2021

THE EFFECTS OF THE LOSS OF PODPC1 IN THE REGENERATION OF THE ZEBRAFISH HEART AND THE CHARACTERISATION OF THE *POPDC1* NULL MUTANT ZEBRAFISH.

NATIONAL HEART AND LUNG INSTITUTE

IMPERIAL COLLEGE LONDON

THESIS SUBMITTED FOR THE DEGREE OF DOCTOR OF PHILOSOPHY

BY

LAUREN BOLAND

OCTOBER 2021

Abstract

Popeye domain containing 1 (Popdc1) is a member of the POPDC gene family, which code for membrane proteins abundantly expressed in heart and skeletal muscle. They bind cAMP and are thought to function as effector proteins involved in stress signalling. *popdc1* null mutant zebrafish have been created using TALENs to cause a premature stop codon resulting in a heavily truncated and non-functional peptide being translated. These mutants survive embryogenesis and larval development and so here I begin to characterise the adults.

Popdc1 null mutants displayed abnormal outflow tracts and heart positioning which may cause cardiac stress. It was also observed that cardiomyocyte size is reduced and heart size is increased in mutants, which could result from cardiac remodelling because of stressors such as pressure overload. Moreover, mutants had a thickened cortical layer and reduced trabecular complexity which may lead to improper heart function. Single nuclear RNA sequencing (snRNA-seq) data show a reduction in presumptive trabecular cardiomyocytes and a unique population of hyper-stressed cardiomyocytes which could explain the morphological differences in the mutant. This data also showed *popdc1* null mutant cardiomyocytes had abnormalities in genes involved in energy metabolism and cardiac regeneration including *fstl1b*, *tbx5a* and *runx1*.

When heart regeneration was tested, mutants displayed reduced regenerative capacity and cardiomyocyte proliferation. Ploidy was also increased in mutant cardiomyocytes, a factor known to hinder cardiomyocyte proliferation. However, this was contrary to the negative regulatory effect that the POPDC proteins have on the proto-oncogene, c-Myc, which would have predicted that the loss of *popdc1* would enhance regeneration.

Overall, the adult *popdc1* null mutant hearts have several morphological phenotypes which are likely caused by or the cause of a hyper-stressed population of cardiomyocytes. High stress along with other factors is also likely to cause the reduced regenerative capacity observed in the mutants.

Statement of originality

I declare that all the work in this thesis has been conducted by myself, Lauren Boland, unless otherwise stated in the document. References to the work of others have been properly cited and full details of these citations can be found in the references section.

Copyright declaration

Acknowledgements

I am truly thankful to everyone who played a role in the submission of this thesis. This huge task has been helped along the way by many people in both my professional and my personal life.

Firstly, I would like to thank my supervisor, Professor Thomas Brand, who always takes the time to explain many scientific details and try to impart to me some of his scientific wisdom. For his enthusiasm in his work which has helped to spur me on in times when I needed some extra motivation. Also, I thank him for the opportunity to complete this degree and to study Popeye proteins in his lab. And finally for being a wonderful host and throwing amazing dinner parties for our lab socials, truly the food is always exquisite. I would also like to thank the other members of the Brand group both past and current for taking the time to talk through technical issues with me and specifically to Lena Gruscheski for keeping me company on some of the lab days that went late into the night. I would like to express special gratitude to Ursula Herbort-Brand, for everything she does for me both in and out of the lab. She keeps the lab running smoothly checks on all my animals and does so much behind the scenes that I probably could never fathom. On top of this, for checking in on me, bringing me delicious homemade snacks and making me tea when she thinks I'm tired. To my second supervisor Dr Tristan Rodriquez and his group, I thank you all for being so open and easy to come to with any issue I might be having.

For the later part of this work, I am grateful for the aid of Dr Michela Noseda and two members of her group, Sam Barnett and Dr Michael Lee. Without you, this work could never have gone ahead and I thank you all for answering many of my questions and helping me to start to put a foot through the door of the labyrinth of bioinformatics. I would like to thank Steven Rothery for answering the many microscope questions. There is never a question or request that seems too much bother for him. To Thomas Adejumo, James Elliott And Bhavik Patel I thank you for all of your help with running the flow cytometers and cell sorters, especially to Thomas who spent a great amount of time explaining and helping me analyse data.

I am grateful for the hospitality of Dr Jeroen Bakkers and his group, specifically Dennis de Bakker, who hosted me for a week at the Hubrecht Institute and taught me many valuable lessons which I have profited from to make gains in this thesis. Also, for introducing me to the *borrel*, it would be grand if this were to happen in England too!

The BHF has been invaluable in this process for funding me as well as providing a network of students and staff that has built a scientific community both within Imperial College London and outside. This community, through conferences and other meet ups, has allowed the discussion and creation of new ideas.

Without my friends and family, this work could never have been completed. My mum and my sister have been rocks throughout this whole process and I'm sorry for the many hours that you have had to listen to me vent about my work. I also thank you both for providing times of distance from my work and allowing me to take my mind from it. To all of my friends, I am so thankful to have you all as a constant source of support. I specifically want to thank Tamzin for being the best emotional support ninja when I needed it in the office and bringing me croughnuts on bad days. And to Amy for allowing me to have the time out than I needed, creating great memories and having amazing adventures!

Finally and in no small part, I am deeply grateful for the animals used in this work who gave their lives for the pursuit of human knowledge. I continually wrestle with the ethics of my work and whether I deem the use of the fish a necessary evil. I hope that life has not been given in vain and that this work has added a little to scientific knowledge. With this, I would also like to thank all of the CBS staff who cared for the fish and upkeep of the system.

"*You are braver than you believe, stronger than you seem, and smarter than you think."* —Christopher Robin, Winnie the Pooh

Table of Contents

List of Figures

List of Tables

Abbreviations

Abbreviation	Full Name
acsl1b	acyl-CoA synthetase long-chain family member 1b
AFOG	Acid fuchsin orange G
aldh1a	aldehyde dehydrogenase 1a
aPKC	atypical protein kinase c
ATP	adenosine triphosphate
AV	atrioventricular
AVN	Atrioventricular node
BA	*bulbus arteriosus*
BMP	Bone Morphogenetic Protein
BSA	Bovine Serum Albumin
BVES	Blood vessel epicardial substance
cAMP	cyclic 3’,5’-adenosine monophosphate
CAP	catabolite activator protein
Cas9	CRISPR Associated 9
cGMP	cyclic guanosine monophosphate
cmlc2	cardiac myosin light chain 2
CoIp	Co-immunoprecipitation
CRISPR	clusters of regularly interspaced short palindromic repeats
CRP	cyclic adenosine monophosphate receptor protein
CCS	Cardiac Conduction System
CTD	Carboxy-terminal domain
CVD	Cardiovascular diseases
DAF-2DA	4,5-diaminofluorescein diacetate
DAPI	4',6-Diamidino-2-Phenylindole
DMEM	Dulbecco's Modified Eagle's Media
dpf	days post fertilisation
DPI	days post-injury
DTA	diphtheria toxin A
ECD	Extracellular domain
ECM	Extracellular matrix
EMT	Epithelial-mesenchymal transition
ENU	N-ethyl-N-nitrosourea
EPAC	Exchange Factor Activates by cAMP
FACS	Fluorescence activated cell sorting
FCS	Foetal Calf Serum
FGF	Fibroblast Growth Factor
FHF	First Heart Field
FIJI	Fiji is just imagej
fstl1b	Folistatin-like 1b
GAPDH	Glyceraldehyde 3-phosphate dehydrogenase
GEFT	Guanine nucleotide exchange factor for Rho-family GTPases

GEM	Gel Bead-In Emulsions
GFP	Green fluorescent protein
GO	Gene Ontology
GSKa	glycogen synthase kinase a
H&E	Haematoxylin and eosin
hand1	heart and neural crest derivatives expressed 1
HCN	hyperpolarisation activated cyclic nucleotide-gated potassium
HER2	human epidermal growth factor receptor 2
HH	Hamburger Hamilton
hpf	hours post fertilisation
HRP	Horseradish peroxidase
IGF	insulin growth factor
LB	Lysogeny Broth
LGMD	Limb-girdle muscular dystrophy
LPM	Lateral Plate Mesoderm
MAP	Mitogen-Activated Protein
metallothionein	mt2
MI	Myocardial Infarction
NGS	Next Generation Sequencing
nppa	natriuretic peptide A
Nrg	Neuregulin
ONS	Office for National Statistics
PAGE	Polyacrylamide gel electrophoresis
PANTHER	protein analysis through evolutionary relationships
PBS	Phosphate Buffered Saline Solution
PCNA	proliferating cell nuclear antigen
PCR	Polymerase chain reaction
PDE	Phosphodiesterase
pdlim	PDZ and LIM domain
PF	Purkinje Fibres
PFA	Paraformaldehyde
PH3	Phospho histone 3
PKA	Protein Kinase A
Popdc	Popeye domain containing
PP2A	Protein phosphatase 2A
qPCR	Quantitative polymerase chain reaction
RA	Retinoic Acid
rpm	revolutions per minute
S62	Serine 62
SAN	Sinoatrial Node
SDS	Sodium dodecyl sulphate
SHF	Second Heart Field
shh	sonic hedgehog
snRNA-seq	Single Nuclear RNA Sequencing

T58	Threonine 58
tal1	T-cell acute lymphocytic leukaemia 1
TALEs	transcription activator-like effectors
TALEN	transcription activator-like effector nucleases
TBST	Tris-buffered saline with tween
TILLING	Targeting Induced Local Lesions In Genomes
TM	transmembrane domain
ToF	Tetralogy of Fallot
TREK-1	TWIX-related K+ channel 1
TUNEL	terminal deoxynucleotidyl transferase dUTP nick end labelling
UK	United Kingdom
UMAP	Uniform Manifold Approximation and Projections
UMI	Unique Molecular Identifier
Vamp3	vesicle-associated membrane protein 3
VEGF	Vascular Endothelial Growth Factor
WCL	Whole-cell lysate
WGA	Wheat germ agglutinin
WHO	World Health Organization
WT	wild type
wt1	Wilm's tumour 1
YFP	Yellow fluorescent protein
ZO-1	Zona occludens-1
ZONAB	ZO-1-associated nucleic acid-binding protein

Notes on nomenclature

According to the human, mouse, chick and zebrafish nomenclature (Crittenden et al., 1995, McAlpine, 1995, Mullins, 1995, Davisson, 1995), I will be using the following nomenclature for naming the different POPDC genes and proteins:

POPDC1 (-2, -3) – Mouse, human or chick Popeye domain containing 1 (-2, -3) protein

Popdc1 (-2, -3) – Zebrafish Popeye domain containing 1 (-2, -3) protein

POPDC1 – Human or chick Popeye domain containing 1 (-2, -3) gene

Popdc1 – Mouse Popeye domain containing 1 (-2, -3) gene

popdc1 – Zebrafish Popeye domain containing 1 (-2, -3) gene

1. Introduction

Cardiovascular diseases (CVD) are a leading cause of death in Western society, with ischemic heart disease producing the highest mortality accounting for almost 20% of deaths (Figure 1) (Bennett *et al*., 2007, Virani *et al*., 2020). In the United Kingdom (UK), 27% of deaths result from CVD (BHF, 2020a), with 167,000 patients dying from myocardial infarction (MI) (BHF, 2020a), although, improved initial responses mean that 70% of patients survive a MI. MI is more commonly known as a heart attack and occurs from coronary artery occlusion which restricts blood flow causing ischemia of the myocardial tissue. The ischemic injury leads to acute death of the myocardial tissue, which is then replaced by fibrotic tissue to maintain integrity as adult cardiomyocytes have a limited ability to proliferate (Bergmann *et al*., 2009). However, the fibrotic tissue does not have the contractile or electrical properties of healthy myocardium (Pfeffer and Braunwald, 1990), resulting in a heart that is unable to retain proper pump function. For these reasons, MI can result in heart failure, causing a lower quality of life, premature death and an increased risk of sudden cardiac death or MI reoccurrence (Yow *et al*., 2021, Anh *et al*., 2010). Although some countries are seeing a drop in the number of mortalities caused by ischemic heart disease (Figure 2A) (Unal *et al*., 2005, Bennett *et al*., 2007, BHF, 2020a, Nowbar *et al*., 2019), heart failure cases are continuing to rise (Figure 2B) (BHF, 2020a, Virani *et al*., 2020, BHF, 2020b). Heart failure can be caused by MI, hypertension and ageing. The rise in cases is likely to be due to an ageing population and increased chances of surviving MI, with 1.4 million survivors in the UK alone. Thus, heart failure is increasing the strain on medical services. Currently, the only treatment option to completely recover from heart failure is receiving a heart transplant, however, limited donor hearts are available, and transplantation is associated with severe side effects. The limited treatment options currently available is why research is ongoing to discover ways to substitute damaged myocardium and reinstate myocardial pump function. Contrary to what is seen in the adult mammalian heart, neonatal hearts (Porrello *et al*., 2011, Haubner *et al*., 2012, Porrello *et al*., 2013, Zogbi *et al*., 2014), hearts of urodele amphibians (Oberpriller and Oberpriller, 1974) and zebrafish

(Poss *et al*., 2002) have retained the ability to recover their heart fully after injury. Zebrafish have recently become a favourable model to study cardiac regeneration and have given valuable insights into the mechanisms involved (Smith and Mommersteeg, 2020, Sanz-Morejón and Mercader, 2020). However, regeneration of the human heart is still currently unattainable.

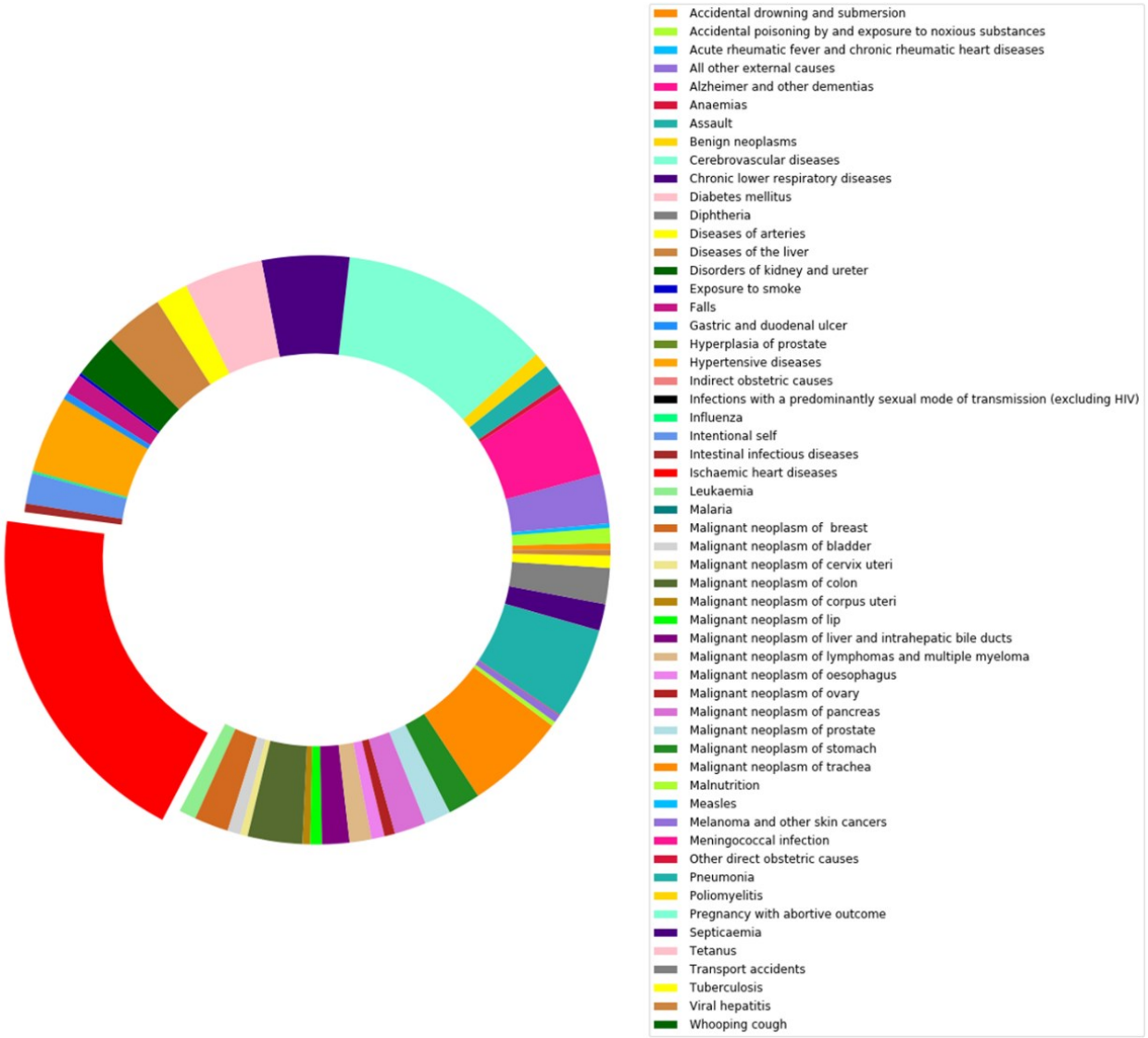

Figure 1 Worldwide causes of mortality in 2015. Deaths by cause across all recorded countries in the latest available year (2015). Ischemic heart disease (red) results in the greatest number of deaths worldwide accounting for 19.37%. Deaths are categorised as according to the World Health Organization (WHO). Data was taken from the WHO mortality statistics (WHO, 2015) and python3 has been used for the representation of the data.

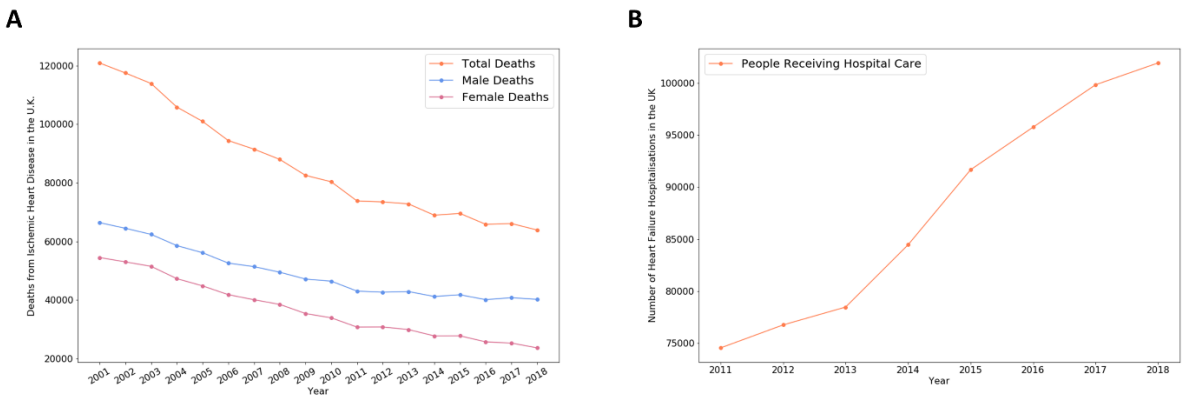

Figure 2 UK heart failure statistics. (**A**) Deaths from Ischemic Heart disease in the UK from 2001 to 2018. Data was taken from the Office for National Statistics (ONS) (ONS, 2020). (**B**) The number of people being hospitalised across the UK due to heart failure between 2011 and 2018. Data were taken from the British Heart Foundation (BHF) Heart and Circulatory Disease Statistics publication (BHF, 2020b) which compiles data from the NHS (Digital NHS, 2020, Digital Health and Care Wales, 2020, Health NI, 2020, Scotland, 2020). Python3 has been used for the representation of the data.

1.1 Zebrafish as an animal model

In recent years, the zebrafish, *Danio rerio,* has become an important model organism. It is a tropical freshwater fish, which has its primary natural habitat in the Ganges River in South Asia. Adult zebrafish typically grow to a length of between 1.8cm and 3.7cm and can be identified by its characteristic striped scale pattern which gave rise to its name. Zebrafish were first used as a model organism by George Streisinger in the 1970's (Streisinger et al., 1981) but really claimed its fame due to the large-scale mutagenesis screens by the groups of Christiane Nüsslein-Volhard and Wolfgang Driever in the 1990's (Mullins *et al*., 1994). Studying the zebrafish can be advantageous, firstly, as they are vertebrates with 71.4% of human reference genes having at least one orthologue (Howe *et al*., 2013). Zebrafish have a rapid, external embryonic development, are largely transparent and are encased in a transparent chorion which allows for embryonic development even at single-cell resolution; addressing scientific questions which cannot be studied in other organisms. They also have a high fecundity; laying up to 200 eggs per week per fish. Furthermore, an ever-expanding range of experimental tools are available to manipulate the zebrafish genome which has allowed large-scale forward and reverse genetic screens to be conducted, allowing the characterisation of many genes. Finally, zebrafish have economical and practical advantages compared to their mammalian

counterparts as large numbers of fish can be kept for a significantly lower cost and require a smaller space relative to mice or rats.

Zebrafish have a large regenerative capacity that has attracted many scientists to work with them. For example, they can regenerate fins (Johnson and Weston, 1995, White *et al*., 1994), maxillary barbel (LeClair and Topczewski, 2010), retinae (Bernhardt *et al*., 1996), optic (Becker and Becker, 2007) and spinal (Becker *et al*., 1997) nerves and skeletal muscle (Rowlerson *et al*., 1997). Kenneth Poss, in the lab of Mark Keating, discovered in 2002 that when 20% of the zebrafish ventricle is amputated it can regenerate (Poss *et al*., 2002), giving rise to the field of study of cardiac regeneration in the zebrafish heart. In this section, I will discuss and describe the similarities and differences between zebrafish and the mammalian heart covering how it develops and regenerates as well as discussing its relevance for human disease.

1.1.1 Structure of the adult zebrafish heart

The heart of zebrafish is typically around 1mm in width and length. The zebrafish heart is unlike the four-chambered mammalian heart as it contains only a single atrium and ventricle (Figure 3) (Hu *et al*., 2000),. Since the blood comes into and leaves the heart deoxygenated it is considered to be a venous heart (Hu *et al*., 2001). The ventricle contains three layers: the endocardium, myocardium and epicardium (Hu et al., 2000, Gupta and Poss, 2012). The myocardium is further subdivided into the cortical, trabecular and primordial layers (Hu et al., 2000, Gupta and Poss, 2012). Unlike the mammalian heart, the trabeculae appear to be more uniformly distributed throughout the ventricle and are much thinner with fewer branching points (Hu *et al*., 2001), allowing the zebrafish ventricle to rely less on the coronary vasculature to provide oxygen and nutrients to the cardiomyocytes. The ventricular wall has coronary vessels in the sub-epicardium, which are penetrating into the myocardium (Hu *et al*., 2000). The wall of the adult atrium is two to three cells thick (Hu *et al*., 2000) and is positioned dorsally to the ventricle and both chambers are separated by the atrioventricular valve which attaches directly to the myocardium (Figure 3). Posterior to the atrium is the inflow tract

or *sinus venous*. Anterior to the ventricle and separated by the bicuspid *bulbo*-ventricular valve is the *Bulbus arteriosus (*BA) (Figure 3), a highly collagenous structure with a thick layer of smooth muscle that contains deep pockets of endocardium that connects the ventricle to the ventral aorta (Hu *et al*., 2000). It is formed of three layers, the intima, media and externa layers (Hu *et al*., 2001). The BA is pear-shaped and thought to prevent high-pressure blood flow over the gills as well as to maintain constant perfusion of blood at a steady pressure over the gill apparatus thereby allowing a continuous uptake of oxygen (Jones *et al*., 1974).

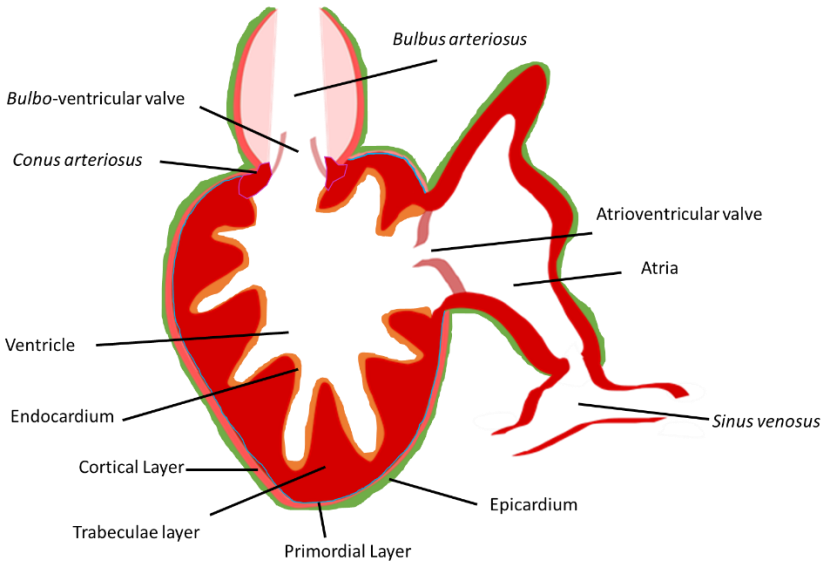

Figure 3 Schematic of the adult zebrafish heart. *Bulbus arteriosus*, ventricle, atrium, *sinus venosus* and *conus arteriosus* are depicted. Blood enters via the sinus venosus and travels through the heart leaving it via the bulbus arteriosus. Different layers of the heart wall are depicted including the epicardial (green) and endocardial (orange) layers. The cortical (pink), trabeculae (red) and primordial (blue) layers of the myocardium are also displayed.

1.1.2 Development of the zebrafish heart

The heart is a fundamentally important organ to mammals and zebrafish. In vertebrates, it is the first organ that completes development and becomes functional. In the human embryo, this takes 35 days while in the zebrafish it only takes 48 hours (Stainier *et al*., 1993, Beis, 2005). Although there are some obvious differences between the mammalian and zebrafish heart, they do share the well-conserved developmental processes and genetic pathways that regulate heart formation. There is wide use of

zebrafish in the study of heart development, they have proven to be an extremely valuable tool, primarily as they can survive for 5 days post fertilisation (dpf) without a functional heart, as the embryo can rely on passive diffusion of oxygen (Hu *et al*., 2001, Hu *et al*., 2000). This has allowed for the study of even severe cardiac phenotypes, which would have caused an early lethality in the mouse model.

In brief, the heart begins to develop shortly after the induction of myocardial progenitor cells which will rapidly differentiate into cardiomyocytes, forming the first heart field (FHF). Endocardial progenitor cells are first seen at the same time as cardiac myoblasts and will migrate and interact with the myocardium to form the cardiac cone. Cells from the second heart field (SHF) are then added to the atrial and venous poles of the cardiac cone and the heart tube will form. The heart tube will loop to form the two compartments and the outflow tract will be added from cells of the SHF. The epicardium will develop from an extracardiac population called the proepicardium which will translocate and adhere to the myocardium before proliferating to cover the surface. The myocardium will also be required to grow and this occurs during trabeculation starting at 60dpf. Other essential structures such as the coronary vessels, the intracardiac nervous system, cardiac valves and the cardiac pacemaker will be essential for the development of the complete heart. Some of these different developmental processes and structures will now be discussed in the following sections.

1.1.2.1 Myocardial Progenitor Cells

The first myocardial progenitor cells can be seen at 5 hours post fertilisation (hpf) in the lateral marginal zone of the blastula (Keegan *et al*., 2004) (Figure 4A). These cells can be defined by their expression of *gata5* (Reiter *et al*., 1999). *Gata5* is essential for generating the proper numbers of myocardial precursors and for the expression of other essential genes in the cardiac development process like *nkx2.5* (Reiter *et al*., 1999). Due to a gene duplication event that took place in teleost evolution, the zebrafish has two orthologues of the mammalian *Nkx2.5* gene, *nkx2.5* and *nkx2.7* (Lee *et al*., 1996) and offer each other some functional redundancy in early development (Tu *et al*., 2009).

Nkx2.5 and *nkx2.7* are targeted for upregulation by *Gata5* just prior to gastrulation in mesodermal progenitor cells (Reiter *et al*., 1999, Kishimoto *et al*., 1997). *Nkx2.5* can first be seen at 12hpf (Lee *et al*., 1996, Chen and Fishman, 1996) and has been considered to mark the beginning of heart field formation (Chen and Fishman, 1996). Fate mapping studies have found that even at roughly 5hpf, there are spatial differences between those cells destined to become atrial or ventricular cardiomyocytes (Keegan *et al*., 2004) and by 15hpf there are two bilaterally aligned cell populations, both with a cardiac fate that form the FHF (Yelon *et al*., 1999) (Figure 4B). In these populations, it is seen that the ventricular cardiomyocyte precursors are more medial and posterior compared to the rostral location of atrial precursors (Keegan *et al*., 2004) and it has been shown that these two different populations have different expression patterns in a number of genes (Yelon *et al*., 1999, Berdougo *et al*., 2003). The two distinct populations will migrate medially at 16hpf and cardiac fusion takes place to form the cardiac primordia (Glickman and Yelon, 2002). Like in mammals (George *et al*., 1997), regulation of extracellular fibronectin is crucial for the correct fusion of these two populations of cells and this is governed by heart and neural crest derivatives expressed 1 (hand1) and lysosphingolipids (Garavito-Aguilar *et al*., 2010).

1.1.2.2 Endocardial Progenitor cells

Endocardial progenitor cells give rise to the cells of the endocardial layer which lines the lumen of the heart and in mammals makes the septum and the valves (Eisenberg and Markwald, 1995). In the zebrafish, endocardial progenitors are first observed 5hpf in the anterior lateral mesoderm in the blastula stage and fate-mapping experiments have shown that they keep a ventral marginal region within the heart field (Lee *et al*., 1994). Time-lapse confocal microscopy has been used to uncover endocardial migration in the zebrafish, at 15hpf these cells rapidly migrate to the site of heart tube formation, proceeding the bilateral myocardial primordia, a process that is governed by T-cell acute lymphocytic leukaemia 1 (tal1) (Bussmann *et al*., 2007). The early endocardial and myocardial progenitors display a huge degree of plasticity, this has been shown by playing with the level of tal1

or the myocardial marker, hand1, which can alter the proportion of cells being recruited into each lineage (Stainier *et al*., 1995, Schoenebeck *et al*., 2007).

Endocardial precursors are thought to make up part of the inner core of the cardiac cone that is made mainly of myocardium during cardiac fusion (Figure 4C), the two cell types are separated by an extracellular matrix called "cardiac jelly" (Glickman and Yelon, 2002, Stainier *et al*., 1993). The endocardial progenitors are now established along the midline, which is critical in allowing the cone to elongate into a heart tube due to the essential interaction between myocardial progenitors and endocardial progenitors (Holtzman *et al*., 2007). Genes that allow the endocardial progenitors to migrate to the midline include *slit1* and *slit2* and their roundabout receptors as well as vascular endothelial growth factor (VEGF), these processes are essential for proper heart tube formation (Fish *et al*., 2011).

Following migration and heart tube formation, the endocardium is then required to mature. One factor in the maturation of the endocardium is biophysical forces including shear stress caused by blood flow (Baeyens and Schwartz, 2016, Haack and Abdelilah-Seyfried, 2016). The endocardium is a specialised endothelium and so it is expected that similar mechanosensory and transduction mechanisms are likely to be used also by other endothelial cells, however, research on this is currently limited. Knockdown of genes of mechanosensory pathways such as VE-cadherin causes cardiac looping defects, defective endocardial junctions and increased endocardial permeability in the zebrafish (Mitchell *et al*., 2010). Morpholino and knockdown experiments in the zebrafish embryo have shown that other genes such as Ets1-related protein/*etv2* and *focx1* are essential for aiding the maturation of the endocardium (Palencia-Desai *et al*., 2011, Pham *et al*., 2007, Sumanas and Lin, 2006).

1.1.2.3 Second heart field development

The presence of SHF has been known for some time in the mammalian heart (Waldo *et al*., 2001, Mjaatvedt *et al*., 2001, Kelly *et al*., 2001), there is a distinct FHF that establishes the primitive heart

tube in early development and contributes primarily to the left ventricle and then the SHF develops slightly later and can be found in the pharyngeal mesoderm with a subpopulation on the dorsal pericardial wall, it helps to create the outflow tract, right ventricle and the atria (Cai *et al*., 2003, Meilhac *et al*., 2004). As zebrafish have a much simpler cardiac structure and contains only one atrium and one ventricle, it was assumed by many that they would not have a SHF during their development. However, a SHF has been discovered and it contributes to the development of the outflow tract, distal ventricle, and the atrium (de Pater *et al*., 2009, Hami *et al*., 2011).

The existence of the SHF was presumed originally due to a second phase of cardiomyocyte differentiation which was temporally and spatially separated from early differentiation of the heart (de Pater *et al*., 2009). It was also noted that this differentiation relied on differing regulation, requiring the expression of Islet1 and fibroblast growth factor (FGF) (de Pater *et al*., 2009). Later publications described the SHF as adding to the arterial and venous poles of the linear heart tube by 36hpf (Lazic and Scott, 2011, Hami *et al*., 2011, Zhou *et al*., 2011b) which requires *tbx1* and sonic hedgehog (*shh*) for normal development (Hami *et al*., 2011). Progenitors in the SHF of the zebrafish express homologues of cardiac progenitor markers such as *nkx2.5* (Lazic and Scott, 2011, Zhou *et al*., 2011b), *mef2cb* (Lazic and Scott, 2011) and *isl1* (Hami *et al*., 2011), which have also been described as mediating SHF development in mammals and thus supports the conservation of the mechanism to generate the SHF, irrespective of the zebrafish's much simpler cardiac structure.

1.1.2.4 Cardiac Looping

The cardiac cone in the zebrafish, in a process known as jogging, will extend to the left of the midline forming the heart tube by 23-28hpf (Stainier *et al*., 1993) (Figure 4D). Southpaw, the zebrafish homologue of Nodal, signals to the cardiac cone to cause the leftward movement (Long *et al*., 2003, de Campos-Baptista *et al*., 2008, Baker *et al*., 2008). Cardiac looping follows this at 30hpf and occurs when the heart tube bends ventrally and rotate to the right forming a dextral S-shaped heart loop with the atria to the left of the ventricle (Figure 4E), this is known to be a complex process involving

many steps (Männer, 2009, Lombardo *et al*., 2019). Nodal is important in ensuring the correct direction of looping, as in mutants there is randomisation of looping with half displaying the correct D-looping and half undergoing incorrect L-looping (Baker *et al*., 2008). Intrinsic bone morphogenic protein (BMP) signalling is also required for ventricular looping specifically for bending at the atrioventricular canal, where it promotes cardiomyocytes to change shape in the superior wall of the canal causing bending (Lombardo *et al*., 2019). Some organ extrinsic factors have also been suggested to affect cardiac looping such as blood flow (Auman *et al*., 2007) and mechanical forces due to restraints by the surrounding tissue (Bayraktar and Männer, 2014). Tbx5a and tbx5b are required for correct cardiac jogging and looping in the zebrafish, if they are knocked down there is randomisation in the directionality of these processes (Garrity *et al*., 2002). During cardiac looping, the two chambers will form in a process named cardiac ballooning (Christoffels *et al*., 2004), here cardiomyocytes on the outer curvature of the wall elongate to create a convex shape, which is promoted by blood flow through the developing ventricle (Auman *et al*., 2007).

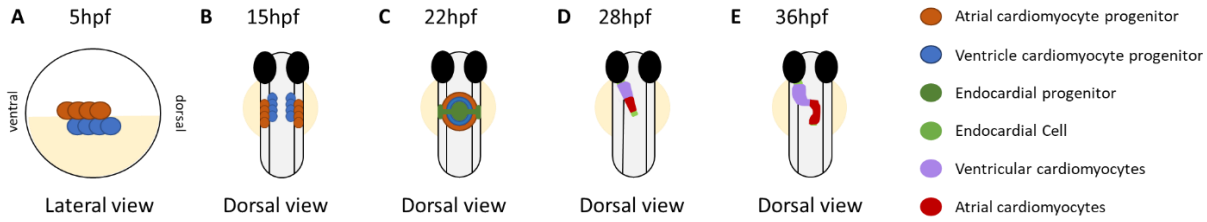

Figure 4 Schematic of heart development in the zebrafish. (**A**) at 5hpf cardiac progenitor cells are located bilaterally in the lateral marginal zone of the blastula with atrial progenitors more ventral than ventricular progenitors. (**B**) Cardiac progenitors migrate bilaterally to the anterior plate mesoderm by 15hpf. (**C**) By 22hpf endocardial progenitors migrate to the midline and fuse with the cardiac progenitors have fused to create the cardiac cone. (**D**) By 28hf the cone has elongated into a tube and has jogged to the left. (**E**) AT 36hpf the heart tube keeps elongating as cardiomyocyte progenitors are added from the second heart field and the linear heart tube has looped dextrally to make the s-shaped heart. Adapted from (Brown *et al*., 2016) and (Bakkers, 2011).

1.1.2.5 Cardiac Maturation

By 48hpf the zebrafish has formed a fully functional two-chambered heart, which is made up of the atrium and the ventricle. However, at this stage, the heart is made up of only two layers; the

endocardium and the myocardium (Stainier *et al*., 1993). To have a fully formed mature heart, outflow tract (*bulbus arteriosus*) formation, epicardial development and trabeculation must occur subsequent to cardiac looping. Further to this, there must be the development of other structures within the heart such as the cardiac conduction system, coronary vessels and valve formation. Finally, the heart must rotate to gain the correct position in the body cavity, with the ventricle becoming positioned more ventrally than the atria (Singleman and Holtzman, 2012). Cardiac maturation is an essential and ongoing process in the fish to cope with the changing demands of the environment, namely the increase in body size and exertion but also perhaps following cardiac injury.

1.1.2.5.1 Epicardial Development

The final layer to develop in the heart is the epicardial layer, this mesothelial cell layer forming the outermost layer of the heart has a vital role by providing nourishment to the myocardium in the form of trophic factors and providing progenitors, which give rise to other important cell lineages in the heart. The epicardium is also essential for the injury response in adult fish by contributing to fibroblasts (González-Rosa *et al*., 2012, Cao and Poss, 2018).

In the zebrafish, the epicardium begins to form at 72hpf and differs in relative time compared with that of the mammalian heart where it is formed in concert with cardiac looping during mid-gestation (Masters and Riley, 2014). The transiently formed proepicardium in the zebrafish can be morphologically distinguished at 48 hpf at the venous pole of the looped heart and at the atrioventricular boundary (Serluca, 2008, Hu *et al*., 2000) and can be identified with the markers Wilm's tumour 1 (*wt1)* and *tcf21* (Kikuchi *et al*., 2010, Liu and Stainier, 2010). At 60 hpf, cells of the proepicardium translocate to the myocardium via cell or cell cluster release into the pericardial fluid (Plavicki *et al*., 2014, Peralta *et al*., 2013). Heart beating is required for this process as it releases epicardial precursors into the pericardial cavity, which eventually attach to the myocardium. However, it is only the contraction that is required for the cell transfer and not the hydrodynamic forces (Plavicki *et al*., 2014). Additional epicardial precursors derive from a second population in the cranial pericardial

mesothelium, which migrates as a cellular sheet to the heart (Plavicki *et al*., 2014). Epicardial layer formation occurs not only through the attachment of proepicardial cells to the myocardium but also through proliferation (Peralta *et al*., 2013). By 6 dpf, the heart is fully covered by the epicardium (Peralta *et al*., 2013).

After the epicardium has formed, a subset of cells undergoes epithelial-to-mesenchymal-transition (EMT) which contribute to the development and maturation of several other cardiac cell types such as cardiac fibroblasts, vascular smooth muscle cells and endothelial cells (Gittenberger-de Groot *et al*., 1998, Takashi and Donald, 1992, Mikawa and Gourdie, 1996, Zhou *et al*., 2008, Kikuchi *et al*., 2011a, Katz *et al*., 2012), a process thought to be governed by Retinoic acid (RA) induced FGF signalling (Pennisi and Mikawa, 2005, Vega-Hernandez *et al*., 2011). They may also contribute towards endothelial cells, however, this is still a matter of discussion in the literature (Red-Horse *et al*., 2010, Poelmann *et al*., 2002). Suggestions have also been made that thymosin beta4 and FGF can push *tbx18*$^{+}$ epicardial cells towards a myocardial lineage in both zebrafish and mammals (Zhou *et al*., 2008, Cai *et al*., 2008, Smart *et al*., 2007, Wills *et al*., 2007). Although, arguments have been made that this is due to the endogenous expression of epicardial markers in a subset of cardiomyocytes (Rudat and Kispert, 2012). The epicardium is also responsible for helping with the maturation, growth and proliferation of the myocardium by secreting several factors (Quijada *et al*., 2020), for example, FGF9 and insulin growth factor (IGF) – 2 (Lavine *et al*., 2005, Li *et al*., 2011). On top of this, it also releases autocrine factors to help with its own maturation (Zhou *et al*., 2008).

1.1.2.5.2 *Bulbus arteriosus* development

The zebrafish outflow tract comprises of the BA and the ventral aorta (Grimes and Kirby, 2009) and regulates the flow through the aorta which sends blood directly to the gills for oxygenation (Grimes and Kirby, 2009). Although the zebrafish heart has only two chambers, the atrium and the ventricle, the bulbus has sometimes had been described as the "subsidiary chamber" that is lacking in the mammalian heart (Hickman *et al*., 1988). A previous lack of specific markers had made understanding

the development of the BA problematic, however, a fluorescent nitric oxide indicator 4,5-diaminofluorescein diacetate (DAF-2DA) was found to specifically label the BA (Grimes *et al*., 2006). DAF-2DA labelling has shown that the striated myocardium does not reach the BA, rather it is made up of a considerable volume of smooth muscle tissue (Grimes *et al*., 2006). In the zebrafish, both the cells of the SHF and the neural crest are also thought to add to BA formation in a process governed by FGF signalling (Felker *et al*., 2018, Cavanaugh *et al*., 2015), similar to what is seen in the mouse and chick (Waldo *et al*., 2005a, Mjaatvedt *et al*., 2001, Waldo *et al*., 2001, Waldo *et al*., 2005b). The addition of SHF progenitors from the anterior lateral plate mesoderm to the outflow tract begins at 26hpf, occurring in multiple waves (Hami *et al*., 2011, Felker *et al*., 2018, Zhou *et al*., 2011c, Paffett-Lugassy *et al*., 2017). By 56hpf elastin expressing immature smooth muscle cells appear at the arterial pole of the heart (Grimes *et al*., 2006, Zhou *et al*., 2011c, Felker *et al*., 2018) and by 72hpf the outflow tract is completely surrounded by smooth muscle cells (Miao *et al*., 2007, Rambeau *et al*., 2017). The BA has an epicardial layer which has different origin from that of the myocardial epicardium (Hu *et al*., 2000, Grimes and Kirby, 2009). Instead of being derived from the proepicardium it is covered as it emerges by flattened pericardial mesothelial cells, in a process similar to that seen in the chick (Pérez-Pomares *et al*., 2003).

The *conus arteriosus* is another portion of the outflow tract that has a role in directing blood and was widely believed that though prominent in more primitive fish species, it had disappeared in teleost fish, like zebrafish (Guerrero *et al*., 2004, Schib *et al*., 2002). However, a region of myocardium in the ventricle surrounding the bulboventricular valve is distinct from the ventricular chamber myocardium as it is non-trabecular and has a strong expression of laminin, suggesting that it may be a residual *conus arteriosus* that is homologous to the conotrucus in the chick (Grimes *et al*., 2006, Icardo, 2006).

1.1.2.5.3 Development of the ventricular myocardial wall

Cardiac trabeculae are highly organised muscular ridges that increase muscle mass prior to the formation of coronary vessels. The purpose of the trabeculae is to increase the myocardial surface

area for blood oxygenation (Samsa *et al*., 2013) and to generate sufficient contractile force to propel the blood around the body. If this process is not properly completed it can lead to embryonic lethality or dilated cardiomyopathy in adults (Liu *et al*., 2010, Gassmann *et al*., 1995, Lee *et al*., 1995, Jenni *et al*., 1999, Crone *et al*., 2002). In zebrafish the ventricular wall is originally only two cells thick; one layer is the endocardium and the other the myocardium. This myocardial layer of cells is the primordial layer that will remain one cardiomyocyte thick throughout the life of the zebrafish. However, cardiomyocytes will begin to delaminate from the primordial layer and proliferate creating trabecular ridges that can be seen by 72hpf (Liu *et al*., 2010, Staudt *et al*., 2014, Gupta and Poss, 2012), thus creating the trabeculae layer. In the zebrafish *erbb2* and neuregulin (Nrg) 2a are vital for trabeculation as mutants fail to form trabeculae (Liu *et al*., 2010, Rasouli and Stainier, 2017). More recent studies have also found that contractility and blood flow are required for trabeculation, which some have attributed to causing an upregulation of the Notch signalling pathway (Staudt *et al*., 2014, Peshkovsky *et al*., 2011, Samsa *et al*., 2015). Crosstalk to the endocardium and myocardium is also essential for development as shown by the *cloche* mutants which cannot form an endocardium and then also fail to undergo trabeculation (Peshkovsky *et al*., 2011). The zebrafish trabeculae are usually two cells thick, although the trabeculae increase during development, suggesting that this process is via hypertrophy (Hu *et al*., 2000). Tbx5a is a marker of the trabeculae and has been shown to prevent trabecular cardiomyocytes from obtaining a different fate (Sánchez-Iranzo *et al*., 2018). After a growth stage, trabeculae will go through remodelling or compaction in mammals to form the compact layer, however, this does not occur in the zebrafish (Sedmera *et al*., 2000). Some Cx40 expressing trabeculae cells in the mammalian heart will not join the compact layer and instead will be fated for a conductive lineage to create the Purkinje Fibres (PF) (Miquerol *et al*., 2010). This process is governed by NKX2.5 (Meysen *et al*., 2007) but does not occur in the zebrafish, it is thought that the ventricular trabeculae serve as a functional equivalent to the PF (Sedmera *et al*., 2003).

If cardiomyocytes in the zebrafish fail to express *tbx5a* then they will take on a cortical layer phenotype (Sánchez-Iranzo *et al*., 2018). The cortical layer is the outer layer of the myocardium that in adulthood

does not exceed four cell layers (Hu *et al*., 2000). The cortical layer begins to develop at approximately 45dpf consisting of cardiomyocytes that primarily originated from two clones of proliferating trabecular myocytes and it is thought that they expand across the primordial layer in a base-to-apex manner (Gupta and Poss, 2012). The cardiomyocytes from different clones converge with one another to have coverage across the whole heart and are laced by coronary vessels (Gupta and Poss, 2012, Harrison *et al*., 2015). It was calculated that approximately eight cardiomyocytes from the trabeculae penetrate the primordial later and contribute to seeding the cortical layer which will then expand via proliferation (Gupta and Poss, 2012).

1.1.3 Modelling cardiac disease in the zebrafish

For some time now, techniques have allowed scientists to make models of a number of genetic diseases in the zebrafish. Studying cardiac disease in zebrafish is convenient due to the ease of genome editing, transparency of embryos to allow observation of aberrant development of the heart and the survival of the embryo for five days without a functional heart as they can rely on diffusion (Hu *et al*., 2001). Large-scale mutagenesis screens have allowed the identification of genes that give rise to specific cardiac pathologies and the creation of fluorescent transgenic reporter lines that label different cardiac cell types within the heart have allowed real-time observations of their in situ development. Furthermore, the fish heart has been used to model diseases, including MI.

1.1.3.1 Genome Editing

Genetic manipulation via reverse genetics has been powerful in the fish for finding genes that are responsible or involved in certain pathologies. However, as the fish has gone through a genome duplication genetic manipulation can cause some difficulties as a single deletion may not lead to a phenotype because of compensation (Meyer and Schartl, 1999). More recently powerful methods have been created to cause targeted mutagenesis relatively easily and quickly.

There are several techniques available to edit the zebrafish genome some transient and some permanent. Morpholinos are a popular method to transiently knock down a gene using anti-sense

technology. They are made to be complementary to mRNA so that they can disrupt ribosome binding and stop translation (Nasevicius and Ekker, 2000). This method has been useful for studying many genes, however, there are drawbacks to this technique; it is only transient lasting up to 5 days, they can cause nonspecific effects such as oedema of the pericardial cavity (Eisen and Smith, 2008), and phenotypes often differ from those of knock out fish (Kok *et al*., 2015, Novodvorsky *et al*., 2015, van Impel *et al*., 2014).

Mutagenesis techniques in the zebrafish include targeting induced local lesions in genomes (TILLING), transcription activator-like effector nucleases (TALEN) and clusters of regularly interspaced short palindromic repeats (CRISPR). TILLING uses (N-ethyl-N-nitrosourea) ENU, a mutagenic chemical that causes the transfer of an ethyl group to nucleotide bases thus causing point mutations (Cox *et al*., 2002) and is used to mutagenize several animals and plants (Gilchrist *et al*., 2006, Taniguchi *et al*., 2006, Till *et al*., 2004, Till *et al*., 2006, McCallum *et al*., 2000, Wienholds, 2002, Wienholds *et al*., 2003, Sood *et al*., 2006). This method is slow, labour intensive and cannot be targeted to specific genes but has produced many important mutant fish (Moens *et al*., 2008).

TILLING was replaced by a method termed transcription activator-like effector nucleases (TALENs), a method that can target specific genes (Huang *et al*., 2011). This method uses Zinc-finger nucleases (ZFNs) to induce targeted double-strand breaks in the genome that are repaired, generating short insertions or deletions by non-homologous end joining or homology-directed repair (Doyon *et al*., 2008). TALENs are created by fusing transcription activator-like effectors (TALEs), which can bind to the gene of interest, to the catalytic domain of the FokI endonuclease. Publicly available reagents have been used by different groups to create TALEs, most of which are based on Golden Gate cloning, this is however labour intensive and not suitable for high throughput. More recently GoldyTALENs was developed, it creates somatic and germline tissue mutations at a high rate and is injected into the embryo and can be used to make large knock-ins of DNA further increasing its use (Bedell *et al*., 2012).

Most recently CRISPR has been used to manipulate the genomes of zebrafish in a way that is much faster and cheaper. CRISPR was discovered in the ’80s (Ishino *et al*., 1987) as a response in archaea and bacteria to protect against bacteriophage (Bhaya *et al*., 2011, Terns and Terns, 2011, Barrangou *et al*., 2007). Bacteria generate RNA complementary to the phage’s genetic information which will bind and recruit CRISPR associated 9 (Cas9) (Deveau *et al*., 2007, van der Oost *et al*., 2009, Wiedenheft *et al*., 2012, Terns and Terns, 2011), this will bind to the phage’s genetic material and cause double-strand breaks (Terns and Terns, 2011). This process has been harnessed for mutagenesis which can be injected into zebrafish at the one-cell stage where it has been adapted to add in, change or remove specific sequences into a section of DNA (Chang *et al*., 2013, Hwang *et al*., 2013, Jinek *et al*., 2012, Bedell *et al*., 2012)

1.1.3.2 Cardiovascular disease models in the zebrafish

Many zebrafish mutant lines have been produced to study human cardiovascular diseases. However, the two-chambered heart means that zebrafish are unsuitable for modelling congenital heart disease such as atrial or ventricular septum defects or studying genes that affect cardiac contractility or that specifically affect the right or left ventricular chamber of the heart. Although zebrafish do share many early developmental pathways and functions with the human heart, which allows for the study of zebrafish in heart development. And so, before modelling human cardiovascular disease in the zebrafish it is important to consider the limitations of the zebrafish heart to determine if this model is suitable in that case. Zebrafish have the capacity to regenerate their heart and so make them suitable for studying regeneration, to help understand the differences compared to humans.

1.1.3.2.1 Cardiac injury models in the zebrafish

Several injury models for the zebrafish heart have been described to mimic MI in patients. These models either rely on surgical techniques to cause physical damage or transgenic lines that allow the specific ablation of cardiomyocytes. Regeneration of the zebrafish heart was first described in 2002 when 20% of the zebrafish ventricle was removed and the fish were shown to survive and hearts were

fully regenerated (Poss *et al*., 2002). This is unlike in humans where cardiomyocyte necrosis leads to inflammation and permanent fibrosis to maintain the integrity of the heart. The following sections will delve into the techniques to model MI and heart regeneration in the zebrafish heart.

1.1.3.2.1.1 Apical resection of the ventricle

The first instance of regeneration of the zebrafish heart was described in 2002 by the Keating lab (Poss *et al*., 2002). The model which they used for this was apical resection, in which 20% of the ventricle is removed (Figure 5A). They found that shortly after cutting the ventricle a large clot was formed, after 2-4 days post-injury (DPI) the clot was replaced by fibrosis and by 30 DPI cardiac muscle was seen to have newly formed in the injured area. The fibrosis in the zebrafish heart differed from what is seen after injury in the mammalian heart as the deposition consisted mainly of fibrin with little collagen, whereas collagen deposition usually dominates the scar in mammalian hearts (Schnitt *et al*., 1993, Cleutjens *et al*., 1995). By 60 DPI the regenerated ventricle appeared normal compared to uninjured fish both histologically and in their contractile function (Poss *et al*., 2002). It was observed however that the usually thin cortical layer of the zebrafish heart was thicker in the injury area and a reduction of the trabecular layer was observed (Poss *et al*., 2002). This suggests that although heart regeneration in the zebrafish can restore cardiac function, there are some permanent alterations of the architecture of the regenerated heart (Hein *et al*., 2015, González-Rosa *et al*., 2014).

Models of surgical resection have also been developed for the neonatal mouse heart and it was found they too recover after partial resection of their ventricle, however, the capacity for this was lost after 7 days of age (Porrello *et al*., 2011) and is injury size-dependent (Bryant *et al*., 2015). Heart regeneration in the neonatal mouse heart resembles the zebrafish with a large clot-forming initially which seals the apical damage, followed by an inflammatory response and extracellular matrix deposition before the scar is resolved and replaced by myocardial tissue (Porrello *et al*., 2011). In the neonatal mouse, this recovery took 21 days and was not associated with any alteration of cardiac function and architecture (Porrello *et al*., 2011). A limitation to this method is that in the human MI

there is necrosis of the cardiomyocytes which have perished from the lack of oxygen caused by the ischemia and need to be cleared, but in this model limited necrosis occurs. Also, a clot is required to form to stem the bleeding caused by the resection, something which is not required in the human MI.

1.1.3.2.1.2 Genetic Ablation

Genetic ablation is a non-invasive method to model MI in zebrafish. Fish are genetically modified to induce the destruction of over 60% of the ventricular myocardium (Wang *et al*., 2011). Transgenic lines were created carrying an inducible Cre recombinase under the control of the *cardiac myosin light chain 2 (cmlc2)* promoter and an inducible cytotoxic diphtheria toxin A (*DTA*) gene (Wang *et al*., 2011). Tamoxifen injection leads to the production of DTA and resulted in the death of ~60% of cardiomyocytes (Wang *et al*., 2011) (Figure 5B). Full recovery is seen 30 days after genetic ablation due to rapid cardiomyocyte proliferation and no changes in the architecture of the heart is observed (Wang *et al*., 2011). However, genetically ablated fish were less capable of handling stress as they did not perform as well as wild types when subjected to heat shock or swim tests, suggesting that they display some signs of heart failure (Wang *et al*., 2011). Despite the robust recovery and similarities to heart failure, the relevance of this model to MI in humans is limited because genetic ablation causes organ-wide cardiomyocyte death rather than necrosis in a defined area and on top of this there is no scar formation, which is the barrier to which the adult mammalian heart fails to overcome. Thus, this model only weakly recapitulates human MI.

1.1.3.2.1.3 Cryoinjury

The final model, which will be discussed is cryoinjury, which was developed in parallel by the groups of Nadia Mercader and Anna Jaźwińska (González-Rosa *et al*., 2011, Chablais *et al*., 2011). In this model localised damage to the heart is caused by a liquid nitrogen cooled probe that is placed on the exposed ventricle until the probe has defrosted (González-Rosa *et al*., 2011). Up to 25% of the ventricle is damaged and within the first 24 hours there is death of cells in the injured area (Figure 5C), this is followed by the clearance of the tissue and the deposition of collagen-rich scar tissue in the first three

weeks (González-Rosa *et al*., 2011). The scar tissue is cleared and replaced by newly regenerated cardiac muscle tissue, the recovery has been shown to take between 60-130 days depending on the size of the initial assault (González-Rosa *et al*., 2011, Chablais *et al*., 2011). It has been observed that the cryoinjured hearts display a thickened ventricular wall upon recovery suggesting that this method does cause changes in the architecture of the heart and may affect cardiac contractility after regeneration has completed (González-Rosa *et al*., 2011, González-Rosa *et al*., 2014).

Cryoinjury models are also used in neonatal mice (Darehzereshki *et al*., 2015), which are known to retain their regenerative capacity for 7 days after birth (Porrello *et al*., 2011). Like in the fish this method can cause transmural damage (damaging the epi-, myo- and endocardium), however, unlike the zebrafish, this does not allow for complete regeneration and the adult mice are left with excessive scarring (Darehzereshki *et al*., 2015). However, when the damage is non-transmural (the injury is only confined to the epi- and myocardium) recovery is more widespread although slight scarring is still apparent (Darehzereshki *et al*., 2015).

Out of the three models, the cryoinjury model is thought to most closely resemble MI in the human heart. Mainly because there is localised tissue damage, which causes necrosis and apoptosis, requiring clearance of the tissue. There is also massive fibrosis, similar to what is seen in mammals (Yang *et al*., 2002, González-Rosa *et al*., 2011, Dobaczewski *et al*., 2010, Susanne *et al*., 2009, Chablais *et al*., 2011), however, unlike humans, the fish can progressively eliminate the scar and regenerate their lost myocardium. Another injury model similar to this is using the application of dry ice instead of a liquid nitrogen-cooled probe to create an injury (Schnabel *et al*., 2011).

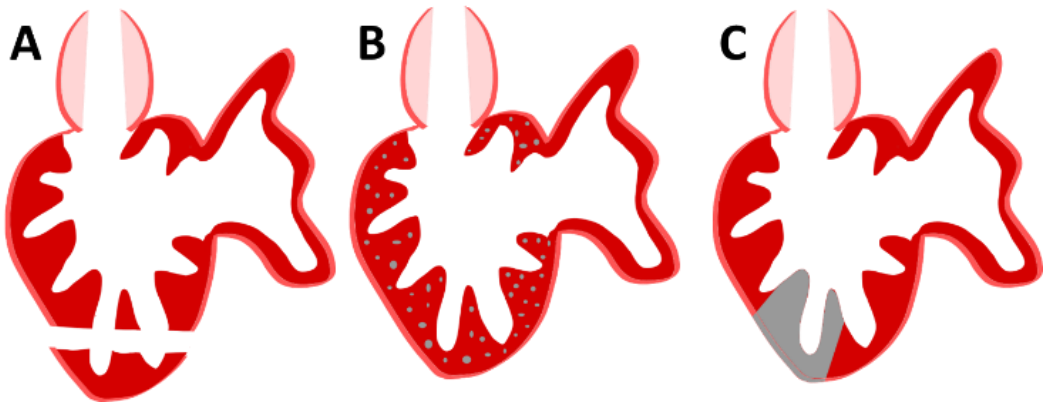

Figure 5 Schematic detailing different models to stimulate MI in zebrafish (**A**) Apical Resection, (**B**) Genetic Ablation and (**C**) Cryoinjury.

1.1.4 Cardiac regeneration in the zebrafish

Regeneration in the zebrafish heart is a constantly evolving process. Regeneration can be broadly subdivided into 4 processes; inflammation, scar formation, cardiomyocyte proliferation and scar removal. Work is ongoing in the zebrafish to understand how this species has maintained the ability to regenerate their heart into adulthood. Many theories have been put forward showcasing the physiological differences between the adult zebrafish and mammalian heart and using them as an explanation as to why adult mammals can no longer regenerate their heart. In this section, I will outline the dynamics of regeneration highlighting genes and differences to mammals that are thought to be essential for proper regeneration.

1.1.4.1 Inflammation

In both the human and the zebrafish after cardiac injury there is the production of damaging molecules such as reactive oxygen species that recruit immune cells to help clear the extracellular matrix using matrix metalloproteinases (Timmers *et al.*, 2012, Etoh *et al.*, 2001). Pro-inflammatory cytokines also mediate the recruitment of immune cells such as phagocytes, neutrophils and macrophages, which are all present by 3 DPI (Huang *et al.*, 2013, Bevan *et al.*, 2020). These cells are essential for the removal of cell debris from the area, the recruitment of other important cell types like fibroblasts and the stimulation of proliferation and angiogenesis through the secretion of cytokines (de Preux Charles *et*

al., 2016, Huang *et al*., 2013). These cytokines are also found after MI in the human heart thus similar initial responses are produced after injury (Ogryzko *et al*., 2014, Stein *et al*., 2007).

This stage of inflammation is essential for the progress of regeneration and if it is inhibited or delayed there is reduced tissue clearance as well as a reduction in cardiomyocyte proliferation (Huang *et al*., 2013, Lai *et al*., 2017). Different types of immune cells are also essential at different time points after injury, as has been described for both macrophages and leukocytes (Bevan *et al*., 2020, Lai *et al*., 2017). The essential role of inflammation is further supported by the finding that leukocyte-derived TGFβ signalling is essential for regeneration (Chablais and Jazwinska, 2012). As well as cytokines stimulating genes like *relaxin3,* which causes cardiomyocyte proliferation (Fang *et al*., 2013). These studies show that inflammation is a prerequisite in allowing regeneration of the zebrafish heart. However, this is a carefully balanced process and if inflammation is too fiercely activated then this can also inhibit regeneration (Xu *et al*., 2019, Bevan *et al*., 2020).

1.1.4.1.2 Scar formation

In mammals, approximately 4 days after injury the reparative stage begins and continues for around 14 days. During this stage, neutrophils go through apoptosis and there is the recruitment of fibroblasts by macrophages through the secretion of TGFβ (Dobaczewski *et al*., 2010, Yano *et al*., 2005). Fibronectin which had been deposited earlier in inflammation to support the heart structure is now allowing endothelial and fibroblast infiltration (Dobaczewski *et al*., 2006). Collagen is deposited into the wound by fibroblasts that have differentiated into myofibroblasts (Dobaczewski *et al*., 2006). The heart will then move into the maturation phase where the collagen is permanently cross-linked with the extracellular matrix (ECM) to provide mechanical support to the heart (Dobaczewski *et al*., 2010).

In the zebrafish, the reparative stage lasts for 3 days starting at 4 DPI and is marked by the secretion of fibronectin and collagen from myofibroblasts after the induction of TGFβ and activin signalling (Chablais and Jazwinska, 2012). Fibroblasts are the primary source of collagen and other ECM proteins and these cells are required for proper regeneration (Sánchez-Iranzo *et al*., 2018) but collagen can also

be deposited by macrophages (Simões *et al*., 2020). The deposition of collagen is mediated by several genes including *midkine-a* and *runx1* (Koth *et al*., 2020, Grivas *et al*., 2021). At the end of the reparative stage at 7 DPI, a fibrin and collagen scar maintains the integrity of the injured zebrafish heart, which is essential for the progression of the healing process, as shown by the inhibition of regeneration when TGFβ is antagonised (Chablais and Jazwinska, 2012). However, limiting collagen and fibrin deposition by ablating *runx1* is beneficial to regeneration (Koth *et al*., 2020).

The epicardium and endocardium are also essential at this stage. Unlike the myocardium, both tissue layers regenerate quite rapidly. The endocardium proliferates between 3-5 DPI and then becomes motile to cover the wound area via migration in a notch dependent manner (Münch *et al*., 2017, Zhao *et al*., 2014) in response to changes in haemodynamic forces (Gálvez-Santisteban *et al*., 2019). The epicardium becomes activated and is highly proliferative as early as 12 hours post-injury expressing genes such as *raldh2*, *tbx18*, *wt1* and *fibronectin 1*; it will then undergo EMT to migrate into the wound (Lepilina *et al*., 2006, González-Rosa *et al*., 2012). Inhibition of proper epicardial activation leads to improper regeneration due to impaired revascularisation and reduced myofibroblast numbers (Lepilina *et al*., 2006, Kim *et al*., 2010a, González-Rosa *et al*., 2011, Kikuchi *et al*., 2011b, Schnabel *et al*., 2011, Wang *et al*., 2013). The epicardium and endocardium are essential in creating a scaffold that will allow for the regeneration of the myocardium, but they also help to lay down extracellular matrix proteins, such as fibronectins and collagen (González-Rosa *et al*., 2012, de Preux Charles *et al*., 2016, Wang *et al*., 2013). Unlike the mammalian heart, this scar deposition is later reabsorbed and substituted by myocardium.

1.1.4.1.3 Cardiomyocyte proliferation

The lack of proliferative capacity in the adult human heart has often been regarded as the limiting factor in cardiac regeneration following MI. Cardiomyocytes of the adult human heart do indeed have a very slow proliferation rate of about 1% in early adulthood (Bergmann *et al*., 2009), with heart growth after birth largely relying on cardiac hypertrophy (Alkass *et al*., 2015). As MI can cause a loss

of around 25% of cells, it is clear that proliferation in the adult human heart is insufficient to regenerate the injured myocardium. However, zebrafish are capable of renewing their myocardium after injury (Poss *et al*., 2002) and myocyte proliferation can even be triggered after multiple injuries to the zebrafish heart, but regeneration becomes less efficient over time (Bise *et al*., 2020). Lineage tracing studies in the zebrafish have shown that the new myocardium after injury is formed from pre-existing myocardium and not from stem or progenitor cells (Jopling *et al*., 2010), with the cardiomyocytes reactivating developmental genes such as *gata4* and *ctgfa* (Kikuchi *et al*., 2010, Pfefferli and Jaźwińska, 2017). To allow for proliferation, the cardiomyocytes revert to a more immature state for example by disassembling their sarcomeres, something that is also seen in the neonatal mouse in cardiac repair (Jopling *et al*., 2010, Kikuchi, 2015, Kikuchi *et al*., 2010, Ben-Yair *et al*., 2019).

Certain genes being expressed in cardiomyocytes have been shown to mark them as being more proliferative. *gata4* is essential in allowing proliferation in cardiomyocytes and lineage tracing reveals that *gata4* expressing cells contribute more highly to the regenerated myocardium, *gata4* is highly expressed in the cortical layer (Gupta *et al*., 2013, Kikuchi *et al*., 2010). More recently the neural crest marker *sox10* was also shown to be expressed in a subset of cardiomyocytes that are more proliferative and contribute more highly to the regenerating myocardium (Sande-Melón *et al*., 2019)

Myocyte proliferation in the zebrafish heart is most apparent at 7 DPI and can be seen largely confined to the border zone of the injury (González-Rosa *et al*., 2011). The cardiomyocytes receive signals to induce their proliferation from non-myocardial cells and these signals include Nrg1, Notch and BMP among many others (Gemberling *et al*., 2015, Wu *et al*., 2016, Münch *et al*., 2017). RA also acts as a proliferation-inducing factor and signals to the border zone myocardium from the epicardium and the endocardium (Kikuchi *et al*., 2011b). Other factors have been proposed to permit the proliferation of cardiomyocytes such as ploidy. Unlike mammals, zebrafish cardiomyocytes are largely mononucleated and diploid, this difference had been highlighted as one that may affect the proliferative potential of

cardiomyocytes, as it also correlates with the regenerative potential across vertebrates (Hirose *et al*., 2019). This has recently been tested as zebrafish have been engineered to become binucleated or polyploid and this caused insufficient proliferation to regenerate the injured zebrafish heart (Patterson *et al*., 2017, González-Rosa *et al*., 2018). The environment is also thought to play a part in the admittance of proliferation in the injured zebrafish myocardium. For example, if hypoxia is not created in the injury area then cardiomyocyte proliferation is blocked (Jopling *et al*., 2012) and when overcrowded tank conditions cause an increase in cortisol there is a reduced regenerative capacity (Sallin and Jaźwińska, 2016).

The different layers of the myocardium do not contribute to the new myocardium evenly and not all of the myocardium is regenerated equally. The cortical layer is important for regenerating the myocardium and can proliferate to add to the cortical layer (Gupta and Poss, 2012). Cardiomyocytes of the trabecular layer have more recently been shown to contribute to the regenerating trabecular layer but are also able to change their fates during regeneration and contribute towards the cortical layer myocardium (Sánchez-Iranzo *et al*., 2018, Pfefferli and Jaźwińska, 2017). The primordial layer on the other hand remains incompletely restored based on the expression of its marker, *careg,* and does not contribute to the regenerating myocardium (Pfefferli and Jaźwińska, 2017). This finding along with the fact that the architecture of the cortical layer and trabeculae layer is not completely restored (González-Rosa *et al*., 2014, González-Rosa *et al*., 2011) suggests that although the myocardium can proliferate, regeneration is not fully achieved in the zebrafish heart and the myocardial histoarchitecture is only incompletely restored. Moreover, functional studies using echocardiography provide evidence for slow recovery after injury and even at 180 DPI some residual impairment still persists (Hein et al., 2015) supporting the conclusions drawn from the histological analysis.

1.1.4.1.4 Scar removal

Scar removal is the final process to occur in myocardial regeneration of the zebrafish heart and is again a process that does not occur in the adult mammalian heart. The ECM that is deposited in the

reparative phase needs to be cleared gradually and replaced by myocardium (González-Rosa *et al*., 2011). Relatively little is known about this process and what cells are involved, however, there is an increase in collagenolytic activity and *mmp2* and *mmp14* expression at 14 – 30 DPI which is thought to aid the degradation of the scar tissue (Gamba *et al*., 2017). Recently osteopontin, a multifunctional cytokine, was shown to have an important role in collagen remodelling and resolution of scarring after being expressed in a subset of macrophages (Bevan *et al*., 2020).

1.1.4.1.5 Angiogenesis

Having vasculature to resupply ischemic tissue after MI greatly reduces adverse remodelling and heart failure, as shown by the overexpression of angiogenic signals after MI (Harada *et al*., 1996, Yanagisawa-Miwa *et al*., 1992). Mammals do naturally express angiogenic signals after MI, triggered by hypoxia and mechanical stress, but still, the injury site remains poorly vascularised and the blood supply to the ischemic area is insufficient (Dimmeler *et al*., 2005, Heil and Schaper, 2004, Lee *et al*., 2000). In the zebrafish heart, new vessels can be seen growing into the damaged tissue as early as 15 hours post-injury, this early onset of vascularisation seems to be essential for the regeneration of the heart (Marín-Juez *et al*., 2016). Vascularisation is dependent on *vegfaa* signalling, which when misregulated will cause a reduction in blood vessel density and a reduction in cardiomyocyte proliferation, which results in permanent scarring of the ventricle (Marín-Juez *et al*., 2016). Mural cells are required for the maturation of new coronary vessels, *pdgfbb* signalling is essential for this as it upregulates mural cell markers and allows endothelial cell proliferation, without proper *pdgfbb* signalling regeneration cannot be completed (Kim *et al*., 2010a).

1.1.4.1.6 Energy metabolism after injury

Cardiac metabolism is essential for creating adenosine triphosphate (ATP) which fuels cells. During embryonic development, the heart primarily uses glucose as an energy source (Piquereau and Ventura-Clapier, 2018), however, as the heart matures metabolic changes occur that cause cardiomyocytes to rely primarily on fatty acid oxidation, which accounts for up to 90% of energy

metabolism in the adult heart (Stanley and Chandler, 2002). However, in disease states, like heart failure and ischemia, cardiomyocytes revert to glucose metabolism as their primary energy source (Das *et al*., 1987, Doenst *et al*., 2013).

It has been shown that after myocardial injury in the zebrafish that there is a transcriptional upregulation of glycolytic enzymes (Fukuda *et al*., 2020, Honkoop *et al*., 2019). Specifically, there is upregulation of pyruvate kinase M1/2 and pyruvate dehydrogenase kinases in the border zone of the injured heart, if this switch is impaired then cardiomyocyte proliferation is reduced and dedifferentiation is attenuated (Fukuda *et al*., 2020). Nrg1/ErbB2 signalling, which is necessary for cardiomyocyte proliferation after injury, mediates the shift to the glycolytic energy metabolism in adult cardiomyocytes (Honkoop *et al*., 2019, Gemberling *et al*., 2015). The switch to glycolysis is also required for fin regeneration in zebrafish (Sinclair et al., 2020). Incidentally, mice switch to fatty acid oxidation away from glycolysis at around 7 days post-birth, coinciding with their loss of regenerative ability (Lopaschuk *et al*., 1992, Porrello *et al*., 2011), leading some researchers to think that the metabolic shift could explain the loss of regenerative capabilities in the mammalian heart (Hirose *et al*., 2019). Recently, a study found that overexpression of glucose transporter, GLUT1, in the neonatal mouse heart leads to a greater regenerative capacity (Fajardo *et al*., 2021). These findings suggest the importance of a switch in energy metabolism away from fatty acid oxidation to permit regeneration of the myocardium.

1.2 Popeye domain-containing gene 1

Popeye domain-containing (Popdc) 1 or blood vessel epicardial substance (BVES) was discovered in 1999 (Reese *et al*., 1999, Andrée *et al*., 2000) and is a member of the Popeye domain-containing gene family, which consists of three family members (*Popdc1, Popdc2* and *Popdc3*) (Reese *et al*., 1999, Andrée *et al*., 2000). The POPDC genes encode for membrane proteins and have notably high expression levels in the heart and skeletal muscle in several species (Reese and Bader, 1999, Andrée *et al*., 2000). However, the expression has also been noted at lower levels in other tissue types (Brand,

2005, Osler and Bader, 2004, Ripley *et al*., 2006, Andrée *et al*., 2002a, Torlopp *et al*., 2006, Froese and Brand, 2008). POPDC1 is known to bind to several proteins, which offers insights into the function of the protein. A notable interaction partner is the proto-oncogene, c-Myc (Parang *et al*., 2016). Moreover, the conserved Popeye domain acts as a binding site for the second messenger, cyclic 3',5'-adenosine monophosphate (cAMP) (Froese *et al*., 2012). Silencing or mutation of the POPDC genes in patients has been reported to be involved with a range of diseases including cardiac arrhythmias, muscular dystrophy, tetralogy of Fallot and cancer (Schindler *et al*., 2016b, De Ridder *et al*., 2019, Indrawati *et al*., 2020, Beecher *et al*., 2021, Shi *et al*., 2019, Vissing *et al*., 2019, Rinné *et al*., 2020). The following sections will give an overview of the research that has been conducted on POPDC1.

1.2.1 Conservation of POPDC proteins across species

POPDC genes are evolutionarily conserved throughout the animal kingdom (Andrée *et al*., 2000). As well as being found in vertebrates, they are also found in basal chordates, such as Ciona intestinalis (Davidson *et al*., 2003, Davidson and Levine, 2003); where there are just two genes, *Popdc1* and *-3* (Brand, 2005), and in some invertebrates where the number of POPDC genes vary largely (Davidson *et al*., 2003, Davidson and Levine, 2003, Brand, 2005, Lin *et al*., 2007, Schindler *et al*., 2012).

The essential role that these proteins play is implied by their highly conserved sequence, as well as their preservation across the animal kingdom (Brand *et al*., 2014). It is also noteworthy that proteins with sequence homology to POPDC proteins have also been described in prokaryotes in the form of the catabolite activator protein (CAP), which is also known as cyclic adenosine monophosphate receptor protein (CRP) and bind cAMP and is involved in metabolic regulation (Schindler *et al*., 2012, Simrick *et al*., 2013). This suggests that these proteins might have a common origin, although, homologues have not been found in plants (Osler *et al*., 2006), perhaps indicating that these genes have either been lost during plant evolution or that the bacterial genes and POPDC genes in the animal phyla have independently evolved. In higher vertebrates *Popdc1* and *Popdc3* are found on the same chromosome (6q21 in humans) in close proximity in a tandem configuration, whereas *Popdc2* is found

on a different chromosome (human chromosome 3q12.33) (Andrée *et al*., 2000); likely affecting the regulation of gene expression. *Popdc2* and *-3* are the most closely related (Andrée *et al*., 2000), and with *Popdc2* being present only in vertebrates, it suggests that it may have its origin from a recent gene duplication of *Popdc3* during vertebrate evolution (Brand, 2005).

1.2.2 Structure of POPDC proteins

The POPDC genes display poor sequence homology to other known genes, a factor that has led to difficulty in determining their function. However, POPDC proteins have a short extracellular amino terminus, of length between 27 and 39 residues, followed by three transmembrane domains, the Popeye domain and the carboxy-terminus that varies considerably in length between the different isoforms (Andrée *et al*., 2002a, Knight *et al*., 2003). The evolutionary conserved Popeye domain is the defining feature of the POPDC family and has been shown to bind cAMP (Figure 6) (Froese *et al*., 2012, Andrée *et al*., 2000). Although the proteins in the POPDC family are similar in structure, they differ in size, which is primarily due to the differences in length of the carboxy-terminal domain. POPDC3 is the smallest at 292 amino acids, followed by POPDC1 at 359 amino acids and the POPDC2 is the largest at 367 amino acids (Andrée *et al*., 2000).

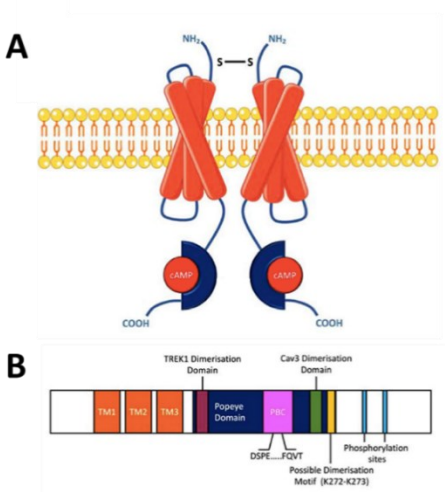

Figure 6 Model of POPDC protein structure. (**A**) A schematic of the quaternary structure of a POPDC dimer. (**B**) A schematic of the linear structure of the POPDC protein. POPDC1 is a membrane protein that forms homo- or heterodimeric complexes. It contains a short extracellular amino terminus and is strongly glycosylated followed by three transmembrane domains. The intracellularly localised Popeye domain is evolutionary conserved and functions as a cAMP binding domain. It is followed by a carboxy-terminal domain, which is variable in sequence and length in the different isoforms. Figure from Swan *et al*. (Swan *et al*., 2019), image reproduced with the permission of the authors.

The predicted molecular weights of POPDC proteins are 37-41kDa (Andrée *et al*., 2000), although sodium dodecyl sulphate polyacrylamide gel electrophoresis (SDS-PAGE) show a larger molecular weight. Moreover, the molecular weight also varies in different tissues and is perhaps due to tissue-specific post-translational modifications or alternative splicing (Andrée *et al*., 2000, Knight *et al*., 2003, Vasavada *et al*., 2004, Schindler *et al*., 2016a). For example, it is known that POPDC proteins get extensively glycosylated and in POPDC1 there are two N-linked glycosylation sites in the extracellular amino terminus (Knight *et al*., 2003), however, it is unknown whether in addition, POPDC1 has any O-linked glycosylation sites or is modified in any other way apart from phosphorylation, as POPDC proteins are getting phosphorylated in response to adrenergic stimulation (Figure 6) (Swan *et al*., 2019).

1.2.3 Expression of the POPDC genes

As well as being highly expressed in the heart and skeletal muscles (Andrée *et al*., 2000), POPDC genes have also been shown to be expressed in other cell types, such as neurons (Brand, 2005), epithelial cells (Osler and Bader, 2004, Ripley *et al*., 2006) and smooth muscle cells (Andrée *et al*., 2002; Brand, 2005; Torlopp *et al*., 2006; Froese and Brand, 2008). A similar and overlapping expression has been noted for the different POPDC genes, though differences are evident, such as *Popdc1* being expressed equally in the heart and skeletal muscles whereas *Popdc2* is expressed strongly in the heart with only little expression in the skeletal muscle. On the other hand, *Popdc3* is expressed highly in skeletal muscle but only weakly in the heart (Andrée *et al*., 2000, Brand, 2005). Both *Popdc1* and *Popdc2* have a higher expression level in the cardiac conduction system, sinoatrial node (SAN) and the atrioventricular node (AVN) as opposed to the working myocardium (Froese *et al*., 2012). Until recently it was assumed that *Popdc3* had a similar expression pattern to *Popdc1* (Andrée *et al*., 2000) due to their chromosomal tandem organisation, although, it has seldom been studied due to its low expression level and the lack of specific antibodies. However, a recent analysis of the LacZ expression

pattern of *Popdc3* in the mouse heart suggests that each of the three POPDC genes have a unique expression pattern but also display overlapping expression domains, with *Popdc3* being unique in displaying an expression in a narrow domain in the subepicardial myocardium (Figure 7). Both *Popdc1* and *Popdc2* show prominent labelling of the cardiac conduction system including the SAN and the AVN.

Within the cardiomyocytes, POPDC proteins are expressed in the plasma membrane and found in multiple compartments including the lateral plasma membrane, t-tubules, caveolae and the nuclear envelope (Brand and Schindler, 2017, Schindler *et al*., 2016a). Interestingly, POPDC1 is also found in the nucleus of satellite cells and cultured neonatal cardiomyocytes (Andrée *et al*., 2002a).

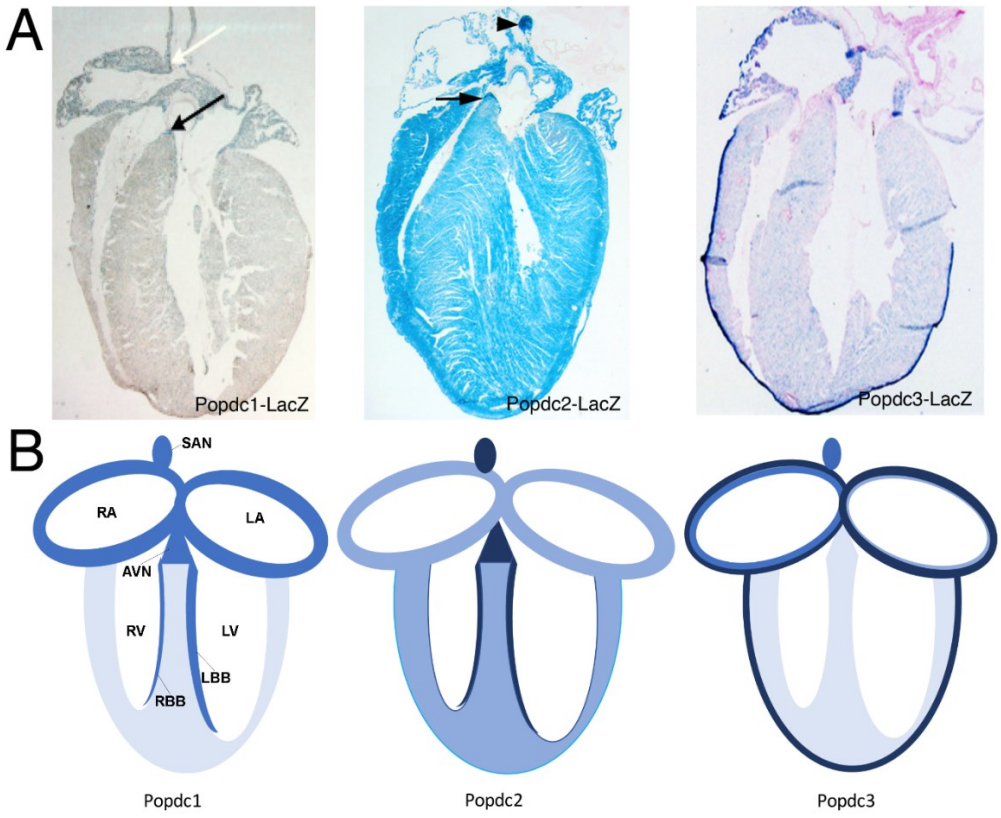

Figure 7 Comparison of LacZ expression pattern of *Popdc1, Popdc2* and *Popdc3* in the mouse heart. The POPDC isoforms display overlapping and isoform-specific expression domains as shown by LacZ staining (upper panel). A schematic of the LacZ staining pattern in the heart covering the right atria (RA), left atria (LA), sinus atrial node (SAN), atrioventricular node (AVN), right ventricle (RV), left ventricle (LV), right bundle branch (RBB) and left bundle branch (LBB), darker shades of blue correspond higher expression in those areas (lower panel). This figure was gifted to me by Professor Thomas Brand.

During development, POPDC1 is expressed in all three germ layers (Osler and Bader, 2004). Arguments haven't been resolved concerning the expression of POPDC1 in the epicardium, with different experimental methods showing contradictory results (Reese *et al*., 1999; Andrée *et al*., 2002). Early work on the developmental expression of POPDC1 came from the chick and mouse. In the mouse, expression analysis by in situ hybridisation first detected expression at E9.5 in the inflow tract and parts of the dorsal ventricle and at E12.5 expression was also observed in the ventral half of the ventricle, however, limited to the subepicardial compact layer (Andrée *et al*., 2000). With lacZ staining, *Popdc1* expression can first be seen at E7.5 in the mesoderm of the cardiac crescent, by E10.5 both atrial and ventricular cardiomyocytes displayed expression of *Popdc1* and as well in parts of the branchial arches. Later at E13.5, there was a strong expression of *Popdc1* in the compact but not the trabecular layer in the heart and by this stage expression could also be seen in other areas of the body such as in the somites and some smooth muscle tissue (Andrée *et al*., 2002a). In the chick, it was observed that protein expression could be seen at (Hamburger Hamilton) HH stage 10 in the presumptive left ventricular segment and after heart looping this staining became specific to the outer curvature of the myocardium (Torlopp *et al*., 2006). Later at stage 31, POPDC1 can be seen in muscle masses in the limb muscle blastema with the protein not being found at the membrane until stage 37 (Vasavada *et al*., 2004). On the other hand, mRNA levels of *Popdc1* in the chick can be seen as early as HH stage 4 and at stage 5 it becomes asymmetric in the Hensen's node and was found in the pharyngeal endoderm and the notochordal plate, by HH stage 9 mRNA occupied a similar location to protein and was found in the cardiac mesoderm (Torlopp *et al*., 2006). So far developmental expression of *popdc1* in the zebrafish has not been studied.

1.2.4 Interaction partners of POPDC proteins

Further analysis of POPDC function shows that these proteins participate in numerous pathways. Importantly, POPDC1 has been shown to interact with the second messenger cAMP and has been heralded as the newest cAMP effector protein (Froese *et al*., 2012). Additionally, POPDC1 is involved

in tight junction formation and maintenance of epithelial layers (Osler *et al*., 2005). Williams and colleagues have also described POPDC1's association with adherens junctions in certain tissues, by observing correlation in expression to known components of adherens junctions (Williams *et al*., 2011). These findings lead to the hypothesis that POPDC1 has a role in controlling EMT (Williams *et al*., 2011, Han *et al*., 2014). Many cancers feature improper regulation of EMT, which causes metastasis (Heerboth *et al*., 2015). Consistent with a role of the POPDC proteins in the control of EMT, *POPDC1* and *-3* are downregulated in various cancer types (Feng *et al*., 2008, Kim *et al*., 2010b, Williams *et al*., 2011, Han *et al*., 2014, Han *et al*., 2015, Luo *et al*., 2012a, Amunjela and Tucker, 2017b).

The below sections will discuss in further detail some of the functions of POPDC proteins and their interaction partners with a more focus on POPDC1 as it has been most extensively studied and is the main subject of this thesis. Whilst discussing these interaction partners I will also give some thought to the potential functions of POPDC proteins.

1.2.4.1 Homo- and heterodimer formation of POPDC proteins

The members of the POPDC family are capable of forming homodimers and heterodimers with different family members. The site mediating this interaction is likely to be found in the carboxy terminus of the Popeye domain (Knight *et al*., 2003, Vasavada *et al*., 2004). Two lysine residues have been discovered in the Popeye domain of POPDC1 that are important for dimerization, however, it is presumed that other sequences are also involved as their removal does not completely inhibit dimerization and the two lysine residues are not conserved between the different isoforms, which suggest that heterodimer formation is controlled via other sequences (Kawaguchi *et al*., 2008, Russ *et al*., 2011). The POPDC family's ability to heterodimerise is thought to be essential for its function (Rinné *et al*., 2020).

1.2.4.2 POPDC proteins and its function as a cAMP effector protein

Protein Kinase A (PKA), exchange factor directly activated by cAMP (EPAC) and the hyperpolarisation activated cyclic nucleotide-gated potassium (HCN) channels are cAMP effector proteins, however,

POPDC proteins have recently been added to this repertoire (Schindler and Brand, 2016). cAMP is a ubiquitous intracellular second messenger that is synthesised by adenylyl cyclase, in response to hormones binding to their receptor such as the beta-adrenergic receptor and is metabolised by phosphodiesterases (PDEs). cAMP has an important role within the heart by modulating heart rate, contractility, relaxation and the speed of conduction (Froese *et al*., 2012). A large number of cardiac diseases have been attributed to the dysregulation of the cAMP pathway (Movsesian, 2004). All three members of the POPDC family can bind to cAMP demonstrated by their ability to be bound and precipitated by cAMP-agarose (Froese *et al*., 2012). POPDC1 can bind to cAMP with a similar affinity as PKA and has a much higher affinity than EPAC, as shown by radioligand binding assays and recombinant POPDC1 protein (Froese *et al*., 2012). Moreover, POPDC1 also displays selectivity and has a 40-fold higher affinity for cAMP than for cyclic guanosine monophosphate (cGMP) (Froese *et al*., 2012).

At the sequence level, the cyclic nucleotide-binding domain in POPDC proteins is divergent from that found in PKA and EPAC, however, homology models have predicted a higher structural similarity to those domains (Froese *et al*., 2012). There are two highly conserved regions within the Popeye domain, the DSPE and the FQVT motifs and these are thought to be essential for cAMP binding and this has been demonstrated by site-directed mutagenesis (Froese *et al*., 2012). Patients carrying the S201F mutation in POPDC1, display a large (50%) reduction in cAMP affinity compared to wild type protein (Froese *et al*., 2012, Schindler *et al*., 2016b). Homology models suggest that these motifs interact directly with cAMP, which are thought to make up at least part of the phosphate-binding cassette, which is essential to bind to cAMP (Froese *et al*., 2012).

It is still not fully understood how cAMP affects POPDC1 protein function, but four models have been put forward, and the underlying mechanisms need to be investigated to determine which model fits best (Amunjela *et al*., 2019). Firstly, is the switch model where POPDC proteins would act after binding cAMP to activate or inhibit an interacting protein. POPDC1's interaction with TWIX-related K+ channel

1 (TREK1) gives some evidence to this as the TREK1 current is only enhanced by POPDC1 at low cAMP levels and this effect is lost when cAMP levels are raised through PDE inhibition (Schindler *et al*., 2016b, Froese *et al*., 2012). Another model is the shield model, in this scenario cAMP binding to POPDC1 could change protein-protein interactions, for example preventing proteins from being phosphorylated by PKA at certain cAMP levels. Evidence for this model comes from the finding that POPDC proteins bind PDE4A and thereby reducing cAMP levels in its vicinity, or keeping POPDC1 in a cAMP unbound state (Tibbo *et al*., 2020). Likewise, POPDC1 function in long term potentiation in hippocampal acute slides appears to be limiting PKA activation in response to electrical stimulation (Shetty *et al*., 2021). The trafficking or cargo model proposes that cAMP can influence POPDC's ability to modulate the trafficking of membrane proteins. Forced expression of the POPDC1^{S201F} mutant, discovered in patients with muscular dystrophy and AV block, reduce membrane trafficking of TREK1 in *Xenopus* oocytes (Schindler *et al*., 2016a). *POPDC1* mutants discovered in patients also show aberrant membrane localisation of POPDC2 (Schindler *et al*., 2016b, De Ridder *et al*., 2019). POPDC1 has also been shown to interact with vesicle-associated membrane protein 3 (VAMP3), a protein involved in vesicle fusion with the plasma membrane. Interestingly, when POPDC1 is compromised, vesicular transport in epithelial cells is abnormal (Hager *et al*., 2010). Finally, in the sponge model, POPDC1 might act to limit cAMP diffusion as it is an abundant protein in muscle cells and bind cAMP with high affinity and thereby could affect the diffusion rate of cAMP. It is thought that cAMP does not freely diffuse in cells, but is actually forming nanodomains, PDEs are known to degrade cAMP shortly after synthesis and thereby limiting its diffusion, however, its enzyme activity is not sufficiently high to solely explain the observed diffusion rate of cAMP in cells (Lohse *et al*., 2017). The high affinity for cAMP by POPDC proteins and their abundance in cardiomyocytes led to suggestions that POPDC proteins could act to 'soak up' cAMP and thereby also participate in defining nanodomains. The activity of the different POPDC isoforms might have the potential to follow different models as well as there being tissue-specific differences in the function of POPDC proteins (Amunjela *et al*., 2019).

1.2.4.3 POPDC proteins in vesicular transport

POPDC1 can interact with the ubiquitously expressed vesicular SNARE protein VAMP3, and further to its interaction when POPDC1 is lost, vesicular transport that is typically mediated by VAMP3 is lost and membrane proteins such as β1-integrin and transferrin become inhibited from being shuttled to the plasma membrane (Hager *et al*., 2010). The interaction of VAMP3 and POPDC1 has been seen in a range of cells including cardiomyocytes and skeletal muscle as well as epithelial cells (Hager *et al*., 2010). POPDC1 has also been shown to display interaction with NDRG4, and this interaction mediates the fusion of VAMP3-positive endosomes with the cell membrane, which further establishes the role of POPDC1 in vesicular transport (Benesh *et al*., 2013). Loss of this interaction causes randomisation of the movement of epicardial cells and they lost their ability to properly secrete and break down ECM (Benesh *et al*., 2013).

1.2.4.4 POPDC proteins and ion channels

Work in *Xenopus* oocytes has demonstrated that PODPC1, -2 and -3 can functionally interact with TREK-1 in a cAMP-dependent manner, where it has been found that co-expression of POPDC isoforms and TREK-1 at low cAMP levels can double the potassium current through the channel and this increase is mainly due to an increase in membrane trafficking compared to cells which express TREK-1 alone (Froese *et al*., 2012). TREK-1 is a two-pore domain potassium channel that can be regulated by many stimuli including membrane stretch, pH and temperature. These findings suggest that POPDC proteins can affect the membrane potential and the excitability of cells which may help to explain the arrhythmias seen in patients carrying mutations in POPDC genes (Schindler *et al*., 2016b, De Ridder *et al*., 2019).

1.2.4.3 POPDC1 and cell-cell contact formations

Theories arose of POPDC1s interaction with cell-cell contacts because of the accumulation of the protein at newly formed cell-cell contact points (Osler *et al*., 2005). Tight junctions regulate the intercellular passage of molecules and block the apical-basolateral diffusion of membrane proteins in

epithelial cells (Sawada *et al*., 2003). POPDC1 has been shown to directly interact with zona occludens 1 (ZO-1) using a GST pull-down assay (Osler *et al*., 2005). ZO-1 is a tight junction protein and it has been concluded that POPDC1 is important in forming tight junctions and also for the formation and maintenance of epithelial monolayers. Adding to this, overexpression of POPDC1 has been shown to increase tight junction formation through RhoA signalling and thus decrease epithelial permeability (Russ *et al*., 2011, Han *et al*., 2015). On top of these studies from the mouse, in the zebrafish, Popdc1 has been seen to interact with atypical protein kinase C (aPKC), which recruits members of the tight junction signalling complex to maintain epithelial integrity (Wu *et al*., 2012).

Subsequently, evidence has been obtained that on top of the role in tight junctions, POPDC1 may also play a role in adherens junctions, which link a cell-cell contact to the cytoplasm of the cell. Adherens junctions can regulate WNT signalling by sequestering β-catenin at the cell membrane (Klinke *et al*., 2015). It was found that POPDC1 could co-localise with both β-catenin and E-cadherin (Williams *et al*., 2011, Han *et al*., 2014), although this overlap of expression does appear to be cell type-specific (Osler *et al*., 2005). Further to this ZO-1, which I have previously mentioned can bind to POPDC1, is also known to interact with key components of adherens junctions (Palatinus *et al*., 2011). The finding that POPDC1 is involved in mediating both tight and adherens junctions is in line with claims that POPDC1 has a role in regulating EMT, which is often deregulated in tumours (Williams *et al*., 2011, Han *et al*., 2014). This is consistent with the finding that the loss of POPDC1 in cancers promotes migration, invasion and metastasis (Amunjela and Tucker, 2017a, Amunjela and Tucker, 2017b, Han *et al*., 2014, Han *et al*., 2015)..

1.2.4.3 POPDC proteins in cell proliferation and cancer

The POPDC proteins in general and with more intensive study, POPDC1, have been shown to interact with several different molecules, which can modulate the cell cycle. Moreover, POPDC proteins are misregulated in a large number of cancers. The role of POPDC2 and POPDC3 in this context is less understood. There is evidence for both POPDC2 and POPDC3 acting as tumour suppressors and in an

oncogenic manner, this may suggest that their roles may be dependent on the tissue in which they are found. For example, both *POPDC2* and *POPDC3* were found to be overexpressed in ductal breast carcinoma, with *POPDC2* being overexpressed at all stages but with *POPDC3* being overexpressed only in the early stages of the disease (Amunjela and Tucker, 2017b). There was also a correlation between POPDC2 and *POPDC3* expression and human epidermal growth factor receptor 2 (HER2)+, a known marker of more aggressive tumours (Amunjela and Tucker, 2017b, Krishnamurti and Silverman, 2014). POPDC3 has been also seen as a potential tumour enhancer in head and neck squamous cell carcinoma, where its expression correlated with poor prognosis and indicated radioresistance (He *et al*., 2019). On the contrary, *POPDC3* suppression in gastric tumours has been liked to oncogenesis. With suppression of *POPDC3* being correlated to poor prognosis, metastasis and invasion (Luo *et al*., 2012b). In these cancers, it has been observed that promoter hypermethylation is responsible for the suppression of *POPDC3* (Luo *et al*., 2012b). No molecular mechanism is yet known regarding *POPDC3* in cancer and cell proliferation, but it is likely that when picked apart that tissue-specific roles will be seen that may explain the different expression levels and functions in the varying forms of cancer.

POPDC1's role in cancer has been more extensively studied, it regulates cell proliferation and when its function is lost or reduced there is an enhancement of malignant cell behaviour. In line with this decreased expression of *POPDC1* has been shown in tumours to enhance cell migration, proliferation and metastasis (Parang *et al*., 2016, Amunjela and Tucker, 2017a, Han *et al*., 2015, Amunjela and Tucker, 2017b, Williams *et al*., 2011, Kim *et al*., 2010b). As POPDC1 can interact with cAMP it has been suggested that the inhibition of cell proliferation could be downstream of cAMP, as it has been shown to inhibit migration and invasion of some types of cancer (del Pulgar *et al*., 2005, Spina *et al*., 2012). In support of this hypothesis is that other cAMP binding molecules have also been involved in tumour progression (Miller, 2002, Kumar *et al*., 2017). However, POPDC1 has other interaction partners that link it to the cell cycle.

For example, POPDC1 can interact with ZO-1 (Osler *et al*., 2005). ZO-1 has been implicated in the inhibition of epithelial cell proliferation through sequestering of ZO-1-associated nucleic acid-binding protein (ZONAB) to the tight junctions removing them from the nucleus which then cannot go on to interact with and promote cell cycle proteins such as proliferating cell nuclear antigen (PCNA) and Cyclin D1 (Balda and Matter, 2009, Balda *et al*., 2003, Matter and Balda, 2000). Thus, when ZO-1 is expressed at low levels, ZONAB is free to enter the nucleus and promote cell proliferation. High POPDC1 levels correlate with high ZO-1 levels, which reduces cell proliferation (Russ *et al*., 2011, Osler *et al*., 2005). This finding has been further substantiated by the suppression of POPDC1 and ZO-1 in some cancers (Amunjela and Tucker, 2017a, Amunjela and Tucker, 2017b, Hoover *et al*., 1998). This is consistent with POPDC1 acting as a tumour suppressor.

POPDC1 can also interact with guanine nucleotide exchange factor for Rho-family GTPases (GEFT) (Smith *et al*., 2008), a guanine nucleotide exchange factor for the Rho-family GTPases Rac1 and Cdc42, that is involved in cell proliferation (Guo *et al*., 2003). On top of affecting cell proliferation, GEFT is also known, when overexpressed, to cause a rearrangement of the microfilaments and affect the morphology and migratory activity of cells. Overexpression of POPDC1 in cells reduces GEFT mediated activity of Rac1 and Cdc42, which will go on to cause a reduction in the cell's mobility (Smith *et al*., 2008). The exact mechanisms that govern the ability of POPDC1 to interact with and affect the Rho-family GTPases Rac1 and Cdc42 are not completely clear. These findings are in line with certain types of cancers where the reduction of POPDC1 causes an increase in tumour cell migration and cell proliferation (Amunjela and Tucker, 2017a, Han *et al*., 2015, Williams *et al*., 2011).

The WNT signalling pathway is a highly evolutionarily conserved pathway that can be found in even the most primitive organisms, it is invaluable in regulating aspects of cell fate determination, cell migration, cell polarity, neural patterning and organogenesis (Komiya and Habas, 2008). The WNT signalling pathway has been shown to regulate cellular processes such as cell proliferation, apoptosis and cell cycle arrest (Teo and Kahn, 2010), linking it to tumorigenesis (Thompson *et al*., 2019, Zhan *et*

al., 2017). The canonical WNT signalling pathway, when activated causes an accumulation of cytoplasmic β-catenin, which will then translocate into the nucleus and will activate the transcription of a number of WNT target genes such as cyclin D1 and c-Jun which can upregulate the cell cycle (Teo and Kahn, 2010, Kaykas *et al*., 2004). POPDC1 has been shown to interact with and/or affect members of the Wnt signalling pathway (Williams *et al*., 2011, Parang *et al*., 2016, Reddy *et al*., 2016, Thompson *et al*., 2019). POPDC1 can also affect β-catenin levels and cause it to have a cytoplasmic localisation, which downregulates Wnt signalling (Williams *et al*., 2011, Thompson *et al*., 2019). In turn, this will reduce WNT mediated cell proliferation.

Finally, POPDC1 has been shown to regulate c-Myc (Parang *et al*., 2016). c-Myc is a nuclear proto-oncogene (Nesbit *et al*., 1999) and a transcription factor controlling the expression of a large number of genes and it recruits histone acetyltransferases which remodel the DNA leading to increased accessibility for transcription (Martinato *et al*., 2008). c-Myc can regulate the cell cycle through upregulating cyclin-dependent kinases and E2F, which are important for cell cycle entrance and suppression of cell cycle inhibitors like p27 (Bretones *et al*., 2015). In normal cells, c-Myc expression is tightly controlled to maintain homeostasis, through transcriptional, translational and post-translational mechanisms (Lang *et al*., 1988, Vervoorts *et al*., 2006). One post-translational modification is the phosphorylation at different amino acids (Sears *et al*., 2000). When c-Myc is phosphorylated at serine 62 (S62) by mitogen-activated protein (MAP) kinase, its cytoplasmic levels are stabilised (Alvarez *et al*., 1991, Lutterbach and Hann, 1994). This phosphorylation will however go on to allow for a second phosphorylation at threonine 58 (T58) by glycogen synthase kinase a (GSKa) (Yeh *et al*., 2004, Arnold and Sears, 2006, Sears *et al*., 2000, Lutterbach and Hann, 1994). T58 phosphorylation can lead to c-Myc degradation as it permits dephosphorylation at S62 by PR61α (also known as B56a) subunit of protein phosphatase 2A (PP2A) (Arnold and Sears, 2006). This dephosphorylation event causes the ubiquitination of c-Myc, which will ultimately target it for proteasomal degradation, reducing c-Myc levels in the cell (Sears *et al*., 2000). Recently, POPDC1 has been shown to interact with c-Myc in cancer models by affecting the phosphorylation status of c-Myc

by interacting with PR61α and c-Myc to help degrade c-Myc (Parang *et al*., 2016). This was discovered after finding that patients with ulcerative colitis often had hypermethylated *POPDC1* causing lower expression levels of *POPDC1* and conversely elevated c-Myc protein levels (Parang *et al*., 2016, Williams *et al*., 2011).

1.2.5 Clinical relevance of POPDC genes

Recently, patients have been discovered with mutations in the POPDC genes and they suffer from heart and skeletal muscle disease (Schindler *et al*., 2016b, De Ridder *et al*., 2019, Rinné *et al*., 2020, Vissing *et al*., 2019, Beecher *et al*., 2021, Indrawati *et al*., 2020) (Table 1). Patients with mutations in *POPDC1* often develop AV-block and limb-girdle muscular dystrophy (LGMD) (Schindler *et al*., 2016b, De Ridder *et al*., 2019, Indrawati *et al*., 2020). In line with the high expression of *POPDC2* in the heart, patients with *POPDC2* mutations show a more severe third-degree AV-block, but no observable muscular phenotypes (Rinné *et al*., 2020). Patients with mutations in *POPDC3* display LGMD, but no observable cardiac defects have been uncovered, which again is in line with its expression pattern (Vissing *et al*., 2019). It has been shown that patients with mutations in *POPDC1* display a mislocalisation of both mutated POPDC1 and POPDC2 protein, however, mutations in POPDC3 did not affect the membrane localisation of the other isoforms (Schindler *et al*., 2016b, De Ridder *et al*., 2019, Vissing *et al*., 2019). Localisation of POPDC3 has not been studied, which is mainly due to the lack of suitable antibodies. These data suggest that the different isoforms can cause overlapping but isoform-specific pathologies.

In-depth studies of a zebrafish model carrying the homologous mutation found in patients (*popdc1* ^{S191F}) revealed that in the homozygous mutant, skeletal muscle displays aberrations in myotendinous junction formation (Schindler *et al*., 2016b, Vissing *et al*., 2019, Kirchmaier *et al*., 2012), which is a structure important for force transmission between muscle cells in adjacent muscle segments. Patients carrying mutations in *POPDC1* and *POPDC3* display high serum creatine kinase levels, suggesting that the sarcolemma might be damaged. Indeed, the muscle biopsy of an older patient

carrying the *POPDC1*^{S201F} mutation displayed membrane discontinuities (Schindler *et al*., 2016b). Moreover, the interaction of POPDC1 with dysferlin (Schindler *et al* 2016b) and annexin 5 (Holt *et al*., 2020) have been reported and both proteins have previously been implicated in membrane repair of skeletal muscle. Interestingly, there is also evidence that membrane repair in other cell types requires an increase in cAMP (Togo, 2019). Thus, POPDC1 could be acting through cAMP to modulate membrane repair, but this will need to be studied further to be confirmed.

POPDC1 variants associated with Tetralogy of Fallot (TOF) have also been reported (Shi *et al*., 2020, Shi *et al*., 2019). TOF is a congenital heart disease affecting ventricular septation, right ventricular hypertrophy, positioning and stenosis of the aorta and pulmonary artery and right ventricular hypertrophy (Morgenthau and Frishman, 2018, Apitz *et al*., 2009). Some single nucleotide polymorphisms of *POPDC1* in TOF patients caused downregulation of *POPDC1* and this was often accompanied by a decreased expression of SHF genes (Shi *et al*., 2020, Shi *et al*., 2019). Zebrafish *popdc1* morphants displayed a narrowing of the outflow tract, which could be partially rescued by injection of *nkx2.5* mRNA, which Popdc1 was shown to regulate (Shi *et al*., 2020). These results suggest that downregulation of *popdc1* may be associated with right ventricular outflow tract stenosis in non-syndromic TOF patients, as it can affect the development of the ventricular outflow tract in zebrafish (Shi *et al*., 2020).

Table 1 Cardiac and skeletal muscle phenotypes in patients with mutations in the POPDC proteins

Gene	Mutation	Heart Phenotype	Skeletal Muscle Phenotype	Reference
POPDC1	p.S201F	2nd-degree AV-block	LGMDR25	(Schindler *et al.* 2016b)
	c.1A>G	1st degree AV-block	LGMDR25	(De Ridder *et al.* 2019)
	p.V217-L272del	1st/2nd-degree heart block	LGMDR25	(De Ridder *et al.* 2019)
	p.R88X	1st-degree AV-block	LGMDR25	(De Ridder *et al.* 2019)
	p.Q153X	1st-degree AV-block and cardiomyopathy	LMGDR25	(Indrawati *et al.* 2020)
	p.S263X	1st-degree AV-block	LGMDR25	(Beecher *et al.* 2021)
	p.R129W	Tetralogy of Fallot	none reported	(Shi *et al.* 2019)
POPDC2	p.W188X	3rd-degree AV-block	none reported	(Rinne *et al.* 2020)
POPDC3	p.L155H	none reported	LGMDR26	(Vissing *et al.* 2019)
	p.L217F	none reported	LGMDR26	(Vissing *et al.* 2019)
	p.R261Q	none reported	LGMDR26	(Vissing *et al.* 2019)

1.2.6 Animal models carrying mutations in POPDC genes

Mutant mice have been developed to ablate *Popdc1* and *Popdc2,* these mice develop a stress-induced sinus node bradycardia, which develops in an age-dependent manner (Froese *et al*., 2012). In double knockouts, there is also the presence of atrial fibrillation, ventricular tachycardia and AV block, as this is a more severe phenotype it infers that there is some redundancy between POPDC1 and POPDC2 (Simrick *et al*., 2012, Simrick *et al*., 2013). Morphological changes are also seen in these mice such as loss of cellular extensions in nodal myocytes and loss of nodal myocytes in the SAN tail (Froese *et al*., 2012, Jianyi *et al*., 2001). Cardiac arrhythmias are also seen in zebrafish *popdc2* morphants and the *popdc1*^{S191F} mutant and both mutants develop an AV block (Schindler *et al*., 2016b, Kirchmaier *et al*., 2012). On top of differences seen in the hearts of these animal models, there is also some skeletal muscle pathologies. Zebrafish *popdc2* morphants display aberrant myotomal segment boundaries and a malformed tail (Kirchmaier *et al*., 2012). In the mouse, loss of *Popdc1* causes a retarded regenerative capacity in their hind limb musculature after cardiotoxin injection. While wild type animals are able to fully recover, the *Popdc1* null mutants have small and immature myotubes and overall display retarded regeneration (Andrée *et al*., 2002a). More recently, animal models have been developed to mimic mutations seen in human patients such as the *popdc*^{S191F} zebrafish, mimicking the *POPDC1*^{S201F} mutation discovered in patients, which display muscular dystrophy and cardiac arrhythmia (Schindler *et al*., 2016b) as well as the POPDC2^{W188X} mouse to model the same mutation in patients, which display cardiac arrhythmia (Rinné *et al*., 2020).

1.3 Hypothesis

POPDC1 is strongly expressed in the heart and skeletal muscle of all vertebrates. An association of POPDC1 in the mouse with skeletal muscle regeneration has been previously established. The zebrafish displays heart regeneration after injury and therefore provides an excellent opportunity to study whether heart regeneration is affected in the *popdc1* null mutant. A *popdc1* null mutant has

been created but its phenotype has not been characterised. I expect that the mutant heart might show some morphological and molecular abnormalities, which I want to characterize. Subjecting *popdc1* mutants to cardiac injury might display an increased regenerative response. This hypothesis is mainly based on the fact that POPDC1 has been found to limit c-Myc levels in cells and act as a tumor suppressor. It is also currently not known whether other members of the POPDC gene family interact with c-Myc and are similarly involved in cell cycle control.

1.4 Aims

In this project I had the following aims:

- To confirm the interaction of Popdc1 and c-Myc in cell lines and to see if this interaction could also be demonstrated in the heart.
- To characterise the morphology of the *popdc1* null mutant heart in zebrafish.
- To use the cryoinjury model to assess whether *popdc1* null mutants display normal heart regeneration.
- If regeneration is affected in the *popdc1* null mutant, I plan to further investigate the dynamics of heart regeneration to uncover the role of Popdc1 in this process.

2. Materials and Methods

Unless otherwise stated chemicals for this project were obtained from Sigma Aldrich.

2.1 Plasmid Preparation

2.1.1 Transformation of competent Escherichia coli bacterial cells

1µl of purified plasmid DNA (Table 2) was added to 100 µl XL1 blue competent cells and incubated on ice for 30 minutes to allow cells time to uptake plasmid DNA. Cells were heat-shocked at 42°C for 45 seconds and then incubated on ice for one minute. 400µl of lysogeny broth (LB) (1% (w/v) tryptone, 0.5% (w/v) yeast extract, 1% (w/v) NaCl) medium was added and cells were incubated in an Eppendorf orbital shaker at 100 revolutions per minute (rpm) at 37°C for 1 hour, to allow the bacteria to express the antibiotic resistance gene. 30µl of bacteria was then plated on an agar plate containing the appropriate antibiotic (either 100µg/ml ampicillin or 50µg/ml kanamycin were used for all plasmid preparations) for the selection of transformants and incubated at 37°C overnight, with the plates positioned upside down to prevent condensation forming on the lid, which could flush the colonies.

Table 2 Plasmids used for transfection of Cos7 cells

Plasmid Name	Tag	Antibiotic resistance	Vector	Source
PPP2R5A (PR61a)	V5	Ampicillin	pcDNA 3.1/V5N	Williams Lab
c-Myc	HA	Ampicillin	pCGN	Williams Lab
Popdc1 [WT]	YFP	Kanamycin	pEYFP-N1	R. Schindler (Brand lab)
Popdc2 [WT]	YFP	Kanamycin	pEYFP-N1	R. Schindler (Brand lab)
Popdc3 [WT]	YFP	Kanamycin	pEYFP-N1	R. Schindler (Brand lab)
pEYFP-N1	YFP	Kanamycin	pEYFP-N1	R. Schindler (Brand lab)
pCS2+MT	N/A	Ampicillin	pCS2+MT	R. Schindler (Brand lab)
Popdc1 [WT]	myc	Ampicillin	pCS2+MT	B. Andree/J. Kuthz (Brand lab)
Popdc1 [Δ116]	myc	Ampicillin	pCS2+MT	R. Schindler (Brand lab)
Popdc1 [Δ127]	myc	Ampicillin	pCS2+MT	R. Schindler (Brand lab)

2.1.2 Purification of plasmid DNA

To obtain large amounts of purified DNA the QIAGEN® Plasmid Midi Kit (#12145) was used according to the manufacturer's instructions. A transformed bacterial colony was picked and used to inoculate

a 3ml starter culture with the appropriate antibiotic added, this was shaken vigorously for 8 hours at 37°C. 100ml of fresh LB media with the appropriate antibiotic added was then inoculated with 1ml of the starter culture and incubated overnight in an orbital shaker at 37°C. The shaker was set to 300rpm to allow for aeration of the bacteria, encouraging growth. The bacteria were then harvested by centrifugation at 1500 x g for 30 minutes at 4°C and resuspended immediately in 4ml buffer P1. After 5 minutes the cells were lysed by adding P2 buffer and incubating for a further 5 minutes. 4ml of pre-cooled P3 buffer was added to the lysate and following a 15-minute incubation, the suspension was centrifuged twice for 30 minutes at 25,000 x g at 4°C. A QIAGEN-tip column was equilibrated with 4ml buffer QBT before the supernatant containing the plasmid DNA was added to the column where it will bind to the resin. The column was washed twice with 10ml of buffer QC before the DNA was eluted with 5ml of buffer QF into a glass centrifugation tube. The plasmid was precipitated using 3.5ml of isopropanol and mixed well before being centrifuged for 30 minutes at 25,000 x g to form a pellet. The supernatant was discarded and the DNA pellet was washed twice in 75% ethanol. The pellet was then allowed to air-dry for 10 minutes to remove all traces of ethanol. The DNA was resuspended in 50µl of TE buffer (10mM Tris-HCL, pH8.0, 1mM EDTA). The amount of DNA was quantified using a Nanodrop spectrophotometer.

2.2 Cell culture

Cos7 cells (Sigma-Aldrich, USA, #87021302) were cultured in Dulbecco's modified Eagle's Medium (DMEM) (Sigma Aldrich, USA, #91031101) with 10% (v/v) foetal calf serum (FCS) (Gibco, 26140-079) and 1% (v/v) L-glutamine (Sigma Aldrich, G7513) at 37°C with 5% CO_2 in a humidified cell culture incubator. All cell culture procedures were undertaken under sterile conditions in a laminar flow hood.

2.2.1 Passage of cells

Cells were passaged by rinsing the plate with phosphate-buffered saline (PBS) (137 mM NaCl, 2.7 mM KCl, 10 mM Na_2HPO_4-$2H_2O$ and 1.8 mM KH_2PO_4 adjusted to 1l with H_2O) and then incubating with

trypsin-EDTA solution (Sigma Aldrich, T4174) for 5 minutes to allow the cells to detach. The detached cells were centrifuged for 5 minutes at 500 x g and resuspended in fresh DMEM before plating.

2.2.2 Transfection of cells

Cos7 cells were transfected using midi-preparation purified plasmid DNA (2.1 Plasmid Preparation). Cells were split one day before transfection and were plated to aim for 90% confluency which translated to 3 million cells per 10cm dish. Lipofectamine™ 2000 (Invitrogen, USA, #11668) was used to transfect the cells using 1µl of lipofectamine per 0.4µg DNA; according to the manufacturer's protocol. The appropriate amounts of plasmid DNA and Lipofectamine™ 2000 were diluted in DMEM in separate tubes and incubated for 5 minutes at room temperature. The DNA and Lipofectamine™ 2000 dilutions were mixed and incubated for a further 20 minutes at room temperature to allow for DNA-lipofectamine complexes to form. The mixture was then added dropwise to the cells. Cells were harvested 24 hours after transfection to allow the cells to express sufficient amounts of the transfected constructs.

2.2.3 Cells Grown in Conditioned Media

Cos7 cells were used to generate conditioned media as depicted by the schematic in Figure 8. Cos7 cells were transfected with a YFP-tagged Popdc1 plasmid cDNA or a vector expressing only yellow fluorescent protein (YFP) and left for 6 hours, cells were then sorted for YFP positivity using a flow cytometer (BD FACSAria™ Fusion) (2.19.2 Cell Sorting). YFP-positive cells were plated and fresh media applied. This was done to enrich for transfected cells. After 24 hours, culture medium was taken from the transfected cells, filtered using a 40µm filter and then mixed with an equal amount of fresh media and transferred onto a plate with non-transfected Cos7 cells. Cells were incubated for 24 hours before being fixed for staining or cell number determination.

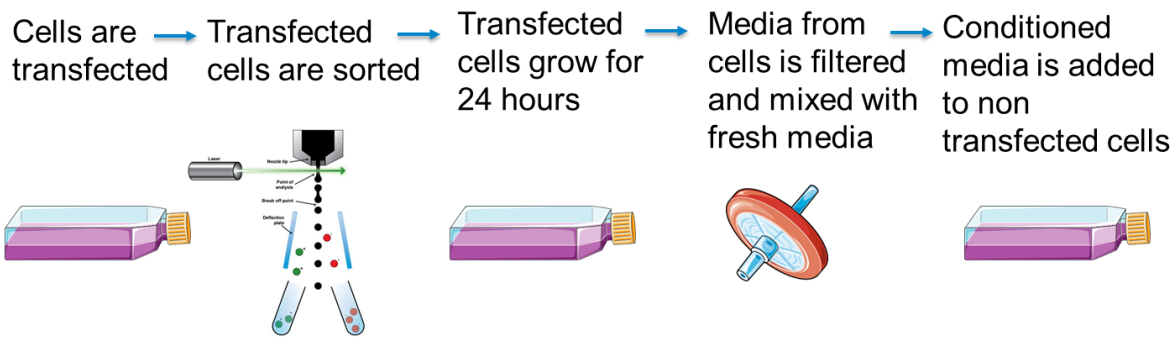

Figure 8 Conditioned Media Protocol. Cells were transfected with a plasmid containing a YFP tag. Cells were left for 6 hours before being sorted based on the YFP expression using a BD FACSAria™ Fusion flow cytometer. YFP-positive cells were then plated and left to grow for 24 hours. Media from these cells was filtered and mixed at a 50:50 ratio with fresh media. The conditioned media was added to non-transfected cells, which were left to grow for 24 hours before being fixed for analysis. Images for this schematic were taken from Servier Medical Art (https://smart.servier.com/).

2.3 Cell lysates

2.3.1 Generation of cell lysates

Cos7 cells were harvested 24 hours after transfection (2.2.2 Transfection), washed three times with ice-cold PBS and then incubated for 20 minutes at 4°C in 700µl of lysis buffer (50mM Tris, pH 8.0, 150mM NaCl, 2mM EDTA, pH 8.0, 1% (v/v) Triton X-100, 0.25% (w/v) gelatine, and 1 protease inhibitors tablet per 10 ml (Roche, Switzerland)). Cell lysates were kept on ice going forward to prevent the degradation of the proteins. Cells were scraped from the culture dishes using a cell scraper (rubber policeman) and then transferred into a 1.5ml Eppendorf tube. To further sheer the cells, they were passed several times through a 23G needle and then sonicated on ice three times for 15 seconds at 4°C at 2mW, with time in between each round to allow the cells to cool down again. Samples were centrifuged to remove cell debris at 16,000 x g for 30 minutes and the supernatant was pipetted in a fresh tube and stored frozen at -20°C.

2.3.2 Determining protein concentration of cell lysates

Protein concentrations were determined using a Bio-Rad DC™ microplate assay, which is based on the Lowry method. In this method proteins react with alkaline copper tartrate (solution A) then are reduced by Folin (solution B), resulting in a blue coloured product with a maximum absorbance of

750nm. The colour intensity is proportional to the amount of protein in the sample. To quantify the amount of protein in the test samples, a standard curve was generated using 0-1.2µg/µl of bovine serum albumin (BSA). 5µl of the sample, diluted 1:10 in lysis buffer was added in triplicate to a 96 well plate. 25µl of a mixture of reagent A (Bio-Rad, #500-0113) and S (Bio-Rad, #500-0115) (1ml of reagent A per 20µl of reagent S) were added and then 200µl of Reagent B (Bio-Rad, #500-0114). The plates were incubated in the dark for 15 minutes to allow the colour to fully develop and a plate reader was used to determine the absorbance at 750nm. SoftMax Pro® software calculated averages for the protein standards and they were plotted against the known protein concentrations, generating a standard curve using linear regression. The software then matches the average of the sample absorbance values to the standard curve to estimate the protein concentration, this value was then multiplied by 10 to account for the dilution.

2.4 Co-immunoprecipitation

Co-immunoprecipitation (CoIP) experiments were undertaken on cells, which had been grown in ø 10 cm dishes and transfected (2.2.2 Transfection of cells) 24 hrs prior to cell lysates being produced (2.3 Cell lysates). 30µl of the lysate was taken as a whole-cell lysate (WCL) input control and 10µl of sodium dodecyl sulphate (SDS) sample buffer (4% (w/v) SDS, 10% (v/v) β-mercaptoethanol, 40% (v/v) glycerol), 250mM Tris-HC: (pH 6.8), 0.05% (w/v) bromphenol blue) was added. The remainder of the lysate was used to conduct the CoIP experiments using a Pierce c-Myc tag IP CoIP kit (Thermo Scientific, USA, #23620) as per the manufacturer's guidelines. Either anti- Green fluorescent protein (GFP) agarose (MBL, USA, #D153-8) or anti-Myc tag agarose (MBL, USA, #M047-8) was added to the lysates and they were incubated overnight at 4°C in spin columns on a wheel rotator, this allowed the antibodies to bind to antigens in the cell lysates. Samples were spun in a centrifuge at full speed for 10 seconds to remove unbound lysates and were then washed 5 times in Tris-buffered saline solution (from the kit, #28376) and then non-reducing sample buffer (from the kit, #1859594) was added. The samples were boiled for 5 minutes at 96°C and samples were collected via centrifugation of the spin

column into a collection tube. 3µl of β-mercaptoethanol was added to the sample to reduce the amount of antibody heavy and light chains in the sample. The WCL input control was also boiled for 5 minutes at 96°C. The samples were then size separated using SDS gel electrophoresis (2.5 SDS-PAGE) and western blot analysis (2.6 Western Blot).

2.5 SDS-PAGE

2.5.1 Gel preparation

For SDS-polyacrylamide gel electrophoresis (PAGE) the mini-PROTEAN® Bio-Rad system was used. Glass plates were cleaned with 70% ethanol to remove any debris and the plates were positioned in the gel cast stand. The 10% SDS-PAGE separation gel (4ml H_2O, 3.3ml 30% (w/v) acrylamide solution, 2.5ml 1.5M Tris-Cl pH8.8, 100µl 10% (w/v) SDS, 100µl 10% (w/v) APS and 4µl TEMED) was made and poured immediately in between the glass plates. To ensure the top of the gel was even, it was overlaid with water. Once the gel had polymerised the water was tipped off and the stacking gel (1.4ml H_2O, 330µl 30% (w/v) acrylamide solution (Bio-Rad, 1610154), 250µl 1.0M Tris-Cl pH6.8, 20µl 10% (w/v) SDS, 20µl 10% (w/v) APS and 2µl TEMED) was poured over the separation gel and a gel comb was inserted. Once the stacking gel had polymerised it was removed from the gel cast stand, rinsed with water and wrapped in a wet paper towel and stored in a plastic bag until it was used, to prevent it from drying out.

2.5.2 Gel electrophoresis

The gel was placed into the gel electrophoresis chamber filled with running buffer (25mM Tris-Cl, pH8.0, 192mM glycine, 1% (w/v) SDS). The comb was removed and the wells were flushed with running buffer to remove any non-polymerised gel. Protein samples were loaded onto the gel along with a molecular weight marker (PageRuler™ Prestained Protein Ladder, Thermo Scientific, #26616) and electrophoresed at 100V until the bromophenol blue dye in the sample buffer had reached the bottom of the gel. The separation gel was removed from the glass plates and separated from the stacking gel for further analysis by western blotting (2.6 Western Blot).

2.6 Western Blot

2.6.1 Transfer to nitrocellulose membrane

Samples were size-separated using a 10% SDS-PAGE (2.5 SDS-PAGE). Gels were incubated in blotting buffer (10% methanol, 25mM Tris-Cl, pH8.5, 150mM glycine) before being electroblotted onto a nitrocellulose membrane (BioTrace^{TM} NT, Pall Corporations, USA, #66485). For the protein transfer, 3 pieces of Whatman filter paper were placed onto the blotter, followed by the separation gel, the nitrocellulose membrane and another 3 pieces of filter paper. The proteins were electrophoretically transferred to the nitrocellulose membrane at 70mA/gel for 1 hour.

2.6.2 Incubation with antibodies

Membranes were washed in Tris-buffered saline with Tween (TBST) (50 mM Tris-HCl, pH 7.4, 150mM NaCl, 0.1% (v/v) Tween-20) and blocked in blocking solution (5% milk powder (w/v) in TBST) for 1 hour. Membranes were then incubated overnight at 4^{o}C gently rotating with the appropriate antibody (Table 3). The membranes were washed three times for 10 minutes with TBST to remove any unbound antibody, before being incubated with the appropriate secondary antibody (Table 3) at room temperature gently rotating for 1-2 hours. Membranes were washed again 3 times in TBST for 10 minutes. Horseradish peroxidase (HRP) substrate (Millipore, USA, #WBKLS0500) was prepared by mixing the components 1:1 and this was then added to the membrane and incubated for 5 minutes. The excess reagent was removed and was placed into the syngene g:box gel imager to capture the light emission from the membrane.

Table 3 Antibodies used in western blotting and peptide binding arrays.

Antibody	Manufacturer	Catalogue number	Dilution
Anti V5- Tag	Abcam	Ab2767	1:5000
Anti HA-tag	Covance	16B12	1:1000
Anti GFP- tag	Abcam	Ab290	1:1000
Anti myc- tag	Abcam	Ab32	1:1000
HRP- conjugated anti Mouse	Vector Laboratories	PI-2000	1:1000
HRP- conjugated anti Rabbit	Vector Laboratories	PI-1000	1:1000

2.7 Peptide binding array

Peptide binding arrays were donated by Professor George Baillie (University of Glasgow). A 25-mer library of overlapping peptides of POPDC1, each shifted by five amino acids at a time, were produced sequentially to increase the reliability of the screening. Immobilised spots containing the peptide sequences were directly synthesised on Whatman 50 Cellulose membranes and used as peptide arrays. The immobilised spots on the filter correspond to POPDC1 residues as depicted in Figure 9. Arrays were blocked in blocking solution before cell lysates (2.3 Cell lysates) were added at a concentration of 3µg/µl and incubated rocking overnight at 4^{o}C. The arrays were washed 3 times in TBST for 15 minutes before being incubated overnight with the appropriate primary antibody (Table 3) rocking at 4^{o}C. The arrays were washed 3 times in TBST for 15 minutes and incubated at room temperature for one hour with the appropriate secondary antibody (Table 3). Arrays were washed again 3 times in TBST for 10 minutes. Horseradish peroxidase substrate (Millipore, USA, #WBKLS0500) was prepared by mixing the components 1:1 and this was then added to the membrane and incubated for 5 minutes. The excess reagent was removed and was placed into the syngene g:box gel imager to capture the exposure from the membrane. If the protein in the lysate can bind to the peptides on the array then a dot becomes visible. The dots with the same sequence are present in duplicates and had 15 overlapping residues with the following peptide. The peptide array allowed us to make predictions on which residues in POPDC1 mediate interaction with the protein of interest.

	1	**2**	**3**	**4**	**5**	**6**	**7**	**8**	**9**	**10**	**11**	**12**	**13**	**14**	**15**	**16**	**17**	**18**	**19**	**20**	**21**	**22**	**23**	
	1-25	5-30	10-35	15-40	20-45	25-50	30-55	35-60	40-65	45-70	50-75	55-80	60-85	65-90	70-95	75-100	80-105	85-110	90-115	95-120	100-125	105-130	110-135	
	24	**25**	**26**	**27**	**28**	**29**	**30**	**31**	**32**	**33**	**34**	**35**	**36**	**37**	**38**	**39**	**40**	**41**	**42**	**43**	**44**	**45**	**46**	
	115-140	120-145	125-150	130-155	135-160	140-165	145-170	150-175	155-180	160-185	165-190	170-195	175-200	180-205	185-210	190-215	195-220	200-225	205-230	210-235	215-240	220-245	225-250	
	47	**48**	**49**	**50**	**51**	**52**	**53**	**54**	**55**	**56**	**57**	**58**	**59**	**60**	**61**	**62**	**63**	**64**	**65**	**66**	**67**	**68**	**69**	
	230-255	235-260	240-265	245-270	250-275	255-280	260-285	265-290	270-295	275-300	280-305	285-310	290-315	295-320	300-325	305-330	310-335	315-340	320-345	325-350	330-355	335-360	340-365	

Figure 9 Schematic to show which residues the dots on the Popdc1 peptide-binding array correspond to. Numbers in bold represent the dot number and the line below represents what residues they correspond to.

2.8 Zebrafish lines and procedures

Fish were cared for in accordance with the guidelines home office.

2.8.1 Zebrafish husbandry

All procedures were performed in line with the Animals (scientific procedures) Act 1986 under the project licences PPL:70/8743 and PP3818670. Zebrafish were raised in mixed-sex tanks, at a maximum density of 10 fish per litre, with a light cycle of 14 hours light, 10 hours dark. Water temperature was 27-29^{o}C with a pH of (7.4) on a diet of Gemma Micro for zebrafish (Skretting). Fish were maintained by the Central Biomedical Services Animal facility staff at Imperial College London. Fish lines used can be seen in Table 4. Tg(cmlc2:mermaidAB) zebrafish were mainly used in my experiments as they had a GFP reporter, which has been used for optical recording of membrane voltage changes (Tsutsui *et al*. 2010), under the cmlc2 (or myl7) promotor, which labelled cardiomyocytes. This line was also crossed with the popdc1-M6 line to create a *popdc1* null line that also expressed GFP in their cardiomyocytes.

Table 4 Details of zebrafish lines used in the study

Name	Component Identified	Referred to in this document
AB-KCL	N/A	wild type (-)
Popdc1-M6	N/A	*popdc1* null (-)
Tg(cmlc2:mermaidAB)	Cardiomyocytes	wild type
Tg(Popdc1-M6/cmlc2:mermaidAB)	Cardiomyocytes	*popdc1* null

2.8.2 Generation of the *popdc1* null mutant

The *popdc1* null mutants were generated in the Brand lab by Dr Kar Lai Poon and Mrs Ursula Herbort-Brand. They were created using TALENS by targeting the first exon of *popdc1* where there was a single deletion which resulted in a frameshift that caused a premature stop codon (Brand Lab, Unpublished). This resulted in a truncated protein that was just 39 amino acids long and would not include the transmembrane domains or the Popeye domain. Mrs Ursula Herbort-Brand regularly performed genotyping on tanks of young zebrafish to confirm their genotype. Briefly, this involved the extraction and amplification of the zebrafish DNA after a caudal fin clip. The following primers were used for amplification: forward “gttatatttcacgccactacgtt”, reverse “taccctataaacacaagcggat”. The amplification product was then digested by BamHI. Wild types would have two bands at 314bp and 205bp,

heterozygous mutants had three bands 519bp, 314bp and 205bp and homozygous mutants would have one band at 517bp (Figure 10). This is because the introduction of the base pair deletion disrupts and BamHI restriction site.

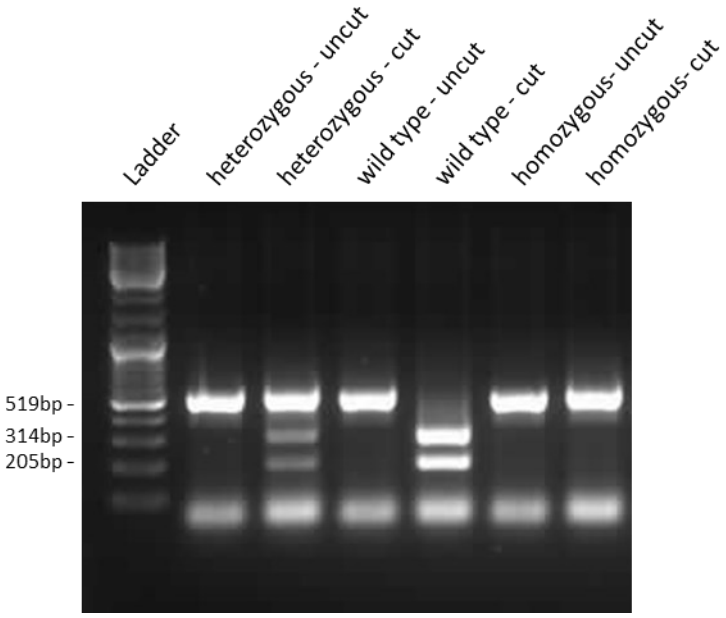

Figure 10 Agarose gel showing the genotyping of *popdc1* null mutant. BamHI digestion of genetic material from wild type, *popdc1* null heterozygous and *popdc1* null homozygous zebrafish show altered digestion because of the disruption of the BamHI restriction site.

2.8.3 Zebrafish mating and maintenance of stock

From 3 months of age onwards, zebrafish were used for breeding to maintain stocks. Matings were set up in the afternoon by placing males and females to a maximum of 5 fish in 500ml mating tanks filled with system water. These tanks had a breeding base insert, which allowed eggs to fall to the bottom but restricted the adult fish, this prevented the eggs from being consumed by the fish after laying. Mating was induced by turning on the light in the morning. After mating, the fish were returned to their stock tanks in the system and eggs were removed by straining the water of the mating tank through a fine sieve. More system water was run over the eggs in the sieve to help clean them and remove any debris. The collected eggs were moved to Petri dishes filled with E3 media (5mM NaCl, 0.17mM KCl, 0.33mM $CaCl_2$, 0.33mM $MgSO_4$) and placed in a 28^{o}C incubator. If fish were intended to

be moved to the main aquarium system the embryos still in their chorion were bleached to clean them at 6hpf. Fish were put into a 0.001% bleach solution (Fisher Scientific, S/5040/PB17) in E3 media for 10 minutes and were then washed 3 times for 5 minutes in E3 media before being moved to a fresh petri dish with pronase (10mg/ml) added to aid removal of the chorion, since bleaching can toughen it. Unfertilised eggs were removed using a plastic pasture pipette at 24hpf. At 48 hours, if necessary, eggs were screened for fluorescence under a stereomicroscope, and those not showing a fluorescent signal were removed. E3 media was changed at least every 48 hours for embryos. At 5dpf fry were moved into the system.

2.8.4 Cryoinjury

Cryoinjuries were performed as described by Gonzalez-Rosa and Mercader (González-Rosa and Mercader, 2012). Fish were anaesthetised by placing them in a 0.032% (w/v) tricaine solution until they were immobilised. Fish were then placed ventral side up on a system water-soaked piece of foam under a dissection microscope, scales were removed and the skin was pulled tort. Scissors were used to make an incision in the body wall. The flanks of the fish were lightly pressed to expose the ventricle which was then dried with a tissue before a 0.3mm copper probe, precooled in liquid nitrogen, was applied to the ventricle for approximately 15 seconds (Figure 11). The fish were then moved to a tank containing 500ml of system water and were aided in their reanimation by gently pipetting system water towards them to aid water motion over the gills. Sham-operated animals were subjected to the same as the above except the probe had not been cooled. Hearts were dissected out of fish at different time intervals.

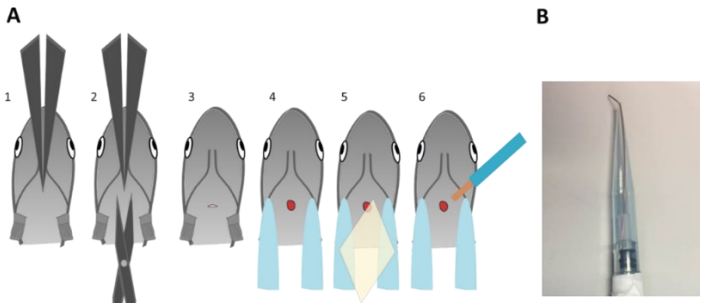

Figure 11 Cryoinjury in the zebrafish (**A**) Schematic of the cryoinjury protocol in zebrafish. Adapted from González-Rosa and Mercader (2012) (**B**) Image of the Cryoinjury probe used in the Brand Lab.

2.8.5 Isolation of zebrafish ventricular cells for single-cell analysis

Zebrafish ventricles were isolated from 3-6-month-old fish and placed in heparin dissection buffer (1M KCl, 2U/ml Heparin in PBS to prevent blood clots. Ventricles were cut into pieces and spun down for 60 seconds at 1000 x g in a centrifuge cooled to 4^{o}C, this was done to remove any remaining blood cells. The supernatant was removed and the ventricles were resuspended in PBS and the washing and centrifugation were repeated. A Pierce™ Primary Cardiomyocyte Isolation Kit (Thermo scientific, 88281) was used to isolate the cardiomyocytes. 100µl of enzyme A and 5µl of enzyme B was added to each heart and the tissue was incubated in a thermomixer for 50 minutes at 30^{o}C and 300rpm. The samples were triturated every 5 minutes using a 100µl Eppendorf pipette. 1ml of HBSS was added to the samples and the samples were centrifuged for 3 minutes at 800 x g. The supernatant was put into a separate microcentrifuge tube and centrifuged again to collect any cells which may have been missed. The pellets from both spin downs were resuspended in 500µl of HBSS+ (HBSS with 0.25% BSA (w/v) and 10mM HEPES).

2.8.5.1 Validation of single ventricular cells

Cells isolated for single-cell analysis were validated, initially by running through a cell counter which was able to give readings on cell numbers, viability and size. The machine does this by mixing cells entering the machine with trypan blue and taking images of the cells passing through, this can then give an estimation of size but also viability and number. Once the validity of isolation was achieved cells could go on for further use in experiments.

2.8.5.2 Isolation of zebrafish ventricular cardiomyocytes for size analysis

Zebrafish ventricular cardiomyocytes were isolated as previously reported (Sander *et al*., 2013). Ventricles were removed from 3-6-month-old fish and placed briefly into heparin buffer (10 U/ml Heparin and 100 U/ml penicillin-streptomycin in PBS). Three ventricles from each genotype were pooled and moved to perfusion buffer (10mM HEPES, 30mM taurine, 5.5mM glucose and 10mM BDM in PBS). Once all ventricles had been excised they were moved to digestion buffer (perfusion buffer plus 12.5µM $CaCl_2$ and 5ug/ml of both collagenase II (Gibco, 17101-015) and IV (Gibco, 17104-019)) and agitated in a thermomixer at 800 rpm at 32^{o}C for 2 hours. Digested cells were spun down in a precooled centrifuge at 250 x g for 5 minutes and the supernatant was discarded. The digested cells were then taken through successive stop buffers (perfusion buffer with 5% (V/V) FCS and with increasing $CaCl_2$; 12µM, 62µM, 112µM, 212µM 500µM and 1000µM), centrifuging between each buffer and discarding the supernatant. Finally, the cells were resuspended in sort buffer (1mM EDTA, 25mM HEPES, 1% FCS in PBS before being used for flow cytometry analysis (2.19.1 ImageStream flow cytometry).

2.9 Mouse lines and care of mice

All procedures were performed in line with the Animals (scientific procedures) Act 1986 under the project licence P2960EB2F. All mouse cells and tissue were collected by and given to me by either Dr Roland Schindler, Dr Navneet Bhogal, Mrs Ursula Herbort -Brand or Dr Laura Fedele. Mice used in this study can be seen in Table 5.

Table 5 Details of mouse lines used in this study

Name	Name used in text	Source
Popdc1 -/-	Popdc1 null	(Andrée *et al*., 2002a, Froese *et al*., 2012)
Popdc2 -/-	Popdc2 null	(Froese *et al*., 2012)
Popdc3 -/-	Popdc3 null	(Brand Lab, Unpublished)
Popdc1 -/- / Popdc2-/-	Popdc1/2 null	(Andrée *et al*., 2002a, Froese *et al*., 2012)
Wild type	Wild Type	Envigo: C57Bl/6J OlaHsd

2.9.1 Isolation of mouse ventricular cardiomyocytes

Isolation of mouse ventricular cardiomyocytes was performed by Dr Navneet Bhogal and excess cells were gifted to me for use in staining and microscopy. 3- 4-month-old mice were sacrificed by inhalation of 5% isoflurane followed by cervical dislocation. The heart was removed and placed on ice-cold Krebs-Henseleit solution (119mM NaCl, 4.7 KClmM, 0.94mM $MgSO_4$, 1mM $CaCl_2$, 1.2mM KH_2PO_4, 25mM $NaHCO_3$, and 11.5mM glucose (pH 7.4)). The aorta was cannulated and the cannula attached to the Langendorff system. The hearts were retrogradely perfused at 37°C with Krebs-Henseleit solution for 1 min. The perfusate was switched to low-Ca2+ solution (120mM NaCl, 5mM KCl, 5mM $MgSO_4$, 5mM Na pyruvate, 20mM glucose, 20mM taurine, 10mM HEPES, 5mM nitrilotriacetic acid and 35µM $CaCl_2$ (pH 6.96) for 4 min, followed by 1 min bacterial protease solution (3.6 mg of protease (Sigma, P8038-1G) in 10 ml of enzyme solution (120mM NaCl, 5mM KCl, 5mM MgSO4, 5mM Na pyruvate, 20mM glucose, 20mM taurine, and 10mM HEPES, 35µM $CaCl_2$ (pH 7.4)) and then by 4-5 min of collagenase V solution (30mg of collagenase (Sigma, C9263-1G) in 30 ml of enzyme solution). The hearts were then removed from the cannula, and the ventricles triturated in the enzyme solution (without enzymes). The solution was passed through a mesh to remove any undigested tissue.

2.10 Preparation of tissue for cryosections and cryostat sectioning

Dissected zebrafish or mouse tissue samples were washed in PBS before being fixed in 4% paraformaldehyde (PFA) at room temperature for 10 minutes or overnight at 4^{o}C. Samples were then washed 3 times for five minutes in PBS before being transferred to 10% (w/v) sucrose in PBS and incubated on ice until the tissue could no longer float; indicating that the solution had equilibrated with the water in the tissue. This was repeated for 20% (w/v) and 30% (w/v) sucrose in PBS. Tissue was then incubated on ice with PolyFreeze (Tissue Freezing Medium) (Polysciences, Inc., USA #19636) at a 1:1 ratio with 30% sucrose in PBS for at least 10 minutes followed by 100% Polyfreeze for at least 10 minutes. Tissue was then placed into a mould filled with PolyFreeze and these moulds were placed into 2-methylbutane which had been cooled with dry ice and stored at -80°C until use. The frozen

samples were then cut on a Leica XM 1850 cryostat and sections were mounted on to superfrost glass slides. Sections were airdried and if required stored at -80^{o}C until used. The sections were encircled with a PAP pen (Sigma-Aldrich, Z377821-1EA) to create a hydrophobic barrier which helped to keep the solutions on the sample and use smaller amounts of liquid.

2.11 Preparation of paraffin sections

2.11.1 Fixation of tissue

Zebrafish tissue samples were fixed in 10% formalin rocking at room temperature for an appropriate amount of time depending on their size. Fry and excised hearts were incubated for 10 minutes at room temperature while whole fish were incubated for 24 hours at room temperature. Samples were then washed with 3 quick washes in PBS and 3 five minute washes in PBS to remove excess fixative.

2.11.2 Embedding of tissue in paraffin

After fixation samples were taken through increasing percentages of ethanol in PBS (30, 50 and 70%), samples were left in each solution for at least 30 minutes, to dehydrate the sample and were then processed by a Tissue Tek® VIP® embedder into paraffin or by hand (Table 6). Samples were then embedded into moulds and the wax was allowed to cool. The blocks of paraffin were cut with a Leica RM 2255 microtome into 6µm sections and mounted on glass slides, where they were left overnight at 60^{o}C to dry. The sections were then stored at room temperature in a box to prevent dust accumulation and damage until further use.

Table 6 Schedule for paraffin embedding samples by hand.

Solution	Time	Temperature
96% Ethanol	3 hours	Room Temperature
96% Ethanol	16 hours	Room Temperature
Isopropanol	8 hours	Room Temperature
Isopropanol	16 hours	Room Temperature
n-Butanol	4 hours	60^{o}C
n-Butanol	4 hours	60^{o}C
n-Butanol : Paraffin	16 hours	60^{o}C
Paraffin	4 hours	60^{o}C
Paraffin	4 hours	60^{o}C
Paraffin	16 hours	60^{o}C

2.12 Immunostaining

2.12.1 Preparation of cells for immunostaining

Cells were seeded into cell culture dishes containing round glass coverslips which were 13mm in diameter by pipetting 100µm of cells in solution on the glass and using water tension to prevent the water bubble from overflowing. If required cells were transfected (2.2.2 Transfection of cells) using lipofectamine. Coverslips that would hold zebrafish cardiomyocytes (2.8.5 Isolation of zebrafish ventricular cells for single-cell analysis) were coated in poly-L-lysine, by placing the coverslips in poly-l-lysine for 10 minutes before washing thoroughly with water and then being allowed to air-dry for at least 2 hours. Coverslips that would hold mouse ventricular cardiomyocytes (2.9.1 Isolation of mouse ventricular cardiomyocytes) were coated in collagen overnight at 4^{o}C, excess collagen was removed and the coverslips allowed to air dry. Once the cells had adhered the cell culture dishes were flooded with media. Cover glasses with cells were removed at the required time point and moved to a humidified chamber for further processing. Humidified chambers were made from Petri dishes containing wet filter paper covered in a layer of parafilm to prevent the sample from drying out. Cells were fixed for 10 minutes using 4% PFA at room temperature and then washed 3 times for five minutes in PBS to remove excess fixative.

2.12.2 Antibody Incubation

Antibody incubation for immunostaining was performed on cells (2.12.1 Preparation of cells for immunostaining) or cryosections (2.10 Preparation of tissue for cryosections and cryostat sectioning). As antigens looked at in this study were localised intracellularly, PFA fixed cells or tissue needed to be permeabilised before antibody incubation to allow the antibodies to penetrate the membrane and to reach the antigen. Therefore, samples were blocked in blocking buffer (2% FCS or donkey serum, 1%BSA and 0.25% Triton X-100 in PBS for 1 hour at room temperature, the triton X-100 in this solution allowed for permeabilisation and the BSA and serum were to saturate any unspecific antibody binding sites. This was then changed for the appropriate primary antibody (Table 7) diluted in blocking buffer

and left overnight at 4^{o}C. Samples were then washed 3 times for five minutes in PBS and incubated with the appropriate secondary antibody (Table 7) diluted in blocking buffer at room temperature for one hour in the dark. Samples were washed 3 times for five minutes in PBS and sections had coverslips mounted using mowiol (Calbiochem, USA, #475904) containing 2µg/ml 4',6-Diamidino-2-Phenylindole (DAPI) (Calbiochem, USA, #268298) on to microscope slides. Samples were stored at 4^{o}C until they could be imaged. For co-staining, if antibodies were raised in different animals then both primary antibodies could be incubated at the same time. Similarly, both secondary antibodies could be incubated at the same time.

2.12.3 Double staining with primary antibodies raised in the same animal

In cases where the primary antibody was raised in the same animal, the binding site for the first primary antibody was saturated using highly concentrated Alexa fluor 555-conjugated Fab fragments (1:50 dilution) for 2 hours. After washing with PBS 3 times for five minutes the next primary antibody was added and incubated overnight at 4^{o}C and the antibody incubation protocol above could continue from the washes before the addition of the secondary antibody.

Table 7 Antibodies used for immunostaining

Antibody Name	Name used in text	Host Species	Manufacturer	Catalogue/identifier number	Dilution
anti-BVES	Popdc1	Rabbit	St John's Laboratory	STJ22848	1:50
anti-BVES	P1 atlas 18176	Rabbit	Atlas	HPA018176	1:50
Popdc2	Popdc2	Rabbit	Sigma Aldrich	HPA024255	1:50
c-Myc	Ab32072	Rabbit	Abcam	Ab32072	1:1000
Anti-rabbit Alexa fluor 488	n/a	Donkey	Invitrogen	A21206	1:1000
Anti- mouse Alexa fluor 488	n/a	Donkey	Invitrogen	A21202	1:1000
Anti- goat Alexa fluor 488	n/a	Donkey	Invitrogen	A11055	1:1000
Anti-rabbit Alexa fluor 633	n/a	Goat	Invitrogen	A21071	1:1000
Wheat germ agglutinin (WGA) tetramethylrhodamine conjugate	n/a	n/a	Invitogen	W849	1:200
Phospho histone 3	PH3	Rabbit	Merck	06-570	1:200
Mef2	Mef2	Rabbit	Abcam	Ab197070	1:50

2.13 Histology

2.13.1 AFOG staining

Zebrafish sections (2.11 Preparation of paraffin sections) were deparaffinised, rehydrated and fixed in Bouin's solution (Sigma, HT1032). Samples were washed in tap water and moved to 1% phosphomolybdic acid (Sigma-Aldrich HT153 diluted 1:10 in distilled H_2O), before being washed in distilled water. Samples were incubated in AFOG solution (Acid fuchsin orange G) (0.5% (w/v) aniline blue diammonium salt (Sigma, 415049), 1.5% (w/v) Acid Fuchsin (Sigma, F8129) and 1% (w/v) Orange G (VWR, 437252Q) in distilled water, pH 1.09) then rinsed in distilled water, dehydrated in 100% ethanol and incubated twice in xylene. See Table 8 for the timing and temperatures for each of these stages. Entellan (Merck, HX57327262) was added to the sections and they were overlaid with coverslips.

Table 8 Schedule for AFOG staining

Solution	Time	Temperature
Xylene	5 minutes	Room Temperature
Xylene	5 minutes	Room Temperature
96% Ethanol	3 minutes	Room Temperature
70% Ethanol	3 minutes	Room Temperature
50% Ethanol	3 minutes	Room Temperature
dH_2O	3 minutes	Room Temperature
Bouin's Solution	2 hours	60^oC
Bouin's Solution	1 hour	Room Temperature
Tap Water	30 minutes	Room Temperature
1% Phosphomolybdic Acid	4.5 minutes	Room Temperature
dH_2O	5 minutes	Room Temperature
AFOG Solution	4.5 minutes	Room Temperature
dH_2O	30 seconds	Room Temperature
50% Ethanol	30 seconds	Room Temperature
70% Ethanol	2 minutes	Room Temperature
96% Ethanol	2 minutes	Room Temperature
Xylene	5 minutes	Room Temperature
Xylene	5 minutes	Room Temperature

2.13.1 Haematoxylin and Eosin (H&E) staining

Zebrafish sections (2.11 Preparation of paraffin sections) were deparaffinised and rehydrated before being incubated with Harris haematoxylin (Sigma, HHS32-1) and then rinsed in tap water with a brief rinse in 1% ammonia water to brighten the haematoxylin stain. The slides were then incubated with eosin Y (Sigma, HT110232) modified with 3.2% Acetic acid and then washed in distilled water. Slides were then dehydrated and moved to xylene. See

Table 9 for the timings of each stage of H&E staining, all stages were conducted at room temperature. Entellan (Merck, HX57327262) was added to the sections and they were overlaid with coverslips.

Table 9 Schedule for H&E staining

Solution	Time
Xylene	3 minutes
Xylene	3 minutes
96% Ethanol	3 minutes
70% Ethanol	3 minutes
50% Ethanol	3 minutes
dH_2O	10 minutes
Harris Haematoxylin	8 minutes
Tap Water	2 minutes
1% Ammonia dH_2O	12-15 seconds
Tap Water	2 minutes
Modified Eosin Y	10 minutes
dH_2O	10 seconds
50% Ethanol	30 seconds
96% Ethanol	30 seconds
Isopropanol	30 seconds
Xylene	30 seconds

2.14 TUNEL staining

Cryosections (2.10 Preparation of tissue for cryosections and cryostat sectioning) were terminal deoxynucleotidyl transferase dUTP nick end labelling (TUNEL) stained according to the manufacture's guidelines (Merck, S7165). In brief, samples were allowed to equilibrate to room temperature for 30 minutes. Then samples were postfixed in an ethanol acetic acid mix at a ratio of 2:1 for 5 minutes at -20^{o}C followed by 2 five minutes washed in PBS. Samples were then incubated with an equilibration

buffer (Merck, 90416) for 10 seconds before incubating the samples in a hydration chamber for 1 hour at 37°C in TdT enzyme (Merck, 90418) in reaction buffer (Merck, 90417). Samples were then incubated in stop/wash buffer (Merck, 90419) for 10 minutes, washed in PBS 3 times for 1 minute each, and then incubated with the anti-TdT Rhodamine (Merck, 90429) in blocking buffer (Merck 90425) for 30 minutes at room temperature before being washed in PBS 2 times for two minutes and then overlaid with a coverslip using mowiol (Calbiochem, USA, #475904) containing 2µg/ml DAPI (Calbiochem, USA, #268298).

2.15 Imaging and image analysis

Fluorescent immunostained and TUNEL stained samples were imaged using ZEN black edition (Zeiss, Germany) using a Zeiss LSM-780 confocal microscope or a Zeiss Axio observer widefield microscope, which are provided by the Facility for Imaging by Light Microscopy at Imperial College London. For the confocal microscope, the argon laser was used for excitation of the respective fluorophores using the 20x or 63x objectives. The widefield images were often taken in tile form using 20x or 40x objective to create a complete image of the tissue or cells. Images were recorded by sequential multi-channel scanning to reduce bleed-through aiming to ensure that only one fluorophore was captured. Images were processed and quantified using Fiji is just ImageJ (FIJI) freeware (Schindelin *et al*., 2012). FIJI has also been used to make the figures for this study.

Histologically stained samples were imaged using ZEN blue edition (Zeiss, Germany) using a Zeiss Axio observer widefield microscope, which is provided by the Facility for Imaging by Light Microscopy at Imperial College London or with a stereomicroscope (Leica M205 FA). The widefield images were taken in tile form using the 20x or 40x objectives to create complete images of the samples using bright field. Images were processed and quantified using FIJI freeware (Schindelin *et al*., 2012). FIJI has also been used to make the figures for this study.

2.15.1 Intensity measurements

FIJI was used to quantify all intensities from fluorescent images. The drawing tool was used to draw around the region of interest or markers, such as DAPI for the nucleus, were used to create masks. The measurement function was then used to calculate the average pixel intensity for the area. A threshold was then set for when the region was deemed to be positive for the fluorophore. Images were compared to negative control which showed unspecific Alexa Fluro binding, to ensure any background staining was not being considered a positive stain. The threshold for positivity was held constant for all images used in the same experiment. The percentage of positive regions could then be calculated from this data.

2.15.2 Estimating ploidy

Estimates of ploidy were based on methods from the Sucov lab (Patterson et al., 2017). Images of isolated DAPI stained isolated zebrafish ventricular cardiomyocytes were used to estimate ploidy. The DAPI stain was used to make a mask of the nucleus using the threshold and then the analyse particles functions in FIJI which then generates a region of interest for each nucleus. The average DAPI intensity and area were then measured of each nucleus using the measure function in FIJI. Wild type nuclei were assumed to be diploid and so were used to generate a control. This information was exported to excel and for each nucleus, the average intensity was multiplied by the area to make the total intensity. The total intensity of all the ventricular nuclei from the different wild type samples was averaged to give the average control intensity. Following this, the total intensity for each nucleus measured was divided by the average control intensity. If a measurement was above 3 standard deviations from the average control intensity it was considered to be polyploid.

2.16 Zebrafish morphological measurements

2.16.1 Body length

Six-month-old zebrafish were anesthetised in 0.02% (w/v) tricaine and then laid against a ruler with their snout places at 0cm and their dorsal side lined up against the ruler. The measurement was then taken to the base of their peduncle fin.

2.16.2 Heart weight

Zebrafish were sacrificed with an overdose of 0.16% (w/v) tricaine. Hearts were then removed and placed into heparin dissection buffer to prevent blood clots. Hearts were then cleaned up to remove any non-heart tissue and any fat. Blood was removed from the heart by perfusing the hearts with PBS. Hearts were then weighed using a fine scale. The heart weight was divided by the body length to give a ratio, this was done as zebrafish heart size correlates with their body length.

2.16.3 Ventricle and BA dimension measurements

Zebrafish were sacrificed with an overdose of 0.16% (w/v) tricaine. Hearts were then removed and placed into heparin dissection buffer to prevent blood clots. Hearts were then cleaned up to remove any non-heart tissue and any fat. The atrium was also removed to give a clear view of the ventricle. A Leica stereomicroscope was used to take pictures of the heart with the atrioventricular valve facing up pictures were taken and lines were drawn from the base to the top of the ventricle for ventricle length (Figure 12A). From the side to side of the ventricle at the widest for the ventricular width (Figure 12A). And from the base to the tip of the BA for the BA length (Figure 12A).

2.16.4 Outflow tract angle

Outflow tract angle measurements were taken in line with work from Singleman and Holtzmann (2012). Zebrafish were sacrificed with an overdose of 0.16% (w/v) tricaine. Hearts were then removed and placed into heparin dissection buffer to prevent blood clots. Hearts were cleaned up to remove any non-heart tissue and any fat. Atria were also removed to give a clear view of the ventricle. A Leica

stereo microscope was then used to take pictures of the heart with the atrioventricular valve facing up pictures were taken and a line was drawn from the apex through to the top of the ventricle. Another line was drawn from the top of the ventricle to the tip of the BA. The angle between the two lines was measured to give the outflow tract angle (Figure 12B).

2.16.5 Ventricular circularity

Ventricular circularity measurements were taken in line with work from Singleman and Holtzmann (2012). Zebrafish were sacrificed with an overdose of 0.16% (W/V) tricaine. Hearts were then removed and placed into heparin dissection buffer to prevent blood clots. Hearts were then cleaned up to remove any non-heart tissue and any fat. Atria were also removed to give a clear view of the ventricle. A Leica stereo microscope was then used to take pictures of the heart with the atrioventricular valve facing up. The ventricle was traced around (Figure 12C). FIJI was then used to give a figure of circularity to the ventricles.

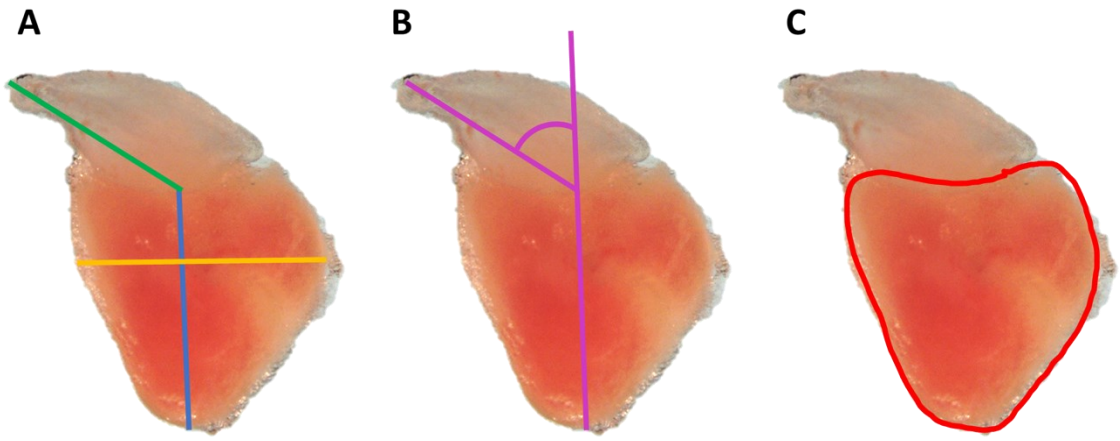

Figure 12 Taking zebrafish heart morphological measurements. (**A**) The blue line represents the measurement of the ventricular length. The yellow line represents the measurement of the ventricular width. The green line represents the measurement of the BA length. (**B**) The two-line represents the lines that go through the ventricular base to the apex and that goes through the tip of the BA and the base of the BA. The curved line represents the angle between the two lines that is the BA angle. (**C**) The red line represents a trace around the ventricle to assess its shape.

2.16.6 Cortical layer thickness

The cortical layer thickness was measured by making paraffin sections (2.11 Preparation of paraffin sections) of excised zebrafish hearts and staining them with H&E. Images were taken and the thickness

of the compact layer was measured with FIJI, compact layer thickness was taken over multiple points in the ventricle and multiple sections and the result was averaged to give an estimation of compact layer thickness for each zebrafish studied (Figure 13).

2.16.7 Quantitative analysis of the trabecular layer

Quantitative analysis of the trabecular layer was made using paraffin sections of excised zebrafish hearts (2.11 Preparation of paraffin sections) and staining them with H&E. Length and width measurements of individual trabeculae were made with the help of FIJI and all measurements taken from one fish were averaged (Figure 13). Trabecular complexity was measured by dividing the length by the width for each trabecula and then averaging this per fish (D'Amato *et al*., 2016). Finally, the percentage trabecular surface area was measured by using FIJI to estimate the total surface area of the trabecular layer. These two values were then used to calculate the percentage that the trabeculae covered within the trabecular layer.

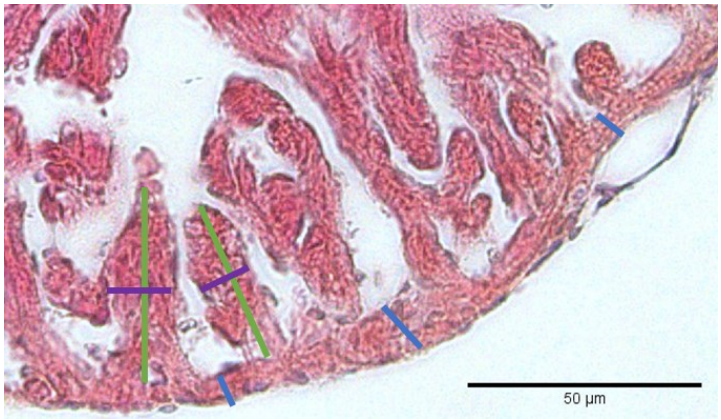

Figure 13 Measurements of the cortical and the trabecular layer. Examples of cortical layer thickness measurements (blue lines), examples of trabecular length (green lines) and width (purple lines) are indicated.

2.17 Quantifying RNA levels

2.17.1 Isolation of RNA from zebrafish ventricles

Zebrafish hearts were dissected out and placed into heparin dissection buffer to prevent blood clots and then the atria and BA were removed. Ventricles were then snap-frozen until the isolation of RNA

occurred. To extract RNA, TRIzol (Invitrogen, 15596026) was used according to the manufacturer's guidelines. Samples were placed into 1ml of TRIzol reagent and tissue was broken down using a pestle and mortar. 0.2ml of chloroform was added and samples were incubated for 3 minutes. Samples were centrifuged for 15 minutes at 12,000 × g at 4°C. The liquid aqueous phase containing RNA was removed and placed into a fresh microcentrifuge tube. 5µg of glycogen was added to each sample to ease the detection of RNA. 0.5ml of isopropanol was added to the sample and inverted a few times before being left to incubate for 10 minutes. Samples were centrifuged for 10 minutes at 12,000 × g at 4°C and the RNA formed a white gel-like pellet. The supernatant was discarded and the sample was washed twice in 75% ethanol centrifuging for 5 minutes at 7500 × g at 4°C after each addition. The supernatant was discarded, and the pellet was left to air dry for 10 minutes before being dissolved in water and concentration and purity tested using a nanodrop spectrophotometer. Samples were then snap-frozen and stored at -80°C until required.

2.17.2 Generation of cDNA from zebrafish ventricular RNA

Isolated RNA from zebrafish ventricles was reverse transcribed and converted to cDNA using the iScript™ cDNA Synthesis Kit (Bio-Rad, 1708890). 250ng of RNA was added 4µl iScript reaction mix, 1µl of iScript reverse transcriptase and nuclease-free water to a total volume of 20µl. The mixture was then transferred to a Polymerase chain reaction (PCR) machine and exposed to the following programme 5 minutes at 25°C, 35 minutes at 42°C and then 5 minutes at 85°C. cDNA was then diluted 1:10 in water and then stored at -20°C until required.

2.17.3 qPCR

Quantitative polymerase chain reaction (qPCR) reactions were set up in triplicate in a 384 well plate using 2µl of cDNA, 0.8µl of each forward and reverse primer (Table 10) at 10mM, 5µl PowerUp™ SYBR™ green (applied biosciences, A25742) and 1.4µl of H2O according to the manufactures instructions. An Applied Biosciences Quanti studio 6 qPCR machine was run using the thermal profile shown in Table 11. The machine gave CT values as an output with a lower CT value conferring to a

higher expression in the sample. The CT values were averaged for the triplicate reaction, if the standard deviation for these values was greater than 0.5 the samples were not used. The average CT values were normalised against Glyceraldehyde 3-phosphate dehydrogenase (GAPDH) by subtracting the GAPDH value to give the ΔCT. To compute the actual relative expression 2 was taken to the power of – ΔCT and this was then multiplied by 100.

Table 10 Primers used for qPCR

Gene	Forward Primer	Reverse Primer	Source (if applicable)
myca	TGTTTCCCTTTCCACTGAC	CTTCATCATCTTCGTCATCG	(Gemberling *et al*., 2015)
mycb	AAGCGGCCAAAGTGGTGATCCT	CACTACTTTGCCACACCCTCGC	(Münch *et al*., 2017)
gapdh	GTGGAGTCTACTGGTGTCTTC	GTGCAGGAGGCATTGCTTACA	N/A
popdc1	CTCATTCCCACCACATTAGCG	CCCTGTCAATCTTAATCGGTCTG	N/A
popdc2	AGTCTATACCATGTCCTTGCC	GATTTCTTGTGCCTGAGCCT	N/A
popdc3	AAGGATCGGTATTTCATCTCGC	AGTTGTCCCAAACAGAAGGC	N/A
nkx2.5	GGACTATGTTAAAGACGCAAAGAC	TCCAGCTTCAGATCTTCACC	N/A
nppa	ACGCATTCAGACACTCAG	TTGCTCTTCATAATCTACGG	N/A
tbx20	ACTCTGGGAGAAGAAGGACATTCAGC	GTGCTGAAAGCCAGAGAAACCAGATG	(Lu *et al*., 2017)
tbx5	GGAATT TAAGGCCTCACGGTA	GATTTGCTGACGGCTGCATTC TGT	(Parrie *et al*., 2013)
mt2	GCACTAATTGCCAGTGTACTACC	CACAGGAATTGCCTTTGCAG	N/A
vegfaa	GTGCAGGATGCTGTAATGATGAGG	AATTATGCTGCGATACGCGTTG	(Marín-Juez *et al*., 2016)
aldh1a	GGGGGAAGCTACTGTTCAAAT	TCCAGAGACTCCAGGGTAGC	(Fang *et al*., 2013)
mmp2	CCTCACCCATCATAAAGTTCC	TTTCTTCAGCGTGTCCTTCAA	(Gamba *et al*., 2017)
mmp13a	GAGGCTCAAGGAGATGC	GTTGAGTAGGCCTTGATGT	(Gamba *et al*., 2017)

Table 11 qPCR thermal profile

Procedure	Temperature	Time
Hold Stage	50°C	2 minutes
	95°C	2 minutes
PCR stage 40 repeats	95°C	15 seconds
	60°C	1 minute
Melt Curve	95°C	15 seconds
	60°C	1 minute
	95°C	15 seconds

2.18 Single Nuclear RNA Sequencing

2.18.1 Nuclear isolation

Five ventricles were pooled for each sample and three samples were used from each genotype. Zebrafish ventricular tissue was broken down using a pre-cooled pestle and mortar. The tissue was

then moved into a precooled Dounce homogeniser with 3ml of HB (250mM sucrose, 25mM KCl, 5mM $MgCl_2$, 10mM Tris-HCL, 1µM DTT, 1x protease inhibitor (Sigma Aldrich, 11873580001), 0.4U/µl RNAsein Plus (Promega, N2611), 0.2U/µl SUPERrasein (ThermoFisher, AM2696) and 0.1% (v/v) Triton X-100) buffer a maximum of 20 strokes of the pestle were carried out on the tissue while incubating it on ice. The homogenised tissue was passed through a 40µm cell strainer into a 50ml falcon tube. The homogeniser was washed twice with 1ml of HB buffer before passing this also through the cell strainer. The suspension was centrifuged at 500 x g for 5 min at 4°C to pellet the nuclei. And the supernatant was discarded. The pellet was resuspended in SB (4% BSA, 0.2U/µl Protector RNAsein (Sigma Aldrich, 03335402001) in PBS buffer and transferred to a fluorescence-activated cell sorting (FACS) tube and 2 drops of NucBlue (ThermoFisher, R37605) was added and incubated for 10 minutes

2.18.2 Purifying the nuclear population

Nuclei with the NucBlue™ stain were sorted using an Aria fusion sorter as described below (2.19.2 Cell Sorting) using the 450nm channel and gated by size to exclude doublets. The nuclei were then counted using a hemocytometer and diluted to make a suspension that is 1000 nuclei/µl in SB buffer

2.18.4 GEM Generation and Barcoding

GEM (Gel Bead-In EMulsions) generation and Barcoding was performed using the Chromium next-generation GEM Single Cell 3' Reagent Kit v3.1 (10x Genomics). Gel beads contain barcoded oligonucleotides which will allow the analysis of the transcriptome on a cell by cell basis. First, the Chromium Next GEM Chip G was assembled by removing the seal and fitted into the holder. In row 1 8.3µl of the purified nuclear sample and 66.8µl of master mix (18.8µl RT reagent B, 2.4µl template switch oligo, 2µl reducing agent B, 8.7µl RT enzyme C and 35µl water) were added. Row 2 was filled with 50µl of gel beads. Row 3 was filled with 45µl partitioning oil. The gasket was attached to the holder and the assembled chip was put into the Chromium Controller and the Machine was allowed to run. Microfluidics allows the formation of vesicles which are the GEMs. The assembled chip was removed from the machine and dissembled. 100µl of the newly made GEMs were aspirated out of

row 3 of the Chromium Next GEM Chip G and moved into PCR tubes. A thermocycler was then used with the thermoprofile in Table 12 to perform the GEM-RT incubation.

Table 12 GEM-RT incubation thermal profile

Step	Temperature	Time
1	53^{o}C	45 minutes
2	85^{o}C	5 minutes
3	4^{o}C	hold

2.18.5 Post GEM-RT Clean up and cDNA Amplification

Post GEM-RT clean up and cDNA amplification was performed using the Chromium Next-generation GEM Single Cell 3' Reagent Kit v3.1 (10x Genomics). This stage causes each nucleus to be lysed and the gel bead dissolved, releasing the oligonucleotide barcode. When the mRNA is reverse transcribed into cDNA there will be the inclusion of this barcode allowing the mapping back of each cDNA to each cell. 125µl of recovery agent was added to the product of the GEM-RT incubation this created a biphasic mixture as the recovery agent bound to the partitioning oil and the GEMs. The recovery agent/partitioning oil mixture was removed and then 200µl of dynabead clean up mix (Cleanup buffer 182µl, 8µl dynabeads MyOne SILANE, 5µl reducing agent B and 5µl nuclease-free water) was added to each sample and incubated at room temperature for 10 minutes. The GEMs are bound to these beads which are magnetic. Samples were then put on a 10x magnetic separator and the supernatant was removed. The sample was washed twice in 80% ethanol and then allowed to air dry. The samples were eluted in 35.5µl elution solution I (98µl buffer EB, 1µl 10% Tween 20 and 1µl reducing agent B) the magnetic separator was then held at the bottom of the samples and then the samples were moved into a new tube, with the magnetic beads remaining in the old tube.

65µl of cDNA amplification reaction mix (50µl Amp mix and 15µl cDNA primers) was added to the sample and it was incubated in a thermal cycler with the conditions described in Table 13.

60µl of SPRIselect reagent was added to each sample and incubated for 5 minutes. Samples were then put on a 10x magnetic separator and the supernatant was removed. The sample was washed twice in

80% ethanol and then allowed to air dry for 2 minutes. 40.5µl of buffer EB was added to the sample and incubated for 2 minutes the magnetic separator was then held at the bottom of the samples and then the samples were moved into a new tube, with the SPRIselect reagent remaining in the old tube. 1µl of the sample diluted with 9µl of nuclease-free water was run on an Agilent Bioanalyzer to give an estimation of the cDNA concentration.

Table 13 cDNA amplification thermal profile

Step	Temperature	Time
1	98°C	3 minutes
2	98°C	15 seconds
3	63°C	20 seconds
4	72°C	1 minute
5	Go to step 2 for a total of 12 cycles	
6	72°C	1 minute
7	4°C	hold

2.18.6 3' Gene Expression Library Construction

The cDNA is then used to create a transcriptome library for each nucleus this is to introduce additional sequence components including the read 1 sequence, the 10x barcode, the unique molecule identifier (UMI) and the poly(dT) primer sequence. 10µl of the purified cDNA sample clean-up was moved to a fresh tube and 25µl buffer EB and 15µl fragmentation mix (5µl fragmentation buffer and 10µl fragmentation buffer) were added. Then samples were run through a thermal cycler with the conditions in Table 14 to fragment, end repair and A-tail.

Table 14 Fragmentation, end repair and A-tailing thermal profile

Step	Temperature	Time
Pre-cool block	4°C	hold
Fragmentation	32°C	5 minutes
End repair and A-tailing	65°C	30 minutes
Hold	4°C	hold

30µl of SPRIselect reagent was added to each sample and incubated for 5 minutes Samples were then put on a 10x magnetic separator and the supernatant was moved to a fresh tube. 10µl of SPRIselect

reagent was added to each sample and incubated for 5 minutes. The supernatant was discarded and the sample was washed twice in 80% ethanol and then allowed to air dry for 2 minutes. 50.5µl of buffer EB was added to the sample and incubated for 2 minutes the magnetic separator was then held at the bottom of the samples and then the samples were moved into a new tube, with the SPRIselect reagent remaining in the old tube.

50µl of adaptor ligation mix (20µl ligation buffer, 10µl DNA ligase and 20µl adaptor oligos) was added and incubated in a thermal cycler at 20^{o}C for 15 minutes and then held at 4^{o}C creating the post ligation sample. This sample was subjected to clean up using SPRIselect reagent. 80µl of SPRIselect reagent was added to each sample and incubated for 5 minutes Samples were then put on a 10x magnetic separator and the supernatant was removed. The sample was washed twice in 80% ethanol and then allowed to air dry for 2 minutes. 30.5µl of buffer EB was added to the sample and incubated for 2 minutes the magnetic separator was then held at the bottom of the samples and then the samples were moved into a new tube, with the SPRIselect reagent remaining in the old tube. The samples then had 60µl of sample index PCR mix added (50µl Amp mix and 10µl SI primer) and incubated in a thermal cycler with the protocol described in Table 15.

Table 15 Sample Index PCR thermal profile

Step	Temperature	Time
1	98^{o}C	45 seconds
2	98^{o}C	20 seconds
3	54^{o}C	30 seconds
4	72^{o}C	20 seconds
5	Go to step 2 for a total of 15 cycles	
6	72^{o}C	1 minute
7	4^{o}C	hold

The PCR product was then cleaned up using SPRIselect. 60µl of SPRIselect reagent was added to each sample and incubated for 5 minutes. Samples were then put on a 10x magnetic separator and the supernatant was moved to a fresh tube. 20µl of SPRIselect reagent was added to each sample and incubated for 5 minutes. The supernatant was discarded and the sample was washed twice in 80%

ethanol and then allowed to air dry for 2 minutes. 35.5µl of buffer EB was added to the sample and incubated for 2 minutes the magnetic separator was then held at the bottom of the samples and then the samples were moved into a new tube, with the SPRIselect reagent remaining in the old tube. 1µl of the sample diluted in 9µl of nuclease-free water was run on an Agilent Bioanalyzer to estimate the concentration and the library size.

2.18.7 Sequencing and analysis

Samples were sent to Genewiz for next-generation sequencing. The samples were subjected to further quality control steps before being processed. Data files with the sequencing were then returned for further computational analysis.

The first step of the analysis was to pre-process these files using the cell ranger pipeline. In this process, cell matrices are created via the alignment of barcodes to identify different cells as well as performing some basic gene expression analysis to normalise different samples. Genes are aligned with one another and their counts are created and added to the matrix alongside the nuclei they originated from.

Once the matrices are created they could continue to be processed with the Scanpy package on Python. Jupyter notebooks were used to operate the Scanpy package. Firstly the samples were combined and taken through quality control steps the nuclei were filtered to have between 500 and 7500 UMIs, to have between 300 and 2500 genes expressed to have less than 5% mitochondrial and ribosomal genes and to have a scrublet score of less than 0.3.

Scanpy was then used to perform dimensional reduction in the form of Uniform Manifold Approximation and Projections (UMAPs). The UMAPs allowed the definition of different clusters and subclusters. Heat maps, dot plots and matrixes were created for the visualisation of gene expression in the different clusters or the different genotypes. Wilcoxon tests were performed within the software to generate lists of differentially expressed genes which could be run in panterdb.org to find differentially regulated biological processes, molecular functions and pathways using Fisher's exact

test. This analysis was run with a Bonferroni correction for multiple testing as statistical tests were performed for each regulated biological process, molecular functions and pathways and was considered significant is $p < 0.05$. Notebooks from this work can be found in the appendix.

2.19 Flow Cytometry

All flow cytometry was conducted at the LMS/NIHR Flow Cytometry Facility at Imperial College London and cell sorting was conducted by the facility technicians.

2.19.1 ImageStream flow cytometry

An ImageStream®X Mark II Imaging Flow Cytometer was used to take images of zebrafish isolated cardiomyocytes (2.8.5.2 Isolation of zebrafish ventricular cardiomyocytes for size analysis) in sort buffer using the IMAGE® programme this programme took an image of every cell going through the machine to create a file. This file was then used in the IDEAS® software, allowing the analysis of the fluorophores expressed and cell size. Cardiomyocytes should emit light upon excitation at 488nm allowing the software to filter the images so only cardiomyocytes were analysed. This software could then be used to make several measurements of the cells such as area.

2.19.2 Cell Sorting

Cell sorting was performed using a BD FACSAria™ Fusion Cell Sorter.

2.19.2.1 Cell sorting

Cells (2.2.3 Cells Grown in Conditioned Media) were detached, resuspended in sort buffer and placed into a fresh FACS tube. The sample cells had been transfected with a YFP expression vector and some were non-transfected to act as a negative control for YFP. 1.5ml microcentrifuge tubes were prepared for collection by adding 200µl of sort buffer. Cells were gated by size to remove debris and doublets. Cells were also gated to be positive for YFP by looking at emission in the 488nm channel. These cells were then used for future experiments.

2.19.2.2 Nuclear Sorting

100µl of nuclei (2.18.1 Nuclear isolation) in SB buffer was placed into a fresh FACS tube to be used as a negative unstained control for FACS. The rest of the suspension had two drops on NucBlue (Invitrogen, R37605) added and were incubated on ice for 10 minutes. 1.5ml Eppendorf tubes were prepared for nuclei collection by adding 200µl of SB buffer. At least 150,000 events were recorded and nuclei were gated to remove doublets and to collect cells that were NucBlue positive in the 405-450/50nm channel.

2.20 Statistical Analysis

GraphPad Prism 5 or Python was used to statistically analyse data. T-tests, Kruskal-Wallis, Wilcoxen tests, Chi-squared goodness of fit tests and Mann-Whitney U tests were used for analysis. Significance was determined by $p \leq 0.05$.

3. Popdc1 and its interaction with c-Myc and the cell cycle

A large number of reports have implicated POPDC proteins in tumour formation in many types of cancer (Amunjela *et al*., 2019). Most studies have focused on POPDC1 where it is thought to act as a tumour suppressor preventing a large range of cancers and its removal or downregulation is known to aid progression of cancer (Parang *et al*., 2016, Wang *et al*., 2014, Han *et al*., 2015, Amunjela and Tucker, 2017b). The tumour suppressor activity has been linked with its ability to promote cell adhesion and inhibit EMT and metastasis (Williams *et al*., 2011, Han *et al*., 2014, Osler *et al*., 2005). But there are also several studies that have observed POPDC1's ability to regulate signalling pathways involved in cell proliferation (Russ *et al*., 2011, Amunjela *et al*., 2019, Smith *et al*., 2008, Parang *et al*., 2016, Thompson *et al*., 2019, Zhan *et al*., 2017, Kliminski *et al*., 2017).

The Williams group recently reported an interaction of POPDC1 and c-Myc (Parang *et al*., 2016). c-Myc is a nuclear proto-oncogene (Nesbit *et al*., 1999) and a transcription factor controlling the expression of a large number of genes, many of which are involved in cell cycle control (Figure 14). Moreover, it also recruits histone acetyl transferases which remodel the DNA, leading to increased accessibility for transcription factors (Martinato *et al*., 2008). In patients with colorectal carcinoma, the *POPDC1* promoter is hypermethylated (Williams *et al*. 2011) and similar observations were made in gastric cancer (Kim *et al*. 2010). In mice, the loss of *Popdc1* leads to the promotion of colitis-associated cancer development (Choksi *et al*. 2018). *Popdc1* null mutant mice display higher expression levels of c-Myc and Popdc1 interacts with both c-Myc and PR61α, a subunit of PP2A (Parang *et al*., 2016). PP2A is known to phosphorylate c-Myc, marking it for proteasomal degradation (Arnold and Sears, 2006). POPDC1 may be involved in controlling the PP2A complex, which provides an explanation to why the loss of POPDC1 leads to more severe colitis-associated cancers in patients (Parang *et al*., 2016).

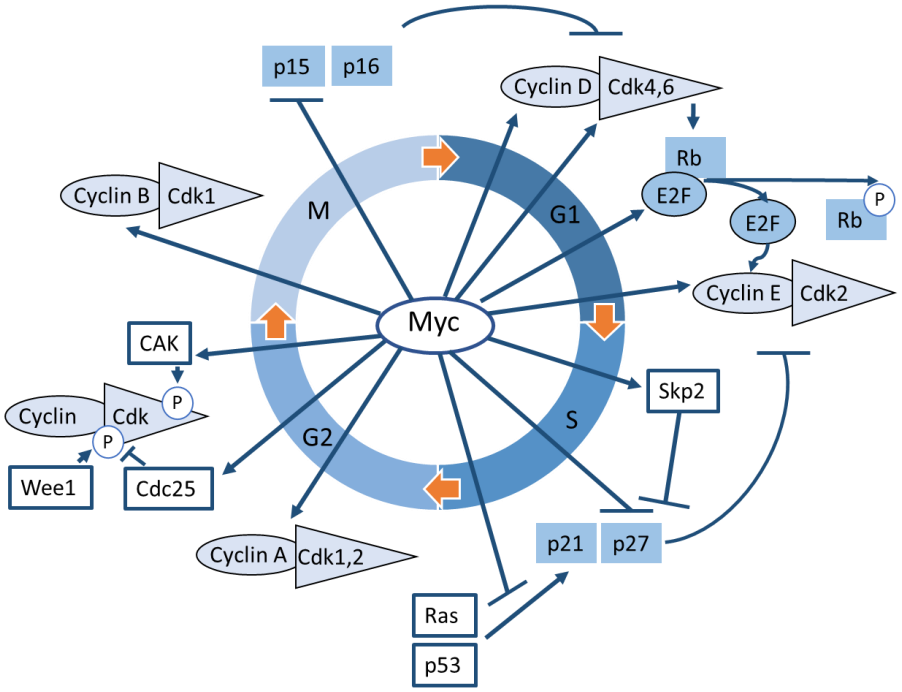

Figure 14 Schematic of the involvement of c-Myc in the cell cycle. Adapted from (Bretones *et al*., 2015).

As the POPDC protein family is expressed predominantly in heart and skeletal muscle (Andrée *et al*., 2000), it would be interesting to study whether the interactions with c-Myc, which links POPDC1 to cell cycle control is also observable in cardiac muscle tissue. There is interest in understanding the cell cycle in cardiomyocytes as in adult mammals there is very limited proliferation (Bergmann *et al*., 2009). This means that after cardiac injury, by myocardial infarction, for example, cardiomyocytes that are lost cannot be replaced and are instead substituted by scar tissue. While the scar is important in enabling the maintenance of heart wall integrity, the contractile function is lost in this area, often leading to myocardial remodelling and eventually to heart failure (Francis Stuart *et al*., 2016). As the number of patients who have survived a myocardial infarction continues to grow (BHF, 2020a), many research groups are trying to find ways to stimulate myocyte proliferation in the uninjured myocardium, something which naturally occurs in the adult heart of non-mammalian model organisms such as the newt and the zebrafish and the neonatal mammalian heart (Porrello *et al*., 2011, Haubner *et al*., 2012, Porrello and Olson, 2014, Poss *et al*., 2002, Bely and Nyberg, 2010).

Zebrafish have two copies of the c-Myc gene; *myca* and *mycb* (Zhang *et al*., 2003). These genes display a high level of homology and similar expression patterns. Like in humans, misregulation of c-Myc can cause tumorigenesis in the zebrafish (Ung *et al*., 2009) and zebrafish c-Myc protein can cause tumours in mammalian tissue when transfected into mammalian cells (Schreiber-Agus *et al*., 1993). Importantly for the interaction with Popdc1, threonine 58 and serine 62 are conserved in both zebrafish Myc proteins. Therefore, it is assumed that c-Myc's regulation via phosphorylation is conserved in zebrafish.

In this chapter, I aimed to further explore the interaction of the POPDC proteins with c-Myc as well as their role in cell cycle regulation. Because of the high sequence similarity between the different POPDC isoforms (Andree *et al*. 2000), I aimed to determine whether apart from POPDC1, also the other POPDC isoforms, i.e. POPDC2 and POPDC3, could interact with PR61α and c-Myc and to attempt to map the binding domains on the POPDC proteins. Moreover, I investigated, whether modulating POPDC levels could affect c-Myc expression and have an impact on the cell cycle. Finally, I wanted to determine whether information that has been obtained in the human and murine gut could be translated into the heart.

3.1 Results: Interaction of c-Myc with the POPDC protein family

3.1.1 POPDC1, POPDC2 and POPDC3 can interact with PR61α and c-Myc

It has previously been shown in cell culture that POPDC1 can interact with c-Myc through the PR61α domain of PP2A and that this has implications in the gut (Parang *et al*., 2016). Here, I aimed to confirm these interactions and to build upon them by testing the interaction with POPDC2 and POPDC3. Using co-immunoprecipitation (CoIP) in Cos7 cells, I demonstrated that POPDC1, POPDC2 and POPDC3 can interact with PR61α, which is the active subunit of PP2A although the band for POPDC3 is weak (Figure 15). GFP antibodies are cross-reactive with the YFP tags on the POPDC proteins and so were successfully used to detect POPDC proteins in the CoIP experiment. Interaction between POPDC

protein family members and c-Myc was also tested and I found that all three POPDC isoforms interact with c-Myc (Figure 16).

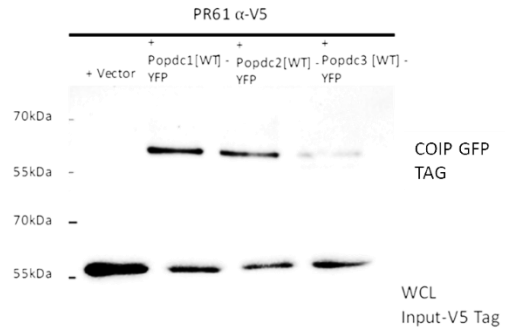

Figure 15 POPDC1, 2 and 3 can bind to PR61α. YFP-tagged POPDC1, -2 and -3 plasmids were co-transfected into Cos7 cells along with V5-tagged PR61α. The top panel shows a Western blot after immunoprecipitation using anti-GFP agarose and incubation with a V5-tag antibody to detect PR61α. The lower panel shows a Western blot using whole-cell lysates (WCL) to confirm the expression of PR61α in each sample. PR61α was co-precipitated with POPDC1, -2 and -3 suggesting that PR61α can interact with all three POPDC isoforms. This experiment was repeated at least twice for each interaction.

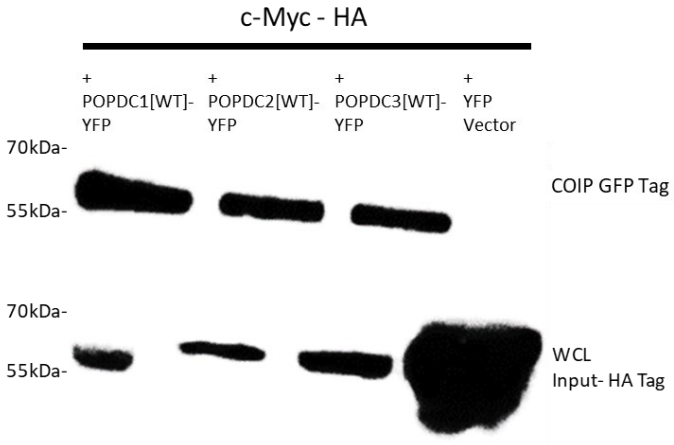

Figure 16 POPDC1, -2 and -3 isoforms can bind to c-Myc. YFP-tagged POPDC1, -2 and -3 plasmids were co-transfected into Cos7 cells along with HA-tagged c-Myc. The top panel shows a Western blot after immunoprecipitation using anti-GFP agarose and incubation with an HA-tag antibody to detect c-Myc. The lower panel shows a Western blot using whole-cell lysates (WCL). c-Myc was co-precipitated with POPDC1, -2 and -3 suggesting that c-Myc can interact with all three POPDC isoforms. This experiment was repeated at least twice for each interaction.

3.1.2 Looking for a binding site for the POPDC proteins on PR61α and c-Myc

The binding site for PR61α on POPDC1 has been recently reported (Parang *et al*., 2016). However, the sequence that was identified is not conserved amongst the three POPDC isoforms (Andrée *et al*., 2000), which would be expected as all three can bind to PR61α (Figure 15). To map a potential binding

site for PR61α on POPDC1, CoIP experiments were performed using full-length myc-tagged POPDC1 and two myc-tagged carboxy-terminal deletion mutants, that had 116 (POPDC1[Δ116]) or 127 (POPDC1[Δ127]) residues removed (Figure 17A). A positive CoIP was seen with both full length POPDC1 and POPDC1[Δ116] (Figure 17B). However, binding was not observed in case of POPDC1[Δ127] and the empty vector used as a negative control (Figure 17B). This suggests that binding of PR61α probably relies on the sequence between POPDC1[Δ116] and POPDC1[Δ127], which corresponds to a putative binding site between amino acid 233 and 244 in POPDC1, and located at the carboxyl end of the Popeye domain (Figure 19A and B).

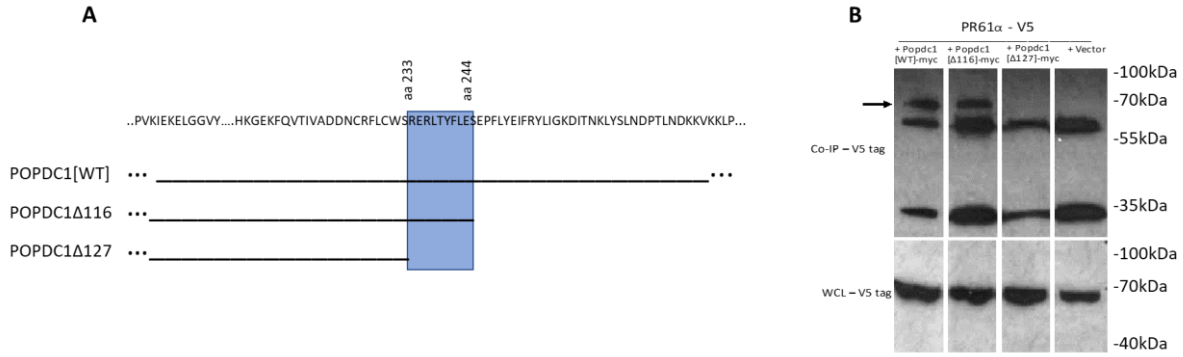

Figure 17 CoIP experiment to identify the interaction site of PR61α on POPDC1 CoIP experiments were performed to map the binding site of PR61α on POPDC1. Myc-tagged full-length POPDC1 (POPDC1[WT]) or carboxy-terminal deletion constructs (POPDC1[Δ116] or POPDC1[Δ127]) were co-transfected into Cos7 cells along with V5-tagged PR61α**.** (**A**) A map of Myc-tagged POPDC1 carboxy-terminal deletion constructs amino acids. (**B**) The top panel shows a Western blot after immunoprecipitation using anti-myc agarose and detection of PR61α using an anti-V5-tag antibody. The lower panel shows a western blot for the WCL to confirm the successful transfection of PR61α using the anti-V5-tag antibody. Bands for co-precipitated PR61α were only seen in the case of full-length POPDC1 and POPDC1 with a deletion of 116 residues. However, precipitation produced no immunoreactive protein band in the vector-transfected control sample, or when 127 residues had been removed. A black arrow points out the band of interest. The other bands on the upper Western blots are presumed to be the immunoglobulin heavy and light chains. The data suggest that a sequence between amino acids 233 and 244 is required for PR61α binding. This co-immunoprecipitation was repeated at least twice for each interaction.

Peptide binding arrays were also employed to investigate the c-Myc binding site on POPDC1. 25-mer peptide arrays were printed on to glass in three peptide increments. From these experiments, the region of binding appears to be over the dots 22-25 (Figure 18), as the sequence overlapped in consecutive dots. It is presumed that single and double dots do not convey binding, due to the overlap in the sequence across neighbouring dots and so are presumed to be non-specific. Dots 22-25

correspond to residues 105-145 (Figure 18, Figure 19B) in the POPDC1 sequence, with the overlap from all dots conferring to residues 120-130. These residues are located in the presumed location of the juxta-membrane region of POPDC1 and are accessible due to their presence on the protein surface (Figure 19C).

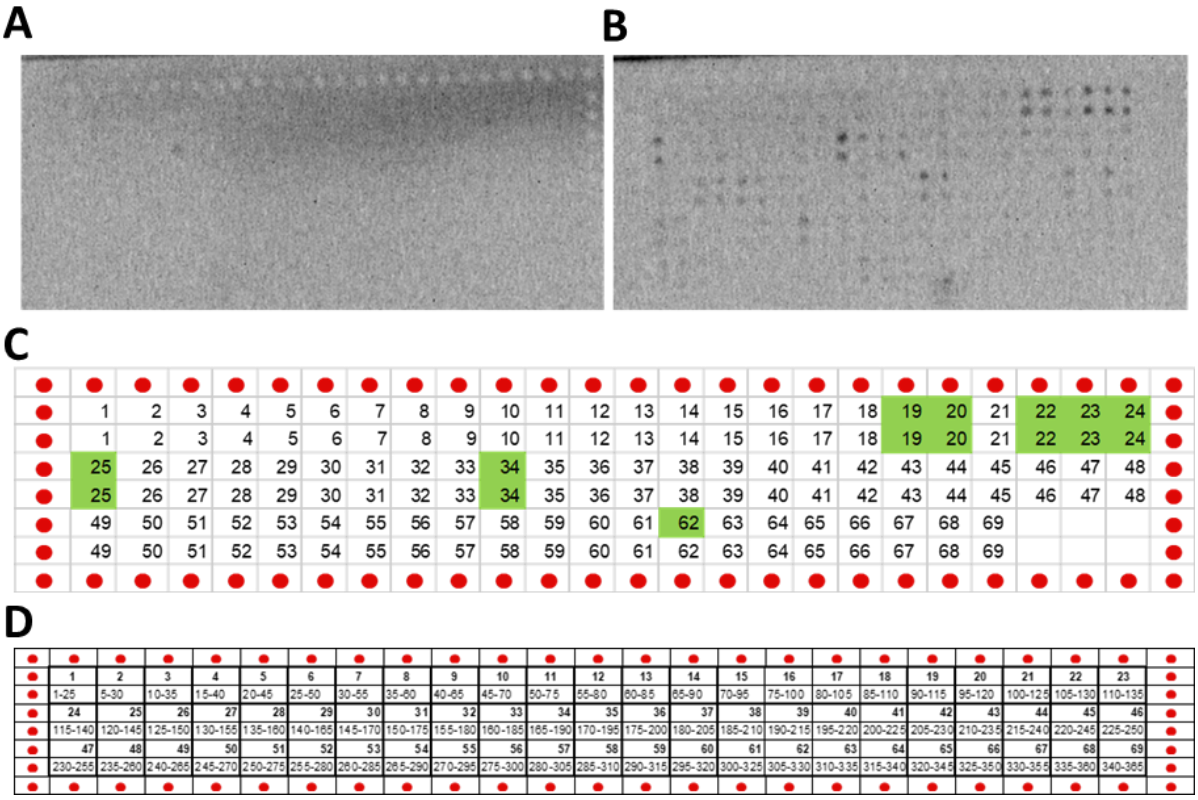

Figure 18 Peptide binding array to map the c-Myc binding site of POPDC1 25-mer POPDC1 peptide array printed on glass was incubated with cell lysates from non-transfected Cos7 cells (**A**) or Cos7 cells transfected with HA-tagged c-Myc (**B**). A schematic of positive dots on the POPDC1 binding array (**C**). Those peptides, which bind to the c-Myc protein were identified by thresholding using FIJI. Dots whose intensity was 3-fold above background level are labelled (green). A schematic to show which residues the dots on the POPDC1 peptide-binding array correspond to is also displayed in Figure 9 (**D**). Numbers in bold represent the dot number and the line below represents what residues they correspond to. Due to the representation of a 5 residue long sequence overlap between dots, it is expected that c-Myc would bind to several consecutive dots. Thus, in this experiment, peptides 22-25 represent the putative c-Myc interaction sequence in POPDC1. The experiment has been repeated twice.

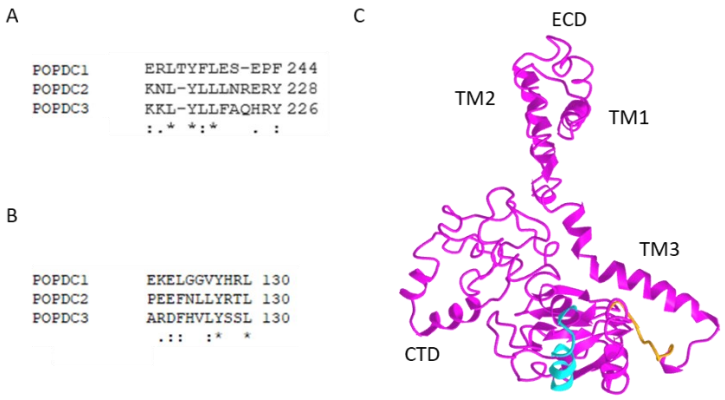

Figure 19 Putative binding site for c-Myc and PR61α on POPDC1 The results of CoIP experiment using carboxy-terminal deletion mutants of POPDC1 from Figure 17 and the peptide array experiment depicted in Figure 18 identified a putative interaction sequence between residues 233-244 mediating the interaction with PR16α and residues 120-130 in case of c-Myc. (**A** and **B**) The amino acid conservation between different POPDC isoforms for residues 233-244 (**A**) and residues 120-130 (**B**). The amount of conservation of each position is represented by symbols at the bottom of each set of proteins *represents an exact match in all sequences, : means that a conserved substitution has occurred so the amino acids are of the same type and. means that a semi-conserved substitution has occurred. (**C**) The putative c-Myc interaction domain (orange) and the putative PR61α interaction domain (cyan) was projected onto 3-dimensional structure predictions of murine Popdc1 secondary structure mode. Abbreviations: ECD-extracellular domain, TM1-3 transmembrane domains, CTD carboxy-terminal domain. Sequence alignments were performed using Clustal Omega (https://www.ebi.ac.uk/Tools/msa/clustalo/). The model was made using Phyre2 (http://www.sbg.bio.ic.ac.uk/~phyre2/html/page.cgi?id=index) and rendered using (https://www.ncbi.nlm.nih.gov/Structure/icn3d/full.htm).

3.2 Results: The effects of POPDC1 on c-Myc levels and the cell cycle

3.2.1 Forced expression of the POPDC proteins can reduce endogenous c-Myc levels in cell culture

As I have shown that POPDC proteins could interact with c-Myc, I then looked at whether the POPDC proteins could affect the c-Myc levels in Cos7 cells. Cells were plated and then transfected with POPDC1 or POPDC2, tagged with YFP, or with an empty vector. These cells were then fixed after 24 hours and endogenous c-Myc protein was stained for and YFP expression was visualised representing POPDC proteins. Pixel intensity for the c-Myc staining was quantified using FIJI. Transfection with both POPDC1-YFP and POPDC2-YFP was able to significantly lower the pixel intensity of the c-Myc staining compared to that of vector-only transfection (Figure 20). Transfection with POPDC2-YFP showed a greater reduction in intensity than those transfected with POPDC1-YFP. These data suggest that overexpression of the POPDC1 and POPDC2 proteins in Cos7 cell lines can cause a reduction in endogenous c-Myc levels.

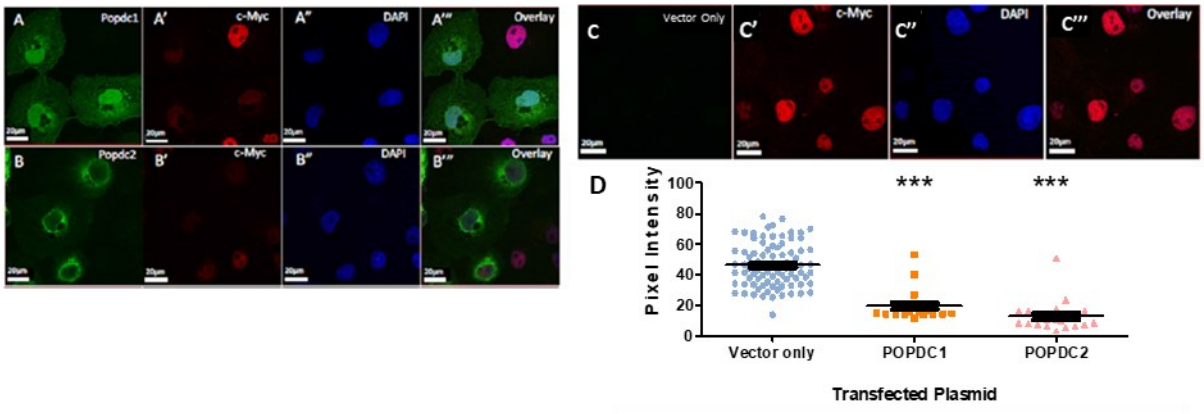

Figure 20 Reduced c-Myc intensity in Cos7 cells transfected with POPDC Proteins. Cos7 cells were transfected with (**A**) POPDC[WT]-YFP. (**B**) POPDC[WT]-YFP or (**C**) an empty vector. Transfected cells were identified by immunocytochemistry with anti-GFP antibody (green) and native c-Myc was detected using an anti-c-Myc antibody (red). Cell nuclei were stained with DAPI (blue). The pixel intensity of transfected nuclei was quantified using FIJI (**D**) quantification and statistical assessment was carried out with GraphPad Prism using a one-way ANOVA ($F(2,124) = 74.35$, $p<0.001$) and Tukey's Multiple comparison test, data are reported as mean ± standard error of the mean. *** represents $p\leq0.01$ compared to vector-only cells. The nuclei of at least 17 cells were measured for each group.

3.2.2 Forced expression of POPDC1 induces secretion of a growth inhibitor

As POPDC1 is thought to be involved in the regulation of c-Myc (Parang *et al*., 2016) (Figure 20), I investigated the effects of POPDC1 on proliferation in Cos7 cells, which had been transfected with either YFP-tagged POPDC1 or a YFP vector control, but no difference was seen (Figure 21). However, when media was conditioned from cells that were transfected with YFP-tagged POPDC1, as verified using FACS sorting, and the conditioned medium was transferred to non-transfected cells, which were left to grow for 24 hours before being stained for the proliferation marker phospho-histone 3 (PH3), there was roughly a 9% reduction in the number of proliferating cells when compared to conditioned media of control cells transfected with a YFP only vector (Figure 22A, D and C). Cells treated with conditioned media were also stained with c-Myc, to observe if conditioned media of POPDC1 transfected cells could have a paracrine inhibitory effect on c-Myc levels, however, no difference between the conditioned medium of vector and POPDC1-transfected cells was observed (Figure 22 B, E, F).

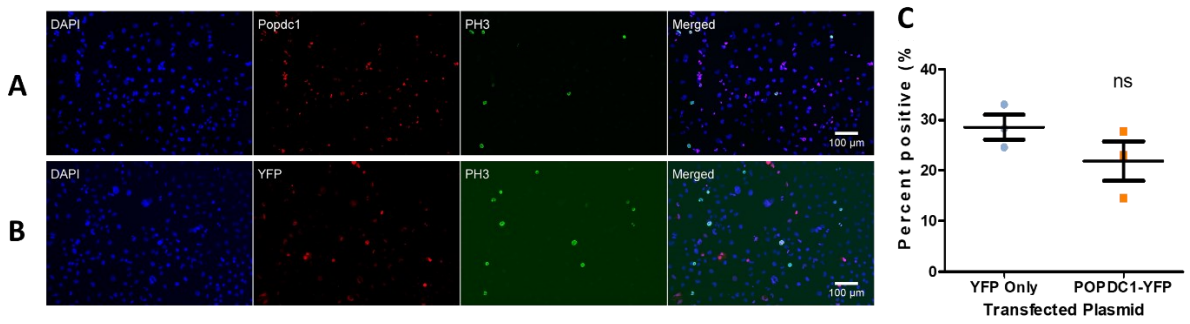

Figure 21 Transfection with POPDC1 does not affect proliferation in Cos7 cells. Cos7 cells were transfected with either Popdc1[WT]-YFP (**A**) or a YFP-only (**B**) plasmid. The number of cells transfected was then determined by looking for co-expression of YFP and the mitosis marker PH3. Staining was determined by using a threshold in FIJI. The data were quantified (**C**) and analysed using a T-test (t=1.478; df=4; p>0.05) in GraphPad Prism but were found to be non-significant (ns) as they had a p> 0.05. 3 replicates were conducted for each condition. Data are reported as mean ± standard error of the mean.

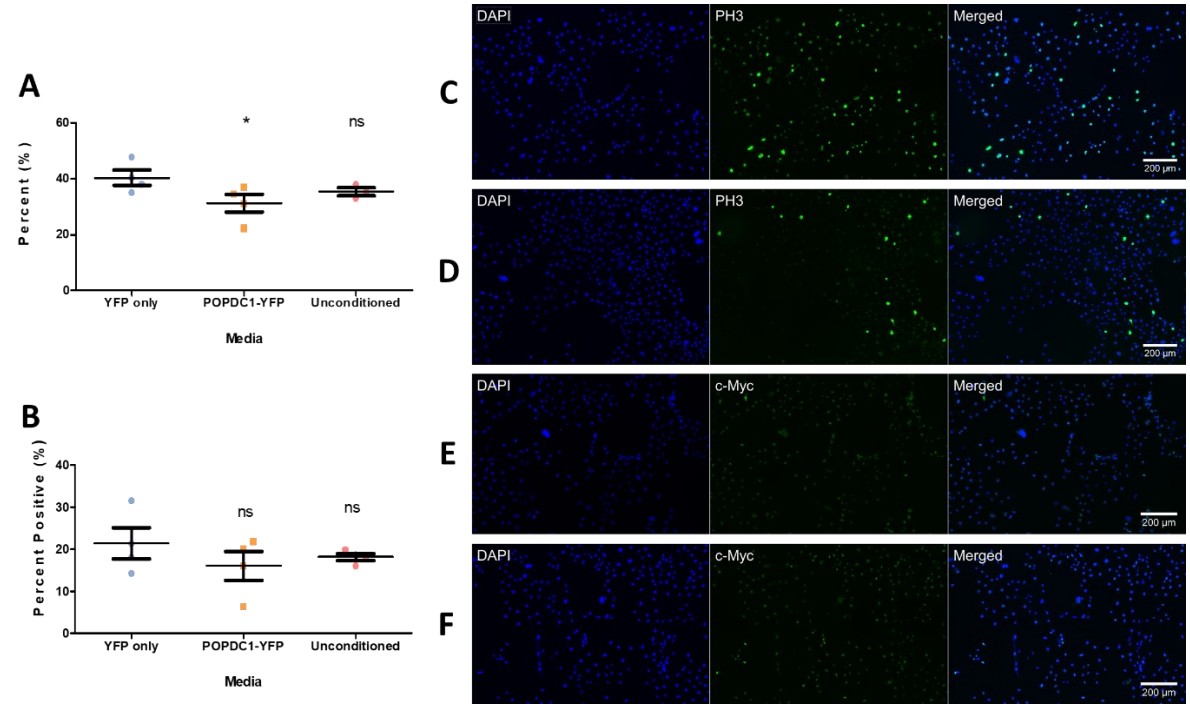

Figure 22 Forced expression of POPDC1 induces secretion of a growth inhibitor. PH3 (**A**, **C**, **D**) or c-Myc (**B**, **E**, **F**) staining of Cos7 cells incubated with 50% (v/v) conditioned medium of Cos7 cells transfected with YFP vector control (**C** and **E**) or POPDC1[WT]-YFP (**D** and **F**). The relative percentage of PH3 (**A**) and c-Myc (**B**) stained cells were quantified using their intensity in FIJI where a threshold was set to confer positivity. POPDC1[WT]-YFP conditioned media significantly reduced proliferation in Cos7 cells (t=2.179; df=6; p<0.05) compared to YFP vector control conditioned media. There was no difference between the YFP vector control and unconditioned media (t=1.447; df=5; p>0.05). The difference in c-Myc positive cell was not significantly different for the POPDC1[WT]-YFP conditioned (t=1.048; df=6; p>0.052) or the unconditioned (t=0.855; df=6; p>0.05) compared the YFP vector control conditioned media. Numerical data were analysed using a T-test in Graphpad Prism. Data are reported as mean ± standard error of the mean. * indicates a significance of p≤0.05 and ns represents no significance when compared to vector-only control. 4 replicates were used for each group.

3.3 Results: c-Myc expression in the mouse heart

Following the finding that forced expression of POPDC1 or -2 could affect the endogenous c-Myc levels in cultured cells (Figure 20), I also wanted to explore whether the loss of POPDC genes could affect c-Myc levels in the heart. Sections were taken from left ventricular tissue of *Popdc1* null mutants and wild type mice and stained for both POPDC1 and c-Myc. Confocal images were collected, and FIJI was used to analyse the images to determine the number of c-Myc-positively stained nuclei. The average percentage of c-Myc-positive nuclei was significantly higher in *Popdc1* null mutant mice compared to wild type (83% in *Popdc1* null mutants and 69% wild type) (Figure 23). This suggests that in the absence of POPDC1 there is an increased expression of c-Myc in the mouse ventricle. In summary, both forced expression of POPDC1 or POPDC2 in Cos-7 cells and loss of function of *Popdc1* in the heart suggests that POPDC negatively control c-Myc expression.

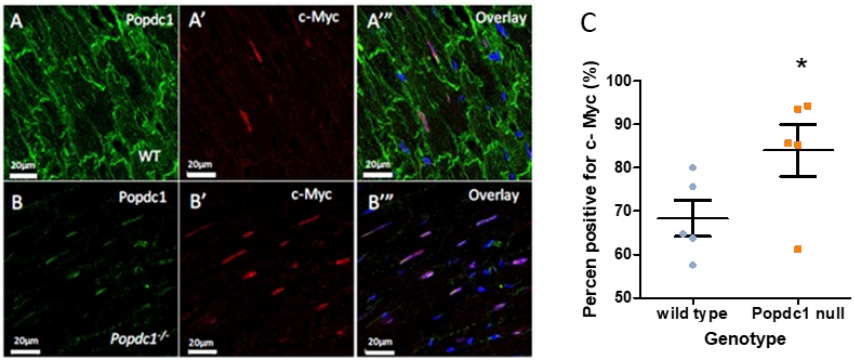

Figure 23 Increased c-Myc staining in ventricular tissue of *Popdc1* null mutants compared to wild type mice. Cryostat sections (10µm) from wild type (**A**) or *Popdc1* null (**B**) mouse left ventricles were made and immunohistochemistry was carried out to detect POPDC1 using an anti-Popdc1 antibody (green) (A-B) and c-Myc using an anti-c-Myc antibody (red) (**A'** and **B'**). Cell nuclei were stained with DAPI (blue) and images were merged (**A'''** and **B'''**). The number of nuclei stained for c-Myc from A and B was quantified in **C**. Nuclei were taken to be positive if they reached an intensity threshold as defined and recorded by FIJI. Numerical data were analysed using T-test in GraphPad Prism and *Popdc1* null mice had significantly higher expression of c-Myc ($t=2.147$; $df=8$; $p<0.05$). Data are reported as mean ± standard error of the mean. * indicates a significance of $p \leq 0.05$ when compared to wild type. Cardiac tissue of five mice was used for each group.

3.4 Discussion

POPDC proteins and specifically POPDC1 have been noted many times for their involvement in different types of cancer (Parang *et al*., 2016, Wang *et al*., 2014, Han *et al*., 2015, Amunjela and Tucker, 2017b). They are thought to act as tumour suppressors due to their involvement in cell cycle control, EMT and cell adhesion (Williams *et al*., 2011, Han *et al*., 2014, Osler *et al*., 2005b, Russ *et al*., 2011, Amunjela *et al*., 2019, Smith *et al*., 2008, Parang *et al*., 2016, Zhan *et al*., 2017, Thompson *et al*., 2018, Kliminski *et al*., 2017). In this study, I was particularly interested in the ability of POPDC proteins to interact with the cell cycle protein, c-Myc. Regulation of the cell cycle in cardiomyocytes is of interest as many MI patients develop heart failure due to the substitution of muscle with scar tissue as cardiomyocytes have poor proliferative ability in the human heart (Bergmann *et al*., 2009). Therefore, it is imperative that research efforts aim to achieve the replacement of lost myocardium so that these patients have a full recovery. My data suggest that POPDC proteins could be a potential target for aiding the recovery of the injured myocardium as they are highly expressed in the heart (Andrée *et al*., 2000) and POPDC1 has been shown to interact with c-Myc (Parang *et al*., 2016).

In this chapter, I have confirmed that c-Myc interacts with POPDC1 and also demonstrated an interaction with POPDC2 and POPDC3. Moreover, I have sought to define the binding sites of c-Myc and PR61α on POPDC1. I have shown that in cell culture this interaction causes downregulation of endogenous c-Myc and may inhibit cell proliferation in a paracrine fashion. Finally, I have shown that when POPDC1 is absent in the mouse heart that there is an increase in c-Myc expression.

3.4.1 The POPDC protein family can interact with c-Myc

CoIPs were used to uncover the interaction between c-Myc and PR61α and the three POPDC isoforms in transfected Cos7 cells. The Williams group first described the interaction of POPDC1 and c-Myc in HEK293 cells, which has been confirmed in this study (Parang *et al*., 2016). Moreover, the interaction of c-Myc with POPDC2 and POPDC3 has been established. Although the POPDC isoforms display sequence similarity (Andrée *et al*., 2000), this finding is unexpected due to the report that c-Myc

binding to POPDC1 is mediated by a sequence, which is not conserved amongst the POPDC isoforms (Parang *et al*., 2016). It is however a significant observation as c-Myc is a "master" regulator of transcription and is also involved in chromatin remodelling making it more accessible for the transcriptional machinery (Vervoorts *et al*., 2006, Frank *et al*., 2003, Liu *et al*., 2003, McMahon *et al*., 2000). Interestingly, PKA, another cAMP binding protein, is also able to regulate c-Myc through phosphorylation (Padmanabhan *et al*., 2013). However, unlike POPDC1, PKA phosphorylation offers protection from proteasomal degradation (Padmanabhan *et al*., 2013) and c-Myc can subsequently go on to upregulate the expression of PKA subunits (Wu *et al*., 2002). Thus, we can understand the promotion of c-Myc degradation by POPDC proteins and the PKA-mediated preservation of c-Myc levels as opposite regulatory inputs on the cell cycle, which is interesting given that PKA and POPDC have also opposite effects on heart rate and hippocampal LTP formation (Froese *et al*. 2012, Shetty *et al*. 2021).

Previous studies suggested the binding site on POPDC1 is located in a sequence near the end of the carboxy-terminal domain (Parang *et al*., 2016), which is a highly divergent region and isoform-specific and so unlikely to be correct as this study has shown that POPDC2 and POPDC3 are also able to interact with c-Myc and PR61α. Therefore, I also started to map the binding site for c-Myc and PR61α on POPDC1. CoIP experiments show PR61α binding to POPDC1 between the 233rd and 244th residues. However, binding array experiments show binding of c-Myc at residues 120th and 130th, which is much more N-terminal than the mapping results from the deletion analysis. Based on 3D model predictions both of the sites found for binding c-Myc and PR61α are located on the outside surface of the protein and so would be accessible for binding. I also see good conservation in these regions both between different POPDC isoforms and between different species (Andrée *et al*., 2000), and as we see that all three isoforms can bind to both PR61α and c-Myc this adds some credibility to the binding sites found. However, I would expect these binding regions to be the same as POPDC1 is expected to bind to c-Myc through PR61α (Parang *et al*., 2016). Both methods could affect the tertiary structure of POPDC1, which may account for the differences. c-Myc may also interact through proteins other than PR61α,

causing differences in binding. Although, 3D models predict that these two putative binding sites are located in close proximity to the POPDC1 protein, and so it is plausible that the complex could be formed with c-Myc and PR61α having separate binding sites on the protein. However, as two different methods were employed for the mapping experiments, further verification is required, ideally by performing the mapping experiments using both methods and getting independent verification and confirming the binding site through site-directed mutagenesis. Both of these experiments were however not performed due to time limitations.

3.4.2 Changes in POPDC1 levels can affect c-Myc levels and cell proliferation

I have demonstrated that overexpression of POPDC1 and POPDC2 in transfected cells reduced endogenous c- Myc levels, suggesting that POPDC1 can not only bind but also cause downregulation of c-Myc. This result is in keeping with the model proposed by the Williams group who suggests that POPDC1 can dephosphorylate c-Myc, through PP2A's catalytic subunit PR61α, targeting it for proteasomal degradation (Parang *et al*., 2016). POPDC1's ability to reduce the levels of the master cell cycle regulator, c-Myc, also supports the role of POPDC1 in cancers, where its knock-down or knockout correlates with a poor prognosis of cancer (Parang *et al*., 2016, Wang *et al*., 2014, Han *et al*., 2015, Amunjela and Tucker, 2017b).

In this chapter, I have also shown that media conditioned by POPDC1 transfected Cos7 cells can cause a reduction in proliferation, as shown by staining with the mitotic marker, phosphohistone 3, this was also seen in C2C12 cells (Adeeba Ali, personal communication). This suggests that POPDC1 may induce the secretion of a yet to be characterised growth inhibitor such as myostatin (GDF8) or GDF11 (Egerman *et al*., 2015, Hammers *et al*., 2017, McPherron *et al*., 1997) into the media, which may have a paracrine effect on the proliferation of neighbouring cells. c-Myc expression was also observed in cells that had been subjected to conditioned media, but no difference was seen between POPDC1 transfected cells and those receiving the empty control vector, suggesting that POPDC1 cannot affect c-Myc expression in a paracrine fashion. I had also expected that POPDC1 transfection would decrease

proliferation in cells that themselves had been transfected as I had seen that c-Myc has a reduced expression in these cells and is capable of regulating the cell cycle on many levels (Martinato *et al*., 2008, Bretones *et al*., 2015). However, this was not seen and proliferation was similar between POPDC1- and vector-only transfected cells. This could indeed be because POPDC1 seems to trigger the release of a yet to be fully characterised paracrine signals, but as proliferation was generally lower in the transfected samples it cannot be ruled out that the stress of the transfection itself could be reducing proliferation in both POPDC1 and vector-only transfection experiments. The finding that cells that are expressing reduced levels of c-Myc do not also have reduced proliferation may be a testament to the fact that the mechanisms of cell proliferation are hugely complex with many different players acting together to determine whether the threshold is crossed to allow a cell to proliferate (Gordon *et al*., 2018).

3.4.3 c-Myc in the heart

Literature from mammalian models suggests that c-Myc is not expressed in the adult heart under normal physiological conditions (Seigo *et al*., 1988, Pollack *et al*., 1994), however, has a role to play in the developing heart (Jackson *et al*., 1990). In this chapter I have shown, that akin to cell culture, when POPDC1 levels are low like in *Popdc*1 null mice, there is an increase in nuclei that are expressing c-Myc. However, unlike previous results in the literature, I did find there to be nuclear staining of c-Myc in wild type hearts that were kept under normal physiological conditions. Reasons for these differences could lie in the different techniques being used to detect c-Myc, immunostaining to look at protein levels in the case of this study and northern blots to see gene expression in the case of the literature. Detection of c-Myc in wild type hearts could also be the result of an antibody that is binding non-specifically, for example, there are other Myc proteins (N-myc and L-myc) present in mice that the c-Myc antibody which has been employed may be also detecting. However, other research groups have not found this to be an issue with the c-Myc antibody used on human samples and so it can likely also be ruled out for the mouse as well (Dammert *et al*., 2019). Further work would have to be

conducted to ensure that it is indeed c-Myc that is truly being detected and upregulated by the absence of POPDC1 in this work.

3.4.4 Conclusions and future directions

Overall, I have confirmed the physical interaction between the POPDC1 and c-Myc, as well as discovering an interaction with the other POPDC isoforms. I have also shown that in cell culture forced expression of POPDC1 reduces c-Myc expression and cell proliferation in a paracrine fashion. Finally, I have shown that c-Myc is expressed in the heart and this changes with *Popdc1* expression in the mouse heart. All of this suggests that the POPDC proteins can interact with and affect the protein levels of c-Myc and that this process may also be present in the heart. Going forward I wanted to focus on Popdc1's effect on the regenerative profile of the zebrafish ventricle and to understand if c-Myc could increase the proliferation after injury.

However, many questions were brought up from the results in this chapter and which may have been interesting to explore but were considered to be out of the scope of this thesis. Such as performing both binding site experiments with c-Myc and PR61α to understand the binding in more depth. From there, site-directed mutagenesis of POPDC1 could be performed to alter the binding site to prove its identity and determine which residues are required for binding. If such a mutation could cause some of the same effects as knocking out *Popdc1*, we can assume that the interaction of POPDC1 with c-Myc is causally involved in these phenotypes. It may also be interesting to follow up on POPDC1 having a paracrine effect on proliferation in cell culture by studying the supernatant and assessing whether there is evidence for enhanced secretion of a growth inhibitor such as myostatin.

4. Further characterisation of the *popdc1* null zebrafish and mouse

Although a *Popdc1* null mutant had been generated in the mouse almost 20 years ago (Andrée *et al*., 2002a), a *popdc1* null mutant in zebrafish has only recently been engineered. The line was created using TALEN-mediated gene engineering, which targeted exon 1 causing a 1 base pair deletion, which resulted in a premature stop codon (Brand Lab, Unpublished). The deletion caused a frameshift and is predicted to encode a 39 amino acid truncated protein, which neither contains the transmembrane or the Popeye domains and will either not be translated or likely be subjected to proteolytic degradation (2.8.2 Generation of the *popdc1* null mutant). Alternatively, the mRNA could be subject to nonsense-mediated decay, a surveillance pathway, which reduces errors in gene expression by removing transcripts that contain premature stop codons (Frischmeyer and Dietz, 1999).

The p*opdc1* null mutant appeared to display normal embryonic and larval development and was able to grow into adulthood. However, it has been observed that in the first week after fertilisation a small number of homozygous mutants suffer from pericardial effusion due to cardiac arrhythmia similar to what has been described for the popdc1^{S201F} mutant (Schindler *et al*. 2016). I focused on the adult *popdc1* null mutant heart, which so far hasn't been properly characterised. I determined the size of the heart and that of isolated cardiomyocytes. Moreover, I analysed the morphology of the adult *popdc1* null mutant heart and its position in the body cavity. Furthermore, the impact of the loss of *popdc1* on the expression and subcellular localisation of the other POPDC isoforms was investigated. The work described in this chapter forms the basis for the molecular analysis described in the following chapters.

4.1 Popdc1 staining is absent in the *popdc1* null mutant

Wild type and *popdc1* null mutant atria were stained for Popdc1. In the wild types, there was a strong membrane stain, however, in the *popdc1* null mutants, there was a greatly reduced staining, which was also present in unstained control tissue and therefore presumed to represent background staining

(**Error! Reference source not found.**). This result confirms that in the *popdc1* null mutants no Popdc1 p rotein was expressed.

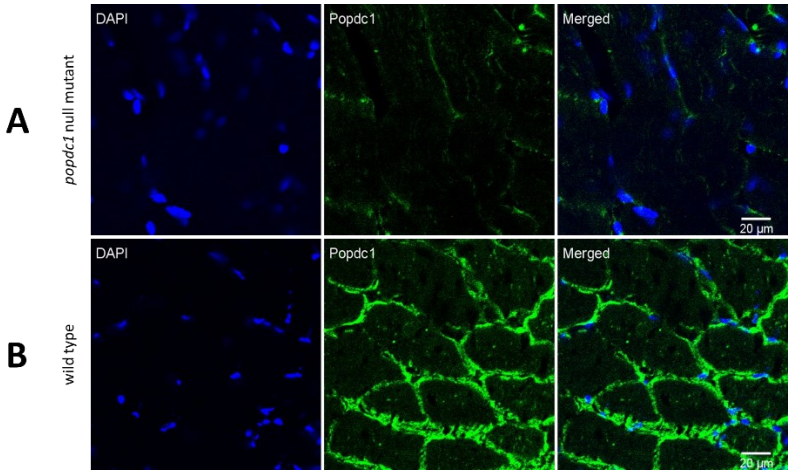

Figure 24 Popdc1 staining is lost in the *popdc1* null mutant zebrafish skeletal muscle. 10µm cryosections of skeletal muscle tissue of *podpc1* null mutants (**A**) and wild type (**B**) were stained for DAPI (blue) and Popdc1 (green). n=3

4.2 Results: The loss of *popdc1* affects the expression and subcellular localisation of the other POPDC isoforms

As patients with mutations in genes of the POPDC family display disruptions to the localisation of other POPDC family members (Schindler *et al*., 2016b, De Ridder *et al*., 2019, Rinné *et al*., 2020), the subcellular localisation of Popdc2 and the mRNA expression of *popdc2* and *popdc3* was studied in the *popdc1* null mutant zebrafish. Moreover, the localisation of POPDC2 was also investigated in *Popdc1* null mutant mice.

4.2.1 Subcellular localisation of POPDC isoforms in the *popdc1* null mutant zebrafish

Sections of wild type and *popdc1* null mutant ventricles were immunohistochemically stained for Popdc2. In wild type ventricular myocytes, Popdc2 was mainly localised at the plasma membrane. However, in the *popdc1* null mutant, no staining was present at the plasma membrane and only some weak and diffuse intracellular staining was observed (Figure 25A and B), suggesting that the ablation of *popdc1* caused a reduction and mislocalisation of Popdc2 protein similar to what has been

described for the *popdc1*^{S201F} mutant (Schindler *et al*. 2016). RT-qPCR analysis was also performed to look at the mRNA levels of *popdc2* and *popdc3* in ventricular tissue of the *popdc1* null mutant and the expression of both genes was significantly reduced in comparison to wild type (Figure 25C and D).

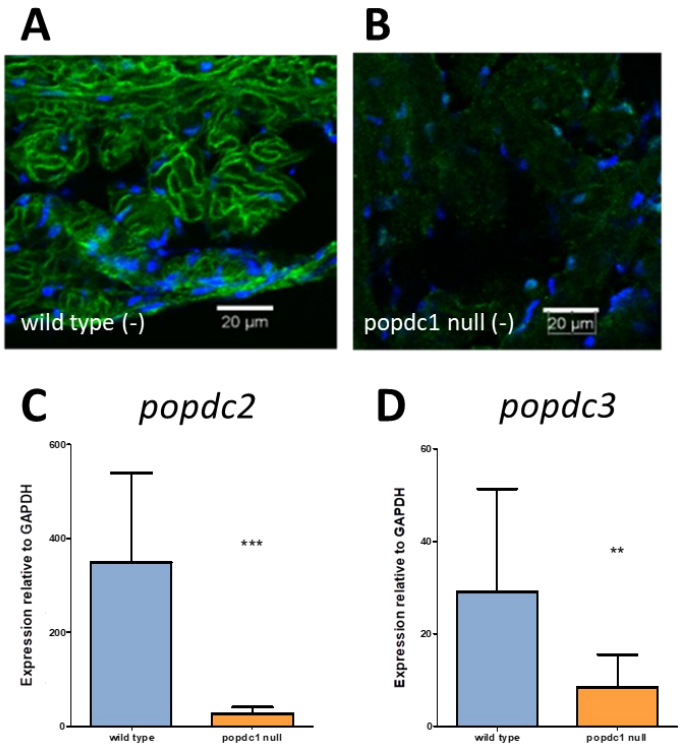

Figure 25 *popdc1* null mutants have reduced RNA and protein expression of the other POPDC family members compared to their wild type counterparts. Immunostaining of zebrafish ventricular tissue of wild type (-) (**A**) and *popdc1* null (-) mutant (**B**) stained with a Popdc2 antibody (green) and counterstained with DAPI (blue) to observe the nuclei. qPCR analysis of zebrafish ventricular tissue isolated from wild type and *popdc1* null mutants, showing significantly reduced levels of *popdc2* (t=1.697; df=14; p<0.001) (**C**) and *popdc3* (t=0.8837; df=14; p<0.01) (**D**) in the *popdc1* null mutant normalised against GAPDH. Statistical analysis was performed using a t-test, ** represents p<0.01 and *** represents P<0.001, n=8. Data are reported as mean ± standard error of the mean.

4.2.2 Popeye family members in the *Popdc1* null mouse

As the subcellular localisation of Popdc2 in the *popdc1* null mutant zebrafish heart was strongly abnormal, the *Popdc1* null mutant in mice was also studied. Similar to the zebrafish, I also saw that Popdc2 staining was greatly reduced in *Popdc1* null mutant compared to wild type (Figure 26). In ventricular tissue, I observed a strong reduction in staining that is believed to be at the membrane and t-tubules of cardiomyocytes, although no secondary markers were used (Figure 26A and B). In the atrium, a strong reduction in membrane staining was observed. However, in contrast to the ventricle

where only faint nuclear staining was present, in atrial myocytes of the *popdc1* null mutant, strong nuclear membrane and perinuclear staining was observed (Figure 26C and D). Moreover, an increase in granular staining, which may correspond to intracellular vesicles was present in both atrial and ventricular myocytes (Figure 26).

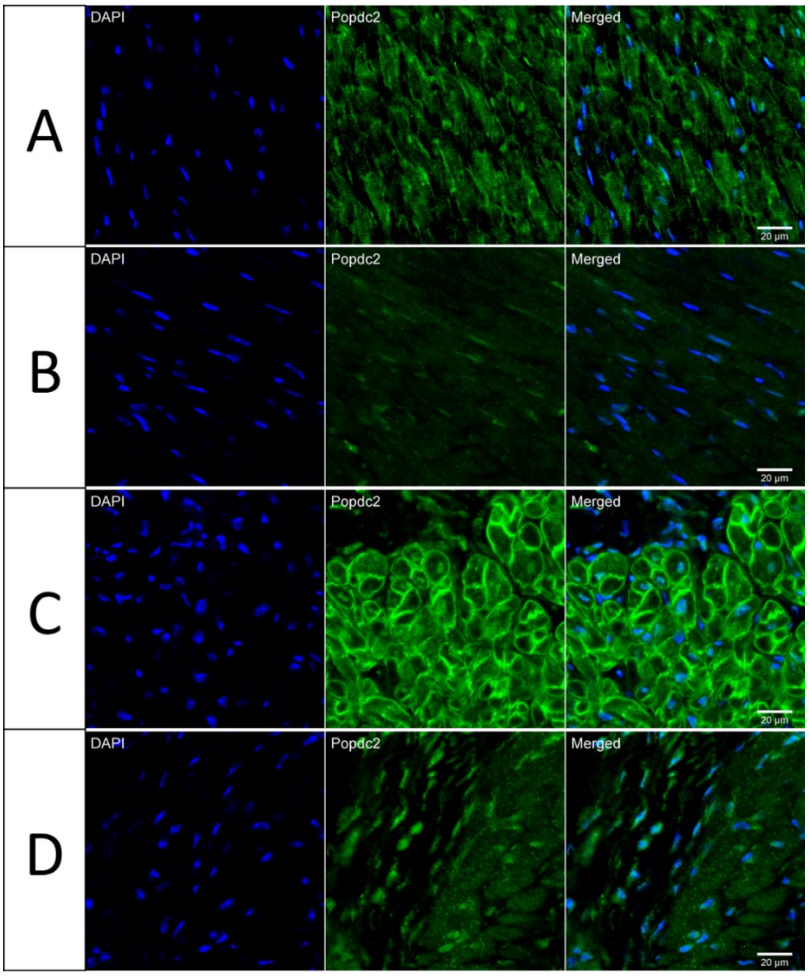

Figure 26 POPDC2 displays an abnormal staining pattern in the heart of *Popdc1* knock out mice. POPDC2 (green) and DAPI (blue) staining of sections of mouse ventricular (**A** and **B**) and atrial (**C** and **D**) tissue isolated from wild type (**A** and **C**) and *Popdc1* null mutant (**B** and **D**). Sections were counterstained with DAPI. n=2.

4.3 Results: *popdc1* null mutant zebrafish display an increased survival rate

A proportion of *popdc1* null mutants encountered pericardial effusion in the first week following fertilisation (Brand Lab, Unpublished), however, this did not cause differences in survival of *popdc1* null zebrafish embryos compared to wild types up to 5 dpf (Figure 27A). However, the survival until

adulthood had not been previously analysed. In this study, zebrafish were monitored for survival between the time of moving the fry from the embryo incubator into the main system at 5dpf until they reached adulthood at 3 months post fertilisation. Fish of both wild type and *popdc1* null mutant genotypes were moved to the system into 3-litre tanks at the same density. Interestingly and unexpectedly, it was found that *popdc1* null mutants had a higher survival rate, which was 47% whereas wild type had a survival rate of 35%, although survival rates of both genotypes were lower than expected (Figure 27B).

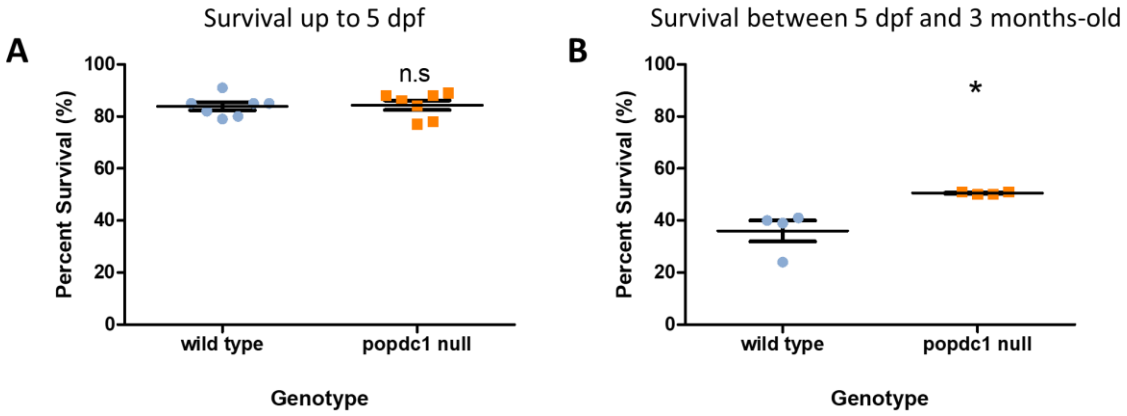

Figure 27 *popdc1* null zebrafish have increased postembryonic survival compared to wild type. Eggs were collected from matings and unfertilised eggs were removed. The embryos were counted at 0 dpf and 5dpf to discover the percent survival until 5 dpf of wild type and *popdc1* null mutants (**A**). Fry was moved to the system at 5dpf and the number of fish per tank was recorded. Wild type and mutant fish were kept at the same density of 50 fish per 3 l tank. The number of fish surviving into adulthood was determined at three months and the percent survival was determined (**B**). *popdc1* null mutants displayed a significantly increased survival ($t=3.079$; $df=6$; $p<0.05$). Statistical analysis was performed using a t-test * represents $p<0.05$, $N\geq4$. Data are reported as mean ± standard error of the mean.

4.4 Results: *popdc* mutants display a reduced heart and body size

Transgenic expression of c-Myc is known to affect cardiomyocyte number and overall organ size in the mouse (Jackson *et al.*, 1990). Moreover, it has recently been described that POPDC1 is a tumour suppressor and can degrade c-Myc (Parang *et al.*, 2016). Therefore, in this section, I determined the heart size, cardiomyocyte size and body size of wild type and *popdc1* null mutant zebrafish (and in some instances, I also obtained some data in mice) to compare it to the published data in transgenic mice with a forced expression of c-Myc in the heart.

4.4.1 *popdc1* null mutants in zebrafish have larger hearts

Jackson *et al* found that c-Myc overexpression in the murine heart caused an increase in organ size (Jackson *et al*., 1990). Zebrafish hearts were assessed for an alteration in heart size at 6 months post fertilisation. I saw that when taking the heart weight-to-body length ratios that *popdc1* null mutant zebrafish had larger hearts compared to wild type (**Figure 28**). This is different from what is seen in the mouse where *Popdc1* null mutants do not have larger hearts (Alcalay *et al*., 2013, Froese *et al*., 2012).

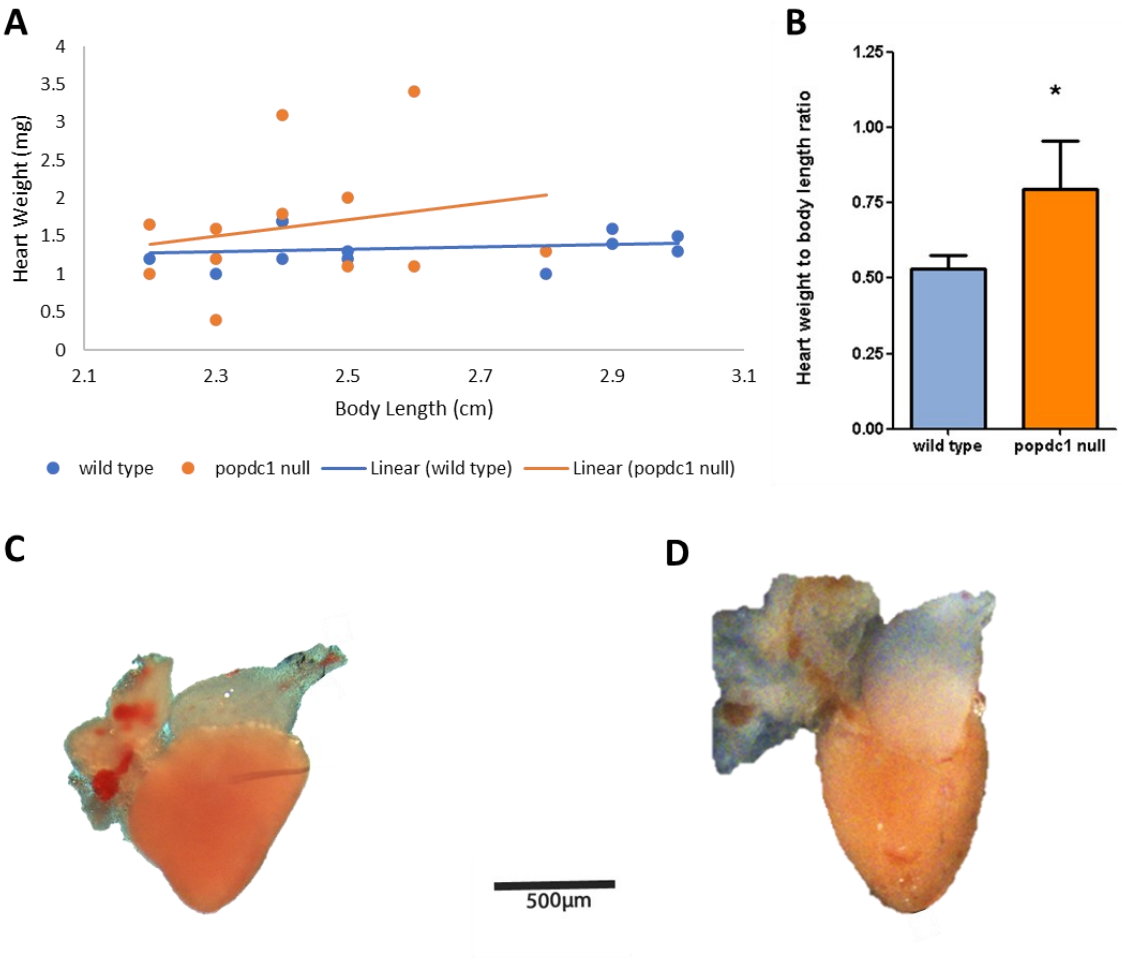

Figure 28 *popdc1* null mutant zebrafishes have larger hearts. (**A**) The absolute heart weight and body length of wildtype and *popdc1* null mutant zebrafish plotted against one another. (**B**) Heart weight-to-body length ratios for *popdc1* null mutant and wild type hearts. Example of a heart of a wild type (**C**) and *popdc1* null mutant (**D**). *popdc1* null mutants had significant larger hearts than wild types (t=1.833; df=12: p<0.05). Statistical analysis was performed using a *t*-test in GraphPad Prism with * representing p<0.05. n=6. Data are reported as mean ± standard error of the mean.

4.4.2 *popdc1* null mutants have a smaller body length

The body length of wild type or *popdc1* null mutants was also determined at 10 months post fertilisation. The fish were kept as siblings in mixed genotype tanks until genotyping occurred at 9 months post fertilisation. The fish were kept at the same density as tank density is known to affect the growth of zebrafish (Ribas *et al.*, 2017). It was observed that the *popdc1* null mutants had a significantly smaller body length than their wild type siblings (Figure 29).

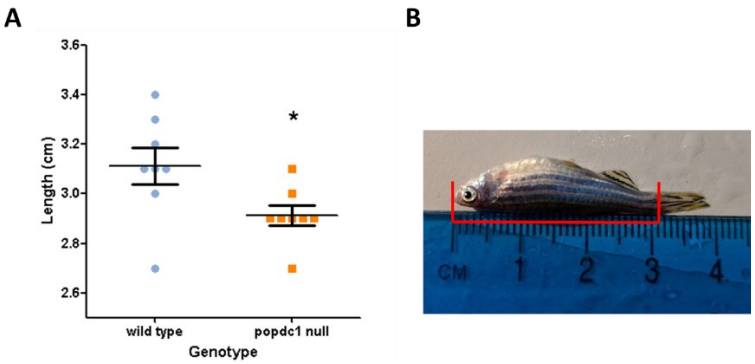

Figure 29 *popdc1* null zebrafish have a smaller total body length compared to wild type siblings. The body length of wild type and *popdc1* null mutants were measured from the snout to the base of the peduncle fin. (**A**) Quantification of the body length of 10 months post fertilisation wild type and *popdc1* null mutant siblings. (**B**) An example of the length measurement, with the fish aligned against a ruler and red lines aligning the snout, the base of the peduncle fin and the distance between the two anatomical markers. *popdc1* null mutants were significantly smaller than wild type ($t=2.374$;$df=14$; $p<0.05$). Statistical analysis was performed using a *t*-test in GraphPad Prism with * representing $p<0.05$. n=8. Data are reported as mean ± standard error of the mean.

4.4.3 popdc1 null mutants in zebrafish and mice have smaller cardiomyocytes

Transgenic overexpression of c-Myc in the mouse heart caused a decrease in cardiomyocyte size (Jackson *et al.*, 1990) and so I studied cardiomyocyte size using different methods in *Popdc1* mutants in both mouse and zebrafish models.

4.4.3.1 Cell size determination of cardiomyocytes in zebrafish

To determine cell size in cardiomyocytes in the zebrafish heart, sections were stained with WGA. WGA is a lectin, which labels the basement membrane and is often used for histological determination of cell size. Animals investigated in this study were three months of age. FIJI was then employed to determine the cell sizes. Ventricular cardiomyocytes of *popdc1* null mutants tended to be smaller

compared to wild type although the difference between genotypes did not reach statistical significance (Figure 30A-C).

Although WGA staining is accepted as a proper means to determine the cross-sectional area, I found that many of the cells were overlapping, making it difficult to be certain of the measurements. As an alternative approach, the cell size was also investigated in isolated cardiomyocytes. Isolated ventricular cells were fed into an ImageStream®X Mark II Imaging Flow Cytometer, this sorted the GFP fluorescent cardiomyocytes from other cell types and then determined the cell area. Ventricular cardiomyocytes of *popdc1* null mutants were significantly smaller compared to wild type using this method (Figure 30D-G).

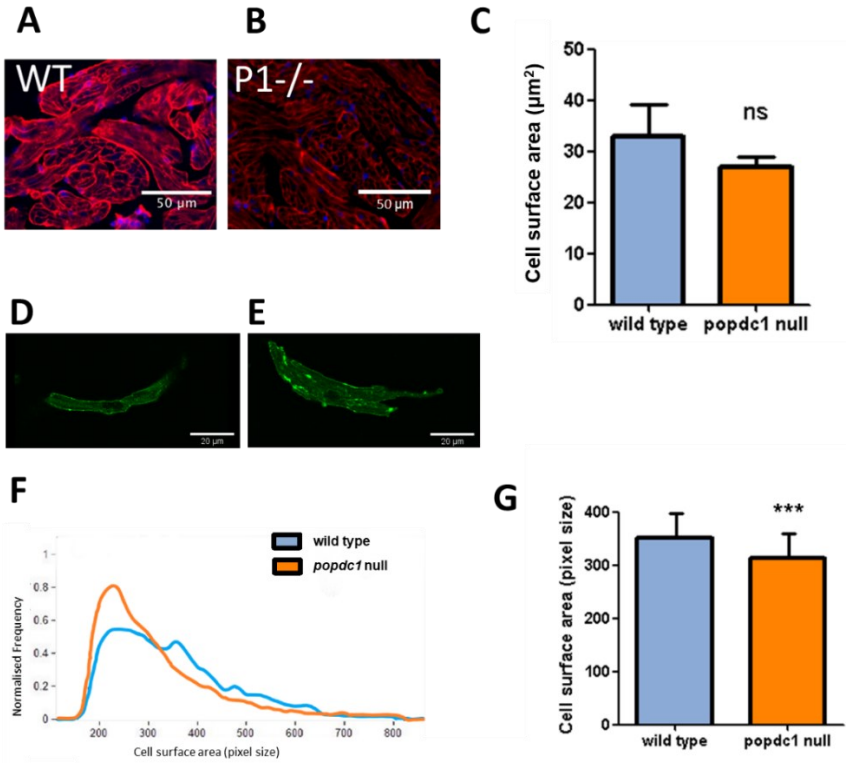

Figure 30 Zebrafish cardiomyocytes of *popdc1* null mutants are smaller than in wild type. (**A-C**) Paraffin sections were cut from whole zebrafish hearts and stained for the membrane marker WGA (red) and DAPI (blue); to detect the boundary of the cell. (**A**) wild type ventricle and (**B**) *popdc1* null ventricle were stained and FIJI was used to make estimations using WGA to label the cell surface area. (**C**) shows a quantification of the cell surface area using GraphPad Prism. With this method cardiomyocyte size was not significantly different (t=08; df=14; p>0.05). ns represents a non-significant result of the *t*-test. (**D-G**) Cardiomyocytes from zebrafish ventricles were isolated and run through an ImageStream®X Mark II Imaging Flow Cytometer to take an image of each GFP expressing cell and then give an estimate of cell surface area. Representative image of cardiomyocytes isolated from *popdc1* null (**D**) and wild type hearts (**E**). The frequency of cells of different sizes is based on these images (**F**). Quantification of the mean surface areas from cells (**G**) where *popdc1* null mutant cells were significantly smaller using a *t*-test (t=9.395; df=1479; p<0.001). GraphPad Prism was used for statistical analysis and *** represents p<0.001. Three fishes of each genotype were used and at least 100 cells were analysed of each specimen. Data are reported as mean ± standard error of the mean.

4.4.3.2 Cell size determination of cardiomyocytes in mice

Since there was tissue available not just of homozygous *Popdc1* null mutants but also of mouse mutants carrying null mutations in the other two POPDC genes, the cell size of ventricular cardiomyocytes using WGA staining was determined in homozygous *Popdc1*, *Popdc2*, *Popdc3* and *Popdc1*/*Popdc2* double knock out null mutants and compared with wild type. Moreover, I determined the cell size of ventricular myocytes isolated from *Popdc1* null mutants and wild type.

As described for the zebrafish heart, sections of mouse ventricular tissue were stained with WGA and analysed with FIJI. *Popdc1* and *Popdc3* null mutants, as well as Popdc1/Popdc2 null mutants, showed a significant reduction in cardiomyocyte size compared to wild type with *Popdc1*/*Popdc2* null mutants displaying the largest size reduction (Figure 31 A-B and D-F). The *Popdc2* null mutant on the other hand did not show a significant reduction in cardiomyocyte size compared with wild type (Figure 31C and F). I also took isolated mouse ventricular cardiomyocytes from wild type and *Popdc1* null mutant mice and determined their size using phase-contrast microscopy and FIJI. With this method, the *Popdc1* null mutant cardiomyocytes were also significantly smaller compared to wild type (Figure 31G-I).

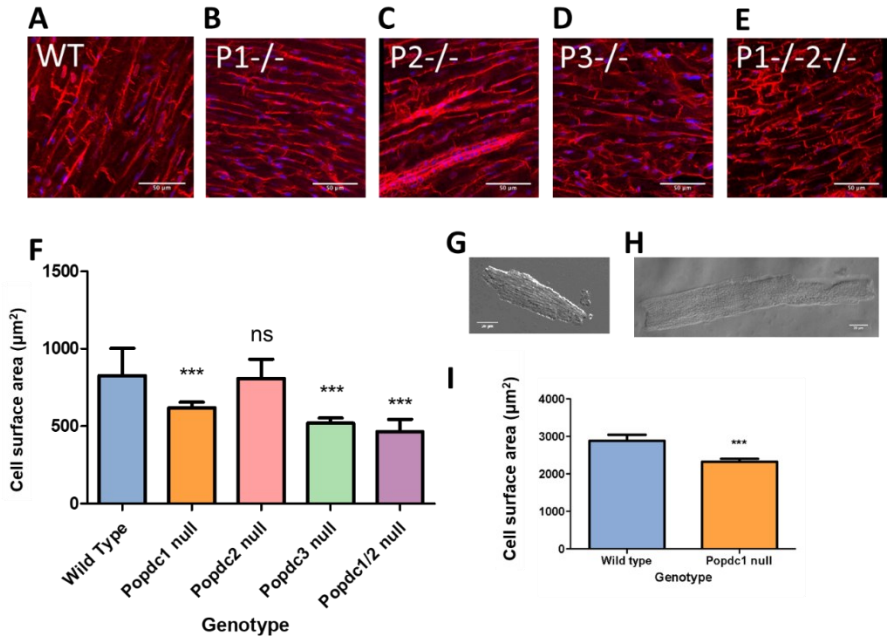

Figure 31 Mouse cardiomyocytes of POPDC null mutants are smaller than in wild type. (**A-F**) Cryosections of mouse hearts were stained for the membrane marker WGA (red) and DAPI (blue). FIJI was employed to estimate the ventricular cell surface area of wild type (WT) (**A**), *Popdc1* null (P1-/-) (**B**), *Popdc2* null (P2-/-) (**C**), and *Popdc3* null (P3-/-) (**D**) and *Popdc1* and *Popdc2* double null mutants ($P1^{-/-}P2^{-/-}$) (**E**) and quantified in **F**. The cell surface area was found to be smaller in the P1-/- (KW=817.9; p<0.001), P3-/- (KW=1632; p<0.001) and P1-/-2-/-(KW=1782; p<0.001) compared to wild type when analysing with a Kruskal-Wallis test in GraphPad Prism. *** represents p<0.001. N=3, n>100. (**G-I**) Isolated left ventricular cardiomyocytes were gifted to me by Dr Navneet Bhogal and imaged using brightfield microscopy. Representative images of a *Popdc1* null cardiomyocyte (**G**) and a wild type cardiomyocyte (**H**). The quantification of cardiomyocyte size (**I**). *Popdc1* null cardiomyocytes were significantly smaller than wild type cardiomyocytes, when analysed using a *t*-test in GraphPad Prism with *** representing p<0.001 (t=3. 39; df=87; p<0.001). N=3, n>10. Data are reported as mean ± standard error of the mean.

4.5 Results: Morphological analysis reveals that *popdc1* null mutants display outflow tract abnormalities and abnormalities in the layers of the myocardium

Assessments were made on zebrafish hearts to determine if the *popdc1* null displayed any other morphological differences apart from the already described difference in organ and cell size. This was investigated both by taking measurements from images of whole hearts as well as by looking at histological sections. It has been described that the shape of the zebrafish ventricle goes from a rectangular shape at the larval stage, to a triangular shape at the juvenile stage to being circular in the adult. Moreover, the angle of the outflow tract axis relative to the ventricular axis increases during development into adulthood as the heart rotates its position in the pericardial cavity (Singleman and Holtzman, 2012). The outflow tract and circularity of the heart was investigated, as well as the size of the cortical and trabecular layer.

4.5.1 Morphological analysis of the *popdc1* null zebrafish

Images were taken of five 6-month-old *popdc1* null mutant and wild type hearts with their atria removed to allow a better view of the ventricular morphology. Measurements were taken from images with a dorsal view of the heart. Several anatomical parameters were determined with the aid of FIJI including ventricular length, ventricular width and length to width ratio, BA length and width, outflow tract angle, ventricle to BA length ratio and circularity. Most of these parameters did not differ between genotypes (Figure 32). However, the *popdc1* null mutants displayed a significantly larger ventricular length-to-width ratio, meaning that the ventricles of the *popdc1* null mutant seemed to be longer and narrower than wild type ventricles (Figure 32C, I-J). Furthermore, the *popdc1* null mutant had a reduced outflow tract angle (Figure 32G and I-J), which is an angle that measures the deviation of the BA axis from base to tip compared to the ventricular axis from apex to base (Figure 12).

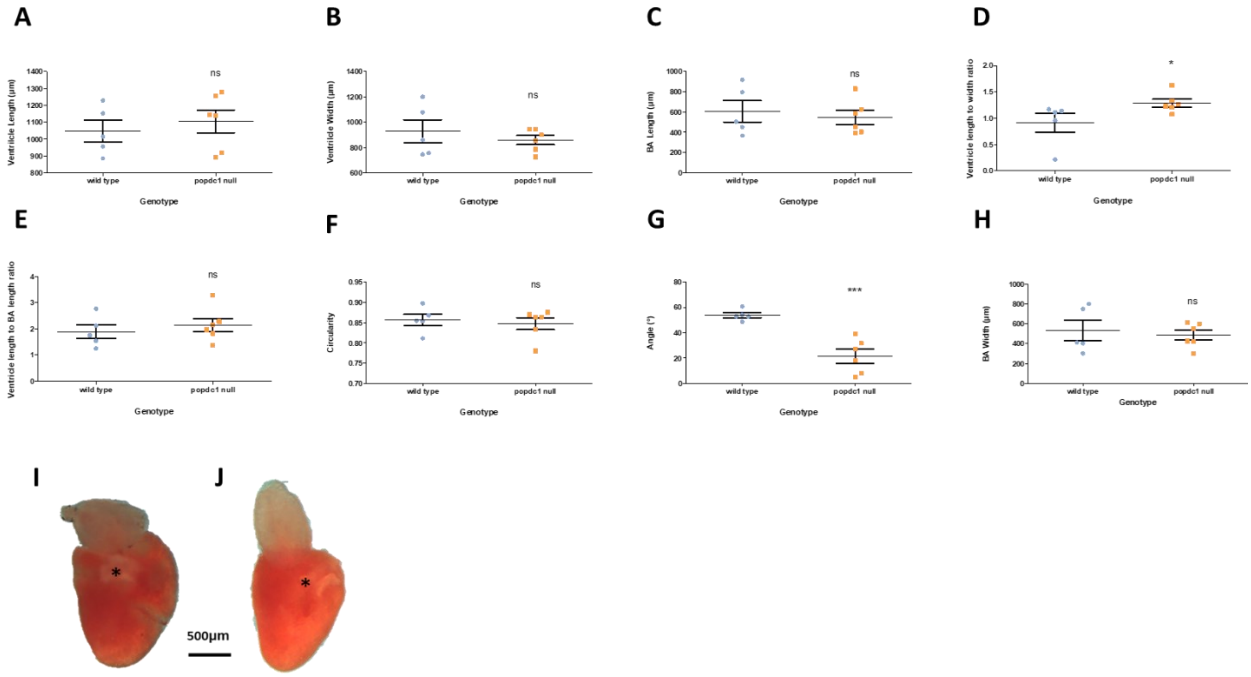

Figure 32 Morphological differences of *popdc1* null mutant zebrafish hearts at 6 months post fertilisation. Several anatomical parameters were measured from images taken from excised zebrafish hearts at 6 months of age including (**A**) ventricular length, (**B**) ventricular width, (**C**) BA length, (**D**) ventricular length-to-width ratio, (**E**) ventricular length to BA length ratio, (**F**) circularity, (**G**) outflow tract angle and (**H**) BA width. The ventricular length to width ratio was significantly larger in the *popdc1* null mutant ($t=2.025$; $df=9$; $p<0.05$) and the outflow tract angle was significantly smaller ($t=5.078$; $df=9$; $p<0.001$).*t*-tests were used to assess statistical differences and the ventricular length-to-width ratio and the BA angle were found to be significantly different with *** representing $p<0.001$ and * representing $p<0.05$, at least 5 fishes were used for each genotype. Data are reported as mean ± standard error of the mean. Representative images were taken of the wild type (**I**) and *popdc1* null mutant (**J**) with the star representing the position of the atrioventricular canal after removal of the atria.

After assessing the morphology of the heart at 6 months of age, I also looked at the same parameters at 3 months of age (Figure 33). Again, I saw that there was a significantly reduced BA angle in the *podpc1* null mutant (Figure 33G and I-J), but there was no significant difference in the ventricular length to width ratio (D and I-J). Instead, *popdc1* null mutants at 3 months of age had a reduced ventricular width (Figure 33B and I-J), BA length (Figure 33Cand I-J), and circularity (F and I-J).

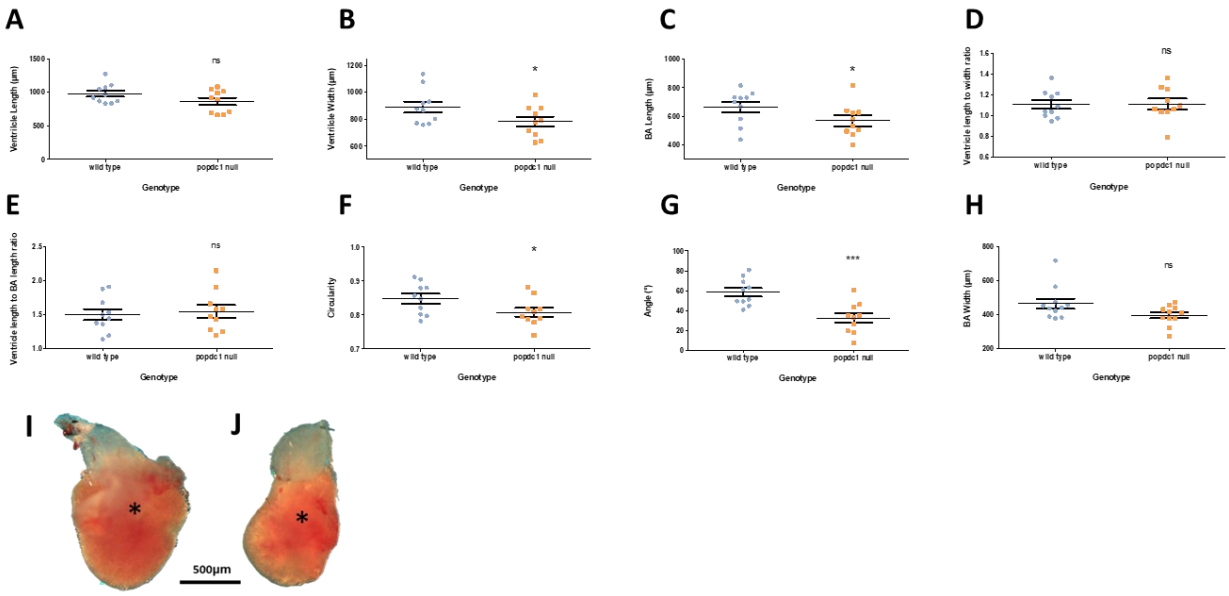

Figure 33 Morphological differences of *popdc1* null zebrafish hearts at 3 months post fertilisation. Several anatomical parameters were measured from images taken from excised zebrafish hearts at 3 months of age including (**A**) ventricle length, (**B**) ventricle width, (**C**) BA length, (**D**) ventricular length to width ratio, (**E**) ventricular length to BA length ratio, (**F**) circularity, (**G**) outflow tract angle and (**H**) BA width. Ventricular width (t=1.959; df=18; p<0.01), BA length (t=1.849; df=18; p<0.05), circularity (t=2.031; df=18; p<0.01) and outflow tract angle (t=3.992; df=18; p<0.001) were all significantly reduced in the *popdc1* null mutants. A *t*-test was used to assess the statistical significance of the differences and ventricular width, BA length, circularity and BA angle were found to be significantly different with *** representing p<0.001 and * representing p<0.05, n=10. Data are reported as mean ± standard error of the mean. Representative images were taken of the wild type (**I**) and *popdc1* null (**J**) with the star representing where the atrioventricular canal is positioned.

Finally, I performed the morphological analysis on hearts at 28dpf (Figure 34). At this stage, the fish and their hearts were too small to isolate them without the aid of a microscope. To ensure that I was looking at the heart during dissection I made use of the GFP expression in the cardiomyocytes of the hearts to ensure the removal of heart tissue. Unlike in hearts at 3 and 6 months of age, there was no significant difference in the outflow tract angle between the *popdc1* null mutant and wild type (E and I-J). However, both ventricular length and width were significantly larger in the *popdc1* null mutants at this time point (Figure 34B-C and I-J). Thus, the observed changes in outflow tract morphology are only developing in early adulthood.

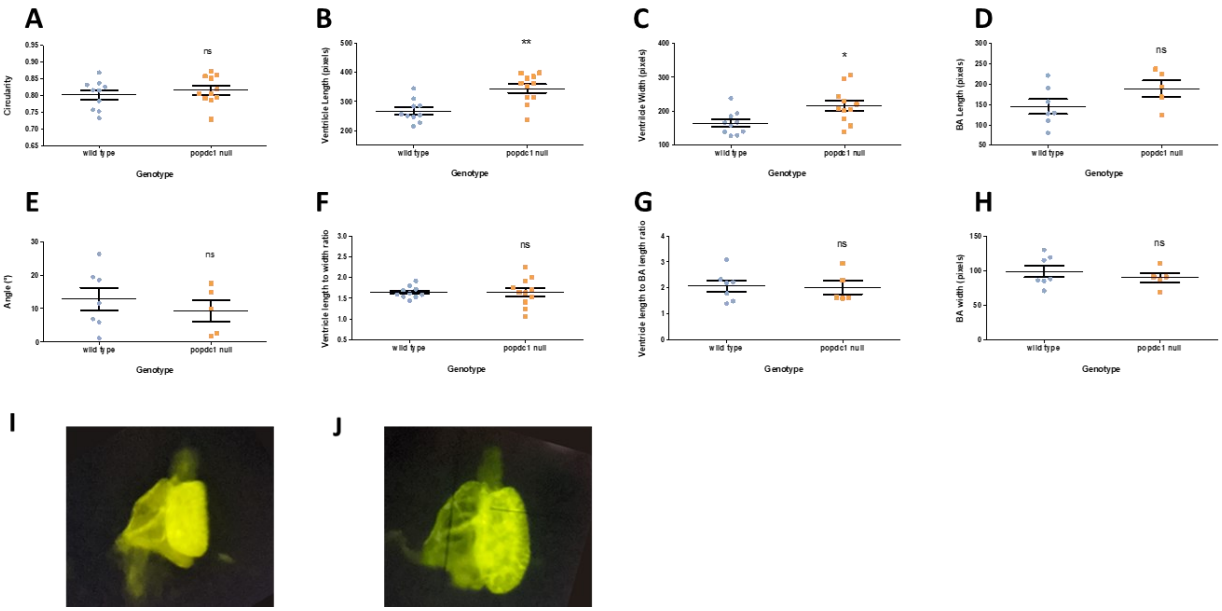

Figure 34 Morphological differences of *popdc1* null zebrafish hearts at 28dpf. Several measurements were made from images taken from excised zebrafish hearts at 28dpf including (**A**) circularity, (**B**) ventricle length, (**C**) ventricle width, (**D**) BA length, (**E**) outflow tract angle (**F**) ventricular length to width ratio, (**G**) ventricular length to BA length ratio and (**H**) BA width. Ventricular width (t=2.684; df=19; p<0.05) and length (t=3.88; df=19; p<0.01) were significantly larger in the popdc1 null mutants at this time point. T-tests were used to assess differences and ventricular length and ventricular width were seen to be significantly different with ** representing p<0.01 and * representing p<0.05, at least 5 fish were used from each genotype. Data are reported as mean ± standard error of the mean. Representative images were taken using a GFP filter on a fluorescence microscope of the wild type (**I**) and *podpc1* null (**J**) hearts after they had been excised.

4.5.2 Histology to reveal outflow tract abnormalities in the *popdc1* null zebrafish

Further to looking at the morphology from the whole heart, I also wanted to see if the difference in the outflow tract angle could also be observed in histological sections. H&E staining was performed on paraffin sections and the outflow tract angle was measured between the line from the base to the apex of the ventricle and the base to the tip of the BA. This was done via taking images under brightfield illumination and taking measurements with the aid of FIJI. It was found that like in the whole hearts when looking at sections there was a significant decrease in the outflow tract angle in the *popdc1* null mutant fish heart (Figure 35).

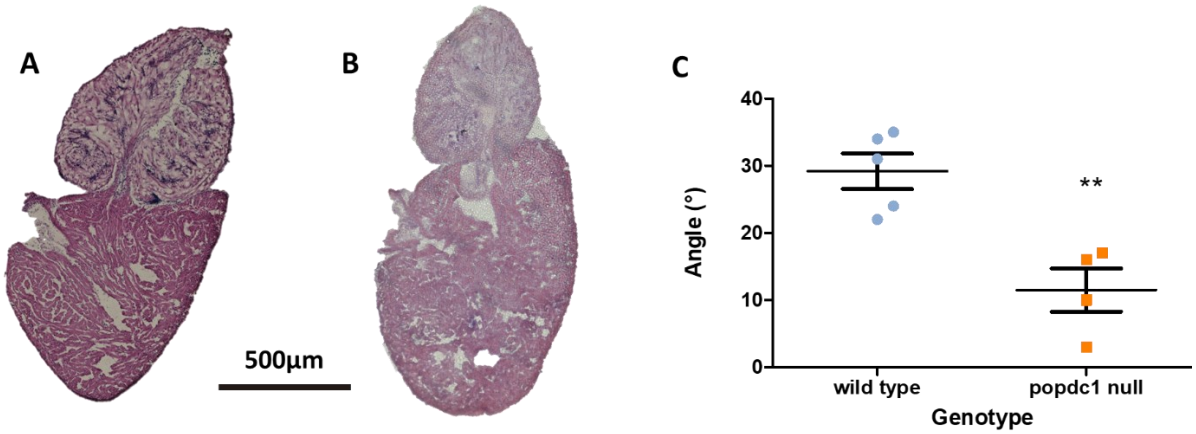

Figure 35 H&E staining to confirm outflow tract angle abnormalities in the *popdc1* null zebrafish. H&E staining of sections of 3-month-old zebrafish wild type (**A**) or *popdc1* null mutant (**B**) hearts. The outflow tract angle from each genotype was quantified (**C**), *popdc1* null mutants had a significantly smaller outflow tract angle (t=4.298; df=7; p<0.01). ** represents p<0.01, n=4. Data are reported as mean ± standard error of the mean

4.5.3 *popdc1* null mutants have an increased thickness of their cortical layer and reduced complexity of their trabeculae

H&E staining was also used to study the differences in the myocardial layers in the *popdc1* null versus wild type zebrafish. The *popdc1* null mutant displayed an increased thickness of the cortical layer (Figure 36A-C). The trabecular layer was also investigated and the *popdc1* null mutants had a reduced length but not width of the trabeculae (A-B and D-E). Trabecular complexity, defined as the average trabeculae-length-to-width-ratio (D'Amato *et al*., 2016), was also reduced in the *popdc1* null mutant as well as the surface area that the trabeculae covered within the trabecular layer in the myocardium (Figure 36A-B and F-G). When looking at H&E images of the trabeculae it was also often observed that they appeared to have less well-defined striations as well as more fragmentation.

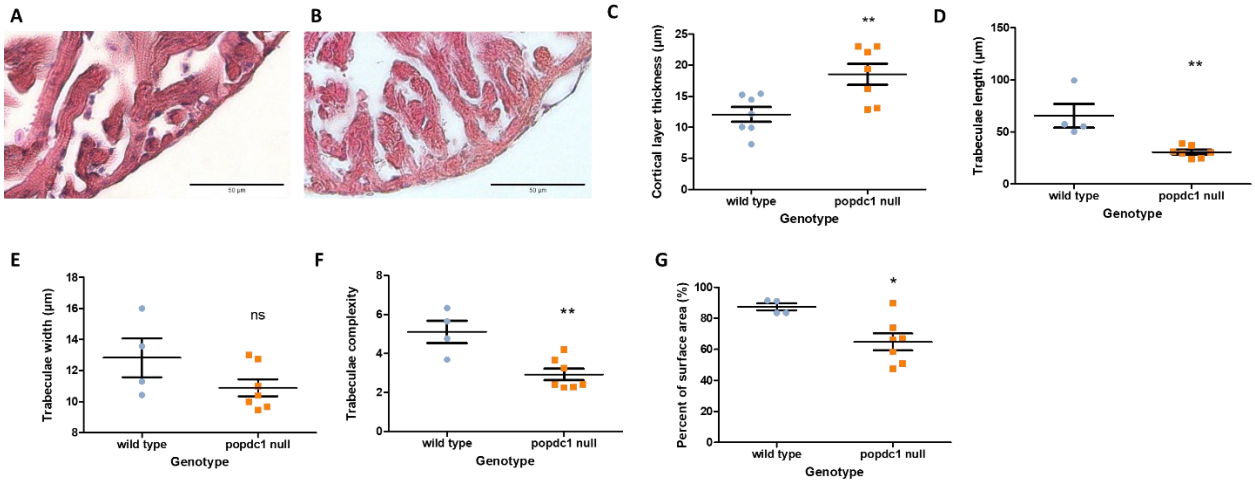

Figure 36 *popdc1* null mutant hearts have an increased thickness of their cortical layer and a reduced complexity of the trabecular layer. H&E staining was performed on sections of the ventricle of 3-month-old zebrafish wild type (**A**) or *popdc1* null mutants (**B**). The cortical layer thickness of each genotype was quantified and found to be thicker in the mutant (t=3.12; df =12; p<0.01) (**C**). The trabecular length was quantified and longer in the mutant (t=3.997; df = 9; p<0.01) (**D**) whereas the width of the trabeculae displayed no difference between genotypes (**E**). Trabecular complexity was calculated by dividing the length of the trabeculae by the width and was found to be reduced in the mutant (t=3.794; df=9; p<0.01) (**F**). Finally, the percent coverage of the trabeculae in the trabeculae layer was calculated for the different genotypes and was reduced in the mutant (t=2.987, df=9; p<0.05) (**G**). At least four specimens were used for each genotype. ** p<0.01, * p<0.05 and ns non-significance. Data are reported as mean ± standard error of the mean.

4.6 Results: Left-right asymmetry in the *popdc1* null zebrafish

The left-right axis determines the appropriate placement of organs in the vertebrate body and determines the correct patterning and the establishment of proper vascular connections during embryonic development (Desgrange *et al*., 2018). In vertebrates, nodal signalling is known to play an important role in creating a gradient from high expression in the left lateral plate mesoderm (LPM) to no expression in the right LPM (Grimes and Kirby, 2009), the expression of other genes is then dependent on what nodal threshold they fall into. The zebrafish heart is positioned to the left of the body cavity and so its placement is under the control of the left-right axis. This can first be morphologically seen during cardiac jogging when the cardiac cone forms a tube and the venous endpoints to the left side (Chen *et al*., 1997, Stainier *et al*., 1993). Cardiac looping is also an essential asymmetric process that makes a flat-S in the fish to place the atrium to the left of the ventricle (Lombardo *et al*., 2019). The fish also goes through a process called cardiac rotation at 5dpf, which

positions the heart into its final position in the body cavity with the atria in a dorsal position relative to the ventricle (Singleman and Holtzman, 2012).

4.6.1 *popdc1* null mutants and wild type generate approximately the same number of embryos that display abnormal cardiac looping defects

Heart looping was studied in 48hpf embryos of both *popdc1* null mutants and wild type fish and embryos were split into 3 categories: embryos with normal or reversed heart loop and middle- where no looping appears to have occurred and the hearts remained in the midline. In both genotypes, I saw that a large proportion of the embryos satisfied normal cardiac looping at 88% in wild type and 86% for the *popdc1* null mutant (Figure 37). In wild type, the remainder of the hearts were reversed (Figure 37), but in the *popdc1* null mutant, only 5% showed reversed heart looping with the remainder being positioned in the midline (Figure 37).

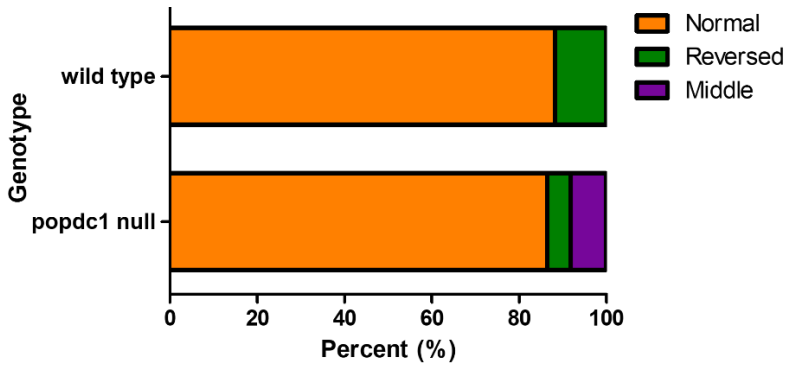

Figure 37 Heart looping in *popdc1* null and wild type embryos. At 48hpf *popdc1* null and wild type zebrafish expressed GFP in their cardiomyocytes under a fluorescence microscope and were laid ventral side up and the position of the atria and ventricle was analysed in relation to one another. Normal situs – the atrium is positioned to the left of the ventricle, reversed situs–the atrium is positioned to the right of the ventricle and middle (or unlooped) - the atrium and ventricle are in line. At least 100 embryos were used for this study using embryos from at least three different breeding pairs. There was a significantly different association between looping and genotype ($\chi 2$ (2, N=100)=17.81, $p<0.001$)

4.6.2 Positioning of the heart in the thoracic cavity of the adult zebrafish

When inspecting the adult zebrafish after opening the thorax it was noticed that the ventricle did not always sit in the same position in relation to the BA and so I decided to quantify this property of the mutant. The body cavity was carefully opened to ensure that the heart was not moved. The position

of the ventricle in relation to the BA was then categorised as being: either position to the left, right or along the midline. At 6 months of age, I saw that in wild type animals, the ventricle was always positioned to the right, whereas in the *popdc1* null mutant this only accounted for 22%, another 22% had their ventricle positioned in the midline and in 56% the ventricle was positioned to the left (Figure 38). At three months of age, in 60% of wild type fish, the ventricle was positioned to the right side and in 40% of the cases at the midline. However, in the *popdc1* null mutant, there was an even split between the possibilities, with a third of the hearts positioned to the left, right or to the midline (Figure 38).

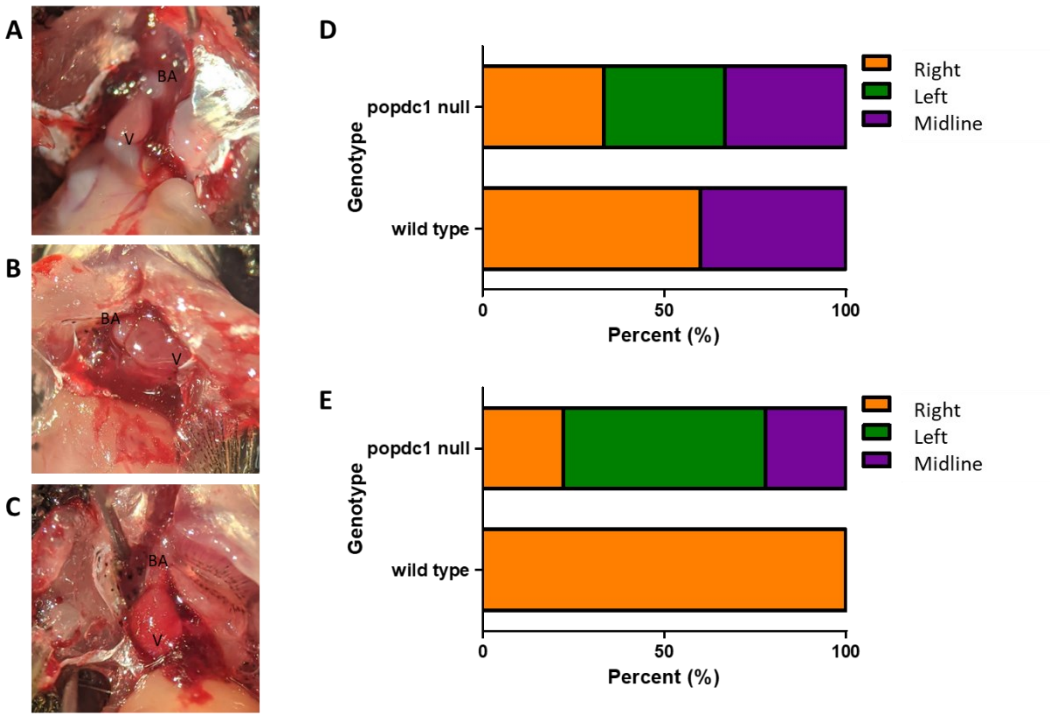

Figure 38 The *popdc1* null mutant display randomised positioning of the ventricle in the body cavity. The body cavity of the zebrafish was carefully opened and the position of the ventricle in relation to the BA from an anterior view was recorded. Images of different heart situses are shown when a ventricle is to the right (**A**), the left (**B**), or midline (**C**) in relation to the BA. The number of fish falling into each of these categories for each genotype was evaluated for animals at 3 (**D**) and 6 (**E**) months post fertilisation. At least 9 fish were used for each group. Abbreviations: BA – bulbus arteriosus, V – ventricle. There was a significantly different association between genotype and the position of the heart in the body cavity at 3 months ($\chi 2$ (2, N=9)=56.15, p<0.001) and at 6 months ($\chi 2$ (2, N=10)=354.55, p<0.001).

4.7 Discussion

The recently generated *popdc1* null mutant has not been well characterised. In this chapter, I have described the morphological analysis of the heart of the *popdc1* null mutant in comparison to the wild

type. It will be useful to identify molecular and morphological differences between *popdc1* null mutants and wild type fish as it may lead to novel and testable hypotheses about the function of POPDC genes, in the heart and other organs.

In this chapter, I have observed several differences between the *popdc1* null mutant and wild type, including, a reduced expression and mislocalisation of the other POPDC family members, enlarged hearts but reduced body size, smaller cardiomyocytes, abnormal morphology of the heart affecting the outflow tract and the compact and trabecular layer in the ventricle as well as an improper situs of the heart in the body cavity. In the following sections, I will explore this further to come up with some reasons for the aberrant morphologies I observed.

4.7.1 Loss of *popdc1* affects the expression of other members of the POPDC family.

In addition to the expected loss of Popdc1 in the *popdc1* null mutant, in both mouse and zebrafish, there was also a reduced expression and mislocalisation of Popdc2. In the wild type heart, in both mouse and zebrafish, Popdc2 is found in the plasma membrane, however, there was also some intracellular staining. Specifically in the mouse, there was also a striated Popdc2 expression domain, which likely represents t-tubules, which has been seen previously in the literature (Holt *et al*., 2020). However, in the *popdc1* null mutant in zebrafish or mice, there is a loss of membrane and t-tubular staining and only some intracellular staining is left behind. In the mouse, the atria were also stained and there was a similar staining pattern in the plasma membrane and some intracellular staining in wild type hearts and membrane staining was lost in the *Popdc1* null mutant, however, an intracellular expression domain was present. Popdc1 and 2 are known to form heterodimers (Brand lab, unpublished), which may explain why Popdc2 cannot localise correctly when Popdc1 is missing. Popdc1 is perhaps required for proper membrane trafficking of Popdc2. Thus, when *popdc1* is lost, only an intracellular expression domain for Popdc2 remains present. This intracellular expression domain appears to be quite granular and could be the result of the protein being localised to vesicles,

however, this has not been further analysed. I have only looked at the localisation of Popdc2 in this study and not that of Popdc3 as currently, no proper antibody is available to study Popdc3.

In the zebrafish, I also saw that the expression of *popdc2* and *popdc3* mRNA was reduced in the *popdc1* null mutant. Suggesting that Popdc1 may upregulate the expression of *popdc2* and *popdc3* in the zebrafish ventricle. Popdc1 is known to have many interaction partners (Amunjela *et al*., 2019), some of which are transcriptional regulators and so it is plausible that Popdc1 could be affecting the expression of *popdc2* and *popdc3.* However, when looking at the *Popdc2*^{W188X} mutant in the mouse it was seen that there was an increase in expression of both *Popdc1* and *Popdc3* compared to wild type (Gruscheski, unpublished). This could mean that the *Popdc2*^{W188X} mutant gained greater ability to upregulate expression of the other Popdc family members or perhaps that Popdc1 and Podpc2 already had differences in their ability to differentially regulate the other POPDC genes.

In zebrafish and mouse null mutants we see that the loss of *popdc1* disrupts Popdc2 membrane localisation and the same is also observed in patients carrying POPDC mutations affecting the subcellular localisation of the mutant protein but also that of other family members (Schindler *et al*., 2016b, De Ridder *et al*., 2019). The same observation was also made in the case of a *popdc1*^{S191F} mutation in the zebrafish, which mirrored the situation in the patients (Schindler *et al*., 2016b). This suggests that the observations made in these models are likely to be also clinically relevant. And in fact, our group is starting to see that mislocalisation of proteins to the membrane may be sufficient to make predictions about the pathogenicity of a mutation, with those causing a mislocalisation having a greater chance of causing cardiac arrhythmias and muscular dystrophy (Rinné *et al*., 2020, Schindler *et al*., 2016b).

4.7.2 Increased survival rate in *popdc1* null fry

The survival of *popdc1* null mutants was studied and it was found that between 5 and 90dpf the *popdc1* null mutant displayed an increased survival rate at 47%, which is up from 35% found in wild type. This result was surprising as it was assumed that survival of the *popdc1* null mutant might be

compromised as in mammalian cardiomyocytes, POPDC1 has been found to have a cardioprotective role (Kliminski *et al*., 2017), and thus, it is expected that its ablation may result in poorer survival of the zebrafish. One explanation for the enhanced survival during late embryonic and larval development may be that by 5dpf null mutant there may have already been death of the fry which were less fit as they did not have the cardioprotection offered by *popdc1* and therefore the surviving fish had a greater chance of making it into adulthood. Whereas in the wild type there may have been more unfit fish surviving for longer and so making it into 5dpf where this investigation was started. It has been noted that about 5% of the *popdc1*^{S191F} mutant develop pericardial effusion and it is assumed that a similar level of null mutant animals also develops a severe embryonic phenotype (Schindler *et al*. 2016). This is a phenotype that is the manifestation of several cardiac defects and can usually be seen as early as 48hpf (Miura and Yelon, 2011). However, from my own observations, I did not see differences in the survival between null mutant and wild type embryos during the first five days of development.

As I did not see great differences between the number of embryos surviving until 5dpf, it suggests that the unfit fish are not dying in greater numbers in the *popdc1* null compared to wild type, and therefore that there really is a difference in survival in the *popdc1* null and the wild type fish. The literature is quite sparse regarding survival between these time points except from optimal and sub-optimal rearing conditions (Siccardi *et al*., 2009), but all of the fish for our studies were subjected to identical environments. Survival was lower however lower than expected for all fish where we would expect many more to have made it to adulthood, which may suggest some sub-optimal conditions in the system. Of note, fish that have been acclimated to hypoxia, as well as those mutations which cause hypoxia, are known to survive better if they are later subjected to hypoxia (Kopp *et al*., 2014, Rees *et al*., 2001). *Popdc1* mutant mice are known to have an upregulation of Bnip3 which usually increases after stress such as through hypoxia (Kliminski *et al*., 2017), suggesting that *Popdc1* null mutant mice may be in a hypoxic state. This may provide some understanding as to the enhanced survival rates of the *popdc1* null mutant zebrafish if the fish were having to suffer hypoxic conditions. However, we

assume that this is not the case as our systems are routinely monitored for functionality to prevent hypoxic conditions from being created. It would be interesting to see if there is any other link to a molecular basis for the increase in survival seen in the *popdc1* null mutant.

4.7.3 Aberrant growth of the zebrafish *popdc1* null mutant

4.7.3.1 Reduced size of mutant cardiomyocytes

The size of zebrafish hearts and individual cardiomyocytes were studied in both zebrafish and mouse *Popdc1* null mutants. This was investigated as transgenic overexpression of c-Myc in the developing hearts of mice has led to a decrease in cardiomyocyte size and an increase of organ size (Jackson *et al*., 1990), suggesting an increase in the total number of cardiomyocytes in the transgenic heart. As Popdc1 is known to downregulate c-Myc (Parang *et al*., 2016) it was hypothesised that a lack of *Popdc1* would cause a similar cardiac phenotype to the overexpression of c-Myc. I found that cardiomyocyte size was reduced in the zebrafish *popdc1* null mutant and likewise in *Popdc1*, *Popdc3* and *Popdc1/Popdc2* double null mutant mice. These findings are in agreement with the fact that Popdc1 plays a role in the degradation of c-Myc (Parang *et al*., 2016) and so we would assume that there would be phenotypic similarities to c-Myc overexpression (Jackson *et al*., 1990). It is however interesting that the mouse *Popdc1* null mutant also appears to display decreased cell size but *Popdc2* null mutants did not, while both can bind to c-Myc. This may suggest that despite all three POPDC proteins having the ability to interact with c-Myc via CoIP, only POPDC1 and POPDC3 have important roles in the pathways that control cardiomyocyte size. Recently it has been suggested that POPDC1 and POPDC3 are co-regulated and have overlapping functions, but that POPDC2 is regulated independently (Kim *et al*., 2010b, Gingold-Belfer *et al*., 2021) which may explain the differences in cardiomyocyte size. It is also interesting that the *Popdc1/Popdc2* double knock out has a more severe effect than the *Popdc1* null mutant alone, as *Popdc2* does not appear to be affecting cell size but perhaps there is some redundancy when Popdc1 alone is knocked out, or else Popdc2 can affect cell size via another mechanism.

4.7.3.2 Impaired heart size

Further to the effect of the POPDC isoforms on cardiomyocyte size, the size of the zebrafish heart was also investigated and was found to be significantly larger in the case of the *popdc1* null mutant zebrafish, although the same was not seen in the mouse (Alcalay *et al*., 2013). This is again in keeping with the phenotype that was seen in the c-Myc overexpression mouse (Jackson *et al*., 1990), and the decrease in cell size and increase in heart size suggests that these hearts are subjected to hyperplasia, which accounts for their overgrowth. The increased size may also be from an increase in other cell types or of extracellular matrix, however, currently, this has not been investigated. Zebrafish hearts have larger hearts with smaller cardiomyocytes suggesting they are phenotypically similar to transgenic mice with forced c-Myc expression. This data suggests that *popdc1* null mutant fish hearts may have more cardiomyocytes than wild type indicating that they may have a higher proliferation level during development, in keeping with their interaction with c-Myc.

It is also plausible that the effect of heart size in the *popdc1* null zebrafish is not, or not entirely, down to the interaction with c-Myc. The cardiomegaly through hyperplasia that I have seen here mimics what is seen when zebrafish are subjected to excessive cardiac stress through a 10 week forced fast-speed swimming exercise regime (Jean *et al*., 2012). Human hearts also enlarge in response to pathological stress, however through hypertrophic growth, which is accompanied by reduced physiological performance (Frey and Olson, 2003). The hyperplastic growth of the heart of the *popdc1* null mutant in zebrafish could be interpreted as being a response to a pathological stimulus similar to stress overload.

4.7.3.3 Reduction in body length of zebrafish popdc1 null mutants

Finally, I found that the *popdc1* null mutants were smaller than their wild type siblings when measuring the body length using fish that were grown at the same density, as this is known to affect their growth (Ribas *et al*., 2017). As groups were siblings and kept under identical conditions, we can assume that the change in body length is a result of the loss of *popdc1*. This growth retardation is similar to *Popdc1*

null mutant mice, which are a third lighter in weight than wild type litter mates (Alcalay *et al*., 2013). I have suggested that null mutant fish may be stressed which has manifested in cardiomegaly, this stress could also cause these fish to be smaller as they have fewer resources to devote to growth. In mice, c-Myc has been found to control body size but not in the same direction as we see here, with the loss of c-Myc causing smaller mice (Oskarsson *et al*., 2001). This suggests that it is not Popdc1's interaction with c-Myc that is causing the difference in body length.

4.7.4 Morphological abnormalities of the *popdc1* null mutant in zebrafish

4.7.4.1 Outflow tract abnormalities

The cardiac morphology was investigated in the *popdc1* null mutant to understand if the heart had a different shape or just differed in size. Previously, it has been shown that during postnatal heart maturation the outflow tract angle changes which might be due to the heart changing its position in the pericardial cavity (intrinsic effect) or alternatively is due to an anterior displacement caused by the growth of abdominal organs (extrinsic effect) (Singleman and Holtzman, 2012). There was a reduction in the outflow tract angle in the *popdc1* null mutant at both, 3 and 6 months post fertilisation but not at 28 dpf. This implies that there is a morphological change that is failing in the mutant, which occurs between 28dpf and 3 months post fertilisation and is responsible for producing the outflow tract angle. Other studies have suggested that the last rotation of the heart is at the larval stage which would cause there to be an increased outflow tract angle (Singleman and Holtzman, 2012). However, I do not see a large outflow tract angle in the 28dpf which is past the larval stage and in the juvenile stage this is perhaps because when the hearts are excised they do not hold their shape as well as the tissue is still developing and so does not have as much integrity.

Hearts within the body cavity were also studied and I saw that the *popdc1* null mutant displayed an unusual positioning in the thoracic cavity with the ventricle often either positioned to the left or linear relative to the BA, as opposed to being positioned to the right side like in wild types at 6 months post fertilisation. The picture is more complicated at 3 months post fertilisation where in wild type too

some hearts were in linear relation to the BA, perhaps because some of the hearts may not yet have fully established their final position in the body cavity. I do not however see any evidence that the *popdc1* null mutant displays an increased frequency of hearts with abnormal looping at 48hpf, suggesting that the abnormal positioning of the BA is not likely the result of a left-right patterning defect but perhaps more of an issue created from the lack of directionality in the mutant outflow tract causing the pressures arising from the posterior organs to cause a randomised positioning of the ventricle. However, it is also possible that heart looping and BA positioning are independently controlled asymmetric processes, which can be experimentally uncoupled from each other. On the other hand, embryos with a morpholino-mediated knockdown of *popdc1* did report looping abnormalities (Shi *et al*., 2020), this difference may have been caused by the different ways the loss-of-function of *popdc1* was achieved. Also, in the chick, POPDC1 has a left-right asymmetrical expression in the Hensen's node at Hamburger Hamilton stage 5 (Torlopp *et al*., 2006) and would be in the right anatomical location to be possibly involved in left-right axis determination. Moreover, it has been reported that PKA signalling, another cAMP effector protein, might be upstream of asymmetric Nodal expression in Hensen's node (Rodríguez-Esteban et al., 2001). Thus, POPDC1 might be involved in left-right asymmetry determination in the chick embryo. However, early mechanisms are species-specific and only later processes such as those involving Pitx2 are conserved in different vertebrate species. At the moment we favour the interpretation of a late-stage process that is involved in the positioning of the BA and which is independent of those processes involved in heart looping.

Another possible reason for the outflow tract abnormalities in the *popdc1* null mutant is the link of POPDC1 and TOF. TOF is a prevalent congenital heart disease known to be associated with several phenotypes, one of which is outflow tract obstruction. In the Chinese Han population, a *POPDC1* polymorphisms was linked to TOF (Shi *et al*., 2019). When *popdc1* morphants were studied in zebrafish they too displayed outflow tract abnormalities in the embryo (Shi *et al*., 2020). No mechanism is currently known to explain how *Popdc1* could cause this phenotype, but SHF regulatory network genes are also downregulated in both TOF patients and *popdc1* morphants, such as *nkx2.5* and *gata4,* which

have previously been shown to be involved in outflow tract development (Laforest and Nemer, 2011). TOF has also been linked to β-adrenergic signalling, which mainly acts through cAMP (Liu *et al*., 2019). Since POPDC1 is a cAMP effector protein may help to provide a mechanism for how the loss of *popdc1* can lead to TOF (Froese *et al*., 2012).

To further confirm the outflow tract abnormalities in the *popdc1* null mutant hearts in explanted hearts, I could take whole zebrafish specimens and H&E stain sections of them. This would allow for confirmation aberrant positioning of the heart within the body cavity as well as to observe any rotational differences and differences in the angle at which the outflow tract comes off of the ventricle.

4.7.4.2 Ventricular rounding

It is known that the hearts become more rounded as they mature (Singleman and Holtzman, 2012). I have seen at 6 months post fertilisation *popdc1* mutants have an increased ventricular length to width ratio compared with their wild type counterparts, meaning that the null mutant ventricle is elongated. However, these differences were not seen at other time points. This may suggest that the *popdc1* null zebrafish is staying in a more immature state as it is failing to reach the rounded shape. On the other hand, *popdc1* null mutant fish hearts are larger due to hyperplasia and so maybe the abnormal elongated shape might be due to the increased number of cells.

4.7.4.3 Cortical layer thickening

Based on H&E staining of sections through the ventricle, I have seen that the *popdc1 null* mutant has a significantly thickened cortical layer. Cortical layer thickening is known to occur after cryoinjury (González-Rosa *et al*., 2011). The cortical layer may have some plasticity depending on environmental factors, for example, a decrease in temperature can decrease thickness (Graham and Farrel, 1989) and increased exercise can increase the thickness (Gamperl and Farrell, 2004). On top of this, there are known differences in cortical layer thickness in heart disease (Singleman and Holtzman, 2012). For further confirmation of the increase in cortical layer thickening, I would need to stain for a cortical

layer-specific marker like laminin (Sánchez-Iranzo *et al*., 2018), this may be important going forward to assess whether the mutants do have more cells that have taken on a cortical layer fate rather than having misplaced cells of non-cortical phenotype. However, we can begin to assume here that the difference seen may be because the *popdc1* null mutant creates a disease state for the hearts, although further work would have to be done to understand the mechanism behind this.

4.7.4.4 Trabeculae abnormalities

Further to differences in the cortical layer, the trabecular layer in the *popdc1* null zebrafish is also abnormal with less elongation, complexity and surface area covered by the trabecular layer, all of which suggests a hypo-trabeculation of the null mutant heart. Tbx5a is known to be a marker of the trabecular layer in the zebrafish heart and studying this gene may be important to understand why trabeculae are perturbed in the mutant (Sánchez-Iranzo *et al*., 2018). The cardiomyocytes of the trabecular layer are known to downregulate *tbx5a* in order to integrate into the cortical layer (Sánchez-Iranzo *et al*., 2018). One possible interpretation that I favour is that in the *popdc1* null mutant an increased number of cells are directed towards the cortical layer fate, which accounts for the increased thickness of the cortical layer as well as the hypo-trabeculation, as fewer cells are left for the trabecular compartment. Alternatively, due to the smaller size of cardiomyocytes in the null mutant, the trabeculae are unable to cover as much area and project as far into the lumen of the heart.

4.7.5 Conclusions and future directions

Little was known about most of the morphological differences that I discovered in the *popdc1* null mutant zebrafish. In this chapter, I have explained some of the observations that were seen in the *popdc1* null mutants and attempted to provide some explanations for why these changes may be occurring.

I have seen that Popdc1 can control both protein localisation and mRNA expression of the other POPDC family members. I have seen that *popdc1* null mutants in zebrafish have increased survival

compared to wild type. When studying whether *popdc1* mutant hearts had shared similarities with c-Myc overexpressing hearts, I found that they both shared reduced cardiomyocyte size and increased organ size. On top of this, I found that the *popdc1* null mutants had a smaller body length compared to wild types. When looking further into the morphology of the *popdc1* null mutant heart I saw that there were outflow tract abnormalities, which may be linked with TOF, as well a decreased roundness of the heart and in increased compact layer thickness and reduced trabeculae complexity. On top of this, it was often seen that *popdc1* null has in proper positioning of the heart in the body cavity.

Overall, the *popdc1* null mutant display several important differences in the heart, many of which have phenotypic similarity to c-Myc overexpression adding to an interaction of Popdc1 and c-Myc in this tissue. Further work could be done with these findings to discover if the differences in heart and cardiomyocyte size result in an increase in cell number and if so at what developmental stage this happens. Moreover, I went on to study the effect of the loss of *popdc1* in cardiac regeneration to study if its interaction with c-Myc can increase the recovery after injury. The number of morphological disparities between the *popdc1* null mutant and the wild type hearts suggests that the mutants fail to go through proper development of the heart leading to incorrect positioning, an altered structure of the heart wall and also causing outflow tract defects. In the future, it would be interesting to study if the morphological changes affect cardiac function and blood flow patterning as well as establishing and adding to theories as to when and how these differences might occur.

Going forward I believe that it would be interesting to see if there is a molecular basis behind some of the findings that are currently left unexplained. One way to do this is to look at the mRNA expression levels of the *popdc1* null mutants with the aid of methods such as next-generation RNA sequencing, this would generate a lot of data and help to unravel some of the misregulated pathways.

5. Impaired cardiac regeneration in the *popdc1* null mutant in zebrafish

Ischemic heart disease accounts for almost 20% of deaths worldwide (Bennett *et al*., 2007, Virani *et al*., 2020). Moreover, the number of patients with cardiovascular diseases is rising in the Western world. This increase is strongly linked to a Western lifestyle, which is characterised by an unhealthy diet, people being sedentary and becoming obese. When patients suffer from a heart attack, 70% of them will now survive due to therapeutic advances (BHF, 2020a). However, the damaged cardiac tissue will be replaced by scar tissue as cardiomyocytes in the human heart do not proliferate at a sufficient level to compensate for the loss after myocardial infarct (MI) (Bergmann *et al*., 2009). The fibrotic scar tissue that substitutes the myocardium can maintain the integrity of the heart wall and prevent a rupture but is acontractile and therefore does not contribute to the pumping function of the heart. The surrounding healthy myocardium will experience higher wall stress, which triggers cardiac hypertrophy and causes an altered geometry of the post-MI heart (De Villiers and Riley, 2020). Post-MI, patients will often in the longer term develop heart failure, which causes a severe reduction in the quality of life and potentially also the death of the patient. Alternatively, the patient could receive a heart transplantation, which however is often not a viable choice given the limited number of hearts available for transplantation. It is therefore imperative to find novel ways to treat the growing number of patients living with heart failure. Many are looking to animal models like the zebrafish, which can regenerate their heart after injury, for the identification of pathways that initiate proliferation to improve healing and even cardiac regeneration in the adult human heart (Price *et al*., 2019).

Unlike mammals, zebrafish can regenerate their heart after cardiac injury (Poss *et al*., 2002). Cryoinjury has become a popular method to injure the heart since many of the cellular responses and processes are comparable to MI in the mammalian heart (González-Rosa and Mercader, 2012). After injury, there is an infiltration of immune cells and a period of scarring, cardiomyocytes are then

stimulated to proliferate to compensate for the loss of functional myocardium and finally, the heart is remodelled to remove the scar tissue and to allow for complete recovery (González-Rosa *et al*., 2017).

Based on our work in the previous chapter and data from the Williams lab it appears that POPDC1 can interact with and downregulate the proto-oncogene c-Myc and that this may also be occurring in the heart (Parang *et al*., 2016). Therefore, I hypothesised that in the *popdc1* null mutant in zebrafish there might be an increase in myocyte proliferation, which may lead to a more rapid recovery from cryoinjury in the *popdc1* null mutant compared to wild type. To test this hypothesis, I used 6 months old wild type and *popdc1* null mutant zebrafish and induced a cryoinjury of the ventricular wall. The hearts were then harvested at different time points post-injury and assessed for their ability to regenerate. I aimed to assess the ability to perform cryoinjury and then to look for evidence for an involvement of *popdc1* and *c-Myc* in the recovery by looking at *popdc1* expression levels post-injury. I assessed the regenerative capacity of the *popdc1* null mutant zebrafish using histological staining and qPCR. Moreover, I studied apoptosis and cell proliferation of cardiomyocytes in the *popdc1* null mutant heart in comparison to wild type. Finally, I assessed the ploidy and the level of binucleation of mutant cardiomyocytes, two parameters, which are known to affect the regenerative ability of the heart.

5.1 Results: Cryoinjury of the zebrafish heart

To ensure the future success of my cryoinjury experiments I wanted to assess my ability to perform a cryoinjury on the zebrafish heart. A liquid nitrogen cooled probe was placed on the ventricle of the anesthetised zebrafish until it had defrosted and then the fish were put in fresh system water to recover for 24 hours. After this time, the fish were sacrificed, hearts were collected and observed under brightfield and GFP illumination to observe the cardiac damage that was experimentally induced (Figure 39A-B). Under brightfield illumination, a red apex could be seen, which demarcated the injury area and with GFP fluorescence there was an absence of GFP fluorescence in the presumptive injury area as the cardiomyocytes had perished (Figure 39A-B). The percent of the

ventricle that was still expressing GFP was estimated from these images and was found to consistently be 75-77% of the total ventricle, giving a total damage of 23-25% (Figure 39C).

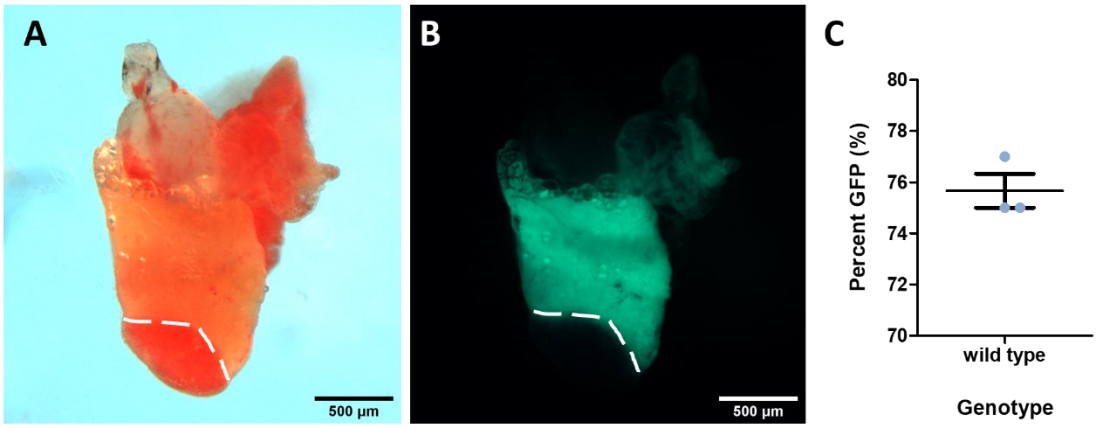

Figure 39 Cryoinjury can be reliably produced in zebrafish. Anesthetised wild type zebrafish were subjected to cryoinjury by a liquid nitrogen cooled probe, allowed to recover for 24 hours and then their hearts were harvested. Images of the heart were taken with brightfield (**A**) and with a GFP filter (**B**), as the cardiomyocytes in these hearts express GFP under control of the cmlc2 (or myl7) promotor. The dashed white line represents the border between the intact myocardium (above) and the perished myocardium (below). The percentage of the ventricle that stained positive for GFP was quantified (**C**), giving an estimation of the healthy myocardium. Data are reported as mean ± standard error of the mean. n=3.

5.2 Results: *popdc1* is upregulated after cryoinjury

popdc1 expression was investigated using qPCR in wild type animals to test whether *popdc1* expression was affected following cryoinjury. Ventricles were excised at different time points after injury and the RNA was isolated, converted to cDNA and used for qPCR experiments. There was a significant rise in *popdc1* expression following cryoinjury with a ~4.5-fold induction, which was sustained between 3 DPI and 14 DPI (Figure 40). However, by 21 DPI expression levels returned to a level comparable with that of sham-operated hearts (Figure 40). The upregulation of *popdc1* suggests that this gene might play a role during the regeneration of the zebrafish heart.

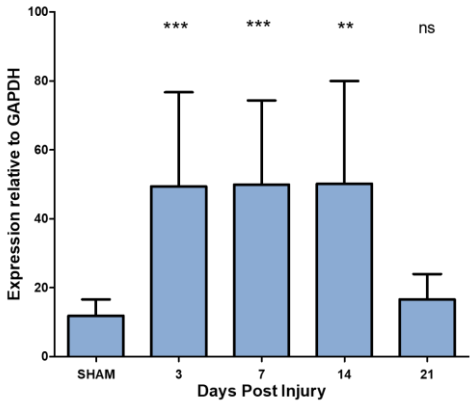

Figure 40 Popdc1 expression level increases following cryoinjury in the zebrafish. RNA from ventricular tissue of wild type (-) fish was isolated at different DPI. RNA was converted to cDNA and was used for qPCR analysis of *popdc1* expression levels. All values were normalised against GAPDH levels. 3 (t=1.252; df=13; p<0.001), 7 (t=1.243; df=13; p<0.001) and 14 (t=1.269; df=10; p<0.01) DPI displayed a significant increase in popdc1 expression compared to SHAM hearts. Statistical analysis was performed using a t-test. *** represents p < 0.001, ** represents p<0.001 and ns represents no significance of an injury time point when compared with SHAM. Data are reported as mean ± standard error of the mean. The ventricles of at least eight animals were analysed for each time point.

5.3 Results: Myc expression in the regenerating zebrafish heart

As Popdc1 has been shown to interact with c-Myc the expression of *popdc1* was investigated in the zebrafish following cryoinjury. Due to a partial genome duplication in bony fish, the zebrafish has two copies of the *c-Myc* gene, *myca* and *mycb* (Zhang *et al*., 2003). However, *mycb* has retained the most functional similarities to mammalian c-Myc in the heart and has a more widespread expression (Kotkamp *et al*., 2014, Münch *et al*., 2017), it has also been used by others as a proliferation marker in the zebrafish heart (Honkoop *et al*., 2019). It is therefore presumed that antibodies used in this section will primarily detect mycb, due to its expression in the heart. As these genes are expected to have a low expression in adult hearts at baseline, wild type hearts before and after cryoinjury were investigated. There was a strong c-Myc expression in the border zone adjacent to the injury area at 7 DPI, but expression was low in the rest of the ventricle comparable to the uninjured ventricle (Figure 41). This suggests an upregulation of c-Myc after injury in the heart.

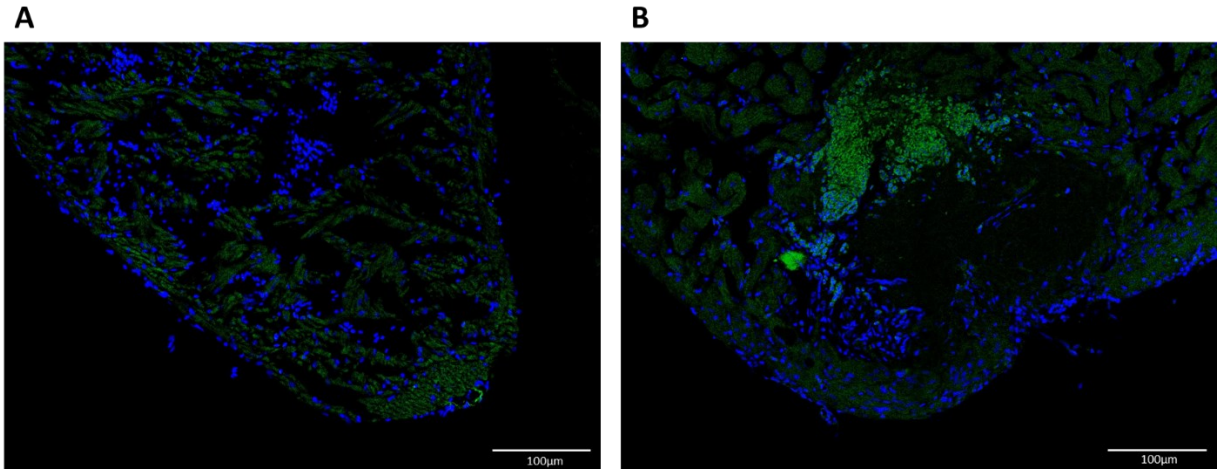

Figure 41 c-Myc is expressed in the regenerating zebrafish heart. Sagittal sections of wild type (-) uninjured (**A**) and 7DPI injured (**B**) ventricles stained with c-Myc antibody ab32072 (green) and DAPI (blue). c-Myc positive cells are clustering adjacent to the wounded myocardium. N=3.

5.4 Results: The *popdc1* null zebrafish display a retarded heart regeneration

To assess the differences between wild type and *popdc1* null mutant hearts in response to cryoinjury, AFOG staining was used on sections of the heart at different time points after injury as it is a sensitive way to look at the scaring of the heart after cryoinjury and is commonly used in the field of heart regeneration (Poss *et al*., 2002). This method allows the visualisation of the injury area as muscle is stained yellow/orange, fibrin is stained red and collagen is stained blue. I investigated sections of injured hearts at different time points post-injury including SHAM, 3, 7, 14, 21, 90 and 130 DPI. Until 14 DPI, the ventricles of both genotypes showed comparable damage after cryoinjury (Figure 42). However, although no scar was observable in wild type hearts at 21 DPI, the scar was on average still accounting for 16% of the ventricle in the case of the *popdc1* null mutants although variation at this stage was very large. However, there was large variability between specimens at this time point (Figure 42). At 90 DPI and 130 DPI, no observable scar tissue was present in wild type, but in the *popdc1* null mutant hearts, a scar was seen, which on average represented about 3% of the ventricle (Figure 42). It should however be noted that at both late time points, approximately one-third of the *popdc1* null mutants displayed a fully regenerated ventricle (Figure 42B).

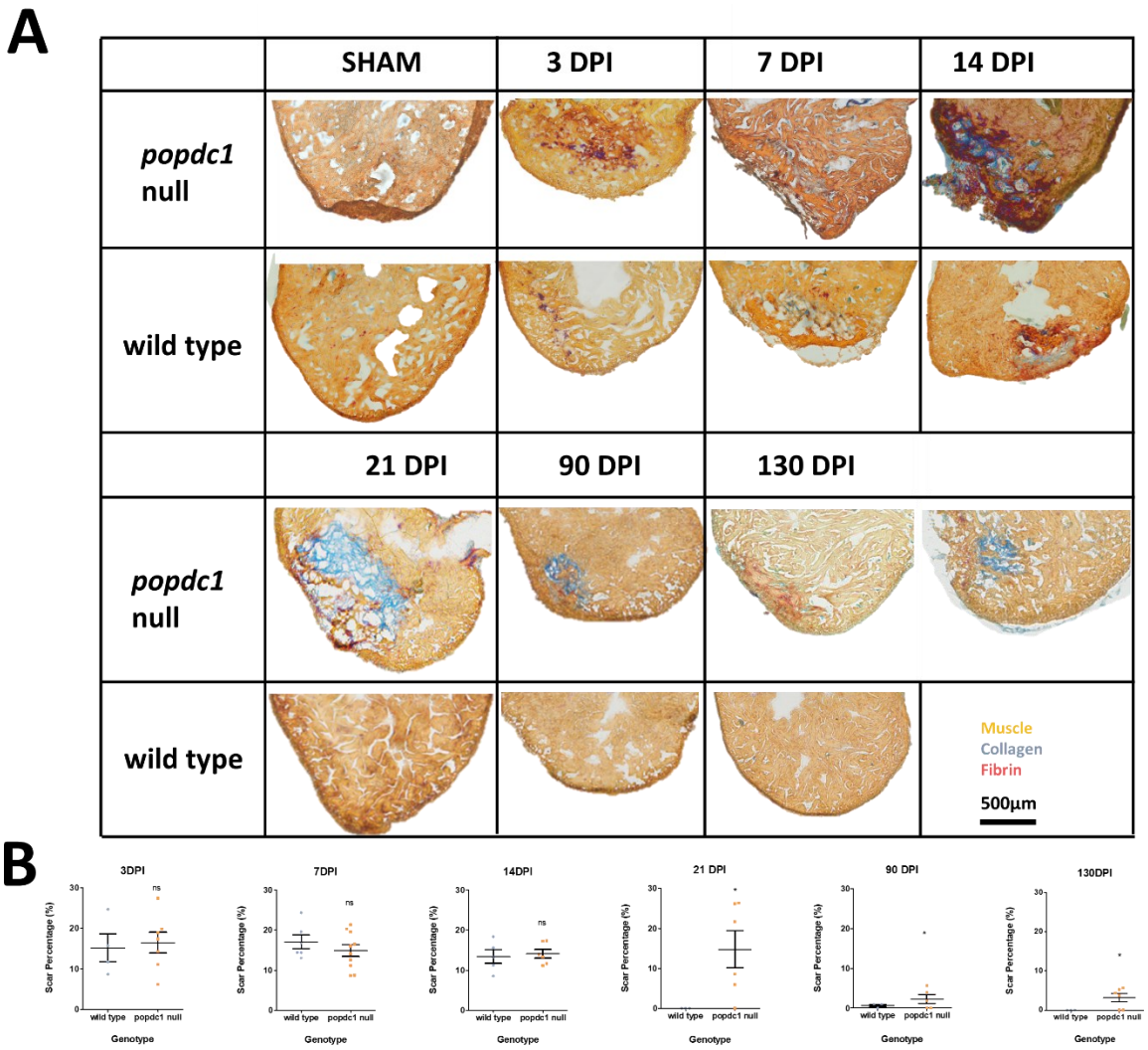

Figure 42 Retardation of the wound healing response in *popdc1* null mutants. Cryoinjured zebrafish hearts were harvested and stained for AFOG (**A**) at different days post-injury (DPI). (**B**) Quantification of the damaged tissue area at 3-130 DPI. At least three zebrafish were used for each time point. The injury size was significantly larger in the popdc1 null hearts at 21 ($t=2.177$; $df=7$; $p<0.05$), 90 ($t=2.190$; $df=10$; $p<0.05$) and 130 DPI ($t=2.087$; $df=7$; $p<0.05$). Data are reported as mean ± standard error of the mean.

5.5 Results: *popdc1* null mutant hearts have a reduced cell proliferation and apoptosis following injury.

The *popdc1* null mutants have a retarded or in some cases have possibly lost the ability to fully regenerate the injured heart (Figure 42). I, therefore, decided to assess whether the *popdc1* null mutant could initiate myocardial proliferation and apoptosis in the same way as wild type.

5.5.1 Proliferation in the injured *popdc1* null mutant heart

For this assessment of proliferation, zebrafish hearts at 7 DPI were stained for the cardiomyocyte marker *mef2* and the proliferation marker phosphohistone3 (PH3) and the number of cells positively labelled for both markers were counted as representing proliferating cardiac myocytes. Cells were only counted if they were in the presumed border zone which was defined as an area, which was at a maximum distance of 100 µm from the injury site. The injury site was defined by the lack of GFP expression, which marks cardiomyocytes. I found that in the border zone of wild type hearts at 7 DPI 43% of cardiomyocytes were PH3 positive (Figure 43A-B and E). On the other hand, in *popdc1* null mutants, there was an approximately 4-fold lower level of proliferating cardiomyocytes with only 10%, displaying PH3 staining (Figure 43C-E).

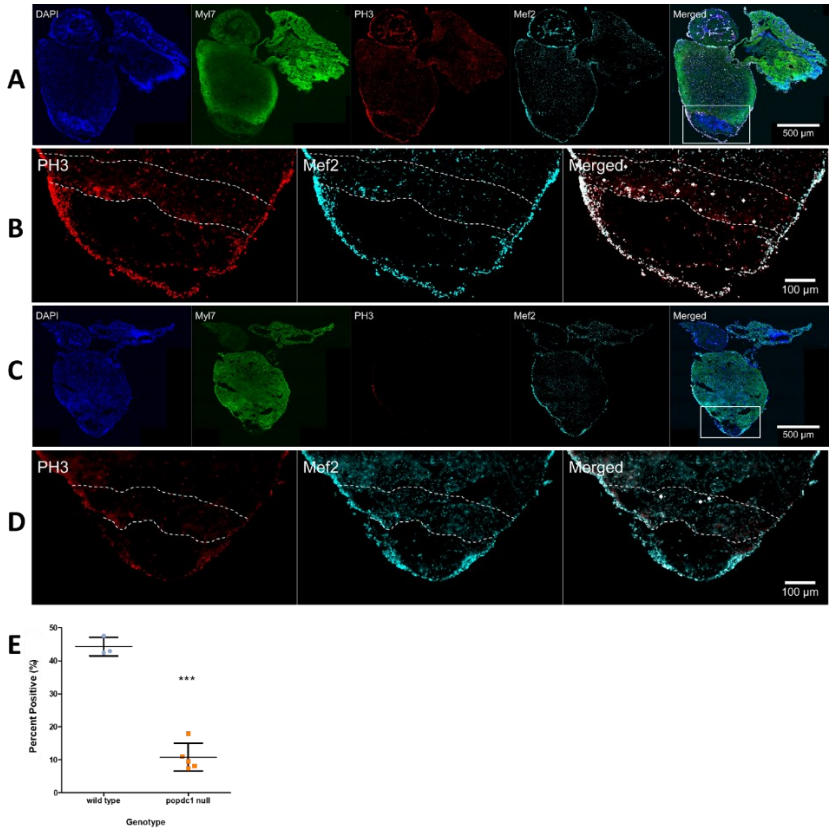

Figure 43 *Se*verely reduced cardiomyocyte proliferation is displayed in *popdc1* null mutant hearts after injury. Cryosections were made from wild type (**A-B**) and *popdc1* null (**C-D**) zebrafish hearts excised at 7DPI. The hearts were then stained for DAPI, Mef2 and PH3 (**A-D**). Whole hearts were imaged (**A** and **C**) as well as the injury area at higher magnification (**B** and **D**). White dashed lines represent the boundary of the border zone, defined as 100µm from the injury into the healthy myocardium, and white arrows point out some nuclei co-stained for Mef2 and PH3. The percentage of co-stained cells in the border zone are quantified in **E**. There was a significant reduction in proliferating cardiac myocytes in injured *popdc1* null mutant hearts (t=12.00; df=6; p<0.001). Statistical analysis was performed using a t-test. ***P < 0.001. At least three zebrafish hearts were used for each group. Data are reported as mean ± standard error of the mean.

5.5.2 Apoptosis in the injured *popdc1* null zebrafish heart

Apoptosis was also investigated by TUNEL staining at 1 DPI, as at this stage, a lot of cell death is expected at the injury site as the damaged myocardium is replaced by scar tissue. TUNEL staining detects the DNA breaks made when DNA fragmentation occurs in the last phase of apoptosis. It was found that in the wild type there were on average 125 nuclei in the injury area that were undergoing apoptosis which accounted for roughly 40% of nuclei (Figure 44A and C-D). In the *popdc1* null mutant ventricles, I saw a similar absolute number of TUNEL positive nuclei of around 125 but the relative number of nuclei undergoing apoptosis in the injured area was significantly lower averaging at around 25% (Figure 44B-D). This much lower relative amount is probably due to the presence of a higher number of unlabeled nuclei in the area. This could either be due to an overall higher number of cells, as implied by smaller cardiomyocytes but larger hearts in the mutant (Chapter 4). However, it is also possible that there is an increased level of infiltrating immune cells present in the injured mutant heart. To answer this question further studies using immune-cell specific markers are required.

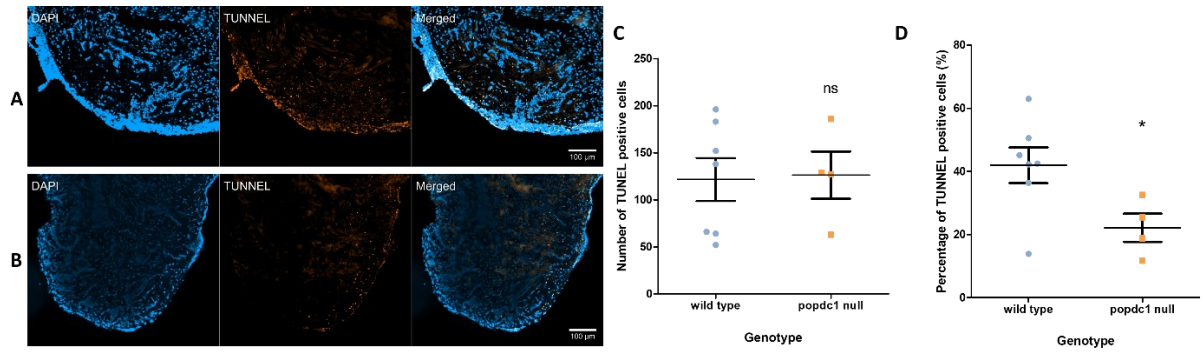

Figure 44 Apoptosis in *popdc1* null mutant and wild type zebrafish ventricles after cryoinjury. Cryosections of wild type (**A**) and *popdc1* null mutant (**B**) zebrafish hearts excised at 1 DPI. The hearts were TUNEL and DAPI stained. The number of TUNEL stained nuclei in the injury area were quantified (**C**) as were the percentage of TUNEL stained nuclei (**D**). Statistical analysis was performed using a t-test. The number of apoptotic nuclei was not significantly different ($t=0.1308$; $df=9$; $p>0.05$) between genotypes but the relative number of apoptotic nuclei was significantly smaller in the *popdc1* null mutants ($t=2.384$; $df=9$; $p<0.05$). *P < 0.05. At least four zebrafish hearts were used for each group. Data are reported as mean ± standard error of the mean.

5.6 Results: Aberrant gene expression in the *popdc1* null following cryoinjury

As heart regeneration after cryoinjury was delayed in the *popdc1* null mutant (Figure 42), I then decided to look at the expression of specific genes, which may be misregulated in the mutant after injury. This was done by qPCR analysis of a selection of genes, which have been involved in heart regeneration at different time points after injury, allowing a better study of the kinetics of the injury response over time. Wildtype and popdc1 null mutant fish were used for this which did not have a GFP reporter on cmlc2 and have been distinguished here in the text as wild type (-) and *popdc1* null (-). The cardiac progenitor marker genes *nkx2.5*, *tbx20* and *tbx5* were investigated as they have been reported to get reactivated in response to injury (González-Rosa *et al*., 2017). In wild type hearts, these genes were expressed stronger in sham-operated wildtypes than in *popdc1* mutant animals. Consistent with the reported peak of cell proliferation at 7 DPI there was an upregulation of these progenitor marker genes at 7DPI, which then fell again at 14 DPI. However, *popdc1* null (-) mutants failed to upregulate these genes (Figure 45), which is consistent with the observed lack of cell proliferation (Figure 43). Matrix metalloprotease genes were also investigated, as they are required to remove or remodel scar tissue that was produced in response to the injury. Expression of both *mmp2* and *mmp13a* was studied and it was expected that the expression of these genes is increased at 14 DPI as the scar begins to clear. There was an upregulation for mmp13a in the wild type (-) at 14 DPI but the levels in the *popdc1* null (-) mutants remained lower, although the difference between genotypes did not reach significance (Figure 45). For *mmp2* there was no large increase in wild type hearts after injury, however, the level of mmp2 was markedly higher in wild type than in the *popdc1* null (-) mutant ventricle at different timepoints (Figure 45). The vascularisation marker *vegfaa* was also studied and again it was consistently expressed at higher levels in the wild type (-) compared to the po*pdc1* null (-) mutant heart (Figure 45). Three stress marker genes were studied and all three genes, metallothionein (*mt2)*, aldehyde dehydrogenase 1a (*aldh1a*) and natriuretic peptide A (*nppa*) were robustly upregulated at 3 DPI, an expected response as these genes protect against oxidative stress (*mt2*), produces RA synthesis, which triggers cardiac regeneration (*aldh1a*), or is a universal

cardiac stress marker (*nppa*), respectively. The *popdc1* null (-) mutants, however, failed to upregulate these stress response markers (Figure 45). Finally, the expression of *myca* and *mycb* was studied. I looked at the *myca* and *mycb* levels firstly at base line in uninjured hearts as this was of interest as in the mouse heart there was increased c-Myc protein and found that both *myca* and mycb were slightly downregulated in the *popdc1* null mutant ventricle, however, this was not significant. *Myca* did not appear to be upregulated in the wild type zebrafish hearts after injury however in the *popdc1* null (-) mutant there was a large increase at 7 DPI (Figure 45). Likewise, mycb was more highly expressed at 3 DPI and 7 DPI in the *popdc1* null (-) mutant compared to wild type (-) (Figure 45). This suggests that the *popdc1* null mutant express higher levels of c-Myc compared to wild type, although variability was high and the observed difference between genotype did not reach statistical significance.

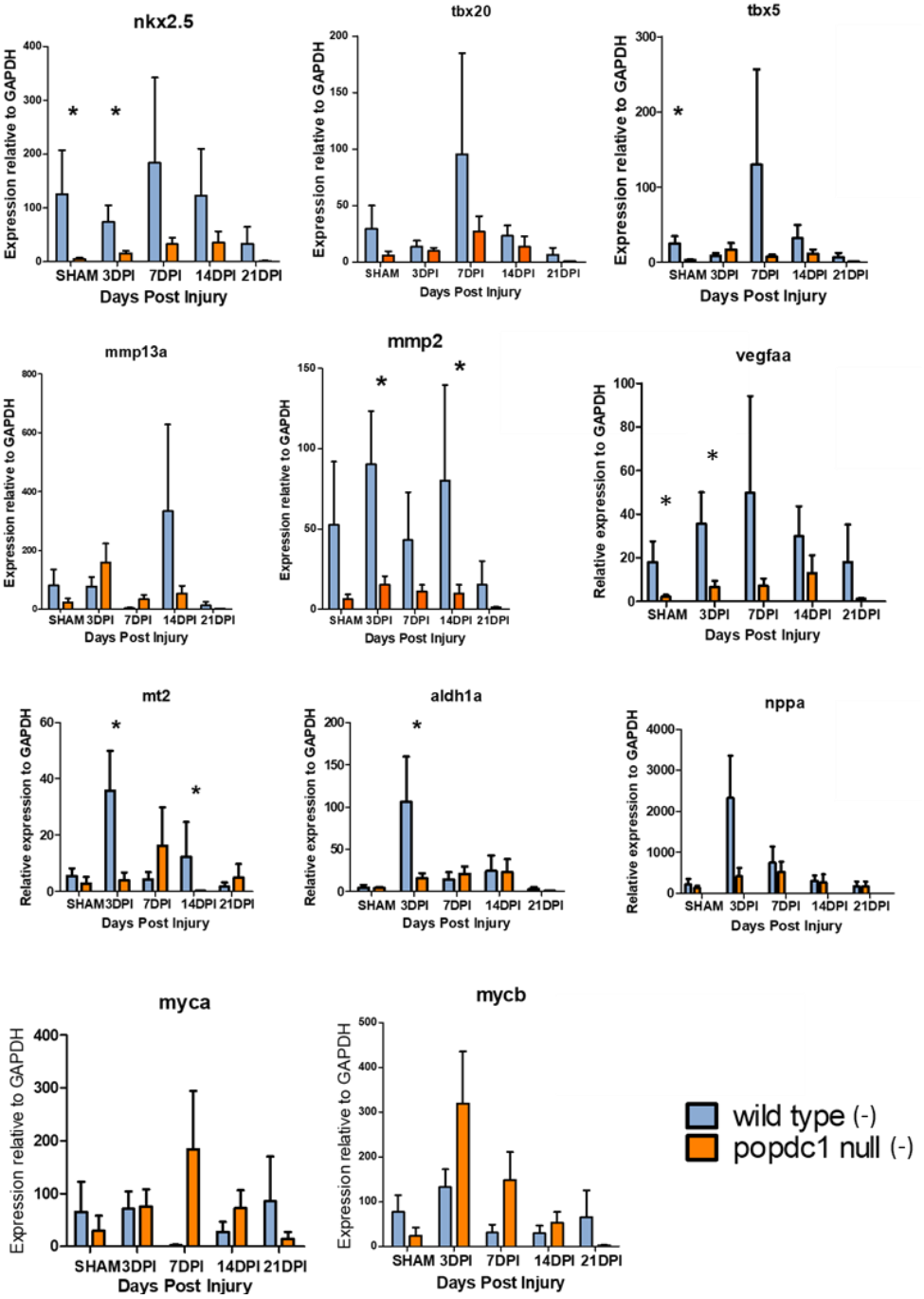

Figure 45 The *popdc1* null mutant displays an abnormal transcriptional response following cryoinjury. RNA from ventricular tissue of popdc1 null (-) and wild type (-) zebrafish were isolated at different DPI. RNA was converted to cDNA and was used for qPCR analysis of markers of different processes involved in heart regeneration; cardiac transcription factors (*nkx2*.5, *tbx20* and *tbx5*), matrix remodelling (*mmp13a*, *mmp2*), vascularisation (*vegfaa*), stress response (*mt2*, *aldh1a* and *nppa*) and *cMyc* (*myca* and *mycb*). All values were normalised against GAPDH levels. Statistical analysis was performed using a t-test on GraphPad Prism. *$p < 0.05$ between genotypes. At least three zebrafish ventricles were used for each group and three technical replicated were made. Data are reported as mean ± standard error of the mean. *nkx2.5* was significantly downregulated in sham ($t=2.007$; $df=6$; $p<0.05$) and 3 DPI ($t=2.234$; $df=10$; $p<0.05$) in *popdc1* null (-) mutants. *tbx5* was significantly downregulates in sham ($t=2.503$; $df=7$; $p<0.05$) hearts in *popdc1* null (-) mutants. *mmp2* was significantly downregulated in 3 DPI ($t=2.231$; $df=8$; $p<0.05$) and 14 DPI ($t=1.794$; $df=14$; $p<0.05$) *popdc1* null (-) mutant hearts. *vegfaa* was significantly downregulated in sham ($t=2.270$; $df=6$; $p<0.05$) and 3 DPI ($t=2.208$; $df=7$; $p<0.05$) *popdc1* null (-) hearts. *mt2* was significantly downregulated in 3 DPI ($t=2.224$; $df=6$; $p<0.05$) and 14 DPI ($t=1.902$; $df=10$; $p<0.05$) *popdc1* null (-) mutants. *aldh1a* was significantly downregulated at 3 DPI ($t=2.289$; $df=9$; $p<0.05$) in *popdc1* null (-) mutant hearts.

5.7 Results: Binucleation and ploidy in the *popdc1* null zebrafish

From previous work, it is known that both binucleation and ploidy can affect cardiac regeneration in the zebrafish by limiting the proliferative ability of the cardiomyocytes (Patterson *et al*., 2017, González-Rosa *et al*., 2018). As the *popdc1* null mutants also display a lack of cell proliferation in response to injury, the level of binucleation and the ploidy status was studied.

5.7.1 Generating single cells from the zebrafish heart

Before the binucleation or the polyploidisation status could be investigated I first had to establish a method for the isolation and attachment of zebrafish cells onto coverslips. Zebrafish cardiomyocytes have been reported to remain viable when incubated at 28°C, however, there was no incubator available set at this temperature and so I tested whether cells could also be incubated at 37°C or room temperature for a short period required for adhesion of the cells to the glass coverslip. I found that I had much better adherence when cells were incubated at 37°C (Figure 46A). I also looked at the effect of clearing the cell suspension to obtain a purer cardiomyocyte population. In mice, this is often done by spinning the cells at low speed or by allowing them to settle for 10 minutes before removing the supernatant and resuspending the cell pellet in fresh media. I found that a large number of cells were lost with both of these clearing methods, although the cell suspensions obtained in this way contained more cardiomyocytes and less cell debris (Figure 46B). I also tested whether cells adhered better when poly-l-lysine coated or uncoated coverslips were used and found there appeared not much difference in adherence between the two substrates (Figure 46). Going forward with my experiments I did not clear the cell suspension and incubated cells for 3 hours at 37°C and on coverslips that had been coated with poly-l-lysine.

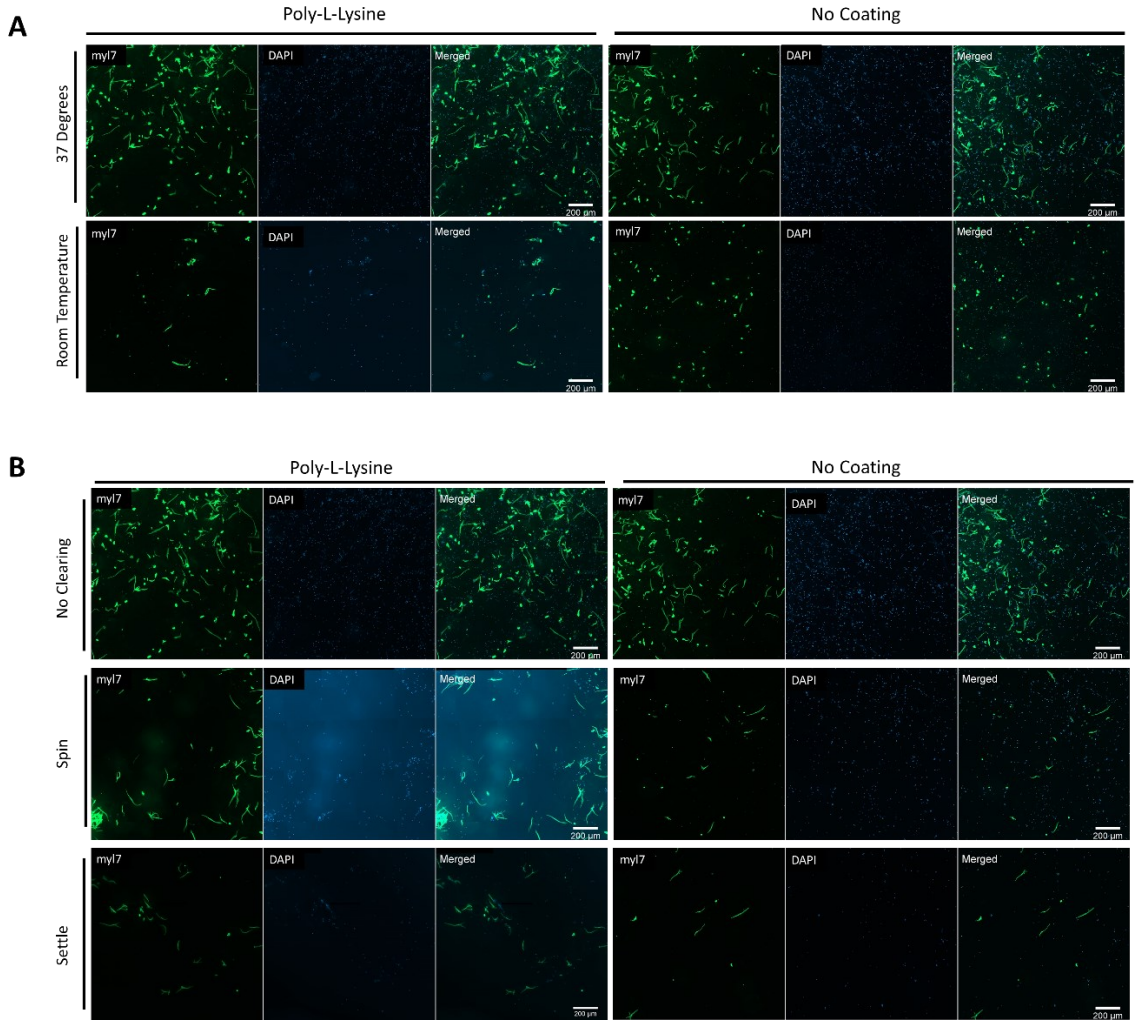

Figure 46 Optimisation of the adherence of isolated zebrafish cardiomyocytes. Enzymatic digestion was used to isolate wild type zebrafish ventricular cardiomyocytes and different conditions were tested to attempt to optimise allowing the cells to adhere. Coverslips were coated with poly-l-lysine or left uncoated to assess the differences. (**A**) the effect of growing in different temperatures was studied as there was no access to a 28°C incubator. Cells grown in a 37°C incubator and at room temperature were compared. (**B**) Cells grown at 37°C were subjected to different clearing methods to attempt to remove debris and other cell types from the isolation material. If nothing was done to the cells they are labelled no clearing, cells that were spun down for 1 minute at 400rpm and are labelled spin, and sells that were allowed to settle for 5 minutes before the supernatant was removed and replaced with fresh buffer are labelled settled.

5.7.2 *popdc1* null zebrafish have increased binucleation

As *popdc1* null mutants fail to regenerate their hearts after cryoinjury (Figure 42) and binucleation is known to be a factor reducing the regenerative ability (González-Rosa *et al.*, 2018), I decided to investigate the nucleation status of cardiomyocytes. This was done by using an enzyme cocktail to digest the ventricles and then plating the cells to let them adhere to coverslips (Figure 46). The nucleus was stained with DAPI and the number of binucleated cells was assessed. I found that the *popdc1* null

fish had a significantly higher number of binucleated cells compared to wild type with about 5% binucleation present in wild type and 11% in the *popdc1* null mutant (Figure 47).

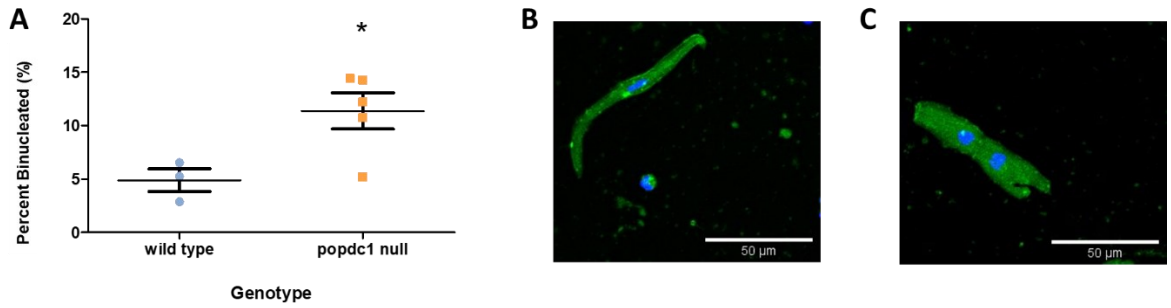

Figure 47 *popdc1* null zebrafish have an increase in binucleated cardiomyocytes. Zebrafish cardiomyocytes were isolated from *popdc1* null and wild type ventricles. Cells expressed GFP in their cardiomyocytes (green) and were counterstained with DAPI (blue) and the number of binucleated cells were counted (**A**), *popdc1* null mutants had a significantly increased number of binucleated cardiomyocytes ($t=2.723$; $df=6$; $p<0.05$), at least three fish were used for each genotype and at least 100 cells were counted per ventricle. Statistical analysis was performed using a t-test on GraphPad Prism. Data are reported as mean ± standard error of the mean with * representing $p<0.05$. Mononucleated and binucleated cells are represented by images **B** and **C** respectively.

5.7.3 *popdc1* null mutants have increased polyploidisation of cardiomyocytes

Polyploidy is also known to limit the regenerative capacity of the zebrafish heart (González-Rosa *et al*., 2018, Patterson *et al*., 2017) and so this was also studied by measuring the total fluorescence of the genomic material after DAPI staining. This was done following a protocol from the Sucov lab (Patterson *et al*., 2017). I found polyploid nuclei in 6 out of 7 ventricles of the *popdc1* null mutant, however, there was large variability in the relative number of polyploid cells (Figure 48). As expected no polyploid cells were found in wild type hearts (Figure 48).

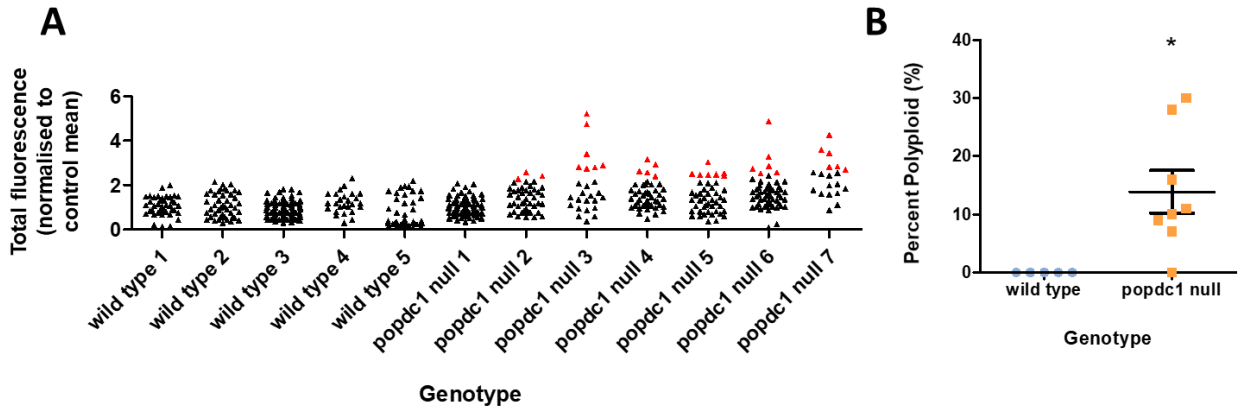

Figure 48 There is an increase in the number of polyploid cardiomyoctes *popdc1* null zebrafish. Zebrafish cardiomyocytes were isolated from *popdc1* null and wild type ventricles and stained with DAPI and the fluorescence intensity was measured. Nuclei showing a fluorescence signal above the threshold and deemed to be polyploid are labelled in red. (**A**) at least 5 fish were used for each genotype and at least 18 nuclei were measured from each ventricle. The percent ploidy are quantified (**B**). There are significantly more polyploid cardiomyocytes in *popdc1* null ventricles (Mdn=71.5) compared to wild type (Mdn=19.5) (U=4.5; p<0.05). GraphPad Prism was used to perform a Mann-Whitney U test, * represents p<0.05 and data are reported as mean ± standard error of the mean.

5.8 Discussion

An increasing number of people in the Western world are suffering from heart failure, we must start to better understand the mechanisms involved in the repair of the heart after injury. Zebrafish have become a prime model to study heart repair after injury as they have retained the ability to regenerate their hearts (Poss *et al*., 2002, González-Rosa *et al*., 2011). Regeneration of the zebrafish heart following injury is a complex process, which involves many genes and pathways, which many labs have already started to untangle (Ryan *et al*., 2020, Sanz-Morejón and Mercader, 2020). Following results in chapter three and based on studies from the Williams Group (Parang *et al*., 2016) it was hypothesised that the *popdc1* null mutant zebrafish might display an increase in myocyte proliferation after injury, thus resulting in a more rapid regeneration because of POPDC1's ability to bind c-Myc and regulate the level of expression by modulating proteolytic degradation. In support of a regeneration-promoting effect of the loss of *Popdc1*, in intestinal epithelial cells, the extent of radiation-induced injury was significantly reduced in *Popdc1* null mutant mice (Reddy *et al*., 2016). However, other forms of injury such as bacterial infection or chemical injury produced larger intestinal injuries in *Popdc1* null mutants, suggesting that the type of injury is important and may determine the outcome (Choksi *et al*., 2018). Possibly, radiation versus bacterial infection or chemical injury trigger different injury

responses, which are activating alternative cellular pathways and depending on the involvement and specific role of POPDC1 in these pathways may have different outcomes.

In this chapter, I was able to demonstrate that the zebrafish *popdc1* mutant *displays* a strongly impaired myocardial regeneration in response to cryoinjury. Although some *popdc1* null mutants were able to regenerate their hearts by 90 DPI, regeneration was strongly retarded when compared to the time course in wild type. Moreover, even at 130 DPI, there were *popdc1* null mutants that had failed to regenerate fully. It was also observed that the *popdc1* null mutants had a reduction in both cell proliferation and apoptosis following injury as well as an abnormal transcriptional response. I also demonstrate that *popdc1* is upregulated following injury, suggestive of a role in the regenerative process. In the following sections, I shall seek to offer some explanations to the findings in this chapter.

5.8.1 *popdc1* is upregulated following cryoinjury

qPCR was employed to monitor the expression levels of *popdc1* following cryoinjury. It was found that in the zebrafish heart at 3, 7 and 14 DPI, *popdc1* was significantly upregulated. However, expression returned to baseline by 21 DPI and expression levels were indistinguishable at that time from sham-operated animals. On top of this, antibody staining for Popdc1 in the injured null mutant ventricle showed an increase in staining at 3 DPI (Brand Lab, Unpublished). Based on these observations and the published involvement of *Popdc1* in the injury response in the murine heart (Alcalay *et al*., 2013), skeletal muscle (Andree *et al*. 2002) and gut (Choksi *et al*., 2018), we hypothesised that *popdc1* might be involved in the regenerative response after myocardial injury in the zebrafish. Interestingly, in contrast to the increased expression of *popdc1* and *popdc2* in the injured zebrafish heart, the expression levels of *Popdc1* mRNA and protein were lowered in mouse hearts subjected to ischemia/reperfusion using a Langendorff preparation (Alcalay *et al*., 2013). These differences in the injury response could be due to the experimental protocol employed, i.e. ischemia/reperfusion versus cryoinjury, but could also be related to species-specific differences. This needs to be further investigated by looking for example at the expression of *Popdc1* in response to injury in the neonate

versus adult mouse heart, to see whether the reported lack of induction of *Popdc1* in response to injury in the adult murine heart correlates with its inability to regenerate.

However, the upregulation of *popdc1* after cardiac injury in the zebrafish heart is not completely unexpected. It is well established that following injury myocytes return to a more developmental-like state, presumably, the de-differentiation of cardiomyocytes helps to stimulate cell proliferation and migration of newly formed myocytes into the wound (Jopling *et al*., 2010). Although the developmental expression of *popdc1* has not been extensively studied in the zebrafish, in the mouse, immunostaining has shown that from E12.5 onwards, POPDC1 is expressed uniformly throughout the cardiomyocytes and then by E17.5 expression is located at the plasma membrane (Smith and Bader, 2006). By in situ hybridisation, it was found that in the mouse at E9.5, *Popdc1* was mainly expressed in the inflow tract, but at E12.5 expression had spread and was now also present in the subepicardial compact layer of the ventricle (Andrée *et al*., 2000). Popdc1 expression at the protein level has also been studied in the developing chick heart where expression steadily increased until E11 at which point POPDC1 levels began to plateau (Vasavada *et al*., 2004, Torlopp *et al*., 2006). Expression analysis by in situ hybridisation studies in the chick detected *Popdc1* in the heart first at Hamburger Hamilton stage 11 in the left ventricular segment but subsequently, *Popdc1* was more widely expressed in the heart (Andrée *et al*., 2000). Assuming that *popdc1* expression in the zebrafish is also upregulated during cardiac development in a similar pattern as seen in other model organisms then its upregulation in response to injury could be interpreted as returning to a more primitive developmental stage to allow for recovery and myocardial regeneration (Jopling *et al*., 2010, González-Rosa *et al*., 2017).

Increased expression in response to injury may however also be interpreted differently since Popdc1 might have a membrane stabilising function in the response to the injury. In this regard, it is worth pointing out that Popdc1 has been found to interact with Dysferlin (Schindler *et al*. 2016) and Annexin 5 (Holt *et al*., 2020), which are both involved in membrane repair in skeletal muscle and similar

processes might also play a role after ischemia-reperfusion injury (Barthélémy *et al*., 2018, Han *et al*., 2007). Moreover, POPDC also interacts with the two-pore tandem potassium channel TREK-1, which recently has been shown to be protective for ischemia/reperfusion injury (Kamatham *et al*., 2019). Thus, the induction in response to injury might represent a protective mechanism to prevent larger damage. In line with this interpretation, it has been found that ischemia-reperfusion injury is more extensively present in *Popdc1* null mutants (Alcalay *et al*., 2013).

Based on our results described in chapter three, it could be postulated that upregulation of *popdc1* may limit cell proliferation due to its inhibitory effect on c-Myc (Parang *et al*., 2016). However, these data were obtained in mice and after transfection in cell lines and thus may not fully translate into the zebrafish heart. Moreover, one has to take into account the complex molecular interactions in the regenerating heart.

5.8.2 *popdc1* null zebrafish have a reduced proliferative ability

5.8.2.1 Retarded regeneration in the popdc1 null mutant

Unlike what was expected of the zebrafish *popdc1* null mutant following the discovery that Popdc1 could interact with and downregulate c-Myc (Parang *et al*., 2016), I found that *popdc1* null mutants displayed a retarded regeneration compared to wild type. Muscle injury and scar formation were similar between genotypes in the first 14 days after injury, however, at 21 DPI I found no evidence of a scar in wild type but in *popdc1* null mutants large scars were present, suggesting retardation of regeneration. Further to this, at both 90 and 130 DPI, where based on the literature we would expect all signs of scaring to be gone in wild type hearts (González-Rosa *et al*., 2011, Chablais *et al*., 2011), there was still scar tissue left in the majority of *popdc1* null mutant hearts. This implies that some of the mutant hearts might be failing to fully recover and might therefore develop a scar that will persist and never resolve. These findings in the zebrafish are in line with findings in the *Popdc1* null mutant mouse model, which displayed a slower skeletal muscle regeneration after injury (Andrée *et al*., 2002a) and a reduced functional recovery after ischemia/reperfusion in the heart of mouse *Popdc1*

null mutants (Alcalay *et al*., 2013). Moreover, *Popdc1* is thought to have a cardioprotective role (Kliminski *et al*., 2017).

It should be mentioned that in this study myocardial regeneration and scar resolution in wild type zebrafish hearts following cryoinjury was more rapid than what has been previously reported in the literature. Some publications still observe a considerable scar at 21 DPI and in some cases a small scar is still detectable at 90 DPI with a full recovery seen by 130 DPI (González-Rosa *et al*., 2011, González-Rosa and Mercader, 2012). However, in this study, I see full regeneration in all wild type fish tested at just 21 DPI. This difference in time course may be related to technical and injury size differences. I see an initial scar size of typically 23-25% when looking from the outside of the heart or 16% when taking averages from AFOG stained sections, whereas others create a scar that amounts to 25% of the ventricle as measured from sections (González-Rosa *et al*., 2011, González-Rosa and Mercader, 2012), which may account for the timing differences. From work in other labs the size of the original injury does appear to play a role in the length of time of recovery, for example, if 20% of the ventricle is cryoinjured then scars are often healed after 60 DPI (Chablais *et al*., 2011). Therefore, due to the consistent injury size in my system and blinded experiments, it is unlikely that the differences in the timeline would affect my conclusions. There was also in some cases a large variability in the scar size at certain time points for example in the mutant at 21dpi, this may be a result of variability in the injury procedure or the variations in the recovery of the fish. As this was sometimes larger than the injury size seen at earlier time point it suggests that initial injury sizes may be variable in some cases, although based on studying the injury technique and getting consistent results we presume this happened minimally and so another explanation could be that the mutant fish are laying down more fibrotic tissue.

5.8.2.2 Altered gene expression in the popdc1 null mutant

Supporting the reduced regenerative ability of the null mutant heart, I also saw a significantly altered gene expression profile by qPCR in the *popdc1* null mutant zebrafish heart following cryoinjury.

popdc1 null mutants failed to upregulate cardiac progenitor marker genes. These genes represent transcription factors involved in early cardiomyocyte specification, which get reactivated in response to injury (González-Rosa *et al*., 2017). It is thought that during zebrafish regeneration, cardiomyocytes dedifferentiate before they can proliferate (Jopling *et al*., 2010). The absence of these transcription factors in injured *popdc1* null mutant hearts suggests that cardiomyocytes are unlikely to undergo dedifferentiation, which however is a prerequisite for the initiation of cell proliferation and cytokinesis. Matrix metalloproteases are required for scar resolution and are typically expressed at 14 DPI (Xu *et al*., 2018, Lien *et al*., 2006), but like the early cardiac transcription factors, these genes were not upregulated in the *popdc1* null mutant. Likewise, the vascularisation marker *vegfaa* was consistently more highly induced in wild type compared to the *popdc1* null mutant heart. This may suggest that the *popdc1* null mutant may also fail to vascularise the damaged area after cryoinjury, a process that is known to be essential in supporting regeneration of the ventricle (Marín-Juez *et al*., 2016). Markers of stress were studied and were highly upregulated in the wild type at 3 DPI. The *popdc1* null mutants, however, failed to upregulate these stress response markers. These results suggest that there must be an impairment of stress signalling in the null mutant as tissue wounding has occurred but does not lead to a proper stress signalling response in the null mutant heart.

Taking these results together, it appears that the *popdc1* null mutant fish is failing to display an induction of expression of several important marker genes involved in myocardial healing and regeneration. However, as we see in the histological analysis ultimately most null mutants still retain the ability to regenerate albeit at a much slower pace. Thus, it may be worthwhile to add some later time points to determine whether the marker genes are still normally activated but may display a different time course. On the other hand, using immunoreagents to identify for example nkx2.5 expressing myocytes in *popdc1* mutants may show that regeneration may be ongoing but in a less coordinated fashion. Mutant and wild type fish displayed a large variability in gene expression, which is likely a result of biological variance and thus, a greater number of animals will be required to obtain more conclusive data, which is essential for proper data interpretation.

5.8.2.3 Loss of proliferative ability in the popdc1 null mutant

Following cryoinjury, a large proportion of the myocardium is damaged and so the cells will go through necrosis and apoptosis (Schnabel *et al*., 2011). This is followed by scar formation and then cardiomyocyte proliferation is triggered at 7 DPI to fully recover after cryo-injury (González-Rosa *et al*., 2011, Schnabel *et al*., 2011, Chablais *et al*., 2011). To test whether in the *podpc1* null mutant myocyte proliferation occurs, hearts were collected at 7 DPI and stained for the mitosis marker phospho-histone 3. It was observed that the *popdc1* null mutants displayed a severe reduction in the number of proliferating cardiomyocytes. As many of the mutant fish can complete regeneration, albeit strongly retarded, it is possible that the *popdc1* null mutant might show continued cardiomyocyte proliferation at a lower level or that the peak of cell proliferation during regeneration might take place at a later time point, however, I did not investigate other time points in this study.

As cardiomyocytes in the *popdc1* null mutant are failing to proliferate at similar levels as in wild type may explain the persistence of scaring. The scar is formed to allow the damaged heart to retain its integrity and will get cleared once there is a suitable number of cardiomyocytes to replace it, therefore without the increase in cardiomyocyte number, the scar cannot be removed (Kikuchi *et al*., 2010). However, the exact role of Popdc1's role in heart regeneration is largely unknown. However, the reduced proliferative capacity provides us with some explanation for aberrant regeneration.

5.8.2.4 Reduction of apoptosis following injury

Although a large proportion of the injured myocardium will undergo necrotic cell death, apoptosis also contributes to the loss of cardiomyocytes following cryoinjury (Schnabel *et al*., 2011). In this study, I measured apoptosis at 1 DPI and found that there wasn't any difference between genotypes in the number of apoptotic nuclei in the injured area of the ventricle, however, there was a decrease in the relative number of apoptotic nuclei. This may be explained by the greater number of nuclei in the injured area of the *popdc1* null mutant. This may suggest that a greater proportion of cells in the injury

area are going through necrosis to complete cell death rather than apoptosis, although this has not been tested or that the mutants have a higher infiltration of immune cells.

It has been shown previously that when *Popdc1* had been silenced in mouse neonatal cardiomyocytes there was an upregulation of the pro-apoptotic marker, Bnip3 (Kliminski *et al*., 2017). This may appear to contradict the finding here where one would expect the upregulation of an apoptotic marker would mean that the cell will more readily go through apoptosis. However, apoptosis is a complex process with many different regulators and processes may differ between mouse and zebrafish. Interestingly, there is an increase in cell number in the *popdc1* null zebrafish in the injury area, this may be explained through POPDC1's regulation of c-Myc (Parang *et al*., 2016). Developmental overexpression of c-Myc in the mouse was able to cause a decrease in cell size but an overall larger heart, suggestive of an increase in cell number (Jackson *et al*., 1990).

5.8.3 Increased binucleation and polyploidy in the popdc1 null zebrafish

Zebrafish unlike mammals are known to have mononucleated, diploid cardiomyocytes (Wills *et al*., 2007, González-Rosa *et al*., 2018). I discovered that there was an over 2-fold increase in binucleation of the *popdc1* null mutant with 11% of cardiomyocytes being binucleated. In this work I found that there was a background of 5% cells that were binucleated in wild type, which is similar to some studies (Patterson *et al*., 2017), however, other studies see a binucleation rate as low as 1% (González-Rosa *et al*., 2018). It is uncertain why these differences arise. However, it could be that the binucleation is seen in replicating cells which may be present in different quantities at different ages.

The DNA content of the cardiomyocyte has been noted as a difference in hearts that permit regeneration and those that do not (Bersell *et al*., 2009, Vivien *et al*., 2016, Smith and Mommersteeg, 2020). More recently it has been demonstrated that cardiomyocyte binucleation is a barrier to regeneration after injury in the zebrafish heart, this was studied by inhibiting Ect2, which blocked cytokinesis (González-Rosa *et al*., 2018). It was found that diploid, mononucleated cardiomyocytes contributed more to heart regeneration than binucleated cells. Moreover, when bi-nucleated

cardiomyocytes accounted for over 50% then regeneration was blocked (González-Rosa *et al*., 2018). Therefore, consistent with the observation that *popdc1* null mutants display a retardation in heart regeneration there is an increased level of binucleated cardiomyocytes.

Polyploidisation has also been shown to block cardiac regeneration, and in both, zebrafish and mouse this is linked to *tnnik3* expression (Patterson *et al*., 2017). On top of having an increase in the number of cells that were binucleated I also found that in the *popdc1* null mutant there were incidences of polyploidisation but not in wild type. The number of polyploid nuclei was quite variable in the individual ventricles that were investigated, which also corresponds to the variability of the regenerative capacity of the *popdc1* null mutant where some mutants were able to fully regenerate after 90 DPI but some still retained scars even at 130 DPI.

Binucleation of cardiomyocytes is linked to animals being endothermic and showing an increase in serum thyroid levels. The link between endothermy and heart regeneration has been tested in the zebrafish where it was demonstrated that by raising thyroid hormone levels, a reduction in heart regenerative capacity was induced (Hirose *et al*., 2019). However, the link of endothermy with binucleation and cardiac regeneration does not fit completely. We see that for example in the case of the Mexican cavefish and medaka, both species are ectotherms, however, they cannot regenerate their heart (Ito *et al*., 2014, Stockdale *et al*., 2018). This is a testament to the sheer complexity of pathways and mechanisms involved in cardiac regeneration.

A possible explanation for the increase in binucleation in the *popdc1* null mutant in zebrafish could be through a mechanistic link to the YAP/TAZ pathway. POPDC1 binds cAMP with high affinity (Schindler and Brand, 2016) and is thought to participate in cAMP signalling although its exact role in the regulation of cAMP is still under investigation. cAMP decreases YAP/TAZ signalling, thus if cAMP levels are reduced, YAP/TAZ signalling is increased causing downregulation of Ect2, a protein known to be essential for cytokinesis (Liu *et al*., 2019). Therefore, if Ect2 is downregulated there will also be downregulation of cytokinesis, providing a potential explanation as to why *popdc1* null mutants have

an increase in binucleation levels. Imbalanced cAMP signalling is likely a phenotype present in *popdc1* null mutants, which may cause an impairment of mitotic spindle formation leading to an increased binucleation and also may be responsible for the increase in polyploidy. Both processes will likely impair the ability of the *popdc1* null mutant heart to undergo myocardial regeneration. However further research will be required to obtain further evidence for this molecular link.

5.8.4 c-Myc and heart regeneration

Before commencing the work for this chapter, I had hypothesised that when *popdc1* was ablated there would be an upregulation of the proto-oncogene c-Myc, which would possibly trigger an increased proliferation of cardiomyocytes and therefore cause an increase in the pace of regeneration. Yet, this was not seen and the *popdc1* null mutant had a reduced proliferative and regenerative ability. Here I will discuss the expression pattern of the Myc genes in the zebrafish and provide some suggestions as to why c-Myc may not be capable of aiding regeneration in the zebrafish ventricle.

In the zebrafish, *myca* and *mycb* expression were expected to be low in the uninjured ventricle based on published data of other species (Seigo *et al*., 1988, Pollack *et al*., 1994), however, in immunostaining performed after injury, I saw that there was c-Myc staining adjacent to the presumptive injury site although staining in the rest of the ventricle and the uninjured ventricle was comparable to a background stain. This suggested that c-Myc may play a role in heart regeneration and agrees with a study of retinal regeneration (Mitra *et al*., 2019), where *mycb* ablation prevented normal regeneration. It also is compatible with the idea that the zebrafish heart needs to activate a heart development-like program for regeneration to occur (Gupta *et al*., 2013, Honkoop *et al*., 2019, Jopling *et al*., 2010) as c-Myc is expressed during the development of the heart as an immediate-early gene in response to growth factor stimulation (Schneider *et al*., 1986, Pollack, 1995). Other labs have also shown that c-Myc is expressed in the regenerating heart (Münch *et al*., 2017, Aguirre *et al*., 2014),

with the de la Pompa Lab having also observed, via in situ hybridisation, that following cryoinjury *mycb* is expressed in the area adjacent to the injury site (Münch *et al*., 2017).

qPCR data suggest that both, *myca* and *mycb* are expressed in the uninjured adult zebrafish heart. Interestingly, there appeared to be a slight reduction of these genes expressed in the *popdc1* null zebrafish ventricles, however, this difference did not reach statistical significance. Based on previous work in the mouse, we would expect there to be an increase in c-Myc expression at the protein level when *popdc1* is knocked out, however, as a post-translational modification governs this change (Parang *et al*., 2016, Arnold and Sears, 2006, Sears *et al*., 2000), it is not unexpected to see that *myca* and *mycb* levels are not significantly different between wild type and the *popdc1* null mutants. *mycb* was also more highly expressed at 3 DPI and 7 DPI in the *popdc1* null mutant compared to wild type but also appeared to be transiently upregulated at 3DPI in the wild type. *Myca* did not appear to be upregulated in the wild type zebrafish cardiac myocytes after injury however in the *popdc1* null zebrafish there was an increase at 7 DPI. Although none of the differences in expression of either of the *myc* genes reached significance the slight upregulation may suggest that the *popdc1* null mutant express higher levels of *myca* and *mycb* compared to wild type, suggesting that the loss of *popdc1* may also have some effect on *c-Myc* expression levels in the zebrafish heart. The qPCR readings from the zebrafish resulted in large variabilities, which may provide some explanation why it was difficult to reach significance in these experiments, however, this maybe due to there not being a real difference. The high variability may be caused by the cryoinjury resulting in differing injury sizes and differences in the injury response. On top of this, differences may not be seen because the whole ventricle was taken and not just the area bordering the injury and so the increased expression may not be visible if the entire organ is investigated.

The loss of *popdc1* in the zebrafish was unable to speed up the regeneration process and in fact appeared to cause it to be delayed. Heart regeneration is a complex process that involves a large number of genes being activated at the correct time. Further to this, many different cell types are

having to act to form the correct microenvironment to facilitate regeneration (Ryan *et al*., 2020, Sanz-Morejón and Mercader, 2020), therefore, looking solely for an increased presence of one protein in one cell type has the potential to vastly oversimplify the regenerative response. Looking specifically at c-Myc, previous reports have suggested that unlike in tumours, the regenerating zebrafish heart displays a reduction in expression of the downstream targets of c-Myc (Dicks *et al*., 2020), although others have reported an increase in c-Myc expression following cardiac injury (Münch *et al*., 2017, Aguirre *et al*., 2014). Moreover, other studies suggested that even when there is a strong c-Myc expression in the heart, cardiomyocytes do not respond with increased proliferation (Bywater *et al*., 2020). It has also been suggested that although cardiomyocytes can re-enter the cell cycle in response to c-Myc overexpression, they are incapable of going through cytokinesis (Xiao *et al*., 2001). Taken together, these studies suggest that c-Myc alone is not sufficient to enhance proliferation in cardiomyocytes.

5.8.5 Conclusions and future directions

To conclude, *popdc1* is upregulated in the ventricle following cryoinjury and if *popdc1* is absent then there is a reduced regenerative ability along with a reduction in both proliferation and apoptosis. The regulation of regeneration in the zebrafish heart is multi-faceted with several genes and cell types having an important role in the regulation of regeneration (Ryan *et al*., 2020, Sanz-Morejón and Mercader, 2020). From the results in this chapter, it is implied that Popdc1 has an essential role in correct regeneration and that it can affect the proliferative ability of the heart, which may be mediated by the binucleation and ploidy status of the cardiomyocytes. I had hypothesised that Popdc1 would act as a negative regulator of proliferation due to its interaction with c-Myc. However, in this chapter, I saw that Popdc1 is essential to have a high level of proliferation after injury. On from this, the *popdc1* null mutant will need to be more intensely studied to better characterise its gene expression pattern at baseline (see chapter 6) and in response to injury, with the hope of uncovering some genes or pathways which could shed light on the reduced proliferative capacity of the *popdc1* null mutant. These insights may also provide novel means to improve myocardial healing and regeneration in the

adult human heart. It would also be interesting to study the *popdc1*^{s191f} zebrafish mutant, which has improper cAMP binding activity (Schindler *et al*., 2016b) to determine if Popdc1's ability to affect the cAMP level in cardiac myocytes is causing the same differences as seen here for the null mutant.

6. Single nuclear RNA sequencing of *popdc1* null zebrafish

Large-scale sequencing used to be a challenging endeavour, for example, the Human Genome Project took over 10 years and cost billions of US dollars (Francis *et al*., 2003). At that time large-scale sequencing and transcriptomic approaches were not available for the average researcher; however, more recently next-generation sequencing (NGS) has become a widely available technique that is high-throughput and can be done at speed with an entire human genome being sequenced in just one day. NGS sequences millions of small fragments of DNA in parallel and then bioinformatic tools are used to map the fragments to a reference genome to piece the fragments together. Transcriptome analysis by RNA sequencing has been able to piggyback off NGS to study tissue-specific gene expression, however, these transcriptome data are derived from different cell types present in a given tissue. Although this yielded large amounts of information and fuelled discoveries single-cell RNA sequencing has been able to take this process a step further and examines the transcriptome of individual cells, using microfluidics to barcode each cell with a unique molecular identifier (UMI), which will then tag the RNA that is later amplified allowing transcripts to be grouped depending on which cell they originated from. Bioinformatic tools can then be applied to group cells with similar transcriptomic patterns. This provides information on the heterogeneity of cells and can help researchers to define different cell types that makeup tissue or organs and make predictions about their roles in a particular microenvironment (Eberwine *et al*., 2014) or can help to identify rare populations of cells that are not visible in bulk tissue RNA sequencing (Miyamoto *et al*., 2015). Dissociating tissue to obtain single cells from tissues to perform single-cell RNA sequencing can be challenging., Moreover, large cells such as cardiomyocytes, which in the fish heart are between 80-120 µm in length, will be too large to be accepted by the GEMs, thus they could not be individually barcoded. For this reason, some transcriptomic studies have used isolated nuclei instead of cells to circumvent the size issue (Bushman *et al*., 2015, Lake *et al*., 2017, See *et al*., 2017, Litvinukova *et al*., 2020). However single nuclear RNA sequencing can only capture the nuclear mRNA and thus any regulations that happen to the cytoplasmic RNA pool will not be represented by these sequencing data (Thrupp *et al*., 2020). Another

problem present in both single-cell and single-nuclear sequencing is the presence of doublets where two cells or nuclei obtain the same UMI as they were not properly segregated. This could skew the data, however, bioinformatic tools like Scrublet have been developed to identify doublets and remove them from the data set before analysis (Wolock *et al*., 2019).

Popdc1 is a complex protein with a large number of interaction partners (Amunjela *et al*., 2019) and its role in the heart is still not completely understood. In this chapter, I aimed to gain a better understanding of the effects of the loss of *popdc1* by performing single-nucleus sequencing on the ventricles of wild type and *popdc1* null mutants in the zebrafish. After ensuring high quality of the transcriptome data, I first aimed to identify transcriptional differences in the ventricle between wild type and *popdc1* null mutant, taking a specific interest in the cardiomyocyte population because in the heart Popdc1 is thought to be mainly expressed by cardiomyocytes (Andrée *et al*., 2000). As there are several anatomical and histological differences apparent between the *popdc1* null mutant and wild type zebrafish (Chapter 4), I expected to also see differences at the transcriptome level that might provide some clues to why these phenotypes might be present. Moreover, I was looking for differences in gene expression that may help to explain the reduced myocardial proliferation and regeneration in the *popdc1* null mutant following cryoinjury (Chapter 5).

6.1 Results: Quality control

Other groups have reported recently single-cell RNA sequencing data for the adult zebrafish heart (Honkoop *et al*., 2019, Koth *et al*., 2020). However, these data were limited by the low numbers of cardiomyocytes sequenced as the single-cell sequencing approach is unable to handle cells that are larger than 50µm in diameter (10x Genomics, 2021). I therefore decided to perform single-nuclear RNA sequencing (snRNA-seq) of ventricular tissue of both *popdc1* null and wild type zebrafish, which would circumvent this issue and ensure an unbiased range of nuclei from different cell types captured by the GEMs.

6.1.1 Purifying the nuclear population

Five ventricles were pooled for each sample and three samples were used from each genotype. Nuclei were isolated from the samples and stained with NucBlue™ and then sorted using a cell sorter to purify the population. The nuclei were gated for size to remove any debris, doublets and finally gated using the 450nm channel to ensure that only those stained for NucBlue™ were retained (Figure 49). This greatly reduced the amount of debris in the sample by removing over 4/5 of the events, leaving purer samples that could go on to be counted and then run through the 10x genomics protocol required to send the samples for sequencing.

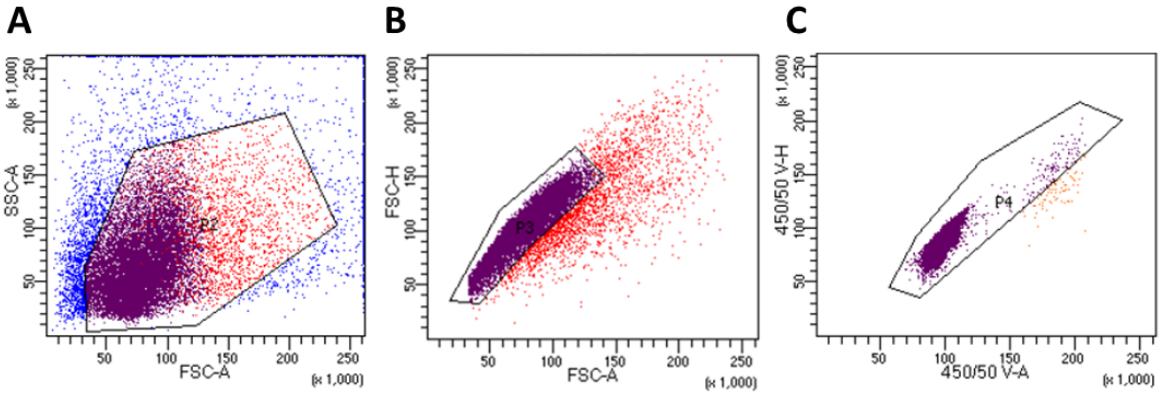

Figure 49 Purifying the nuclear population. An example of the output from a nuclear extraction sample stained with NucBlue™ and ran through the FACS Aria fusion sorter. Nuclei were gated to remove debris (**A**) and doublets (**B**). Nuclei were also gaited to retain those that had been stained with the NucBlue™ dye (**C**). 18% of the events were collected and taken forward to the next stage.

6.1.2 Quality control before NGS.

The nuclei were taken through GEM generation and barcoding stages before being cleaned up, the nuclear RNA was isolated and reverse transcribed and the resulting cDNA was amplified. Gene expression libraries were then created from each sample and subjected to some quality controls steps both in our laboratory and once they had been sent to Genewiz, where the next generation sequencing took place. Firstly, the cDNA concentration was assessed using a Bioanalyzer, in house, and then a Tapestation and Qubit Bioanalyzer at Genewiz to ensure that comparable concentrations were found for each sample (Table 16). These different types of equipment use electrophoresis as a

basis to assess the quality and quantity of cDNA in the samples. The average library length was also extrapolated from bioanalyzer measurements at both Imperial College London and at Genewiz to check if they were comparable (Table 17). Both cDNA concentration and library size were similar enough from the different estimations to proceed (Table 16 and Table 17), differences in the estimates are thought to have occurred from different sensitivities in the equipment and perhaps some degradation upon transport.

Table 16 cDNA concentration for samples for NGS as measured in house and by Genewiz

	Library Concentration		
Test location	Imperial	Genewiz	
Sample	Bioanalyser ng/µL	Tapestation ng/µL	Qubit ng/µL
wild type a	7.27795	5.44	8.35
wild type b	4.8837	3.67	5.75
wild type c	5.64185	4.8	6.97
***popdc1* null a**	10.5029	8.36	12.4
***popdc1* null b**	6.00375	5.42	8.63
***popdc1* null c**	3.6377	3.85	3.94

Table 17 Average library size for samples for NGS as extrapolated from bioanalyzer measurements in house and by Genewiz

	Library Average Size	
Sample	Imperial	Genewiz
wild type a	439	403
wild type b	477	404
wild type c	473	422
***popdc1* null a**	464	415
***popdc1* null b**	411	400
***popdc1* null c**	511	395

6.1.3 Post sequencing quality controls

Once sequencing was completed, data files were returned to us from Genewiz and put through Cell Ranger 5.0.1 (Zheng *et al*., 2017). Cell Ranger is a set of analysis pipelines that process the single-nuclear data to align reads to the zebrafish reference genome (*Danio rerio*, GRCz11.102) and create a feature-barcode matrix. From this step, I found that I had 3917 nuclei from *popdc1* null zebrafish

ventricles and 4621 nuclei from wild type ventricles, combined from the replicates from each genotype. There was an average of 264,063 reads per nuclei, 25,107 different genes detected and 1319 was the mean number of transcripts detected per cell, across all of the samples. These numbers were suitably high enough to continue the analysis and move through the quality control steps.

From this stage, the analysis could begin using the Scanpy 1.7.0 package in Python 3.6.10, which is software for analysing single-cell or -nuclear RNA sequencing (Wolf *et al*., 2018). The samples were filtered so that nuclei had a UMI count of between 500 and 7500 which indicated the total number of transcripts found in each nucleus. They were also filtered to have between 300 and 2500 different genes expressed per nucleus and to have less than 5% mitochondrial and ribosomal genes (Figure 50). Scrublet is a computational tool that scores nuclei to help identify doublets (Wolock *et al*., 2019), nuclei were only retained if they had a score of less than 0.3 (Figure 50). This reduced the number of nuclei that were further studied from a total of 8,538 to 7,422, however, the number of genes remained the same at 25,107. The distribution of the number of genes and the number of UMI is bimodal in our sample, although this can represent more than one nuclei being captured in the GEM or poor quality of some nuclei it can also represent differences between cell types, with some cell types having a more active transcriptome than others (Harvard Chan Bioinformatics Core, 2021). Another study has also seen a bimodal distribution when looking at ventricular tissue (Honkoop *et al*., 2019).

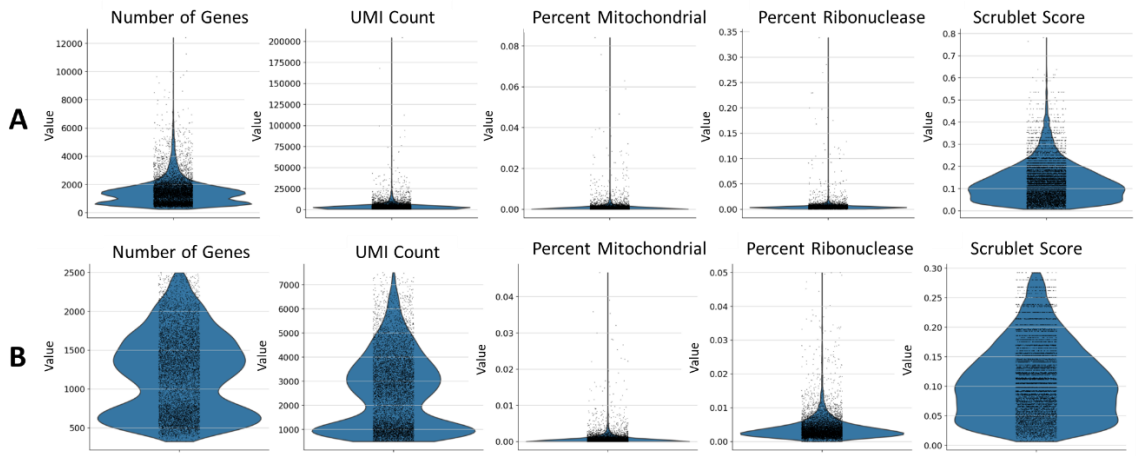

Figure 50 Filtering of nuclei for use in snRNA-seq analysis. Violin plots of the number of UMI count, number of genes, percent mitochondrial, percent ribonuclease and scrublet score of nuclei from all samples before (**A**) and after filtering (**B**).

6.2 Results: Annotation of major cell types

Once the nuclei had been filtered by the quality control measures described in the previous section, they were clustered to identify cell types. Firstly, the quality control filters and the genotypes were plotted in UMAPs (Figure 51), this was to check for specific clusters which were doublet (two nuclei that had ended up with the same UMI) or had high levels of ribosomal or mitochondrial genes. Here it can be seen that the higher numbers of UMIs and genes as well as scrublet scores are from nuclei in the top right of the UMAP. This could mean that these nuclei clusters are doublets, however, nuclei from certain cell types are known to have higher RNA expression especially if the cell has an active role, which could give rise to the difference (Zhang *et al.*, 2019). The percent ribonuclease and mitochondrial was low across the whole UMAP. The data were also plotted by genotype (Figure 51) to ensure that there was no genotype-specific effect on these scores.

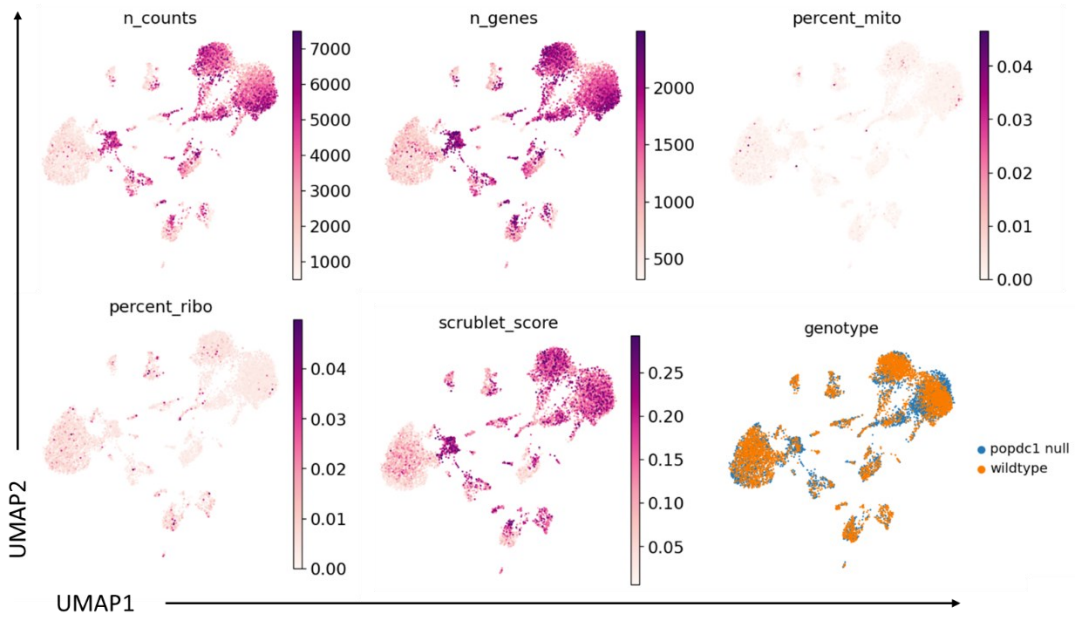

Figure 51 UMAP plot of all the nuclei combined from both genotypes. UMAP plots showing the number of UMI counts (n_counts), number of genes (n_genes), percent mitochondrial (percent_mito), percent ribonuclease (percent_ribo), scrublet score, with a high score represented as dark pink and a low score represented as white as shown in each UMAPs colour scale bar. The genotype for all nuclei is also shown in the final UMAP with wild type nuclei in orange and *popdc1* null nuclei in blue.

All nuclei from the three samples of both genotypes were plotted on a UMAP and were split into 11 clusters based on their similarities (Figure 52). Annotations were made as to what each cluster was presumed to be and is comprised of atrial cardiomyocytes (atrial CM), three types of ventricular cardiomyocytes (cardiomyocyte 1, cardiomyocyte 2, cardiomyocyte 3), three different types of endothelial cells (endothelial, endothelial 2, lymphatic endothelial cells (endothelial – lymphatic)), epicardial fibroblasts, immune cells, pericytes and thrombocytes (zebrafish thrombocytes have a nucleus). These annotations were based on the differential expression of marker genes in the different clusters (Figure 53). All cardiomyocytes showed a high expression of genes encoding sarcomeric proteins (*tnnt2a* and *ttn.2*) and proteins involved in calcium transport (*ryr2b*). The atrial CM population was mainly defined by the expression of the atrial specific myosin heavy chain isoform *myh6* and the ventricular cardiomyocyte populations (cardiomyocyte 1-3) were mainly defined by the expression of the ventricle-specific marker *myh7l* (Berdougo *et al*., 2003). Endothelial nuclei were identified based on the expression of the pan-endothelial marker genes *kdrl, cdh5* and *flt1*, with lymphatic endothelial

nuclei being differentiated from other endothelial cells by the expression of *flt4*, which is considered to be specifically expressed in lymphatic vessels (Küchler *et al*., 2006). Some of these nuclei may also represent an endocardial population, with other studies also clustering endocardial and vascular endothelial populations together due to their similarity (Koth *et al*., 2020), a more in-depth study of the endothelial clusters would be required to assess this further. Thrombocytes were identified based on the expression of the pan-thrombocyte markers *itga2b, itgb3b* and *mpl*. Nuclei in the epicardial fibroblast cluster were classified based on their expression of *tbx18*, *tcf21*, *pdgfra* and *col1a1a*. Immune nuclei were identified by their high expression of the immune cell markers genes: *ctsd, sla2* and *cd74a*, while pericytes were classified due to the expression of markers, *pdgfrb, rgs5a* and *abcc9*.

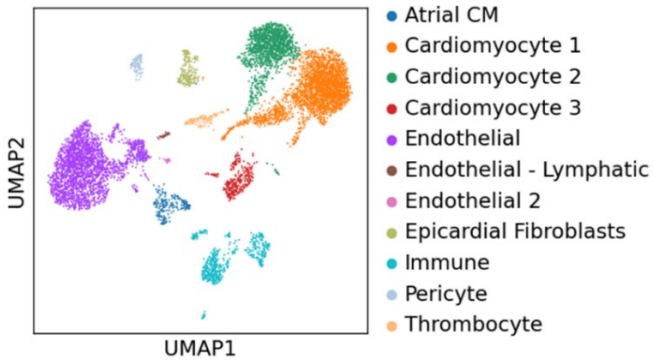

Figure 52 UMAP plot of all the nuclei combined from both genotypes. UMAP (left) of all nuclei from the three samples from each genotype split into 11 clusters with their annotation (right).

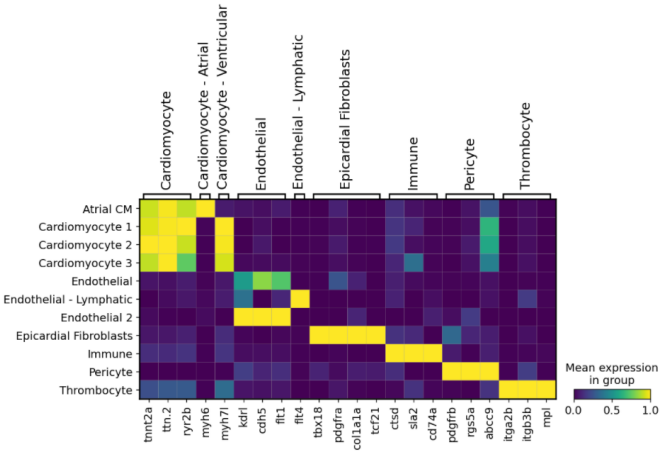

Figure 53 Heatmap showing example genes used to determine the identity of different cell clusters. Genes (bottom labels) which are known markers of different ventricular cell types (top labels) were used to identify and give names to the different clusters produced by the UMAP plot (left labels). High mean expression is shown in the heat map in yellow and low in blue as shown by the colour scale bar, with the values normalised between 0 and 1.

The percentage of nuclei in each cluster was calculated for the different genotypes (Figure 54). The *popdc1* null mutant had more atrial cardiomyocytes than wild type. They also displayed a reduction of the cardiomyocyte 2 population, although the overall number of cardiomyocytes was comparable and the reduction in cardiomyocyte 2 was compensated by an increase in cardiomyocyte 1. The relative level of cardiomyocyte 3 was comparable in both genotypes. There were also differences in some of the non-muscle cell populations, which were made up of only small numbers of nuclei. For example, *popdc1* null mutant samples had a reduction of endothelial 2, lymphatic vessel endothelial cells and pericytes populations. However, only the difference in the cardiomyocyte 1 cluster reached significance (Figure 54).

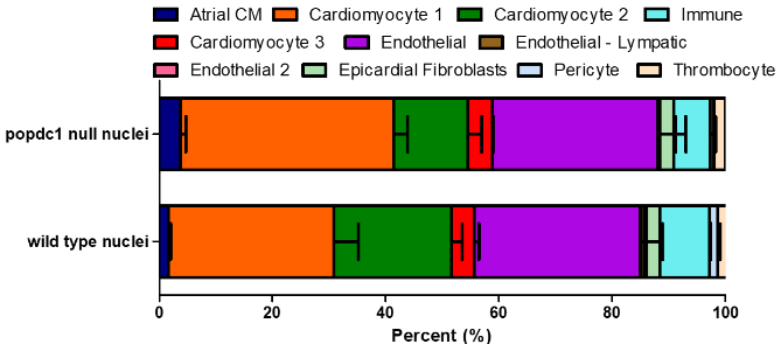

Figure 54 The percentage of nuclei forming each cluster between genotypes. Nuclei from each genotype were separated and the percentage that made up each cluster was averaged across the three samples and are reported as mean ± standard error of the mean. Statistical analysis was performed using a 2-way ANOVA with a Bonferroni post hoc test where it was found that genotypes did affect percentage per cluster ($F=2.07$; $df=10$; $p<0.05$). However, only the cardiomyocyte 1 cluster was significantly different between genotypes, with *popdc1* null mutants having a larger number of them ($t=2.11$; $df=1$; $p<0.05$).

6.3 Results: Popdc1 expression

The expression of *popdc1* was assessed from the snRNA-seq data. The *popdc1* null mutant was created using TALENS by targeting the first exon of *popdc1* resulting in a single base pair deletion, which resulted in a frameshift causing a premature stop codon (Brand Lab, Unpublished). This would likely result in the mRNA being transcribed but would encode a peptide of 39 amino acids that is not expected to be able to perform its biological function and would be targeted for degradation suggested by its inability to be detected in immunostaining. Upon assessing the expression of *popdc1*

in the nuclei of *popdc1* null mutants and wild type ventricles, I found that the RNA expression levels in the *popdc1* null mutant were actually increased compared to wild type (Figure 55).

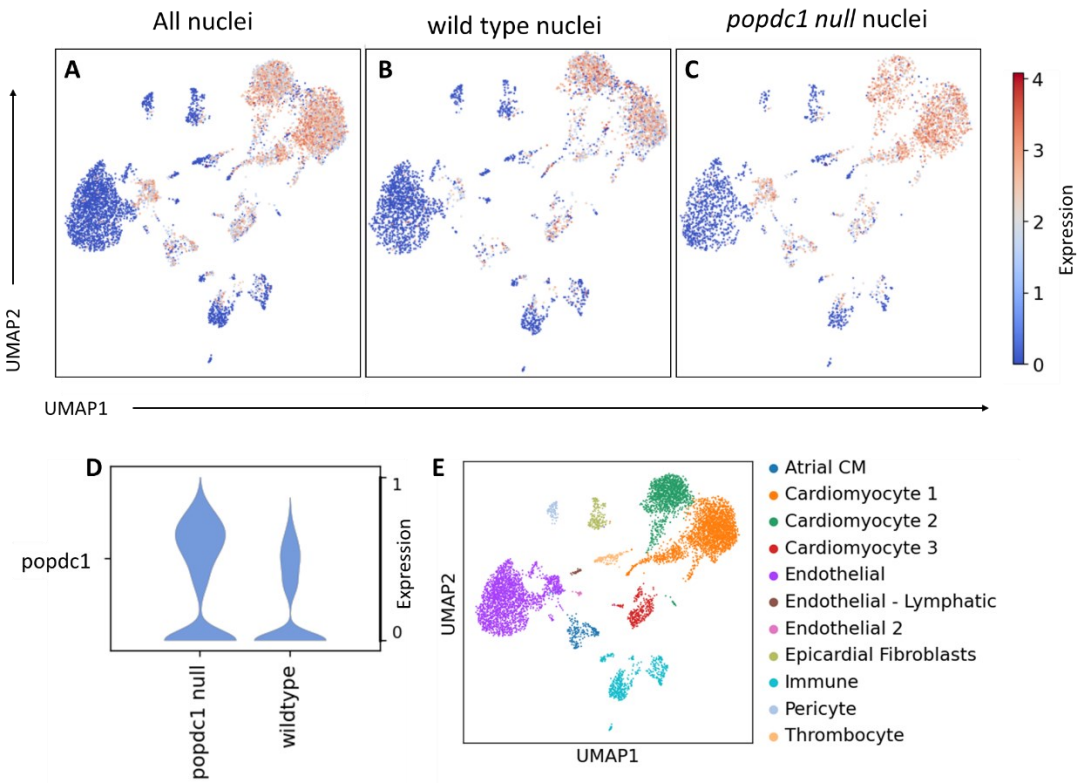

Figure 55 *popdc1* expression in all nuclei. *popdc1* UMAPs were made for all nuclei combined (**A**), wild type nuclei (**B**) and *popdc1* null mutant nuclei (**C**), the expression level was normalised for values between 1 and 4 as visualised in the scale bar. Violin plots were made to visualise the *popdc1* expression between genotypes, with expression normalised between 0 and 1 (**D**). An annotated UMAP is shown for all the nuclei in the ventricle for reference (**E**). was more highly expressed in the *popdc1* null mutant compared to the wildtype (Z=1.330398, p<0.001).

When looking at the *popdc1* expression across different clusters, *popdc1* was found to be enriched in the different cardiomyocyte populations (atrial CM and cardiomyocyte 1-3) as expected (Figure 56). In all the other clusters *popdc1* expression was on average low or absent, although small populations of *popdc1* expressing nuclei can be found in endothelial, immune, thrombocyte and epicardial fibroblast nuclei (Figure 55 and Figure 56). Notably, there is a subset of mutant endothelial cells with nuclei that display high *popdc1* expression (Figure 55).

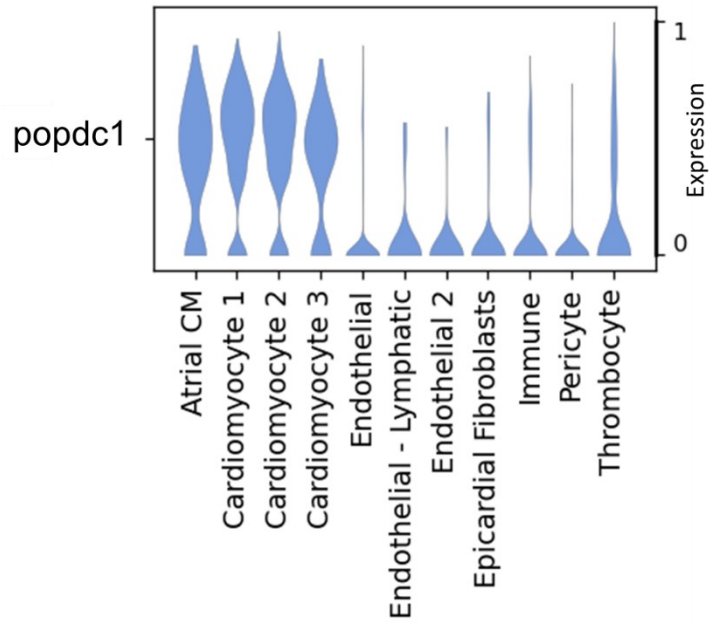

Figure 56 Expression of *popdc1* in different ventricular clusters. Violin plots were made to visualise the *popdc1* expression between different clusters found in the zebrafish ventricle, their expression has been normalised between 0 and 1. *popdc1* was significantly more highly expressed in the atrial CMs (Z=2.2618594, p<0.001) and the Cardiomyocyte 2 population (Z=1.568, p<0.001).

6.4 Results: Cardiomyocyte heterogeneity

As *popdc1* is expressed at high levels in the cardiomyocytes, going forward with the analysis of the single-nuclei seq data I focused on the cardiomyocyte 1, cardiomyocyte 2 and cardiomyocyte 3 populations. The atrial CM population was not included as I wanted to limit my study to ventricular cardiomyocyte nuclei, with the hope of identifying possible reasons for the loss of heart regeneration in the null mutant. The three ventricular populations were isolated from the global population of nuclei and Scanpy was used to cluster these cardiomyocytes into subclusters. The quality control metrics and the genotypes were plotted on a UMAP (Figure 57). The UMI counts and the number of genes were high and the Scrublet score and the percent ribonuclease and mitochondrial genes were low throughout most of the nuclei (Figure 57). Interestingly when looking at the genotype UMAP I see that the *popdc1* null mutant nuclei form distinct clusters compared to wild type nuclei, some clusters are specifically populated by wild type cells, but the null mutant-specific clusters are much larger (Figure 57).

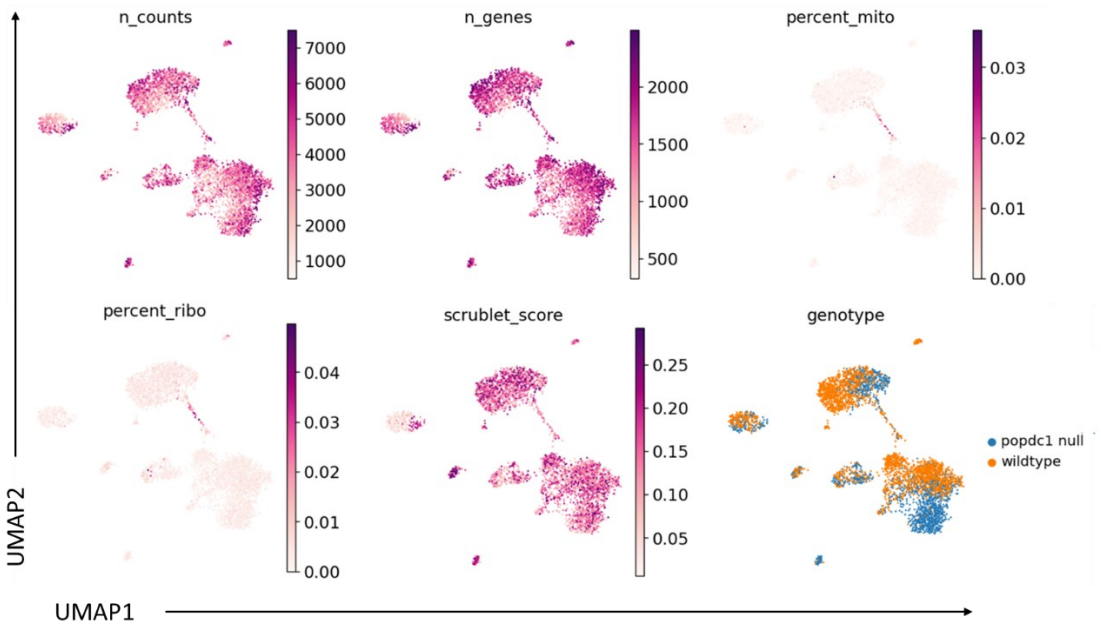

Figure 57 UMAP plot of all cardiomyocyte nuclei combined from both genotypes. UMAP plots showing the number of UMI counts (n_counts), number of genes (n_genes), percent mitochondrial (percent_mito), percent ribonuclease (percent_ribo), scrublet score with a high score represented as dark pink and a low score represented as white as shown in each UMAPs colour scale bar. The genotype for all nuclei is also shown in the final UMAP with wild type nuclei in orange and *popdc1* null nuclei in blue.

Clustering of cardiomyocytes at a higher resolution than in the global clustering split the nuclei into 10 sub-clusters to represent the different types of cardiomyocytes (Figure 58A). The sub-clusters were labelled CM1-10. UMAPs were also created for nuclei from wild type and *popdc1* null mutant samples to compare their profiles (Figure 58B-C). The UMAP projections of cardiomyocytes indicated the existence of sub-clusters that were populated primarily by only one of the genotypes.

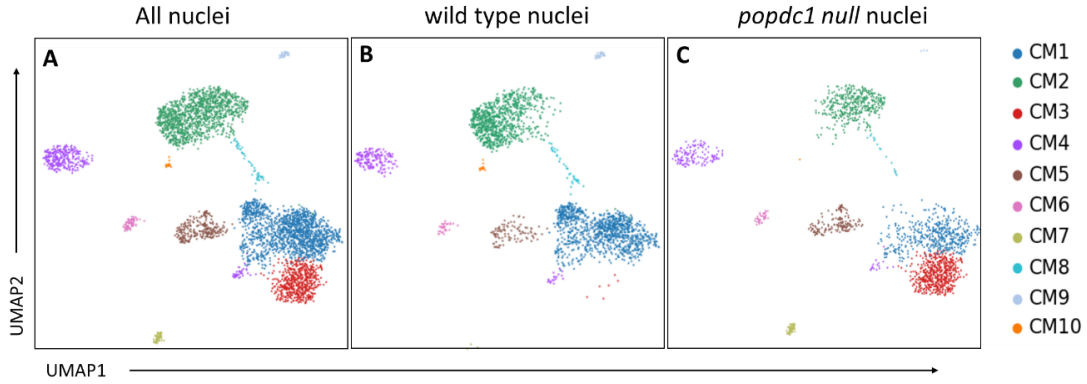

Figure 58 UMAP of all cardiomyocyte nuclei. UMAPs were made for all the nuclei (**A**), wild type only nuclei (**B**) and *popdc1* null nuclei (**C**). The clusters were labelled CM1 to CM10 and each had a unique colour as per the key to the right of the figure.

The relative number of nuclei from each CM sub-cluster was quantified for both genotypes and the representation of nuclei looked quite different. The *popdc1* null mutant nuclei were less represented in CM1 and CM2 but had a 100-fold increase in the CM3 population. CM3 was nearly absent in the wild type samples, having only a few nuclei present with this expression profile (Figure 59). Furthermore, the *popdc1* null mutant samples had a roughly 20-fold increase in CM7 nuclei compared to wild type (Figure 59). However, *popdc1* null mutants had 8- and 12-times fewer nuclei in CM9 and CM10 respectively (Figure 59), although these both represent very small cell populations. The differences for CM1, CM2 and CM3 reached statistical significance (Figure 59).

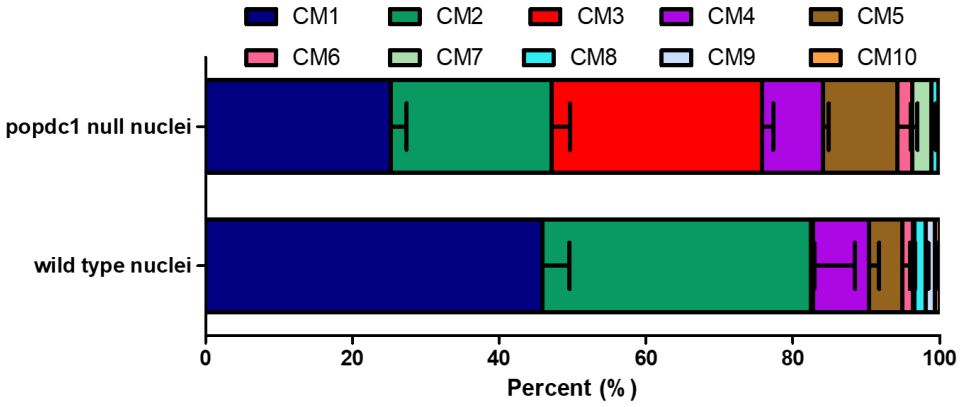

Figure 59 The percentage of nuclei from each cardiomyocyte sub-cluster in null mutant and wild type ventricles. Nuclei from each genotype were separated and the percentage that made up each sub-cluster was averaged across the three samples and are reported as mean ± standard error of the mean. Statistical analysis was performed using a 2-way ANOVA with a Bonferroni post hoc test where it was found that genotypes did affect percentage per sub-cluster ($F=23.18$; $df=10$; $p<0.0001$). CM1, CM2 and CM3 sub-clusters were significantly different between genotypes, with *popdc1* null mutants having a greater percentage in CM3 ($t=10.64$; $df=1$; $p<0.001$) and significantly smaller percentages of CM1 ($t=7.729$; $df=1$; $p<0.001$) and CM2 ($t=5.478$; $df=1$; $p<0.001$).

To begin to understand what roles the different cardiomyocyte sub-clusters might have, the significantly differentially expressed genes were calculated for each of the clusters and the 4 most differentially expressed genes for each cluster was included in a dot plot (Figure 60).

CM1 was enriched for *tbx5a*. Interestingly, it has recently been shown that the ventricular trabecular layer displays a high level of *tbx5a* expression(Sánchez-Iranzo *et al*., 2018), which suggests that the CM1 population may potentially represent the trabecular layer. Although, another trabeculae marker,

nppa (Jensen et al., 2012), is not specifically upregulated here (Figure 61), unfortunately, no other markers have been identified in the literature to substantiate this interpretation any further. CM2 had no obvious functional role but gene expression was enriched for *dab2*, *gabrb2a* and *sox4a,* which are known to be involved in the inhibition of WNT/β-catenin signalling (Hofsteen *et al*., 2016), inhibition of neural transmission (Jurd *et al*., 2008) and outflow tract development (Paul *et al*., 2014) respectively. CM2 also displayed a high expression of *lama5* which is known to be a marker specifically expressed in the cortical layer (Sánchez-Iranzo *et al*., 2018), but none of the other cortical layer marker genes (*xirp2a* and *hey2*) were enriched in this cell population (Figure 61). CM3 nuclei were almost exclusively derived from the *popdc1* null mutant and these nuclei showed an expression of stress markers such as *nppa* and *atf3* (Zhou *et al*., 2018, Sergeeva *et al*., 2014). *acta1b* was also heavily upregulated and codes for skeletal muscle α-actin that is upregulated when the mammalian heart is under mechanical stress (Schwartz *et al*., 1986). This suggests that this cell population are probably induced in response to stress that the *popdc1* null mutant heart is under, from results in chapter 4 I can suggest that the stress may be caused due to the morphological differences in the hearts. CM3 also demonstrates high levels of *cryabb*, encoding the crystallin alpha B isoform, which is a cytoprotective and antioxidant heat shock protein (Fittipaldi *et al*., 2015). Upregulation of these stress-related genes indicates that these ventricular cardiomyocytes are probably outfitted to perform a higher workload than other ventricular cardiomyocytes. The CM4 population has the highest expression of *lama5*, xirp2a and hey2 (Figure 61), which are known to specifically mark the cortical layer (Sánchez-Iranzo *et al*., 2018, Otten *et al*., 2012), although *lama5* was also highly expressed in CM2, this suggests possibly a role for CM2 and CM4 in the cortical layer of the myocardium. CM4 was also enriched for *pdlim5a, bcam, fhod3b* and *tns1b,* which are genes involved in cell adhesion and actin filament cross-linking and polymerisation. Genes such as *ank1a* and *hbba1-1* are enriched in CM5 and are also expressed in erythrocytes and so may represent an erythrocyte-like population in the cardiomyocytes. CM6 had a high expression of genes such as *grb10a, spock3* and *coro1ca* which are presumed to have insulin receptor signalling, calcium-binding and actin-binding filament activity

respectively, but had no clear function. CM7 was almost exclusively found in the *popdc1* null mutant and like CM3 displayed high expression levels of stress markers as well as hypoxia-related genes like *hif1al2* again suggesting that this population of cells are characterised by an upregulation of stress-related genes. CM8 was enriched for mitochondrial genes that are associated with apoptosis like *mt-co1, mt-co2* and *mt-co3* and so it is likely that CM8 represents a population of nuclei which are dying or of low quality. CM9 has high expression of endosomal associated genes such as *laptm4b* and *chmp6b* and is represented mainly by wild type cells. CM10 again mainly contains wild type nuclei and is enriched for genes associated with the immune system such as *rorc, dapp1* and *runx3* suggesting an immune cell-like function for these nuclei.

Popdc1 null enriched sub-clusters, CM3 and CM7, showed similar transcriptional profiles to one another especially regarding the expression of stress-related genes. These two populations also appeared to be a subset of nuclei that fell under the same umbrella as CM1, which might represent cells, which form the trabecular layer. This assumption is mainly based on its expression of *tbx5a* (Sánchez-Iranzo *et al*., 2018). Interestingly, however, *tbx5a* expression was very low in CM3 and CM7 (Figure 61). These three sub-clusters are then parallel to a branch that contains CM5 and CM8. These five cell clusters are grouped together. On the other side is CM2, which possibly is representing the cells, which form the cortical layer of the zebrafish heart and is clustered together with CM9. Related to these two subclusters are CM4, CM6 and CM10 (Figure 60).

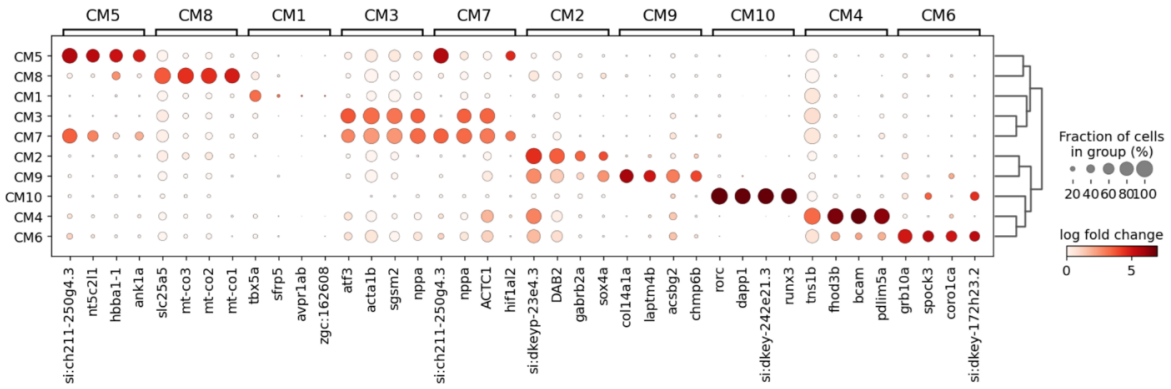

Figure 60 Dot plot of the differentially regulated genes for the different cardiomyocyte sub-clusters. The top 4 most differentially regulated genes for each cardiomyocyte subcluster are shown in a dot plot, with the size of the dot representing the percentage of nuclei that express the gene and the colour of the dot representing the log of the fold change away from the average expression with the scale running from white (low expression) to red (high expression). To the right of the dot plot is a dendrogram that maps out the relatedness of the different clusters to one another.

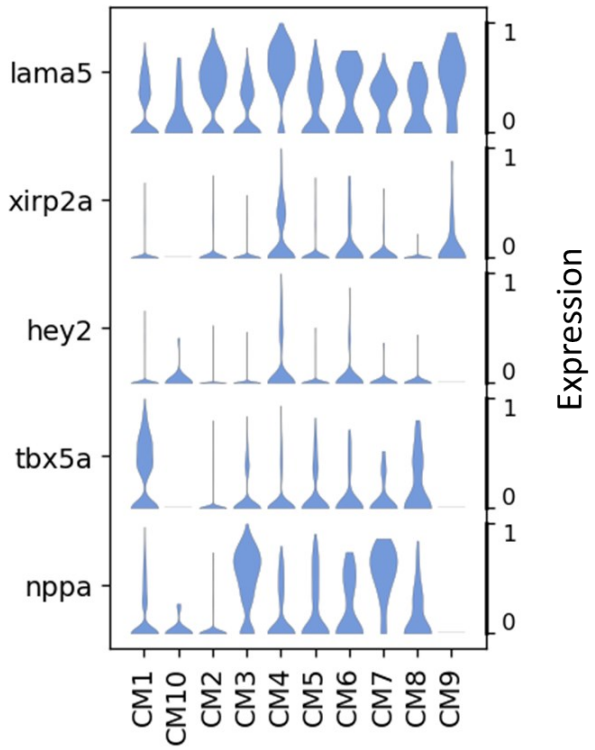

Figure 61 Expression of cortical and trabecular layer markers in different ventricular clusters. Violin plots were made to visualise the expression of cortical layer (*lama5a*, *xirp2a* and *hey2*) and trabecular layer (*tbx5a* and *nppa*) markers between different clusters found in the zebrafish ventricle. Their expression has been normalised to fall between 0 and 1. *lama5* was significantly more highly expressed in CM2 (Z=1.1199, p<0.001) and CM4 (Z=2.2011, p<0.001). *xirp2a* (Z=3.349, p<0.001) and *hey2* (Z=4.2778, p<0.001) were significantly upregulated in CM4. *tbx5a* was significantly upregulated in CM1 (Z=3.3431, p<0.001). *nppa* was upregulated in CM3 (Z=3.6252, p<0.001) and CM7 (Z=3.4311, p<0.001).

6.5 Results: A comparison of *popdc1* null vs wild type ventricular nuclei

As *popdc1* is primarily expressed in cardiomyocytes, my investigation of the differences between the mutant and wild type began here. All of the ventricular cardiomyocytes that form the 10 subclusters were pooled together and different methods were employed to assess any differences that might be present.

6.5.1 GO biological process

Wilcoxon tests were performed in the Scanpy software in Python to provide a list of genes that were significantly differentially expressed between genotypes (with significance defined by a p-value of less than 0.05 and a fold change of at least 1). This list was then compared against lists for gene ontologies (GO) (Gene Ontology Consortium, 2006) with a Bonferroni correction for multiple testing applied to determine if any GO's were differentially regulated. When looking at GO biological processes I found 22 upregulated and 19 downregulated processes in *popdc1* null mutants (Figure 62). Upregulated processes involved the actin and cytoskeletal organisation as well as cardiac and skeletal muscle development. GO biological processes that were downregulated formed a broad range of categories including those involved in heart looping and morphogenesis as well as regulation of metabolic processes.

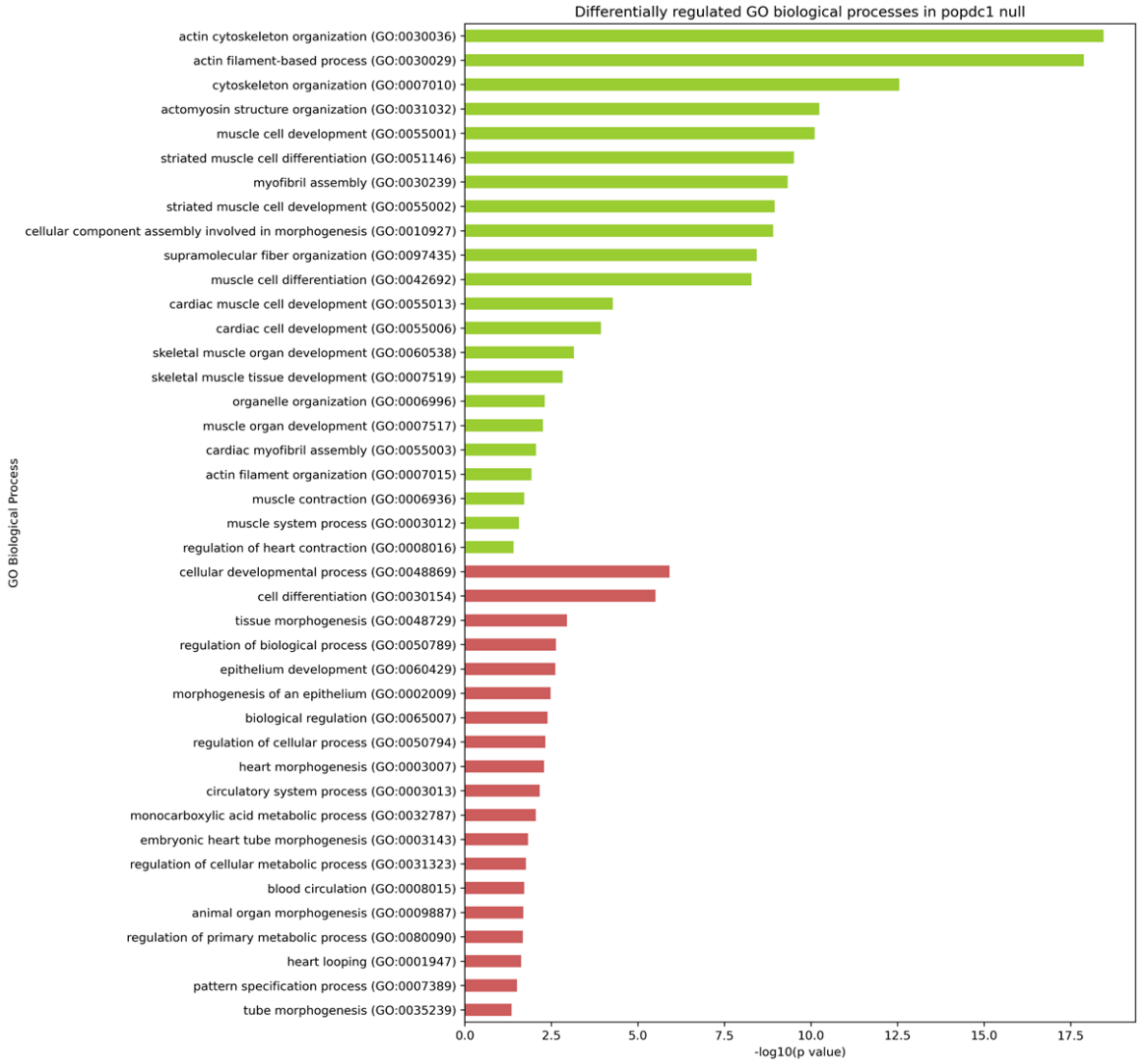

Figure 62 GO biological processes analysis results for combined ventricular cardiomyocyte clusters. Showing significantly enriched GO terms associated with significantly upregulated genes between *popdc1* null and wild type cardiomyocytes. With those in green being upregulated in *popdc1* null and those in red being downregulated.

6.5.2 GO molecular pathways

Differentially regulated GO molecular pathways were also generated from genes that were found to be significantly differentially regulated in the *popdc1* null mutant vs wild type zebrafish. *popdc1* null mutants had upregulation of *actin-binding*, *muscle-alpha actinin binding*, *alpha-actinin binding*, *protein-containing complex binding* and *3',5'-cyclic AMP phosphodiesterase activity* (Figure 63). The *popdc1* mutants had an underrepresentation of genes involved in *transmembrane receptor activity*, *molecular transducer activity* and *signalling receptor activity* (Figure 63).

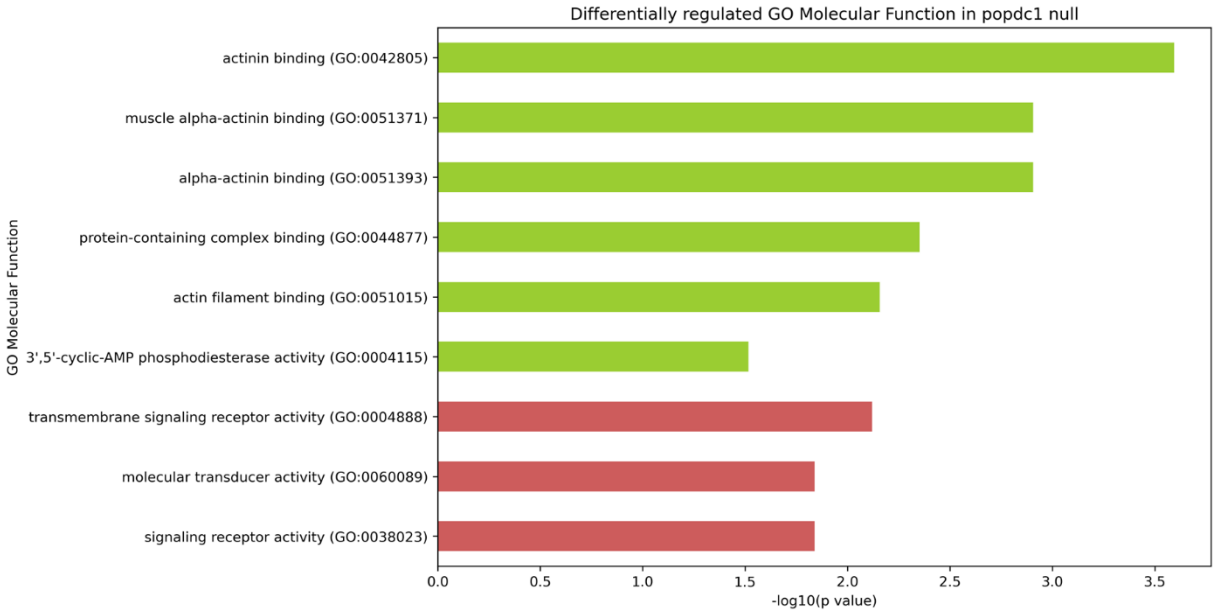

Figure 63 GO molecular function analysis results for combined ventricular cardiomyocyte clusters. Showing significantly enriched GO terms associated with significantly upregulated genes between *popdc1* null and wild type cardiomyocytes. With those in green being upregulated in *popdc1* null and those in red being downregulated.

There was an overlap in the upregulated genes involved in actin binding, muscle alpha actinin binding, alpha actinin binding and actin filament binding. I decided to look at the alpha-actinin binding in more detail. When looking at the upregulated genes from this pathway I saw an upregulation in a number of PDZ and LIM domain (*pdlim*) genes; *3a, 3b, 7,5b* and *5a* as well as upregulation in *ldb3a* (Figure 64) Although all were significantly upregulated in the *popdc1* null mutant *pdlim3b* and *pdlim7* showed the largest difference in expression.

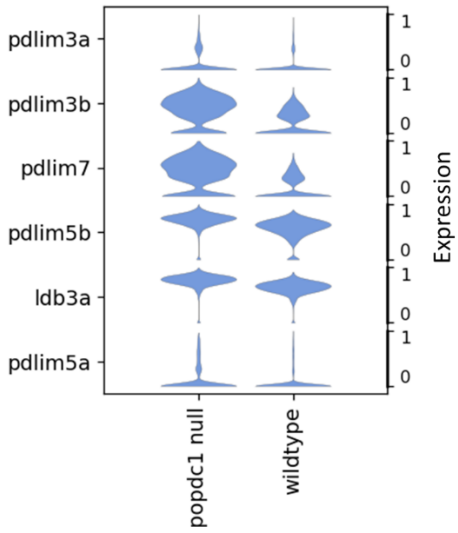

Figure 64 Differentially regulated alpha-actinin binding genes. Violin plots of genes from the alpha actinin binding function that were upregulated in *popdc1* null mutant cardiomyocytes. Their expression has been normalised to fall between 0 and 1. *pdlim3a* (Z=1.0385, p<0.001), *pdlim3b* (Z=5.2704, p<0.001), *pdlim7* (Z=5.2572, p<0.001), *pdlim5a* (Z=1.4305, p<0.001), *pdlim5b* (Z=9.2462, p<0.001) and *ldb3a* (Z=28.9238, p<0.001) were upregulated in the *popdc1* null mutant cardiomyocytes.

As POPDC1 is known to be a cAMP binding protein (Froese *et al*., 2012), I also looked at the genes upregulated in the 3',5'-cyclic AMP phosphodiesterase activity function. POPDC1 is already known to bind with the pde4A isoform (Tibbo *et al*., 2020). I found that there was an upregulation of several PDE genes, including *pde3b, 4d, 3a* and *7a* in the *popdc1* null mutant cardiomyocytes (Figure 65). With *pde3a* being the most highly upregulated.

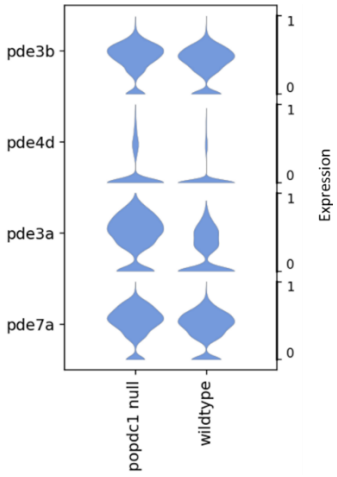

Figure 65 Differentially regulated 3'5'-cyclic AMP phosphodiesterase activity genes. Violin plots of genes from the 3'5'-cyclic AMP phosphodiesterase activity function that were upregulated in *popdc1* null mutant cardiomyocytes. Their expression has been normalised to fall between 0 and 1. *pde3a* (Z=3.7716, p<0.001), *pde7a* (Z=2.5071, p<0.001), *pde3b* (Z=1.8616, p<0.001) and *pde4d* (Z=1.3393, p<0.001) were upregulated in the *popdc1* null mutant cardiomyocytes.

6.5.3 PANTHER pathways

Differentially regulated protein analysis through evolutionary relationships (PANTHER) pathways (Thomas *et al*., 2003) were also generated from genes that were found to be significantly differentially regulated in the *popdc1* null mutant vs wild type. Popdc1 null mutants displayed an upregulation of genes involved in *CCKR signalling*, *oxidative stress response*, *p38 MAPK pathway*, *Insulin/IGF pathway-mitogen activated protein kinase kinase/ MAP kinase cascade*, *Insulin/IGF pathways-protein kinase B signalling cascade*, *cytoskeletal regulation by RhoGTPase and PI3 kinase pathways* (Figure 66).

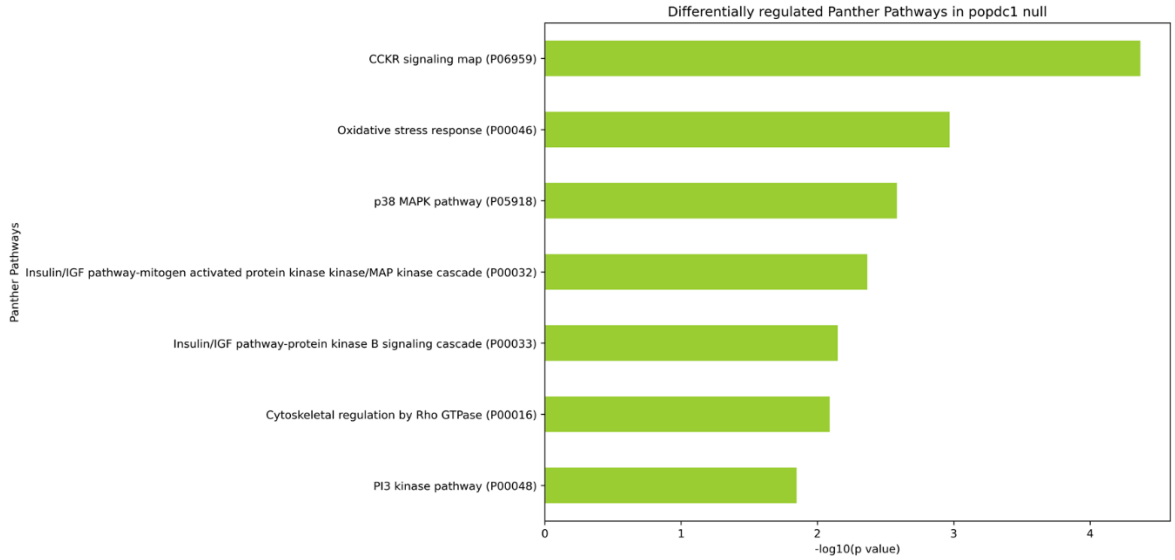

Figure 66 PANTHER Pathway analysis results for combined ventricular cardiomyocyte clusters. Showing significantly enriched PANTHER pathways associated with significantly upregulated genes pathways between *popdc1* null and wild type cardiomyocytes. With those in green being upregulated in *popdc1* null.

6.5.4 *popdc1* null cardiomyocytes are stressed

Cardiac stress occurs when there are transcriptional, epigenetic or morphological changes to the heart that are commonly due to pathological stressors, including but not limited to, MI, hypertension and genetic heart conditions. It was observed that there was an upregulation of genes that are commonly upregulated after cardiac stress such as *nppa*, *acta1b* and *atf3* in the *popdc1* null mutant cardiomyocytes (Figure 67). Although more highly expressed in *popdc1* null mutant cardiomyocytes

as a whole, *nppa* and *atf3* were most highly upregulated in the CM3 population, which was the sub-cluster that contained nuclei primarily derived from the *popdc1* null mutant (Figure 67).

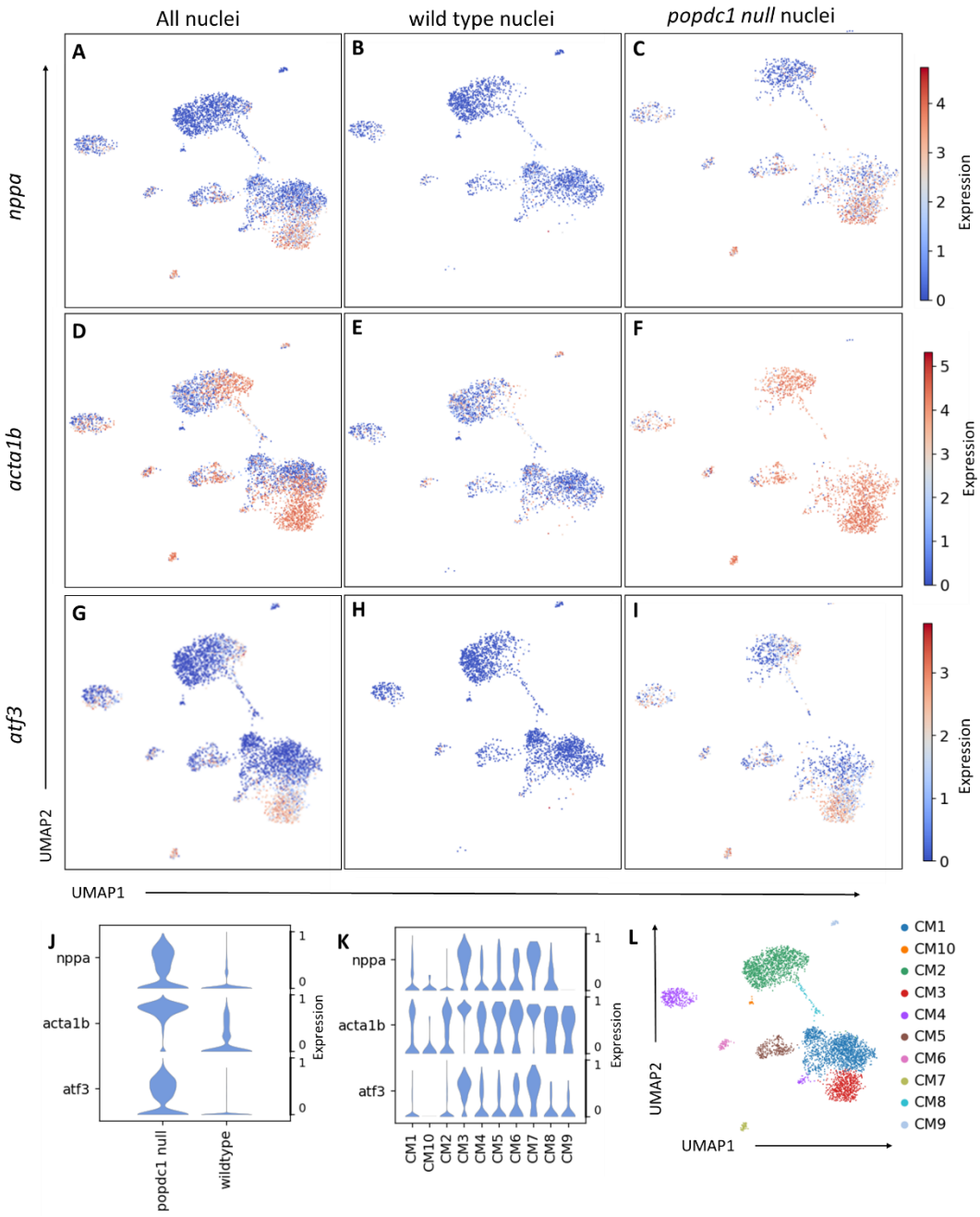

Figure 67 stress markers are upregulated in *popdc1* null ventricular cardiomyocytes. *nppa* (**A-C**), *acta1b* (**D-F**) and *atf3* (**G-I**) UMAPs were made for all the nuclei (**A, D, G**), wild type only nuclei (**B, E, H**) and *popdc1* null nuclei (**C, F, I**) and colour scale bars are shown to the right of the UMAPS to illustrate the normalised expression level. Violin plots were made to visualise *nppa*, *acta1b* and *atf3* expression between genotypes (**J**) and between cardiomyocyte clusters (**K**), where the data has been normalised to fall between 0 and 1. A UMAP showing the cardiomyocyte subclusters has been included for reference (**L**). *nppa* (Z=7.4479, p<0.001), *acta1b* (Z=25.7824, p<0.001) and *aft3* (Z=7.7738, p<0.001) were upregulated in the *popdc1* null mutant cardiomyocytes. *nppa* (Z=3.6252, p<0.001), *acta1b* (Z=3.3637, p<0.001) and *atf3* (Z=3.8062, p<0.001) were significant upregulated in CM3. *nppa* (Z=3.4311, p<0.001), *acta1b* (Z=2.4564, p<0.001) and *atf3* (Z=2.8595, p<0.001) were significant upregulated in CM7.

A heat map was also made using genes that are upregulated after stress, many of which are known to have cardioprotective functions. From the heat map, it is seen that the *popdc1* null mutant cardiomyocytes display a higher expression level of stress-related genes (Figure 68).

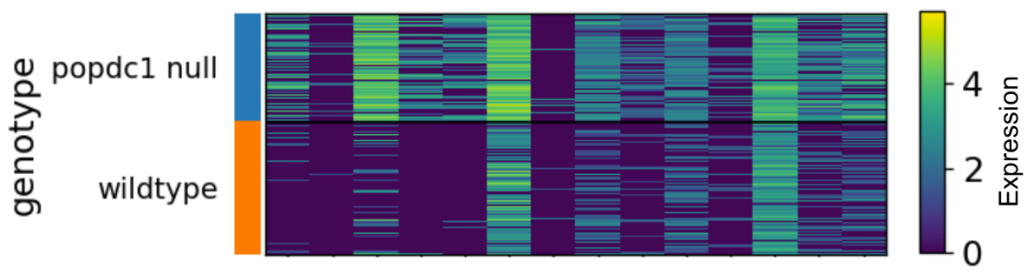

Figure 68 Heat map showing the expression of some cardiac stress-related genes in cardiomyocytes from *popdc1* null mutant and wild type nuclei.

6.5.5 Mis-regulation of genes known to be involved in regeneration

In chapter 5, it was demonstrated that the *popdc1* null mutant had a reduced regenerative ability compared to wild type. To try and comprehend the lack of regenerative potential in the *popdc1* null mutant ventricle I looked for differentially regulated genes in the *popdc1* null mutant that are known to affect cardiac regeneration in zebrafish.

6.5.5.1 Runx1 is upregulated in popdc1 null cardiomyocytes

The *runx1* null mutant in both mouse and zebrafish display an improved regenerative response after cryoinjury (McCarroll *et al*., 2018, Koth *et al*., 2020). Because of this, the nuclear RNA expression of *runx1* was looked at in the *popdc1* null and wild type cardiomyocytes. *popdc1* null mutants have an increased expression of *runx1* with the highest expression in CM3 and CM7, which contain primarily mutant nuclei (Figure 69).

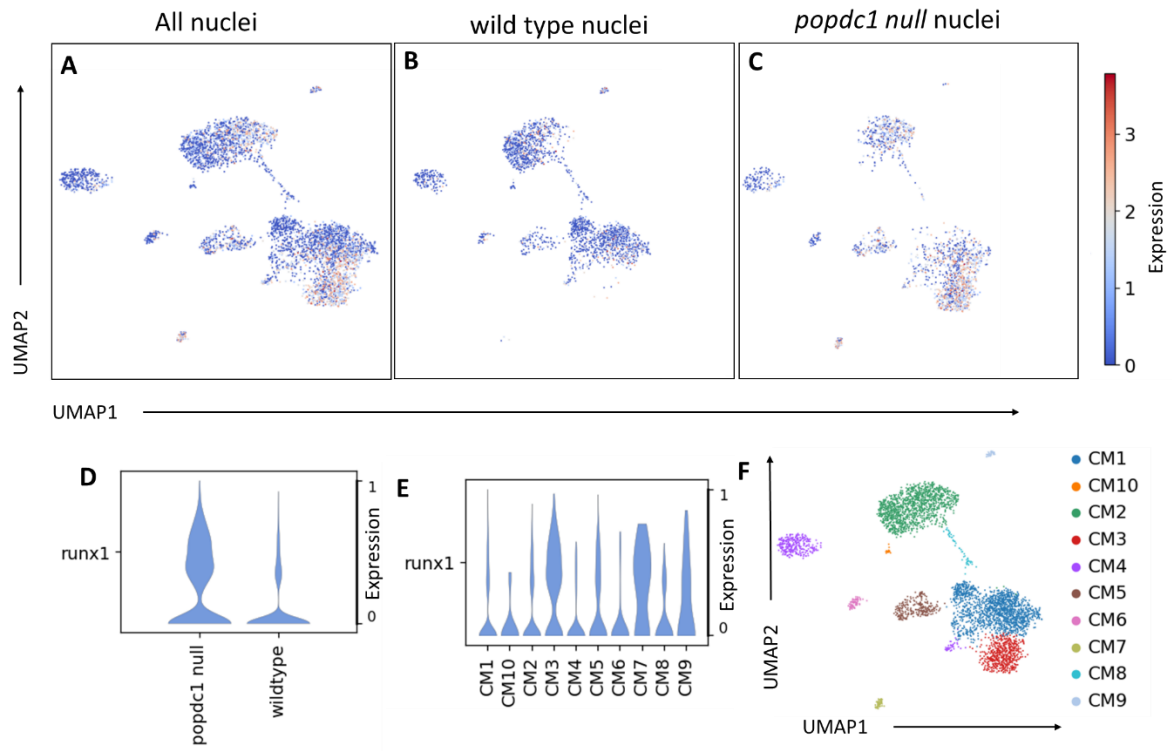

Figure 69 *runx1* is upregulated in *popdc1* null ventricular cardiomyocytes. *runx1* UMAPs were made for all the nuclei (**A**), wild type only nuclei (**B**) and *popdc1* null nuclei (**C**) and a colour scale bar is included to illustrate the expression level normalised to fall between 0 and 5. Violin plots were made to visualise the *runx1* expression between genotypes (**D**) and between cardiomyocyte clusters (**E**) where data has been normalised to fall between 0-1. A UMAP showing the cardiomyocyte subclusters has been included for reference (**F**). *runx1* was significantly upregulated in the *popdc1* ($Z=2.6244$, $p<0.001$) null mutant cardiomyocytes. *runx1*) was significantly upregulated in the CM3 population ($Z=1.8554$, $p<0.001$.

After cryoinjury, an increase in *runx1* expression in the endothelial/endocardial cells was reported and thought to induce *myh11a* (Koth *et al*., 2020). I therefore also looked into the expression of *runx1* and *myh11a* in presumptive endothelial nuclei at baseline and found a small but significant increase in expression of both genes in *popdc1* null mutant (Figure 70).

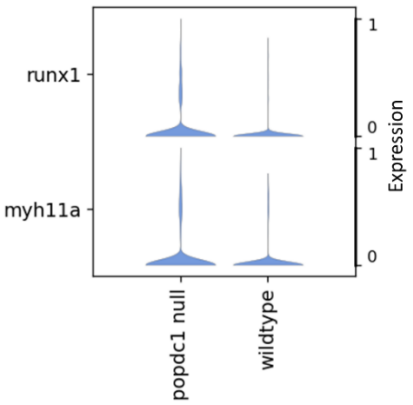

Figure 70 *runx1* and *myh11a* expression are upregulated in *popdc1* null endothelial nuclei. Violin plots were made to visualise the expression of *runx1* and *myh11a* in *popdc1* null vs wild type endothelial nuclei with data normalised to have values between 0 and 1. *runx1* (Z=2.7882, p<0.001) and myh11a (Z=1.3654, p<0.001) was significantly upregulated in the popdc1 null mutant endothelial nuclei.

6.5.5.2 tbx5 downregulation in popdc1 null cardiomyocytes

As well as being known to be a marker of the trabecular layer in the zebrafish heart (Sánchez-Iranzo *et al*., 2018), *tbx5a* is also known to be necessary for regeneration of the zebrafish ventricle after injury (Grajevskaja *et al*., 2018). Interestingly, there was a decrease in the amount of both *tbx5a* and *tbx5b* in the *popdc1* null mutant cardiomyocytes (Figure 71). The reduction of *tbx5a* in the *popdc1* null mutant was also confirmed by qPCR (Figure 72) where whole ventricles were used and so this would represent mRNA from all cell types in the ventricle and not just those from cardiomyocytes like in the snRNA-seq results, although tbx5a is only expected to be expressed in cardiomyocytes (Sánchez-Iranzo *et al*., 2018).

As *tbx5a* is most highly expressed in the CM1 subcluster of cardiomyocytes (Figure 71H), I also looked at the difference in expression of *tbx5a* between the *popdc1* null mutant and wild type nuclei specifically in this subcluster. I found that there was a reduction in the number of nuclei expressing *tbx5a* and also an overall reduction in its expression level (Figure 73). From work earlier in this chapter it is suggested that CM3 represent a *popdc1* null mutant-specific cell cluster, which probably represents trabeculae-like cells that are closely related to the CM1 population, however, in the CM3 population, I also see a low expression of *tbx5a* (Figure 71H).

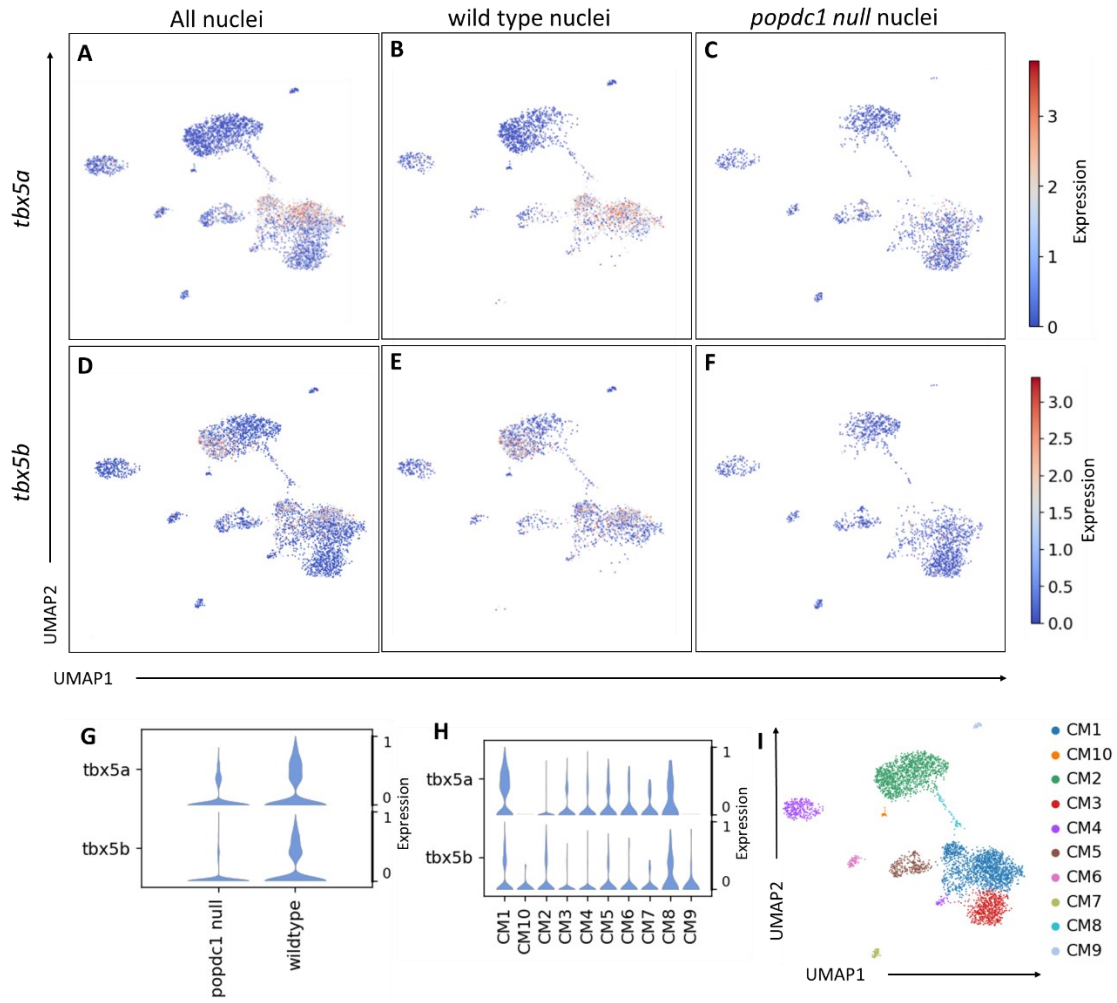

Figure 71 *tbx5* is downregulated in *popdc1* null ventricular cardiomyocytes. *tbx5a* (**A-C**) and *tbx5b* (**D-F**) UMAPs were made for all the nuclei (**A, D**), wild type only nuclei (**B, E**) and *popdc1* null nuclei (**C, F**), colour scale bars have been included to illustrate the expression level in the UMAPS. Violin plots were made to visualise *tbx5a* and *tbx5b* expression between genotypes (**G**) and between cardiomyocyte clusters (**H**), with this data being normalised to fall between 0 and 1. A UMAP showing the cardiomyocyte subclusters has been included for reference (**I**). *tbx5a* (Z=2.3655, p<0.001) and *tbx5b* (Z=2.9147, p<0.001) were significantly downregulated in *popdc1* null cardiomyocytes. *tbx5a* (Z=1.0479, p<0.001) and *tbx5b* (Z=3.3431, p<0.001) were significantly upregulated in CM1

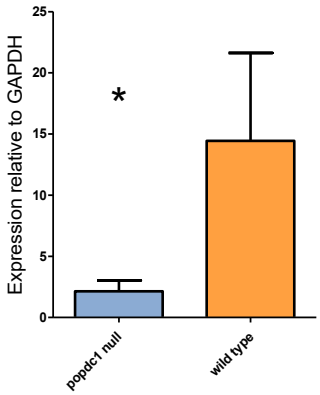

Figure 72 *tbx5a* expression is reduced in zebrafish ventricles. qPCR was used to confirm the reduction of *tbx5a*. *tbx5a* expression was plotted for popdc1 null and wild type ventricles relative to their expression of GAPDH. *tbx5a* expression was significantly reduced in the mutant with * representing p<0.05 (t=1.819; df=13; p<0.05), at least three fish were used for each genotype. Data are reported as mean ± standard error of the mean.

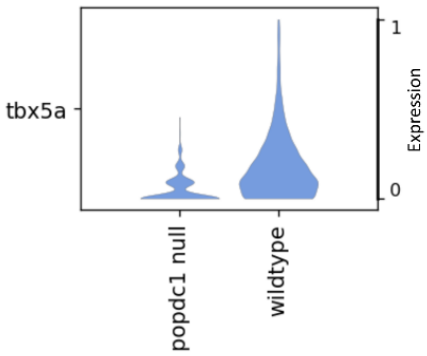

Figure 73 *tbx5a* expression is downregulated in *popdc1* null cardiomyocytes in CM1. Violin plots were made to visualise the expression of *tbx5a* in *popdc1* null vs wild type CM1 cardiomyocytes, the data have been normalised to fall between 0 and 1. *tbx5a* (Z=3.1829, p<0.001) was significantly downregulated in the *popdc1* null in the CM1 population compared to the wildtype.

6.5.5.3 fstl1b is downregulated in popdc1 null cardiomyocytes

Follistatin-like 1b (fstl1b) has been implicated in cardiac regeneration and loss of *fst1b* in zebrafish results in impaired cardiac regeneration after cryoinjury (P. Ruiz-Lozano, personal communication). Moreover, in the mouse and porcine heart it has been shown to aid the repair of the mammalian heart after delivery via an epicardial patch (Wei *et al*., 2015). *popdc1* null mutant cardiomyocytes had a large and significant reduction in *fstl1b,* with expression being uniformly low across all *popdc1* null nuclei (Figure 74). When looking at the expression in different subclusters, CM3 which constituted primarily *popdc1* null mutant nuclei had the lowest expression of *fstl1b* (Figure 74E).

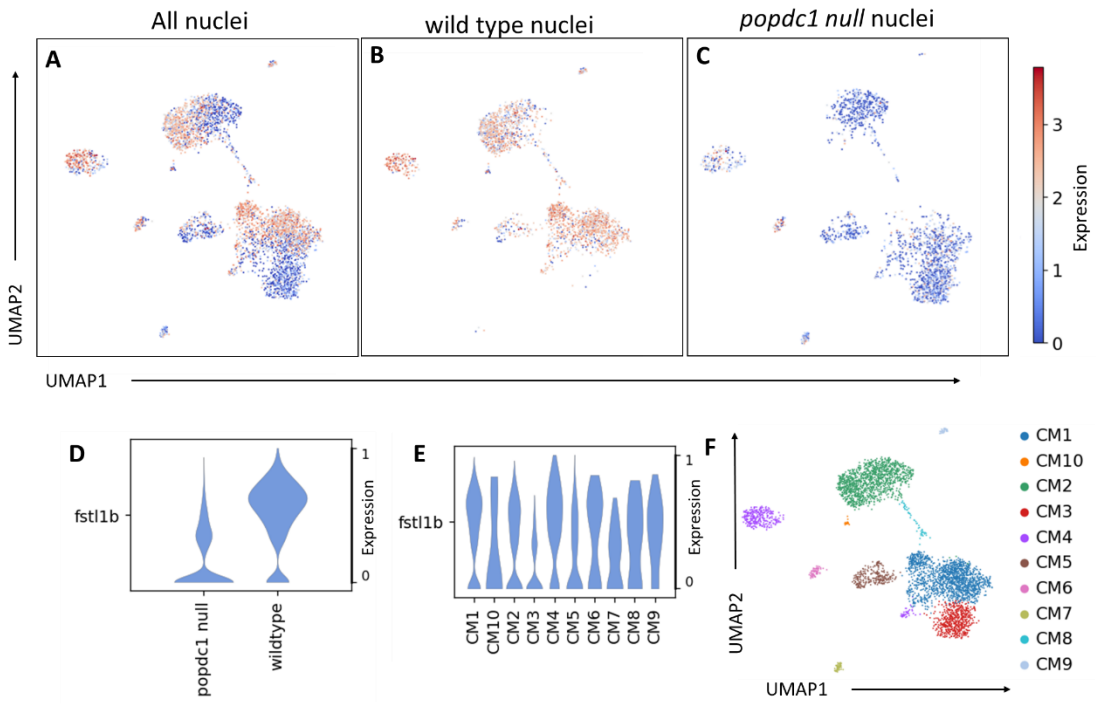

Figure 74 *fstl1b* is downregulated in popdc1 null ventricular cardiomyocytes. *fstl1b* UMAPs were made for all the nuclei (**A**), wild type only nuclei (**B**) and *popdc1* null nuclei (**C**) a colour scale bar has been included to illustrate the expression level in the UMAPS. Violin plots were made to visualise the *fstl1b* expression between genotypes (**D**) and between cardiomyocyte clusters (**E**), the data has been normalised to fall between 0 and 1. A UMAP showing the cardiomyocyte subclusters has been included for reference (**F**). *fstl1b* (Z=5.7624, p<0.001) was significantly downregulated in the *popdc1* null mutant. *fstl1b* (Z=1.0052, p<0.001) was significantly upregulated in the CM4 population.

6.5.6 Misregulation of energy metabolism in *popdc1* null mutants

The adult heart usually uses fatty acid oxidation as a way to produce energy (Fukuda *et al.*, 2020, Kreipke *et al.*, 2016). When looking at differentially regulated genes in the *popdc1* null mutant cardiomyocytes I found that one of the strongest downregulated genes was *acyl-CoA synthetase long-chain family member 1b* (*acsl1b*), which was downregulated across all *popdc1* null cardiomyocytes (Figure 75A-D). The Acsl1b protein is required to convert long-chain fatty acids into fatty acyl-CoA esters, allowing fatty acid degradation and so it is involved in energy metabolism (Black and Dirusso, 2003). I predict that CM3 is a subset of trabeculae which are made up primarily of nuclei from the CM1 population. Although interestingly, CM1 has the highest expression of *acsl1b* of all the clusters and that CM3 has very low expression of *acsl1b* (Figure 75E).

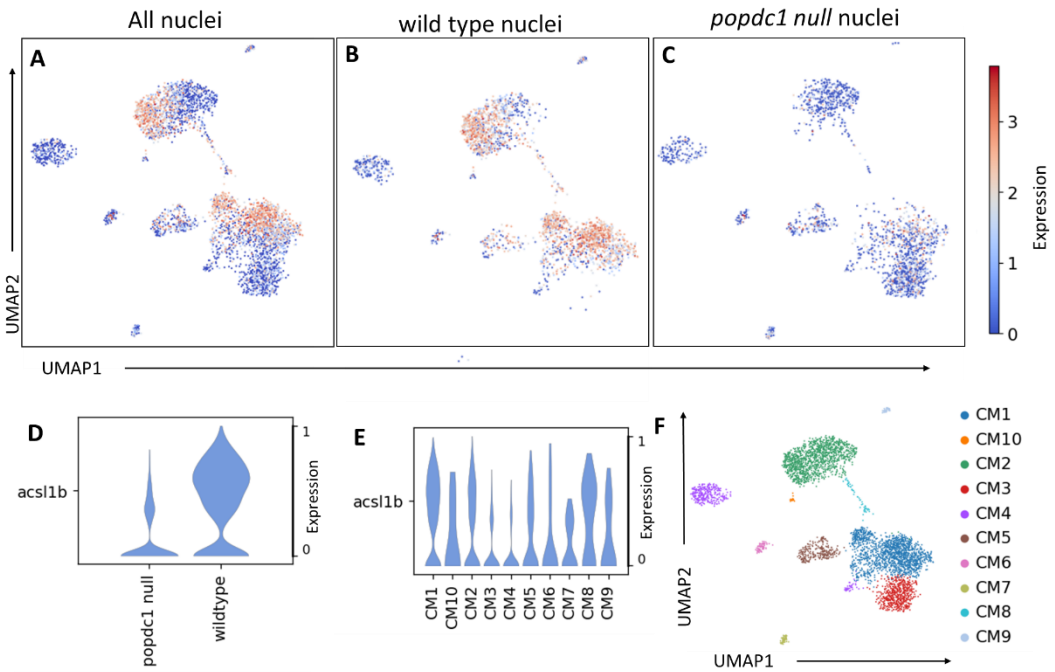

Figure 75 *acsl1b* is downregulated in popdc1 null ventricular cardiomyocytes. *acsl1b* UMAPs were made for all the nuclei (**A**), wild type only nuclei (**B**) and *popdc1* null nuclei (**C**) and a colour scale bar of the clusters were made to visualise the expression level which has been normalised for fall between 0 and 4. Violin plots were made to visualise the *acsl1b* expression between genotypes (**D**) and between cardiomyocyte clusters (**E**), with data normalised to fall between 0 and 1. A UMAP showing the cardiomyocyte subclusters has been included for reference (**F**). *acsl1b* (Z=4.5222, p<0.001) is significantly downregulated in *popdc1* null cardiomyocytes. *acsl1b* (z=1.4489, p<0.001) was significantly upregulated in the CM1 population.

If cardiomyocytes cannot produce energy by metabolising fatty acids they must switch to another energy resource to not enter into an energy deficit. After injury and in heart disease the heart will rely on glucose metabolism for energy production as it is more efficient and requires less oxygen (Fukuda *et al*., 2020, Martik, 2020). Therefore, I looked into the expression of some genes in the glucose metabolism pathway. I found that there was a significant increase in glycolysis related transcription factors *foxo1a* and *foxo3b* and an increase in the number of nuclei expressing glucose transporter *slc2a1b* in the *popdc1* null mutant cardiomyocytes (Figure 76).

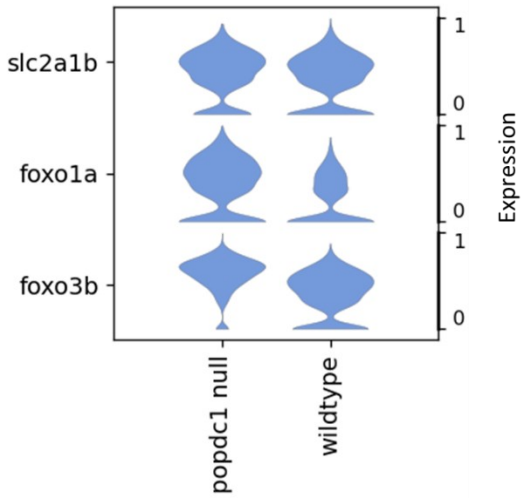

Figure 76 Upregulation of some glycolysis related genes in *popdc1* null cardiomyocytes. Violin plots of *slc2a1b, foxo1a* and *foxo3b* that are upregulated in *popdc1* null mutant cardiomyocytes with data normalised to fall between 0 and 1. *slc2a1b* (Z=1.1665, p<0.001), *foxo1a* (Z=3.2555, p<0.001) and *foxo3b* (Z=8.8510, p<0.001) are significantly upregulated in *popdc1* null cardiomyocytes.

6.5.7 Misregulation of genes related to binucleation and polyploidisation

In chapter 5, I saw that *popdc1* null mutant cardiomyocytes had an increase in binucleation and polyploidisation. Here, I looked at the expression of two genes known to affect binucleation (*ect2*) and polyploidisation (*tnni3k*) (Tatsumoto *et al*., 1999, Patterson *et al*., 2017). *ect2* displayed a low expression level in cardiomyocytes and there was no difference in expression between *popdc1* null mutant and wild type (Figure 77A-C and G). Expression of *tnni3k* was reduced in *popdc1* null mutant cardiomyocytes compared to wild type (Figure 77D-F and G).

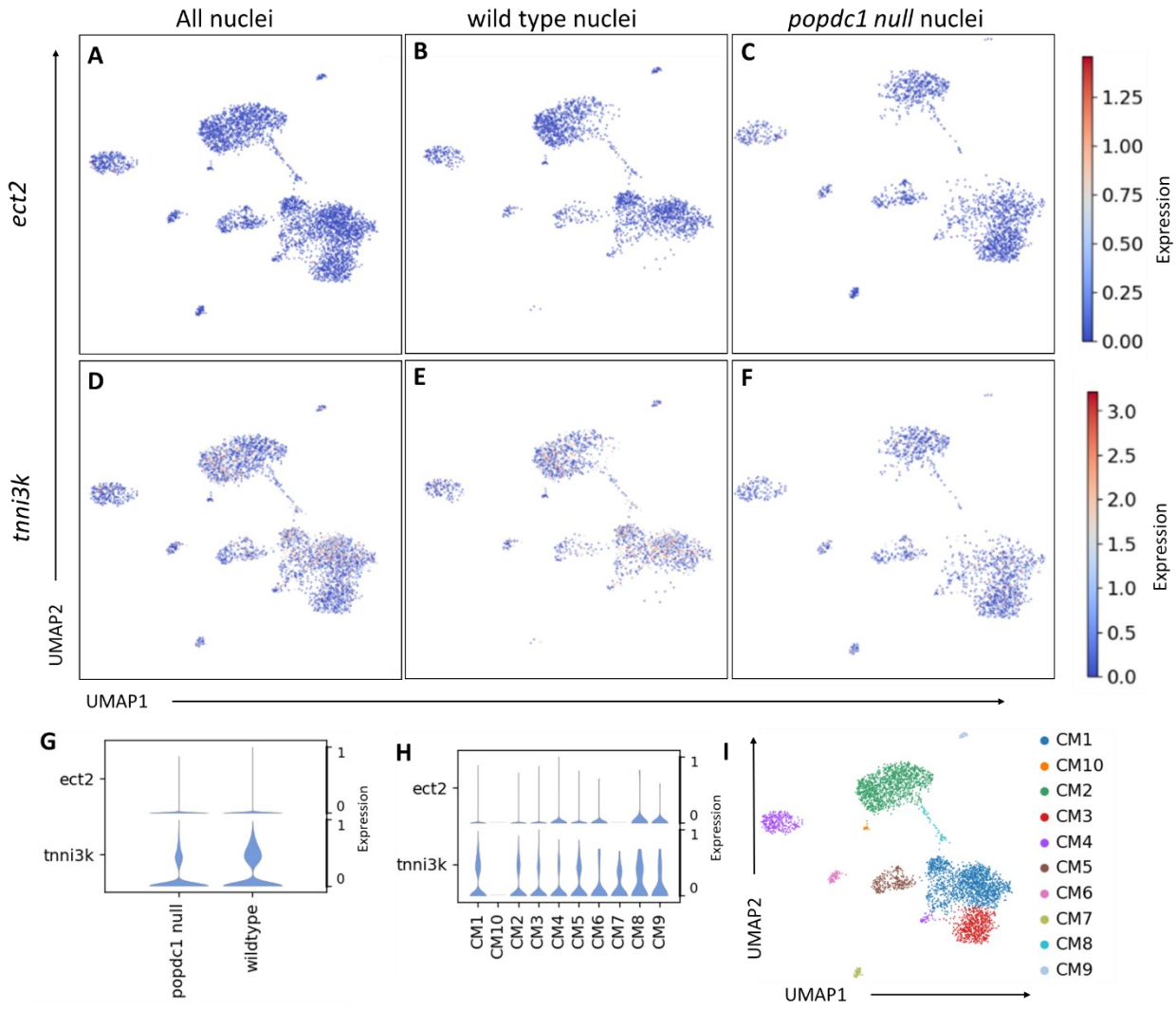

Figure 77 Expression of polyploid associated genes in cardiomyocytes. *ect2* (**A-C**) and *tnni3k* (**D-F**) UMAPs were made for all the nuclei (**A, D**), wild type only nuclei (**B, E**) and *popdc1* null nuclei (**C, F**) with a colour scale bar of the UMAPs made to visualise the expression level. Violin plots were made to visualise *ect2* and *tnni3k* expression between genotypes (**I**) and between cardiomyocyte clusters (**J**) with data normalised to fall between 0 and 1. A UMAP showing the cardiomyocyte subclusters has been included for reference (**F**). *tnni3k* (Z=1.2165, p<0.001) is significantly downregulated in the *popdc1* null cardiomyocytes.

6.5.8 Expression of the other POPDC isoforms in the *popdc1* null mutant

In chapter 4, I saw that loss of *popdc1* could affect the expression and subcellular localisation of the other POPDC isoforms. Something which has also been seen in patients with mutations in POPDC1 (Schindler *et al*., 2016b, De Ridder *et al*., 2019, Rinné *et al*., 2020). When looking at the expression of *popdc2* and *popdc3* in the *popdc1* null cardiomyocytes I saw that they were both reduced (Figure 78). *popdc3* is significantly downregulated in the *popdc1* null cardiomyocytes (Figure 78D-G). More

cardiomyocyte nuclei do not express *popdc2* in the *popdc1* nulls, however, the spread of expression level of *popdc2* is similar and there is no significant difference in the expression of *popdc2* in the *popdc1* null mutant (Figure 78A-C and G).

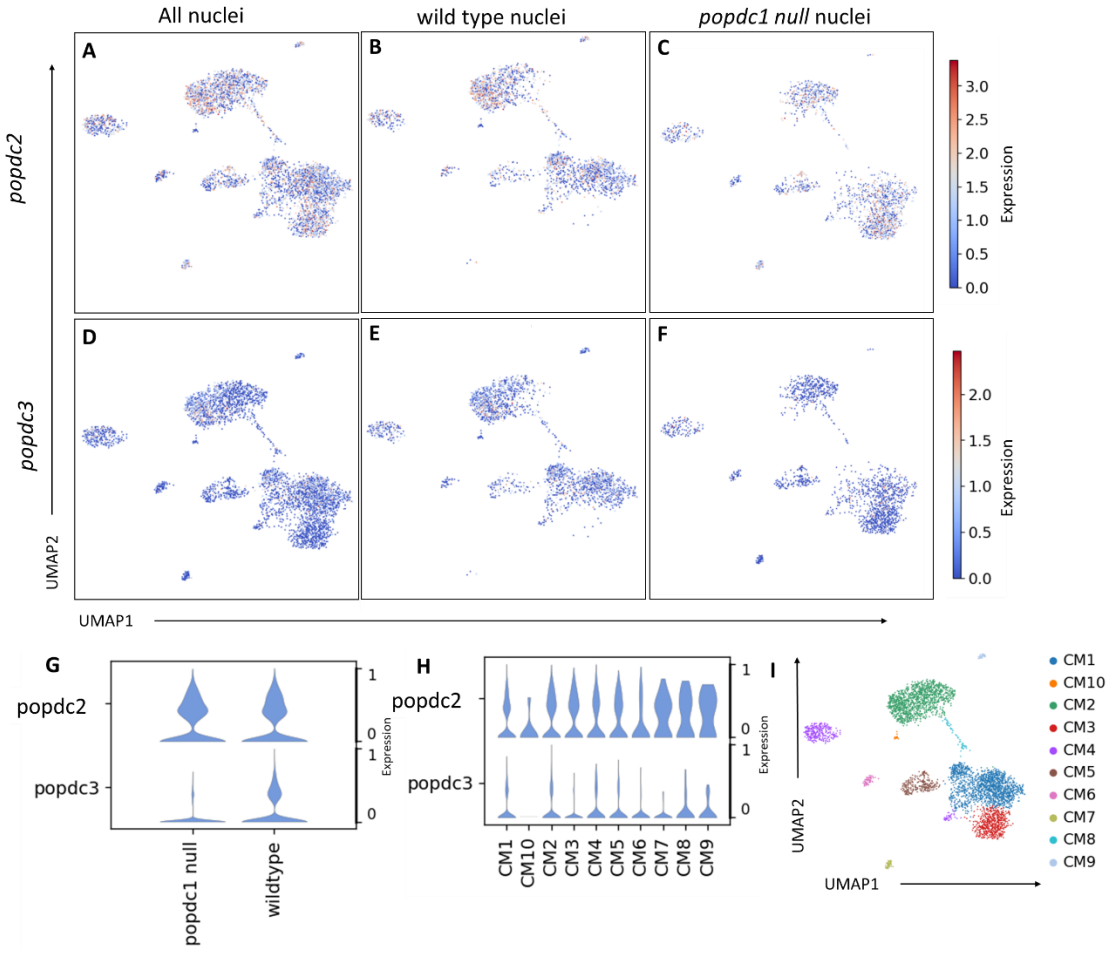

Figure 78 *popdc* expression in cardiomyocytes. *popdc2* (**A-C**) and *popdc3* (**D-F**) UMAPs were made for all the nuclei (**A, D**), wild type only nuclei (**B, E**) and *popdc1* null nuclei (**C, F**) and a colour scale bar were made for the UMAPS to visualise the normalised expression. Violin plots were made to visualise *popdc2* and *popdc3* expression between genotypes (**G**) and between cardiomyocyte clusters (**H**), with data normalised to fall between 0 and 1. A UMAP showing the cardiomyocyte subclusters has been included for reference (**F**). *popdc3* (Z=2.5223, p<0.001) is significantly downregulated in the *popdc1* null cardiomyocytes.

6.5.9 Investigating the CM3 *popdc1* null enriched sub-cluster

As CM3 was a large subcluster that was mostly represented by *popdc1* null mutant cardiomyocyte nuclei, I decided to look at the subcluster in more detail.

6.5.9.1 GO biological processes

Significantly differentially expressed genes were calculated using a Wilcoxon signed-rank test for subcluster CM3 compared to the other cardiomyocyte subclusters, significance was defined by a p-value of 0.05 and a fold change of 1. The differentially expressed genes were used to determine if there were differentially regulated GO biological processes with a Bonferroni correction for multiple testing applied to determine if any GO's were differentially regulated. There were 13 upregulated and 18 downregulated GO biological processes. The upregulated processes involved those to do with actin, actin filament, the cytoskeleton and myofibrillar assembly as well as those involved in striated muscle development and differentiation (Figure 79). There was downregulation of genes involved in cardiomyocyte and cardiac development and differentiation as well as heart looping and morphogenesis (Figure 79).

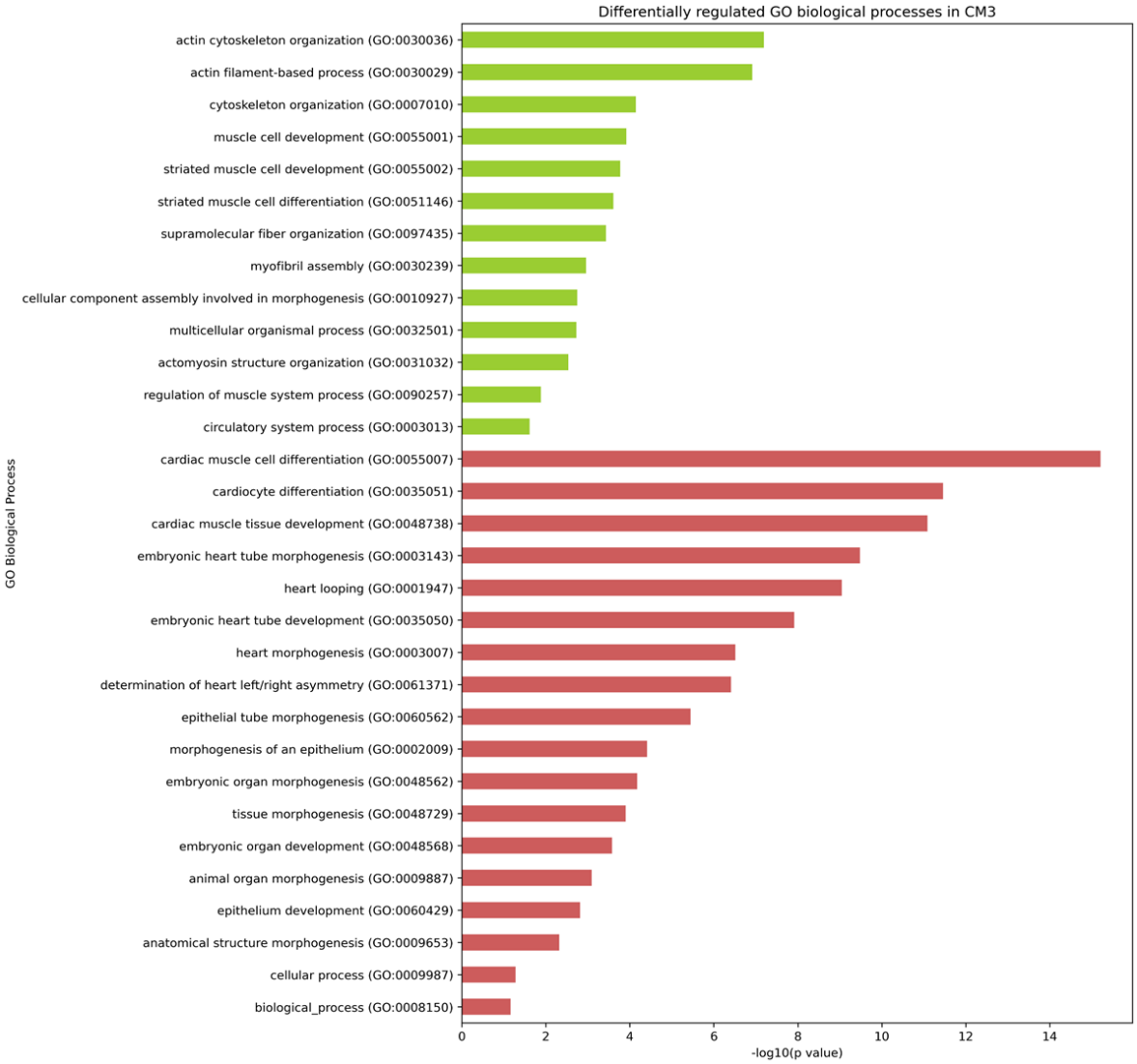

Figure 79 GO biological processes analysis results for the CM3 subcluster. Showing significantly enriched GO terms associated with significantly upregulated genes between subcluster CM3 and the remaining subclusters. With those in green being upregulated in the CM3 subcluster and those in red being downregulated.

6.5.9.2 GO molecular functions

Significantly differentially expressed genes were calculated for subcluster CM3 compared to the other cardiomyocyte subclusters and the differentially expressed genes were used to see if there were differentially regulated GO molecular functions. CM3 nuclei displayed an upregulation of *actin binding* (Figure 80). There was downregulation of *glycogen branching enzyme activity*, 4-*alpha-glucotransferase activity* and *amylo-alpha-1,6 glucosidase activity* (Figure 80).

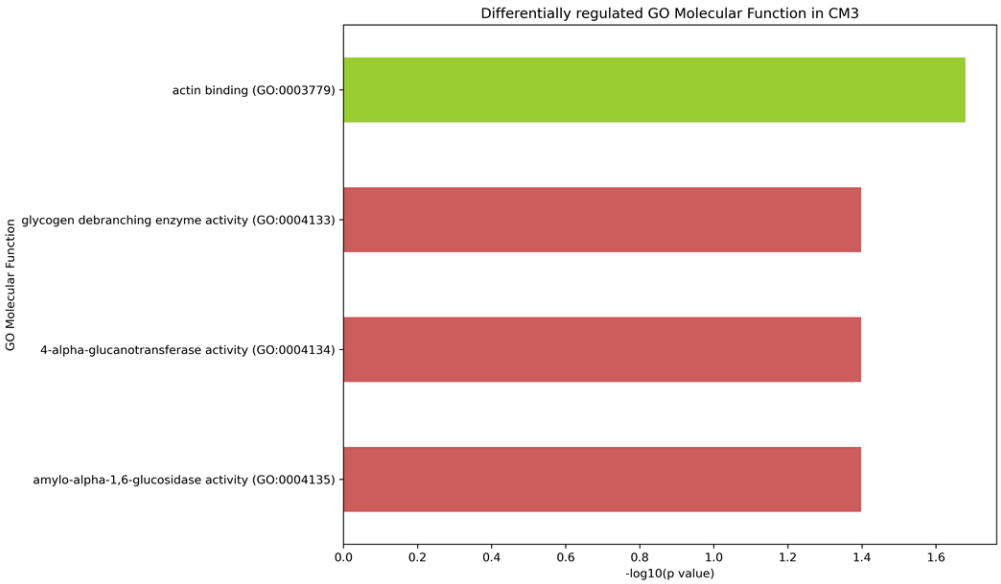

Figure 80 GO molecular function analysis results for the CM3 subcluster. Showing significantly enriched GO terms associated with significantly upregulated genes between subcluster CM3 and the remaining subclusters. With those in green being upregulated in the CM3 subcluster and those in red being downregulated.

6.5.9.3 PANTHER pathways

Differentially expressed genes were calculated for subcluster CM3 compared to the other cardiomyocyte subclusters and the significantly differentially expressed genes were used to see if there were differentially regulated PANTHER pathways. There were no downregulated pathways in the CM3 subcluster, but there was upregulation of *CCKR signalling*, *nicotinic acetylcholine receptor signalling*, *Alzheimer's disease-presenilin*, *cadherin signalling* and *cytoskeletal regulation by Rho GTPase pathways* (Figure 81). The latter is of note as previously it has been seen that POPDC1 interacts with GEFT, a GEF for Rho-family GTPases to control cell shape and locomotion (Smith *et al*., 2008) and included upregulation of genes such as *actb2*, *rhoca*, *acta1b*, *acta1a*, *actb1*, *actc1a* and *myh9b* (Figure 82).

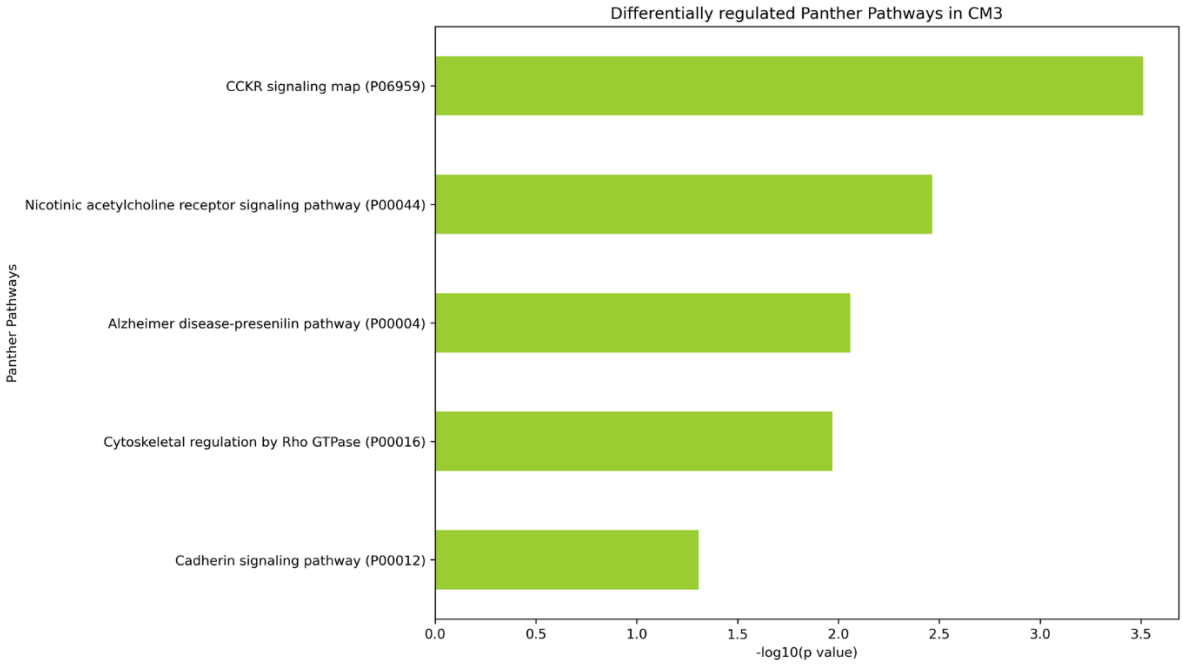

Figure 81 PANTHER pathway analysis results for the CM3 subcluster. Showing significantly enriched PANTHER pathways associated with significantly upregulated genes between subcluster CM3 and the remaining cardiomyocyte subclusters. With those in green being upregulated in the CM3 subcluster.

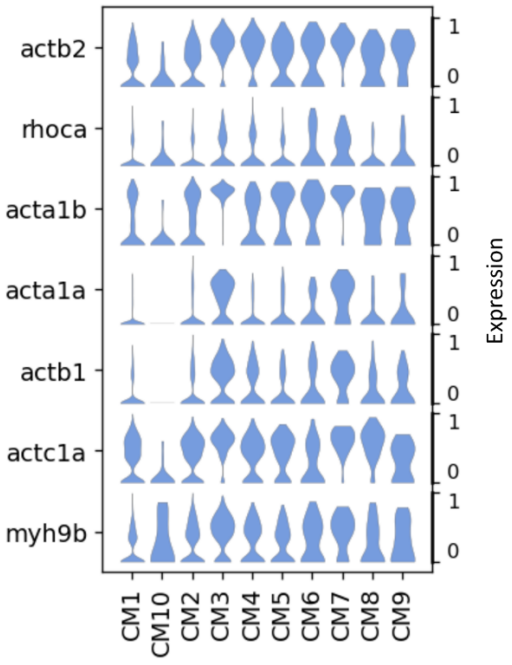

Figure 82 Differentially regulated cytoskeletal regulation by Rho GTPase pathways genes in the CM3 cardiomyocyte population. Violin plots of genes from the cytoskeletal regulation by Rho GTPase pathway genes that were upregulated in CM3 cardiomyocytes. Their expression has been normalised to fall between 0 and 1. *actb2* (Z=1.6805, p<0.001), *rhoca* (Z=1.1538, p<0.001), *acta1b* (Z=3.3637, p<0.001), *acta1a* (Z=3.3432, p<0.001), *actb1* (Z=3.3637, p<0.001), *actc1a* (Z=1.3393, p<0.001) *and myh9b* (Z=1.2803, p<0.001) were significantly upregulated in the CM3 cardiomyocytes.

6.6 Discussion

Single-cell and single-nuclei RNA sequencing are novel, powerful methods that sequence the mRNAs in the cell or nucleus population. This allows the identification of different cell populations whereas traditional bulk RNA sequencing could only generate the total expression level of genes in tissues, and therefore cellular heterogeneity would not be seen (Wen and Tang, 2018). Technological progress has allowed for the development of these novel single-cell (or -nucleus) RNA sequencing methods at an affordable price, which is now accessible and widely used in various fields. In this chapter I have used 10x Genomics' chromium single-nuclear RNA sequencing to begin to understand the transcriptional differences of the ventricle in the *popdc1* null mutant ventricle compared to wild type, hoping to identify some changes, which may also provide us with an explanation for the phenotypic differences that have been described in the previous chapters.

In this chapter, I ensured the proper quality of the samples sent for sequencing and also carefully evaluated the sequencing data returned for analysis. I clustered the data and assigned cell types as well as looking at the relative numbers of each cluster represented by the two genotypes. Moreover, I separated the ventricular cardiomyocytes into subclusters to uncover differences between wild type and *popdc1* null mutant. In general, *popdc1* null mutant ventricular cardiomyocyte nuclei appeared to be stressed, display differences in genes involved in energy metabolism and heart regeneration.

6.6.1 Cell types and differences in all ventricular nuclei

Previous omics studies of adult zebrafish hearts relied on single-cell RNA sequencing rather than single-nucleus RNA sequencing resulting in a relatively small population of cardiomyocytes for which sequencing data were obtained (Koth *et al*., 2020, Honkoop *et al*., 2019). Here I have shown that through single-nucleus RNA sequencing that robust numbers of cardiomyocyte nuclei can be obtained along with a range of other cell types that are expected to be present in the ventricle. This method also has allowed for further analysis of the cardiomyocyte populations, however, this method does have its limitations. Although single-nucleus RNA sequencing created a less biased cell type coverage

(Lake *et al*., 2016), it has been found in some studies to be less sensitive than single-cell RNA sequencing (Thrupp *et al*., 2020). Predictably, mRNA that is found in the cytoplasm is typically underrepresented and estimates have been made that nuclear mRNA make up between 20-50% of total RNA depending on the cell type (Thrupp *et al*., 2020, Bakken *et al*., 2018). However, the extensive ECM between cardiomyocytes and also the strong adhesion between cardiomyocytes means that isolation of intact single zebrafish cardiomyocytes is challenging without damaging the cells (Sander and Joung, 2014). While adult cardiomyocytes can be isolated, they are too large to fit into the microfluidic channels used for single-cell sequencing and therefore will unavoidably result in an underrepresentation of cardiomyocytes relative to other cell types and a biased representation of smaller sized cardiomyocytes. Thus, presently there is no alternative to snRNA-seq to study the transcriptome of cardiomyocytes.

The initial analysis resulted in the clustering of the nuclei into 11 different populations, which included 4 cardiomyocyte and 3 endothelial cell populations and single immune, pericyte, epicardial fibroblast and thrombocyte populations. Overall, the cardiomyocyte populations had a comparable relative number of nuclei. In previous chapters, I had suggested that the *popdc1* null mutants may have a greater number of cardiomyocytes in their ventricle due to the smaller cardiomyocyte size and heart size but the equal representation of cardiomyocytes in both genotypes does not support this. Within the ventricular cardiomyocyte populations, *popdc1* null mutants had less representation of cardiomyocyte 1 and a greater representation of cardiomyocyte 2 which probably can be explained by the *popdc1* null mutant having nearly exclusive sub-clusters within the cardiomyocyte population, which will be discussed in further detail in the next sections. It was interesting to see an atrial cardiomyocyte cluster in the samples, as identified by the expression of *myh6* (Berdougo *et al*., 2003). This was unexpected as the atrium was surgically removed from the ventricle. Thus, it is likely that these atrial cardiomyocytes come from cells in the atrioventricular canal. *popdc1* null mutants had a greater representation of the atrial cardiomyocyte population although the difference was not significant. If this population does represent the atrioventricular canal then this increase in number

could be as a result of the increased capturing of these cells because of the abnormal position of the heart within the body cavity and morphological differences of the heart as described in chapter 4. It cannot however be ruled out that this population is a product of contamination from atrial tissue. *popdc1* null nuclei were also underrepresented in endothelial 2, endothelial – lymphatic and pericytes populations. However, these populations were very small and varied between samples differences were not significant and may be due to the random capturing of these cells rather than actual differences between genotypes.

6.6.2 Expression of *popdc1*

The *popdc1* null mutant was made by TALENs targeting of exon 1 which caused a 1 base pair deletion (Brand Lab, Unpublished). This resulted in a frameshift that caused a premature stop codon. It was predicted that the mutant transcript would encode a truncated protein that if translated is likely targeted for ubiquitination. However, it is also possible that the mRNA is subjected to nonsense-mediated decay (NMD), a process that scans the mRNA for premature stop codons and triggers degradation (Frischmeyer and Dietz, 1999). Because *popdc1* is strongly expressed in the *popdc1* null mutant it suggests that the mutant transcript is not subject to NMD. snRNA-seq works by sequencing many fragments of the cDNA, accounting usually for only 10-20% of the transcript (Kolodziejczyk *et al*., 2015, Islam *et al*., 2014), software is then used to piece the fragments together to determine gene expression and so a single nucleotide change can be missed, allowing for the recognition of mutated genes like *popdc1*. It is of note that the expression of *popdc1* is higher in the *popdc1* null mutant than in wild type, this may suggest that there might be a feedback mechanism in place to upregulate *popdc1* when protein levels are low. However, as demonstrated by immunostaining, Popdc1 protein is absent in the *popdc1* null mutant, showing that a truncated protein is likely made that is degraded (**Error! R eference source not found.**).

As expected *popdc1* had high expression levels in all of the cardiomyocyte clusters from both atrial and ventricular populations. This is in line with the strong expression of POPDC in striated muscle cells

(Andrée *et al*., 2000). The expression of *popdc1* in the heart has been subject to dispute, with the first reports claiming expression in the epicardium and coronary vasculature (Reese *et al*., 1999), however using immunohistochemistry, in situ hybridisation, and RT-PCR analysis in both mouse and chick models, expression was not found in the epicardium, proepicardium or coronary vessels (Andrée *et al*., 2002a, Andrée *et al*., 2002b, Torlopp *et al*., 2006). Here, in the zebrafish, I also see that there is expression of *popdc1* in nuclei presumably to be from epicardial derived fibroblasts and endothelial cells, which may suggest some expression in the epicardium and in the coronary vessels, which are made partly from endothelial cells. The differences in expression seen may be due to different methods, as only small subsets of these nuclei have *popdc1* expression and it could also be related to differences between species. Clearly, without further studies specifically devoted to this question, no firm conclusions can be drawn.

6.6.3 Popdc isoform expression

The expression levels of the other two POPDC isoforms was taken from the snRNA-seq data. Previously I had seen that in mRNA from whole ventricles there was a significant reduction in *popdc2* and *popdc3* expression in the *popdc1* null mutant when performing qPCR. However, with snRNA-seq, there was only a significant reduction in *popdc3* levels and no difference in the case of *popdc2* levels. This was an unexpected finding but may be explained as only the nuclear mRNA level are looked at with this method, and so perhaps the difference in *popdc2* mRNA levels can be more severe in the cytoplasmic RNA pool, but would not be visible with this method. However, there is an annotation error with *popdc2* on ensemble, which was what was used to identify the genes in this data, where another gene appears to have the same sequencing. This may cause irregularities in the information that we have found on *popdc2* in this work and so would require further investigation. The reduction of *popdc3* expression further supports the claim from chapter 4 that *popdc1* may be able to regulate the expression of *popdc3*, likely through one of its many interaction partners.

6.6.4 Cardiomyocyte heterogeneity

11 different ventricular cardiomyocyte subclusters were found when completing a more in-depth analysis of the three clusters; cardiomyocyte 1, cardiomyocyte 2 and cardiomyocyte 3. This is the first time in the zebrafish that heterogeneity of the cardiomyocytes has been seen by large scale sequencing, although other studies have been conducted in the hearts of other animals (Litvinukova *et al*., 2020). Although further bioinformatic analysis and confirmation of the differential gene expression patterns of these subclusters will be required to assign concrete functions, we can start to make some predictions about the populations that have been identified. CM1 had a high enrichment of *tbx5a* compared to the other clusters, tbx5a:GFP transgene expression is limited to the trabeculae suggesting that this population may represent the trabecular layer cardiomyocytes in the ventricle (Sánchez-Iranzo *et al*., 2018). Interestingly, it has recently been shown that *tbx5*a is required for cardiac regeneration (Grajevskaja *et al*., 2018), which suggests that although *tbx5a* labels exclusively the cardiomyocyte population in the trabecular layer and a recent paper from the Poss group suggests that most myocytes involved in cardiac regeneration are derivatives of the cortical layer (Gupta and Poss, 2012), that the contribution of trabecular myocytes to the regenerating ventricle seems to be essential. Although I see low mRNA expression of *nppa*, another marker of the trabecular layer in the zebrafish (Jensen *et al*., 2012), in cardiomyocytes of the wild type zebrafish and CM1. This may be explained by the fact that in healthy cardiomyocytes *nppa* mRNA has been found predominantly in the cytoplasm (Celik *et al*., 2019), so may not be captured by the methods used in this study. The cortical layer specifically expresses *lama5* (Sánchez-Iranzo *et al*., 2018). CM2 and CM4 both show enrichment for *lama5* suggesting that both lineages are probably part of the cortical layer. However, apart from *lama5*, these two populations had many differences, with CM4 more highly enriched for genes involves in cell adhesion. CM4 also showed upregulation in other genes marking the cortical layer like *xpir2a* and *hey2*, although they were both still expressed at relatively low levels. CM5 was enriched for genes involved in gas transport and erythrocyte homeostasis. They are unlikely to represent a precursor to both erythrocyte and cardiomyocyte as these cell types are formed by distant

lineages (Martin-Puig *et al*., 2008), but may represent cardiomyocytes that re-express some hematopoietic genes. However further work is required to substantiate this claim, as this is not something that has previously been described in the literature. The role of CM6 remains largely unknown at this time. The genes that are characterising this cell population (*grb10a, spock3matrix protein* and *coro1ca*) are involved in cellular signalling, extracellular matrix regulation and cell migration. Many apoptosis markers were found in CM8 and so CM8 most likely represents a population of cells undergoing apoptosis. Subcluster CM9 displayed an increased expression of endosomal related genes suggesting that this small population of cardiomyocytes may be responsible for the secretion of proteins in the ventricle and so may be important for signalling to other cell in the tissue. CM10 had a strong and specific upregulation of a number of genes traditionally associated with immune cells suggesting that these myocytes are possibly involved in the communication with immune cells.

There were two cardiomyocyte subpopulations almost uniquely present in the *popdc1* null mutant; CM3 and CM7. Both displayed a strong upregulation of genes involved in cardiac protection and of genes that are typically upregulated after stress. And so, these subclusters have likely arisen due to the physiological stress that the *popdc1* null mutant heart is under, triggering these differences in the gene expression. Apart from one another, their gene expression is most similar to CM1. This suggests that both may be a subset of the trabeculae, although they do not express *tbx5a*. This may also help to explain the differences seen in the trabeculae of *popdc1* null mutant ventricles. The significant enrichment of CM3 in *popdc1* null cardiomyocytes may be explained by the reduction of nuclei expressing the CM1 and CM2 pattern probably as a result of the increase in cardiac stress.

Further analysis will however be required to further delve into the differences between the cardiomyocyte clusters to confirm some of the hypotheses that have been put forward. Heterogeneity of cardiomyocytes has been seen in the development of the zebrafish heart and it has been recently

suggested that heterogeneity of cardiomyocytes allows for some cells to more easily assist in regeneration (Tsedeke *et al*., 2021).

6.6.5 Stress in *popdc1* null cardiomyocytes

The *popdc1* null mutant cardiomyocytes are stressed as evident by enrichment of stress-related genes. Although some stress markers were confined to the *popdc1* null mutant-enriched cell populations, CM3 and CM7, others like those involved in cytoskeletal changes and myofibrillogenesis were widely spread across the different nuclei populations found in *popdc1* null mutants. Upregulation of these genes may be suggestive of remodelling of the ventricle (Machackova *et al*., 2006). There was also upregulation of the oxidative stress pathways in the *popdc1* mutant, from work in mice, it is known that *Popdc1* null mutants are more susceptible to oxidative stress (Alcalay *et al*., 2013). Contrary to these findings, in transcriptome analysis after injury in chapter 5, where I saw that at baseline there was not a significant upregulation of stress markers such as *nppa* in ventricles of *popdc1* null mutants. This may be as the whole ventricle was taken and so the upregulation of stress markers in specific subsets of populations was too dilute to cause changes in global ventricular transcriptomic analysis. It was also found that after injury the mutants failed to upregulate their stress response, from work in this chapter this could be because the ventricles or at least specific cardiomyocyte populations are already in a state of stress and so are less receptive to new stress signals.

In mice and humans, it has long been known that in response to pathological stress there is a re-expression of 'foetal' genes, which are normally expressed in the embryonic and foetal heart and are downregulated after birth. However, these genes get upregulated and play a role in the remodelling of the heart to compensate for the damage (Seigo *et al*., 1988, Chien *et al*., 1991, Komuro and Yazaki, 1993). The catalogue of foetal genes re-expressed in the mouse in response to stress includes a number of isoforms of contractile genes such as *β-myosin heavy chain* (*Myh7*), *skeletal α-actin* (*acta1*), *smooth muscle α-actin* (*Acta2*), *β-Tropomyosin* (*Tpm2*) and the *natriuretic peptide* (*Nppa*). While this molecular response is probably present in most vertebrate hearts in response to injury and has also

been described in the human heart, there are species-specific differences. Nonetheless, I see an upregulation of *nppa* and *acta1b* which are orthologues of some of the foetal reprogramming genes. Similar to what was seen here in the *popdc1* null mutant fish heart, early work on the *Popdc1* null mouse mutant also reported an upregulation of some of these foetal reprogramming genes (Andrée *et al*., 2002a). It is unknown why hearts upregulate these foetal genes but it has been put forward that these genes may help to cope with the adverse remodelling in the pathological heart (van der Pol *et al*., 2020). As morphological changes are also observed in the *popdc1* null mutant hearts, this expression could represent an explanation for why we are seeing an upregulation of some foetal reprogramming genes.

One gene that was highly upregulated in the *popdc1* null enriched subclusters, CM3 and CM7, was *atf3*. This gene encodes for a transcription factor that belongs to the basic leucine zipper family (Hai *et al*., 1989), which has a low expression during homeostasis but can be upregulated by several stressors including angiotensin II, suggesting mechanical stress, and also in response to oxidative stress (Hai *et al*., 2010). Ectopic expression of ATF3 in cardiomyocytes of the mouse promote hypertrophy, fibrosis and cardiac dysfunction (Koren *et al*., 2013, Okamoto *et al*., 2002), but other studies have suggested that this gene has a protective role in the atria and under high-fat diet conditions (Zhou *et al*., 2011a, Kalfon *et al*., 2017). These data might suggest that this protein has different roles in different areas of the heart and potentially with different stressors. ATF3 has also been reported to have anti-inflammatory properties in immune cells (Gilchrist *et al*., 2008). Thus, it is presently unclear if *atf3* is being upregulated in response to stress or whether it is causing stress in the CM3 and CM7 clusters. Interestingly, with regard to the role of POPDC1 as a cAMP effector protein is the fact that ATF3 is also mediating transcriptional responses of cAMP signalling, binds to the cAMP responsive elements and may be regulated in a cAMP-dependent manner (Chu *et al*., 1994, Hertz *et al*., 2009). An increase in *ATF3* expression in response to mechanical stress in rat cardiomyocytes has been found to be mediated by cAMP and PKA (Koivisto *et al*., 2014). However, many other regulators and pathways can also affect ATF3 expression levels (Zhou *et al*., 2018). Further work would be

required to understand if Popdc1 was also able to regulate Atf3 expression through its cAMP effector activity.

Previously, I had suggested that the increased size of the hearts and smaller cardiomyocyte size is mimicking phenotypes seen in stress overload in the fish. The increase in several stress markers from the snRNA-seq is adding to this hypothesis. Although it is not completely clear right now what is the cause of the stress overload at present, one theory could be that the abnormal outflow tract and position of the heart in the body cavity is causing some form of pressure overload and an increase in wall stress hence is causing the morphological changes of the heart and the increase in cardioprotective and stress marker gene expression in the *popdc1* null mutant cardiomyocyte population.

6.6.6 Upregulation of PDEs in *popdc1* null cardiomyocytes

In the *popdc1* null cardiomyocytes, there was an upregulation of several PDEs. This was of interest as PDEs can degrade cAMP and thus modulate cAMP signalling and they have also been shown to create nanodomains for cAMP signalling which can depend on their interaction partners (Baillie *et al*., 2019). POPDC1 has been shown to preferentially bind to PDE4A and the interaction with other PDEs is currently being tested (Tibbo *et al*., 2020). This interaction is essential for the maintenance of a proper action potential in cardiomyocytes as the application of a disruptor peptide in rabbit cardiomyocytes caused a prolongation of repolarisation (Tibbo *et al*., 2020). I did not find *pde4a* to be affected in the null mutant, however, *pde3a*, *pde3b, pde4d* and *pde7a* were significantly upregulated. PDE3 and PDE4 are the isoforms that are highly expressed in the heart, and so likely most relevant here (Maurice *et al*., 2014). This finding suggests that *popdc1* may provide a level of transcriptional control to PDEs. This may add to the stress phenotype seen in the *popdc1* null cardiomyocytes as there will be an alteration of cAMP compartmentalisation if PDE levels are upregulated and this may be further affected if like with PDE4A there is an interaction with Popdc1, which may affect cAMP localisation and signalling (Tibbo *et al*., 2020). The upregulation of PDEs may however also be interpreted as an

attempt of the cell to recover control of cAMP signalling as the loss of POPDC1 may cause an aberrant increase in PKA activity and thus, the observed upregulation of PDEs may represent an attempt to compensate for this aberrant increased PKA activity in the null mutant heart.

6.6.7 Gene expression and regeneration

In chapter 5 I described that the *popdc1* null mutant displays retarded regeneration after cryoinjury. I used my snRNA-seq data to look into some genes which are known to be involved in regeneration to assess if they are misregulated in the *popdc1* null mutant.

6.6.7.1 Genes involved in ploidy

There is an increase in binucleation and ploidy in the *popdc1* null mutant cardiomyocytes. Both of these factors negatively affect the regenerative capacity of the zebrafish heart (Patterson *et al*., 2017, González-Rosa *et al*., 2018). *ect2* is the gene that is known to affect the binucleation status of cardiomyocytes in zebrafish causing an increase in binucleation when a dominant-negative mutant of ect2 is expressed (González-Rosa *et al*., 2018). Here, I saw consistently low levels of *ect2* in cardiomyocytes across both genotypes, which was unexpected as higher levels of this gene is what is thought to be required to prevent binucleation from occurring. This may be explained if the cells are dormant in the cell cycle, which may be the case as they were taken from adult hearts that had not suffered any injury, thus any cell proliferation will be low. The increase in binucleation may have occurred during an earlier phase of heart growth during larval and juvenile stages. Looking into these earlier stages may allow us to see differences in *etc2* that may account for the differences in binucleation status.

I did however see a significantly reduced expression of *tnni3k*, a gene known to regulate the ploidy of cardiomyocytes in zebrafish (Patterson *et al*., 2017). In the fish overexpression of this gene has been shown to promote polyploidisation (Patterson *et al*., 2017). This result is the inverse of what was to be expected based on the increase in ploidy in the *popdc1* null mutant cardiomyocytes. But again, if the cells are in a state of quiescence and not progressing through the cell cycle then tnni3k is not likely

to affect the ploidy status in the adult cardiomyocytes, and so its expression may need to be looked at earlier in the zebrafish's life. It is unclear why there is in fact a significant reduction of *tnni3k* in the *popdc1* null mutant cardiomyocytes, but one suggestion could be because *tnni3k* is known to cause oxidative stress and cardiac remodelling (Vagnozzi *et al*., 2013), thus lowering levels may help to prevent this from happening in the already stressed *popdc1* null ventricle.

Overall, the expression of the genes involved in binucleation and ploidy did not support the earlier evidence of increased binucleation and ploidy in the *popdc1* null mutant cardiomyocytes, which has been put forward as an explanation for the reduced proliferative and regenerative ability of the cryoinjured zebrafish heart of the *popdc1* null mutant.

6.6.7.2 tbx5 downregulation in popdc1 null mutant cardiomyocytes

Studies have been conducted to observe fish that contain an inactive form of *tbx5a* to assess whether they can regenerate their hearts. The researchers found that regeneration was severely impaired with the loss of *tbx5a* (Grajevskaja *et al*., 2018). Although no specific mechanism was proposed for the loss of regeneration, it is possible, that the loss of *tbx5a* prevents the cells from entering dedifferentiation, which is known to be crucial for zebrafish heart regeneration (Jopling *et al*., 2010, Gupta *et al*., 2013). It had been previously reported that the cortical layer was the source of most new cardiomyocytes and so important in regeneration (Gupta and Poss, 2012), however, the importance of *tbx5a* in regeneration and more recent reports of the trabeculae too contributing to the new myocardium after injury are implying that the trabecular layer is also important for heart regeneration (Grajevskaja *et al*., 2018, Tekeli *et al*., 2017).

In this chapter, I saw that there was a decrease in both *tbx5a* and *tbx5b* in the *popdc1* null mutant cardiomyocytes. Reduction of *tbx5a* in the *popdc1* null mutant cardiomyocytes could help to explain the loss of regenerative capacity. There is no clear link to the downregulation of *tbx5a* in the *popdc1* null mutant from the literature, however, one gene from the alpha-actinin binding pathway, *pdlim7*,

is known to downregulate *tbx5* and was significantly upregulated in the mutant cardiomyocytes (Camarata *et al*., 2006).

6.6.7.3 downregulation of fstl1b in popdc1 null cardiomyocytes

Across all sub-clusters, there is a reduction of *fstl1b* in the *popdc1* null mutant cardiomyocytes. This encodes for a non-glycosylated isoform of Fstl1 and in the zebrafish is upregulated in the epicardium and regenerating zones after injury (P. Ruiz-Lozano, personal communication). Further to this, it is necessary for regeneration, as when it is knocked down in the fish they are unable to regenerate their heart following cardiac resection (P. Ruiz-Lozano, personal communication). On top of this in mouse and swine models restoration of FSTL1 in the epicardium through an epicardial patch improved cardiac function and survival after myocardial infarction (Wei *et al*., 2015), usually after infarction, the protein becomes absent from the epicardium and the infarcted area. However, only the epicardial and not the myocardial form of FSTL1 has this benefit which is due to its hyperglycosylated state (Wei *et al*., 2015, Magadum *et al*., 2018). The glycosylation state appears to be important in the zebrafish as well, where the non-glycosylated *fstl1b* isoform but not the glycosylated isoform *fstl1a* is upregulated after injury (P. Ruiz-Lozano, personal communication). Although the exact mechanism as to how FSTL1 provides its cardioprotective function after injury is not known, it is thought that it might provide resistance to hypoxia through Akt and Smad1/5/9 signalling (Chen *et al*., 2016, Shen *et al*., 2019). The severe downregulation of *fstl1b* in the *popdc1* null mutant cardiomyocytes may represent an explanation as to the reduced regenerative capacity in *popdc1* null mutants.

6.6.7.4 Upregulation of runx1 in popdc1 null cardiomyocytes

Runx1 is a transcription factor that is involved in determining the proliferation and differentiation of multiple cell types in development and adulthood (Sood *et al*., 2017). It has been shown that in mice with a cardiomyocyte-specific conditional knock out of *Runx1* there is less adverse cardiac remodelling after myocardial infarction (McCarroll *et al*., 2018) and in the zebrafish knock out of *runx1* causes an improvement in heart regeneration and scar resorption after cryoinjury (Koth *et al*., 2020). I have seen

that there is upregulation of *runx1* in the *popdc1* null cardiomyocyte nuclei with most upregulation occurring in the mutant enriched subclusters as well as an upregulation of this gene *popdc1* null mutant nuclei in the endothelial cluster. After injury in the zebrafish, a higher *runx1* expression is known to cause an increase in smooth muscle and collagen genes such as *myh11a* in their endothelial/endocardial and thrombocyte populations, which is thought to explain why higher levels of *runx1* lead to an increase in the collagen content of the scar after cardiac injury (Koth *et al*., 2020). I also see a small but significant increase in *myh11a* even before injury has occurred in the endothelial population. The increased expression of *runx1* and *myh11a* in the p*opdc1* null mutant even at baseline may explain the persistence of the scar tissue after cryoinjury, although experiments would also need to be conducted in the injured fish heart to assess if this caused exaggerated runx1 and *myh11a* expression after injury.

6.6.8 Energy metabolism in popdc1 null cardiomyocytes

The heart requires a large amount of energy and so is dependent on a constant production of ATP by oxidative phosphorylation in the mitochondria. In a healthy human, fatty acid oxidation account for 60-90% of ATP generation with 10-40% coming from pyruvate oxidation, formed from lactate or glycolysis (Stanley and Chandler, 2002).

In the *popdc1* null mutant, there is severe downregulation of *acsl1b*, the gene that encodes for acyl-CoA synthetase long-chain family member 1b, across all cardiomyocyte sub-populations. Acsl1b is a cardiac-specific enzyme that catalyses the conversion of fatty acids to acetyl-CoA, a necessary step to allow for β-oxidation and energy production, with *Acsl1* knock out mice having a 90% reduction of fatty acid oxidation (Ellis *et al*., 2011). As expected I see some genes and pathways that are upregulated, which are related to glucose metabolism and uptake, suggesting a transition to glycolysis to compensate for the energy deficit. Although contrary to this, in the CM3 subcluster that is enriched for *popdc1* null mutant nuclei, there is downregulation of functions related to debranching glycogen, which is required to release glucose for glycolysis, suggesting that these nuclei are trying to store

rather than spend glucose. During heart failure and hypertrophic heart growth there is a switch to glycolysis and away from fatty acid oxidation, returning to a more foetal like state of metabolism, this is thought to limit the adverse remodelling of the heart (Heather *et al*., 2006, Osorio *et al*., 2002, Kato *et al*., 2010). Fatty acid oxidation is not the most efficient way to produce energy in the heart, it has been found that when there is inhibition of fatty acid oxidation there is increased mechanical efficiency (Lopaschuk *et al*., 2010). Glycolysis is more energy-efficient especially in terms of the amount of oxygen used which can be particularly important in the ischemic heart (Lopaschuk *et al*., 1994). However, the switch away from fatty acid oxidation could result in lower energy production as the heart is now not using all available substrates for energy metabolism as well as more energy being spent on ion uptake for glycolysis to occur (Wende *et al*., 2017). The switch in energy metabolism could be interpreted as the result of the heart being stressed and so trying to produce energy more efficiently and circumvent adverse remodelling events.

On the other hand, the stress signals being seen in the *popdc1* null could be a product of the switch in energy metabolism. It has been shown that when you remove genes involved in fatty acid oxidation including ACSL1 there is contractile dysfunction and there is likely to be insufficient compensation by other metabolic pathways which could lead to a stressed heart (Wende *et al*., 2017, Ellis *et al*., 2011). On top of this, the build-up of un-oxidised fatty acids could cause lipotoxicity, leading to the expression of stress markers like those seen in the *popdc1* null heart (Wende *et al*., 2017, Opie and Knuuti, 2009). Taken together, aberrant metabolism of energy could be a product of the *popdc1* null heart being stressed or it may be what is causing the stress. Further work would have to be conducted to assess this to determine what factor is causing the stress.

A switch to glycolysis is also seen in heart regeneration. In the mouse there is a metabolic shift from glycolysis to oxidative phosphorylation of fatty acids in the first week after birth, correlating with the loss of heart regeneration and cardiomyocyte cell proliferation (Porrello *et al*., 2011, Lopaschuk *et al*., 1992, Menendez-Montes *et al*., 2016). In the zebrafish, one theory that has recently been put forward

to explain why they have retained the ability of heart regeneration in the adult heart is the ability to revert to embryonic metabolism with the upregulation of glycolysis after injury (Honkoop *et al*., 2019, Ogawa *et al*., 2021). This might suggest that in the *popdc1* null mutant we would expect an increased regenerative ability as even at baseline we are seeing a shift away from fatty acid oxidation to glycolysis. However, if this switch has been because the heart is stressed perhaps the type of energy metabolism used is not enough to allow the heart to regenerate particularly if the heart might have an energy deficit. Especially as stress itself has also been found to be sufficient to prevent heart regeneration (Sallin and Jaźwińska, 2016).

6.6.9 Conclusions and future directions

In this chapter, I have described the categorisation of different cell populations in the ventricle as well as different sub-populations of cardiomyocytes. Ten subpopulations were discovered with two being highly enriched with the *popdc1* null mutant nuclei and two populations being highly enriched with wild type nuclei. Theories have been put forward for the location and function of some of these sub-populations within the ventricle, with the presumed trabeculae population having a subset that is enriched for *popdc1* null nuclei and does not express important trabeculae markers. On from this, I have gone on to highlight some of the important differences that I have found between the *popdc1* null mutant and wild type cardiomyocytes, which has focused mainly on the increase in stress markers and the aberrant metabolic function of the *popdc1* null mutant cardiomyocytes. Currently, it is not possible to pinpoint what is the cause of the stress, especially as aberrant metabolic function can be both a stressor and a downstream effect of stress. Finally, I investigated some genes which are known to affect heart regeneration and found that some are misregulated in the *popdc1* null mutant.

Going forward, some of the differences seen will have to be further confirmed using qPCR analysis, in situ hybridisation or immunostaining, with the latter two allowing me to discover the location of different subsets within the ventricle. On top of this, there will have to be a more in-depth pathway analysis to unpick the metabolic dysfunction seen in the *popdc1* null mutant and to help to confirm

where the cardiomyocytes are getting their energy from as well as to explore other misregulated pathways, which at this point have not been given attention. Finally, it could be important to look at nuclei from different clusters other than from cardiomyocytes. Although *popdc1* is primarily expressed in cardiomyocytes, cell-cell interactions within the ventricle could lead to different expression patterns in other cell types which may produce interesting findings that are yet to be uncovered. Although the uninjured heart studied here has provided some clues in understanding the loss of regeneration in the *popdc1* null mutant, in the future injured hearts will have to be looked at to generate more concrete theories regarding this phenotype.

7. General Discussion

7.1 Background and summary of the study

POPDC1 is a membrane protein that is highly expressed in the heart and skeletal muscle (Andrée *et al*., 2000). After its discovery, efforts were made to uncover interaction partners to help describe a function of POPDC1. Although numerous interaction partners were found (Amunjela *et al*., 2019), it wasn't until more recently that the involvement of the POPDC proteins with cAMP signalling was discovered, marking it the newest member of the cAMP effector protein family (Froese *et al*., 2012). The functions of POPDC1 appear to be quite complex based on its many protein-protein interaction partners while so far only little knowledge has been gained about the mechanism of how cAMP may control these interactions. However, recently several working models have been formulated and some evidence has been put forward, for example, cAMP binding modulates Popdc1's interaction with TREK-1 (Swan *et al*. 2019).

In mice, POPDC1 is expressed at high levels in the sinoatrial and atrioventricular nodes and is equally strong in the atrium. In the ventricle, expression is weaker than in the atrium and higher levels are seen in the His bundle, bundle branches and Purkinje fibres (Froese *et al*. 2012). Experiments with mutants carrying null or missense mutations in mice and zebrafish have revealed the importance of *Popdc1* in the regulation of the heartbeat (Schindler *et al*., 2016b, Froese *et al*., 2012). *Popdc1* null mutant mice develop stress-induced sinus bradycardia, which is induced by physical exercise, mental stress or after isoproterenol injections (Froese *et al*., 2012). Cardiac arrhythmias are also seen in patients with mutations in *POPDC1* (Schindler *et al*., 2016b, De Ridder *et al*., 2019, Beecher *et al*., 2021, Indrawati *et al*., 2020). These observations suggest that POPDC1 has an essential role in the development and maintenance of electrical conduction of the heart. Furthermore, skeletal muscle phenotypes are seen when *POPDC1* is mutated with many patients showing limb-girdle muscular dystrophy (Schindler *et al*., 2016b, De Ridder *et al*., 2019, Beecher *et al*., 2021, Indrawati *et al*., 2020),

and *Popdc1* null mutant mice displaying retardation of skeletal muscle regeneration following injury (Andrée *et al*., 2002a).

Further to the role of POPDC1 in striated muscles, there are many reports of the misregulation of POPDC1 in cancer. The involvement of POPDC1 in tight and adherens junctions has long been hypothesised due to the role of some of its interaction partners in this context (ZO-1) and colocalisation with these junctions (Osler *et al*., 2005, Russ *et al*., 2011, Williams *et al*., 2011, Wu *et al*., 2012, Han *et al*., 2014). This has led to claims that POPDC1 has a role in regulating EMT, thus its misregulation can promote the migration and metastasis of cancers (Amunjela and Tucker, 2017b, Amunjela and Tucker, 2017a, Han *et al*., 2015, Han *et al*., 2014). On top of this, POPDC1 can interact with several proteins known to be involved with the cell cycle such as ZO-1 (Osler *et al*., 2005), GEFT (Smith *et al*., 2008) and c-Myc (Parang *et al*., 2016). In the gut, POPDC1 aids in the proteasomal degradation of the proto-oncogene c-Myc by amending its phosphorylation status with a reduction in POPDC1 expression in the gut leading to more acute cancer phenotypes (Parang *et al*., 2016).

The expression of POPDC1 in the heart and its role in mediating cell cycle progression has led to the current project to test its role in myocardial regeneration following injury. Unlike the mammalian heart, the adult zebrafish heart can regenerate after injury (Poss *et al*., 2002). Cryoinjury of the zebrafish heart has become popular to model MI and to try to understand the differences that permit regeneration of the fish heart (González-Rosa *et al*., 2011). For the zebrafish heart to regenerate it must go through successive stages including inflammation, scar formation, cardiomyocyte proliferation and scar removal (González-Rosa *et al*., 2017). This process has been reported to take between 60-130 days depending on the injury size (González-Rosa *et al*., 2011, Chablais *et al*., 2011). Many genes and processes have already been discovered as being essential for cardiac regeneration, but work is still ongoing to understand this process at a higher resolution. This work hopes to find clinically relevant targets that may culminate in the generation of new therapies for the human heart to aid in the repair of the myocardium following cardiac injury such as MI.

Results presented in this thesis have explored the interaction with POPDC1 and the master cell cycle regulator c-Myc. All three POPDC proteins have been found to interact with c-Myc as well as PR61α, the active subunit of PP2A which dephosphorylates c-Myc leading to its instability. Putative binding sites for both PR61α and c-Myc have been mapped onto POPDC1. Further to this, it has also been found that manipulation of POPDC protein levels affects c-Myc expression. Loss of *Popdc1* in the mouse ventricle causes an upregulation of c-Myc, while forces expression of POPDC1 in cos7 cells causes a reduction in c-Myc expression. Overexpression of POPDC1 also displays paracrine inhibition of cell proliferation suggesting that POPDC1 controls the release of a chalone that affects the cell cycle. The hearts of *popdc1* null mutants zebrafish were studied for phenotypic similarities to hearts of transgenic mice with overexpression of c-Myc and were found to also display enlarged hearts with smaller cardiomyocytes compared to wild types hearts. Other morphological differences were observed in the zebrafish null mutant heart including a reduced outflow tract angle, hypotrabeculation, an increase in cortical layer thickness and randomised positioning of the heart within the body cavity. Aside from the morphological difference in the heart, the *popdc1* null mutants display a smaller body size than wild type but have an increased survival to adulthood and display a reduction in the expression of the other POPDC isoforms at mRNA and proteins level.

Cryoinjuries were performed on wild type fish which showed an upregulation of *popdc1* until 14 DPI, and an increase in Popdc1 protein expression was also seen and simultaneously an upregulation of *mycb*. However, contrary to the expectation of an enhanced myocardial regeneration in the *popdc1* null mutant due to its role of controlling the expression of the proto-oncogene c-Myc, cardiac regeneration in the *popdc1* null mutant was retarded and/or remained incomplete with the persistence of scar tissue even at 130 DPI. Further studies uncovered that the mutants had a reduced proliferative response in cardiomyocytes following injury. Gene expression was altered following injury with a failure to upregulate marker genes for cardiac progenitors, stress, angiogenesis and scar remodelling at the proper time points. Studies were undertaken to uncover the reasons for the impairment of cardiac regeneration in the *popdc1* null mutants and it was found that the mutants had

an increase in ploidy and binucleation of their cardiomyocytes, which has been associated with loss of proliferation following injury (González-Rosa *et al*., 2018, Patterson *et al*., 2017). snRNA-seq was used to analyse the transcriptome of the adult ventricle of *popdc1* null mutants before injury and a misregulation was seen in genes known to be involved in heart regeneration such as *tbx5a*, *runx1* and *fstl1b* (Koth *et al*., 2020, Grajevskaja *et al*., 2018) (P. Ruiz Lazano, personal communication). Transcriptome data have also indicated that the *popdc1* null mutant hearts have aberrations in the expression pattern of energy metabolism genes across all the cardiomyocyte nuclei and importantly a unique population of hyper-stressed cardiomyocytes, which was only present in mutant hearts and likely involved in the impaired cardiac regeneration, but their involvement needs to be further characterised.

7.2 Major Findings

7.2.1 Popdc1 is required for the correct regeneration of the zebrafish ventricle

A major aim of this project was to investigate the role of Popdc1 in regeneration of the zebrafish heart. It was hypothesised that *popdc1* null mutants would show increased proliferation following cryoinjury because of the interaction of Popdc1 and c-Myc (Parang *et al*., 2016). However, in this study, the opposite was found, with the loss of *popdc1* causing retardation or possibly the incomplete regeneration of the myocardium. The regeneration process is complex and Popdc1 has numerous interaction partners and so potentially also multiple functions, suggesting that the increase in c-Myc levels following the loss of Popdc1 may not be sufficient to cause an increase in proliferation and that the loss of Popdc1 through one of its other interaction partners is causing the reduction in regenerative capabilities. With this in mind, the focus of the project became trying to understand how Popdc1 levels can affect the healing of the myocardium.

Following cryoinjury, there is an increase in both mRNA and protein expression of Popdc1, which may be indicative of an essential role in the regeneration process. It was found that Popdc1 was essential to not delay recovery after injury and to have a robust increase in proliferation at 7 DPI. Ploidy and

binucleation of cardiomyocytes are linked to the regenerative potential in many organisms, with those with mononucleated cardiomyocytes and a diploid state being more likely to regenerate their hearts (Bersell *et al*., 2009, Vivien *et al*., 2016, Smith and Mommersteeg, 2020). Zebrafish are diploid and mononucleated, but when binucleation is experimentally induced, the ability to regenerate is lost, with multinucleated or polyploid cardiomyocytes being unable to contribute to the myocardial regeneration (Patterson *et al*., 2017, González-Rosa *et al*., 2018). Cardiomyocytes in the *popdc1* null mutant display an increase in binucleation and ploidy, however, expression of genes associated with spindle formation and ploidy (such as *ect2* or *tnni3k*) did not corroborate with this. This may be because the myocardium is only proliferating at a low level in steady-state and only uninjured hearts were investigated in the case of the sn-RNA-seq. Thus, the increased DNA content and nucleation may be a relic from a time of more extensive myocardial growth during embryonic and larval growth. Based on the literature, neither the DNA content nor the ploidy level is high enough to be responsible for a complete block of heart regeneration (González-Rosa *et al*., 2018). However, this might explain why typically retardation was seen in the null mutant rather than a complete block of heart regeneration.

Although genes associated with binucleation were not misregulated in the *popdc1* null mutant, there were differences seen in other genes which are known to affect cardiac regeneration including *tbx5a,* which is known to demarcate the trabecular layer of the adult zebrafish heart (González-Rosa *et al*., 2018) *Tbx5a* is, essential for heart development and together with some other cardiac transcription factors can reprogram cardiac fibroblasts into cardiomyocytes (Ieda *et al*., 2010). Conditional ablation of *tbx5a* just prior to heart injury provided evidence for an essential role of *tbx5a* for heart l repair and that a persistent injury is not a product of mal-development (Grajevskaja *et al*., 2018). In the *popdc1* null mutant, there is a reduction of *tbx5a* expression in the adult heart, which may be one of the reasons for the retardation in cardiac regeneration.

runx1 is a transcription factor that is essential in haematopoiesis (Meyers *et al*., 1993, Okuda *et al*., 1996). It has recently been reported to be upregulated in the zebrafish ventricle following injury and

that when ablated there is an increase in myocardial survival and a decrease in scar formation (Koth *et al*., 2020). Wild type zebrafish have a *runx1*-positive endocardial population, that express smooth muscle and collagen genes, which are not found in *runx1* knock out zebrafish hearts and are thought to be responsible for the increase in scarring (Koth *et al*., 2020). Even prior to injury in the *popdc1* null mutant, there is an increase of *runx1* expression in cardiomyocytes and endothelial cells as well as an upregulation of smooth muscle genes in endothelial cells. This may help to explain the persistence of scaring at 130 DPI, long after wild type hearts have fully recovered.

Finally, there was a severe downregulation of *fstl1b* in all *popdc1* null cardiomyocytes. *Fstl1b* is encoded a secreted glycoprotein that carries a follistatin-like domain, which binds BMP4 preventing it from binding to the BMP receptor complex and thereby negatively regulating BMP signalling (Zhou *et al*., 2006). Whether fstl1b functions in the context of BMP antagonism or has some other biochemical function is currently poorly understood. Epicardial patches releasing FSTL1 in mice and pigs after coronary artery ligation were shown to induce an increase in cardiomyocyte proliferation and result in improved functional recovery (Wei *et al*., 2015). Interestingly, recent work in zebrafish demonstrated that loss of *fstl1b* but not the related *ftsl1a* impairs heart regeneration (P. Ruiz Lazano, personal communication). Thus, the downregulation of *fstl1b* may be another mechanism resulting in impaired heart regeneration in the *popdc1* null mutant.

From these data, we can already draw some conclusions and formulate a hypothesis that helps to explain the reduced proliferation and persistence of scaring in the injured *popdc1* null mutant heart. But aside from these, there are other considerations to be made for example haemodynamic forces are also required in activating the endocardium following injury (Gálvez-Santisteban *et al*., 2019). In the *popdc1* null mutant, we observed several morphological aberrations, which may lead to altered blood flow and so haemodynamic forces, which could interfere with regeneration following injury. There is also the upregulation of a number of stress-related genes (*nppa*, *acta1a*) prior to injury in the *popdc1* null cardiomyocytes. If the heart is already in a stressed state then perhaps it is unable to

properly deal with any additional stress upon cryoinjury leading to the reduced regenerative response. Overall, there are several potential reasons for the loss of correct regeneration in the *popdc1* null mutant. As the process is complex, Popdc1 may likely affect regeneration at different levels. To unpick this process further it would be interesting to try and link Popdc1 to some of the genes that are misregulated at baseline or to assess the transcriptome of the *popdc1* null mutant after injury.

7.2.2 *popdc1* null mutants have improper morphology in the adult heart

Whilst characterising some of the differences in the *popdc1* null mutant compared with wild type it was noted the mutant had larger hearts and smaller cardiomyocytes. It is currently unknown if this results in an overall greater cardiomyocyte number for the heart, although this is what the data suggests. This implies that the heart has been subjected to hyperplasia, which is thought to happen in the zebrafish in response to pressure overload (Jean *et al*., 2012), whereas mammals would respond to pressure overload with cardiac hypertrophy (Frey and Olson, 2003). Pressure overload in mammals can be caused by aortic stenosis or in response to hypertension (Cooper *et al*., 1981). It is plausible that the *popdc1* null mutant heart may be exposed to pathological hemodynamic conditions because of the improper positioning of the heart in the thorax and alterations in the outflow tract morphology, both of which may cause an increase in wall stress, which possibly mimics pressure overload conditions in the zebrafish. Further evidence that the hearts are stressed comes from the snRNA-seq data where an upregulation of a number of stress markers such as *nppa* and *atf3* was observed; both genes having implications in remodelling the heart after stress (Seigo *et al*., 1988, Chien *et al*., 1991, Komuro and Yazaki, 1993, Koren *et al*., 2013). There is also the upregulation of genes involved in cytoskeletal assembly, which may indicate that cells are changing their shape in response to an increase in wall stress, adding to the remodelling (Hein *et al*., 2000). It must also be mentioned that c-Myc, which has been shown to interact with POPDC proteins and trigger its degradation, is also known of causing hyperplasia in the heart (Jackson *et al*., 1990, Parang *et al*., 2016). Further to the upregulation of stress markers, differences are also seen in energy metabolism with an important gene involved in fatty acid oxidation being strongly downregulated in the *popdc1* null mutant and

some genes and pathways relating to glucose metabolism being upregulated. This is of significance as stressed hearts or injured hearts often switch to glucose metabolisms as a means to generate energy (Heather *et al*., 2006, Osorio *et al*., 2002, Kato *et al*., 2010). Currently, the epistatic relationships between the different gene regulatory responses remain unclear. Thus, it is unclear whether the transcriptional changes are a result of the stress that the loss of *popdc1* puts on the heart, or whether the loss of *popdc1* is triggering some of the transcriptional changes, which then are causing the stress in the mutant heart. Further work would have to be conducted to pinpoint the cause of the stress in the *popdc1* null mutant heart, although due to the numerous interaction partners of Popdc1 it may be that there are multiple reasons.

Further, morphological differences are seen in the heart, with a noticeably thickened cortical layer and trabeculae, which do not project as far into the lumen, have less complexity and cover less surface area. On top of this, when looking at the trabeculae they seem to be more fragmented and striations are not as easily seen, suggesting they have abnormal sarcomere organisation. *tbx5a,* a marker of the trabecular layer in the adult ventricle (Sánchez-Iranzo *et al*., 2018), is expressed at low levels in *popdc1* null mutants. On top of this, when looking at the different cardiomyocyte populations present in the ventricle there is a presumptive trabecular myocyte population based on their *tbx5a* expression and a separate but related population that is almost exclusively found in the mutant and is *tbx5a* negative. The failure to upregulate *tbx5a* may be responsible for the abnormal trabecular layer in the mutants as the expression of *tbx5a* is necessary to prevent cardiomyocytes from shifting to a cortical layer identity (Sánchez-Iranzo *et al*., 2018). The loss of *tbx5a* in *popdc1* null cardiomyocytes may stimulate more cells to become part of the cortical layer, which could explain the thickening of this layer in the null mutant. It is a possibility that there are also cells, which are in 'limbo' as they have not received proper direction to become cells of either layer. The PF in the postnatal mammalian heart after compaction are remnants of the trabecular layer of the embryonic heart (Choquet *et al*., 2020, Jensen *et al*., 2017). Interestingly, *Popdc1* expression in the mouse heart is higher in the cardiac conduction system (CCS) including the PF (Schindler *et al*., 2016a). The localisation and upregulation of POPDC1

in the CCS might suggest a function here and add to the argument of the abnormal trabecular layer when *popdc1* is ablated in the zebrafish.

The extensive trabeculation of the embryonic mammalian hearts serves as an intermediate state before compaction to allow for efficient contractility of the heart and at the same time allowing for a sufficient supply of oxygen and nutrients via diffusion. Coronary vessels will form alongside compaction of the ventricular wall, taking over the role of delivery of oxygen and nutrients (Sedmera *et al*., 2000). In zebrafish, the coronary vasculature never acquire the dense network seen in the mammalian heart and the ventricular wall never undergoes compaction and this diffusion delivering oxygen and nutrients persists in the adult zebrafish heart (Sedmera *et al*., 2000). The hypotrabeculation seen in the *popdc1* null mutants may add to the stress phenotype as it could cause oxygen diffusion to be impeded across the tissue. And so it may be that the abnormal morphologies are interlinked with differences that may be formed much earlier causing later morphological changes due to increased stress in the heart.

Future studies would have to be conducted to understand if the abnormal myocardial layering seen in the *popdc1* null mutants are causing functional abnormalities, which could be observed by looking at the blood flow and conduction of the mutant heart and may help us to understand the stress phenotype observed in the mutant.

7.3 Future Work

There are many different avenues, which could now be explored based on the discoveries in this work, with many of the specific next steps having been alluded to in the discussions for individual chapters. Here I will discuss in more depth some of the broader lines of exploration. Firstly, I have established that the loss of *popdc1* can cause retardation of heart regeneration. It would however be interesting to study the reverse situation by looking at heart regeneration in zebrafish with overexpression of *popdc1* in the ventricle to determine if elevating *popdc1* expression could accelerate the recovery of injured myocardium. If this would be the case then there would be the potential for investigating

Popdc1 as a therapeutic target for patients to help to improve myocardial recovery after MI. To aid the uncovering of the mechanism behind *popdc1*'s effect on myocardial regeneration, one could use for example the *popdc1*^{S191F} mutant. This zebrafish mutant encodes a mutant Popdc1 protein, which binds cAMP with low affinity. If these fish too display an aberrant regeneration phenotype it may suggest the interaction of Popdc1 with cAMP is what is necessary for permitting regeneration of the heart. Unfortunately, the *popdc1*^{S191F} mutant displays an impaired membrane localisation of POPDC1 and POPDC2 and thus may not be the appropriate model to test the role of cAMP binding of POPDC proteins in heart regeneration (Froese *et al*., 2016). Alternatively, the identification and use of a small molecule Popdc1 inhibitor, to block Popdc1 function would be an approach to specifically address the question of the role of cAMP in cardiac regeneration. It is also advisable to generate a conditional *popdc1* allele. The ablation of *popdc1* could be triggered before the injury and would allow us to determine if Popdc1 is specifically required during cardiac regeneration or if the loss of popdc1 during development is causing stress to the heart, which is responsible for the retardation of cardiac regeneration. In the case of the small molecule approach to modulate a molecular inhibitor of Popdc1 function, there is the potential to block different functions such as agonist peptides to prevent certain protein-protein interactions or antagonists molecule that could mimic cAMP to prevent cAMP binding, this may allow the further identification definition of the role of Popdc1 in regeneration.

snRNA-seq is a powerful method applied in this thesis generating large amounts of data. Much of this data could be further mined to allow for the analysis of pathways that are misregulated in the *popdc1* null mutants. Moreover, in this work I have focused on the study of cardiomyocytes, other cell types present in the ventricle may generate specific differences which could aid in explaining some phenotypes seen and/or bring up further questions leading to new areas fit for exploration. To understand the regeneration phenotype in more depth, it would be beneficial to perform snRNA-seq of hearts that have been injured at one or more time points to provide further information of the pathways and genes that are aberrantly expressed in the mutant and may lead to a more thorough

understanding of the mechanism behind the retarded regeneration phenotype in the *popdc1* null mutant.

Finally, it will be important to study the *Popdc1* null mutant mouse to uncover if they too show some of the phenotypes that have now been observed for the first time in the zebrafish. Specifically, it will be important to investigate if any of the morphological differences observed in the zebrafish are also present to some level in the mouse heart and to look at the RNA expression of some differentially expressed genes to determine if some anomalous expression patterns and pathways are similarly perturbed in the mouse mutant. The phenotypes present in both species may be indicative of common functions of POPDC1 in vertebrate hearts and therefore likely also apply to the human heart making this observation more clinically relevant.

7.4 Final Conclusions

My work demonstrates that *popdc1* is essential for the proper time course of regeneration of the zebrafish heart, as when it is lost, hearts either fail completely or display a severely retarded regeneration in the 130-day period that I have studied following injury. Since the discovery that zebrafish can regenerate their hearts after injury (Poss *et al*., 2002), a large number of genes and pathways have been implicated in cardiac regeneration (Ryan *et al*., 2020, Sanz-Morejón and Mercader, 2020, Smith and Mommersteeg, 2020). A specific link to any of these previously identified regeneration pathways has not become apparent in this work but a number of hypotheses have been put forward to explain the loss of proliferation and regeneration in the *popdc1* null mutant heart, such as the increase in binucleation and ploidy, increase of *runx1* and the decrease of *tbx5a* and *fstl1b* in cardiomyocytes. In addition to the regeneration phenotype, *popdc1* null mutants display differences in their myocardial layers with a thickened cortical layer and hypotrabeculation. As *popdc1* null mutants display abnormally low expression levels of *tbx5a*, a marker of the trabecular layer (Sánchez-Iranzo *et al*., 2018), this may cause a greater proportion of cardiomyocytes to gain a cortical identity

and a reduction in cells with a trabecular identity potentially explaining the alterations observed in the mutant heart at the histological level. Additionally, the mutant ventricles display changes in gene expression, associated with impaired energy metabolism and stress; factors are known to trigger myocardial remodelling (Heather *et al*., 2006, Osorio *et al*., 2002, Kato *et al*., 2010, Machackova *et al*., 2006), which also may contribute to the morphological alterations in the mutant heart. Further work will have to be performed to find the underlying cause of the stress, although abnormal outflow tract positioning in the mutants may cause altered blood flow through the heart giving rise to mechanical stress. Overall, this work has resulted into a much more in-depth characterisation of the zebrafish *popdc1* null mutant specifically concerning the morphological changes and the transcriptomic profile of the mutant heart, generating lots of novel questions, which need to be explored and hopefully answered in the future.

References

10X GENOMICS. 2021. *What is the range of compatible cell sizes?* [Online]. https://kb.10xgenomics.com/hc/en-us/articles/218170543-What-is-the-range-of-compatible-cell-sizes-: 10x Genomics. [Accessed 15th June 2021].

AGUIRRE, A., MONTSERRAT, N., ZACCHIGNA, S., NIVET, E., HISHIDA, T., KRAUSE, MARIE N., KURIAN, L., OCAMPO, A., VAZQUEZ-FERRER, E., RODRIGUEZ-ESTEBAN, C., KUMAR, S., MORESCO, JAMES J., YATES, JOHN R., CAMPISTOL, JOSEP M., SANCHO-MARTINEZ, I., GIACCA, M. & IZPISUA BELMONTE, J. C. 2014. In Vivo Activation of a Conserved MicroRNA Program Induces Mammalian Heart Regeneration. *Cell stem cell,* 15**,** 589-604.

ALCALAY, Y., HOCHHAUSER, E., KLIMINSKI, V., DICK, J., ZAHALKA, M. A., PARNES, D., SCHLESINGER, H., ABASSI, Z., SHAINBERG, A., SCHINDLER, R. F. R., BRAND, T. & KESSLER-ICEKSON, G. 2013. Popeye domain containing 1 (Popdc1/Bves) is a caveolae-associated protein involved in ischemia tolerance. *PLoS ONE,* 8**,** e71100.

ALKASS, K., PANULA, J., WESTMAN, M., WU, T.-D., GUERQUIN-KERN, J.-L. & BERGMANN, O. 2015. No Evidence for Cardiomyocyte Number Expansion in Preadolescent Mice. *Cell,* 163**,** 1026-1036.

ALVAREZ, E., NORTHWOOD, I. C., GONZALEZ, F. A., LATOUR, D. A., SETH, A., ABATE, C., CURRAN, T. & DAVIS, R. J. 1991. Pro- Leu- Ser/ Thr- Pro is a consensus primary sequence for substrate protein phosphorylation. Characterization of the phosphorylation of c-myc and c-jun proteins by an epidermal growth factor receptor threonine 669 protein kinase. *J Biol Chem,* 266**,** 15277-85.

AMUNJELA, J. N., SWAN, A. H. & BRAND, T. 2019. The Role of the Popeye Domain Containing Gene Family in Organ Homeostasis. *Cells,* 8**,** 1594.

AMUNJELA, J. N. & TUCKER, S. J. 2017a. Dysregulation of POPDC1 promotes breast cancer cell migration and proliferation. *Biosci Rep,* 37**,** BSR20171039.

AMUNJELA, J. N. & TUCKER, S. J. 2017b. POPDC1 is suppressed in human breast cancer tissues and is negatively regulated by EGFR in breast cancer cell lines. *Cancer Lett.,* 406**,** 81-92.

ANDRÉE, B., FLEIGE, A., ARNOLD, H.-H. & BRAND, T. 2002a. Mouse Pop1 Is Required for Muscle Regeneration in Adult Skeletal Muscle. *Mol Cell Biol.,* 22**,** 1504-1512.

ANDRÉE, B., FLEIGE, A., HILLEMANN, T., ARNOLD, H.-H., KESSLER-ICEKSON, G. & BRAND, T. 2002b. Molecular and functional analysis of Popeye genes: A novel family of transmembrane proteins preferentially expressed in heart and skeletal muscle. *Exp Clin Cardiol.,* 7**,** 99-103.

ANDRÉE, B., HILLEMANN, T., KESSLER-ICEKSON, G., SCHMITT-JOHN, T., JOCKUSCH, H., ARNOLD, H.-H. & BRAND, T. 2000. Isolation and Characterization of the Novel Popeye Gene Family Expressed in Skeletal Muscle and Heart. *Dev Biol.,* 223**,** 371-382.

ANH, L. B., TAMARA, B. H. & GREGG, C. F. 2010. Epidemiology and risk profile of heart failure. *Nat Rev Cardiol.,* 8**,** 30-41.

APITZ, C. M. D., WEBB, G. D. P. & REDINGTON, A. N. P. 2009. Tetralogy of Fallot. *The Lancet,* 374**,** 1462-1471.

ARNOLD, H. K. & SEARS, R. C. 2006. Protein Phosphatase 2A Regulatory Subunit B56a Associates with c- Myc and Negatively Regulates c- Myc Accumulation. *Mol Cell Biol.,* 26**,** 2832-44.

AUMAN, H. J., COLEMAN, H., RILEY, H. E., OLALE, F., TSAI, H.-J. & YELON, D. 2007. Functional Modulation of Cardiac Form through Regionally Confined Cell Shape Changes. *PLoS Biol,* 5**,** e53.

BAEYENS, N. & SCHWARTZ, M. A. 2016. Biomechanics of vascular mechanosensation and remodeling. *Mol Biol Cell.,* 27**,** 7-11.

BAILLIE, G. S., TEJEDA, G. S. & KELLY, M. P. 2019. Therapeutic targeting of 3',5'-cyclic nucleotide phosphodiesterases: inhibition and beyond. *Nat Rev Drug Discov.,* 18**,** 770-796.

BAKER, K., HOLTZMAN, N. G. & BURDINE, R. D. 2008. Direct and Indirect Roles for Nodal Signaling in two Axis Conversions during Asymmetric Morphogenesis of the Zebrafish Heart. *Proc Natl Acad Sci U S A.,* 105**,** 13924-13929.

BAKKEN, T. E., HODGE, R. D., MILLER, J. A., YAO, Z., NGUYEN, T. N., AEVERMANN, B., BARKAN, E., BERTAGNOLLI, D., CASPER, T., DEE, N., GARREN, E., GOLDY, J., GRAYBUCK, L. T., KROLL, M.,

LASKEN, R. S., LATHIA, K., PARRY, S., RIMORIN, C., SCHEUERMANN, R. H., SCHORK, N. J., SHEHATA, S. I., TIEU, M., PHILLIPS, J. W., BERNARD, A., SMITH, K. A., ZENG, H., LEIN, E. S. & TASIC, B. 2018. Single-nucleus and single-cell transcriptomes compared in matched cortical cell types. *PloS one,* 13**,** e0209648-e0209648.

BAKKERS, J. 2011. Zebrafish as a model to study cardiac development and human cardiac disease. *Cardiovasc Res.,* 91**,** 279-288.

BALDA, M., S., GARRETT, M., D. & MATTER, K. 2003. The ZO-1-Associated Y-Box Factor ZONAB Regulates Epithelial Cell Proliferation and Cell Density. *J Cell Biol,* 160**,** 423-432.

BALDA, M. S. & MATTER, K. 2009. Tight junctions and the regulation of gene expression. *Biochim Biophys Acta.,* 1788**,** 761-767.

BARRANGOU, R., FREMAUX, C., DEVEAU, H., RICHARDS, M., BOYAVAL, P., MOINEAU, S., ROMERO, D. A. & HORVATH, P. 2007. CRISPR Provides Acquired Resistance Against Viruses in Prokaryotes. *Science,* 315**,** 1709-1712.

BARTHÉLÉMY, F., DEFOUR, A., LÉVY, N., KRAHN, M. & BARTOLI, M. 2018. Muscle Cells Fix Breaches by Orchestrating a Membrane Repair Ballet. *J Neuromuscul Dis.,* 5**,** 21-28.

BAYRAKTAR , M. & MÄNNER, J. 2014. Cardiac looping may be driven by compressive loads resulting from unequal growth of the heart and pericardial cavity. Observations on a physical simulation model. *Front Physiol,* 4**,** 112.

BECKER, C. G. & BECKER, T. 2007. Growth and pathfinding of regenerating axons in the optic projection of adult fish. *J Neurosci Res.,* 85**,** 2793-2799.

BECKER, T., WULLIMANN, M. F., BECKER, C. G., BERNHARDT, R. R. & SCHACHNER, M. 1997. Axonal regrowth after spinal cord transection in adult zebrafish. *J Comp Neurol.,* 377**,** 577-95.

BEDELL, V. M., WANG, Y., CAMPBELL, J. M., POSHUSTA, T. L., STARKER, C. G., KRUG, N. R. G., TAN, W., PENHEITER, S. G., MA, A. C., LEUNG, A. Y. H., FAHRENKRUG, S. C., CARLSON, D. F., VOYTAS, D. F., CLARK, K. J., ESSNER, J. J. & EKKER, S. C. 2012. In vivo genome editing using a high-efficiency TALEN system. *Nature,* 491**,** 114-118.

BEECHER, G., TANG, C. & LIEWLUCK, T. 2021. Severe adolescent-onset limb-girdle muscular dystrophy due to a novel homozygous nonsense BVES variant. *J Neurol Sci,* 15**,** 117259-117259.

BEIS, D. 2005. Genetic and cellular analyses of zebrafish atrioventricular cushion and valve development. *Development,* 132**,** 4193-4204.

BELY, A. E. & NYBERG, K. G. 2010. Evolution of animal regeneration: re-emergence of a field. *Trends Ecol Evol.,* 25**,** 161-170.

BEN-YAIR, R., BUTTY, V. L., BUSBY, M., QIU, Y., LEVINE, S. S., GOREN, A., BOYER, L. A., BURNS, C. G. & BURNS, C. E. 2019. H3K27me3-mediated silencing of structural genes is required for zebrafish heart regeneration. *Development,* 146**,** dev178632.

BENESH, E. C., MILLER, P. M., PFALTZGRAFF, E. R., GREGA-LARSON, N. E., HAGER, H. A., SUNG, B. H., QU, X., BALDWIN, H. S., WEAVER, A. M. & BADER, D. M. 2013. Bves and NDRG4 regulate directional epicardial cell migration through autocrine extracellular matrix deposition. *Mol Biol Cell.,* 24**,** 3496-3510.

BENNETT, K., SHELLEY, E., UNAL, B., CRITCHLEY, J. A., CAPEWELL, S. & KABIR, Z. 2007. Comparing Primary Prevention with Secondary Prevention to Explain Decreasing Coronary Heart Disease Death Rates in Ireland, 1985–2000. *BMC Public Health,* 7**,** 117.

BERDOUGO, E., COLEMAN, H., LEE, D. H., STAINIER, D. Y. R. & YELON, D. 2003. Mutation of weak atrium/atrial myosin heavy chain disrupts atrial function and influences ventricular morphogenesis in zebrafish. *Development,* 130**,** 6121.

BERGMANN, O., BHARDWAJ, R. D., BERNARD, S., ZDUNEK, S., BARNABÉ-HEIDER, F., WALSH, S., ZUPICICH, J., ALKASS, K., BUCHHOLZ, B. A., DRUID, H., JOVINGE, S. & FRISÉN, J. 2009. Evidence for cardiomyocyte renewal in humans. *Science,* 324**,** 98.

BERNHARDT, R. R., TONGIORGI, E., ANZINI, P. & SCHACHNER, M. 1996. Increased expression of specific recognition molecules by retinal ganglion cells and by optic pathway glia accompanies the successful regeneration of retinal axons in adult zebrafish. *J Comp Neurol.,* 376**,** 253-64.

BERSELL, K., ARAB, S., HARING, B. & KÜHN, B. 2009. Neuregulin1/ErbB4 Signaling Induces Cardiomyocyte Proliferation and Repair of Heart Injury. *Cell,* 138**,** 257-270.

BEVAN, L., LIM, Z. W., VENKATESH, B., RILEY, P. R., MARTIN, P. & RICHARDSON, R. J. 2020. Specific macrophage populations promote both cardiac scar deposition and subsequent resolution in adult zebrafish. ***Cardiovasc Res*** . 116**,** 1357-1371.

BHAYA, D., DAVISON, M. & BARRANGOU, R. 2011. CRISPR-Cas Systems in Bacteria and Archaea: Versatile Small RNAs for Adaptive Defense and Regulation. *Annu Rev Genet,* 45**,** 273-297.

BHF. 2020a. *BHF CVD statistics UK factsheet* [Online]. https://www.bhf.org.uk/what-we-do/our-research/heart-statistics. [Accessed 27th May 2020].

BHF. 2020b. *Heart and Circulatory Disease Statistics 2020* [Online]. https://www.bhf.org.uk/what-we-do/our-research/heart-statistics. [Accessed 28th May 2020].

BISE, T., SALLIN, P., PFEFFERLI, C. & JAŹWIŃSKA, A. 2020. Multiple cryoinjuries modulate the efficiency of zebrafish heart regeneration. *Sci Rep.,* 10**,** 11551.

BLACK, P. N. & DIRUSSO, C. C. 2003. Transmembrane Movement of Exogenous Long-Chain Fatty Acids: Proteins, Enzymes, and Vectorial Esterification. *Microbiol Mol Biol Rev.,* 67**,** 454-472.

BRAND, T. 2005. The Popeye domain-containing gene family. *Cell Biochem Biophys.,* 43**,** 95-103.

BRAND, T. & SCHINDLER, R. F. R. 2017. New kids on the block: The Popeye domain containing (POPDC) protein family acting as a novel class of cAMP effector proteins in striated muscle. 40**,** 156-165.

BRAND, T., SIMRICK, S. L., POON, K. L. & SCHINDLER, R. F. R. 2014. The cAMP-binding Popdc proteins have a redundant function in the heart. *Biochem Soc Trans.,* 42**,** 295-301.

BRETONES, G., DELGADO, M. D. & LEÓN, J. 2015. Myc and cell cycle control. *Biochim Biophys Acta.,* 1849**,** 506-516.

BROWN, D., SAMSA, L., QIAN, L. & LIU, J. 2016. Advances in the Study of Heart Development and Disease Using Zebrafish. *J Cardiovasc Dev Dis,* 3**,** 13.

BRYANT, D. M., O'MEARA, C. C., HO, N. N., GANNON, J., CAI, L. & LEE, R. T. 2015. A systematic analysis of neonatal mouse heart regeneration after apical resection. *J Mol Cell Cardiol.,* 79**,** 315-318.

BUSHMAN, D. M., KAESER, G. E., SIDDOWAY, B., WESTRA, J. W., RIVERA, R. R., REHEN, S. K., YUNG, Y. C. & CHUN, J. 2015. Genomic mosaicism with increased amyloid precursor protein (APP) gene copy number in single neurons from sporadic Alzheimer's disease brains. *eLife,* 4**,** e05116.

BUSSMANN, J., BAKKERS, J. & SCHULTE-MERKER, S. 2007. Early Endocardial Morphogenesis Requires Scl/Tal1 (Scl/Tal1 Function during Endocardial Development). *PLoS Genet.,* 3**,** e140.

BYWATER, M. J., BURKHART, D. L., STRAUBE, J., SABÒ, A., PENDINO, V., HUDSON, J. E., QUAIFE-RYAN, G. A., PORRELLO, E. R., RAE, J., PARTON, R. G., KRESS, T. R., AMATI, B., LITTLEWOOD, T. D., EVAN, G. I. & WILSON, C. H. 2020. Reactivation of Myc transcription in the mouse heart unlocks its proliferative capacity. *Nat Commun.,* 11**,** 1827-1827.

CAI, C.-L., LIANG, X., SHI, Y., CHU, P.-H., PFAFF, S. L., CHEN, J. & EVANS, S. 2003. Isl1 Identifies a Cardiac Progenitor Population that Proliferates Prior to Differentiation and Contributes a Majority of Cells to the Heart. *Dev Cell.,* 5**,** 877-889.

CAI, C.-L., MARTIN, J. C., SUN, Y., CUI, L., WANG, L., OUYANG, K., YANG, L., BU, L., LIANG, X., ZHANG, X., STALLCUP, W. B., DENTON, C. P., MCCULLOCH, A., CHEN, J. & EVANS, S. M. 2008. A myocardial lineage derives from Tbx18 epicardial cells. *Nature,* 454**,** 104-108.

CAMARATA, T., BIMBER, B., KULISZ, A., CHEW, T.-L., YEUNG, J. & SIMON, H.-G. 2006. LMP4 Regulates Tbx5 Protein Subcellular Localization and Activity. *J Cell Biol.,* 174**,** 339-348.

CAO, J. & POSS, K. D. 2018. The epicardium as a hub for heart regeneration. *Nat Rev Cardiol,* 15**,** 631-647.

CAVANAUGH, A. M., HUANG, J. & CHEN, J. N. 2015. Two developmentally distinct populations of neural crest cells contribute to the zebrafish heart. *Dev Biol.,* 404**,** 103-12.

CELIK, S., KARBALAEI SADEGH, M., MORLEY, M., ROSELLI, C., ELLINOR, P. T., CAPPOLA, T., SMITH, J. G. & GIDLOF, O. 2019. Antisense regulation of atrial natriuretic peptide expression. *JCI insight,* 4**,** e130978.

CHABLAIS, F. & JAZWINSKA, A. 2012. The regenerative capacity of the zebrafish heart is dependent on TGFβ signaling. *Development,* 139**,** 1921-1930.

CHABLAIS, F., VEIT, J., RAINER, G. & JAŹWIŃSKA, A. 2011. The zebrafish heart regenerates after cryoinjury-induced myocardial infarction. *BMC Dev Biol.,* 11**,** 21.

CHANG, N., SUN, C., GAO, L., ZHU, D., XU, X., ZHU, X., XIONG, J.-W. & XI, J. J. 2013. Genome editing with RNA-guided Cas9 nuclease in Zebrafish embryos. *Cell Res.,* 23**,** 465-472.

CHEN, J. N., EEDEN, F. J. V., WARREN, K. S., CHIN, A., NUSSLEIN-VOLHARD, C., HAFFTER, P. & FISHMAN, M. C. 1997. Left-right pattern of cardiac BMP4 may drive asymmetry of the heart in zebrafish. *Development,* 124**,** 4373-4382.

CHEN, J. N. & FISHMAN, M. C. 1996. Zebrafish tinman homolog demarcates the heart field and initiates myocardial differentiation. *Development,* 122**,** 3809-16.

CHEN, W., XIA, J., HU, P., ZHOU, F., CHEN, Y., WU, J., LEI, W. & SHEN, Z. 2016. Follistatin-like 1 protects cardiomyoblasts from injury induced by sodium nitroprusside through modulating Akt and Smad1/5/9 signaling. *Biochem Biophys Res Commun,* 469**,** 418-23.

CHIEN, K. R., KNOWLTON, K. U., ZHU, G. & CHIEN, S. 1991. Regulation of cardiac gene expression during myocardial growth and hypertrophy: molecular studies of an adaptive physiologic response. *FASEB J.,* 5**,** 3037-3064.

CHOKSI, Y. A., REDDY, V. K., SINGH, K., BARRETT, C. W., SHORT, S. P., PARANG, B., KEATING, C. E., THOMPSON, J. J., VERRIERE, T. G., BROWN, R. E., PIAZUELO, M. B., BADER, D. M., WASHINGTON, M. K., MITTAL, M. K., BRAND, T., GOBERT, A. P., COBURN, L. A., WILSON, K. T. & WILLIAMS, C. S. 2018. BVES is required for maintenance of colonic epithelial integrity in experimental colitis by modifying intestinal permeability. *Mucosal Immunol.,* 11**,** 1363-1374.

CHOQUET, C., KELLY, R. & MIQUEROL, L. 2020. Nkx2-5 defines distinct scaffold and recruitment phases during formation of the murine cardiac Purkinje fiber network. *Nat Commun.,* 11**,** 5300-5300.

CHRISTOFFELS, V. M., BURCH, J. B. & MOORMAN, A. F. 2004. Architectural plan for the heart: early patterning and delineation of the chambers and the nodes. *Trends Cardiovasc Med,* 14**,** 301-7.

CHU, H. M., TAN, Y., KOBIERSKI, L. A., BALSAM, L. B. & COMB, M. J. 1994. Activating transcription factor-3 stimulates 3',5'-cyclic adenosine monophosphate-dependent gene expression. *Mol Endocrinol,* 8**,** 59-68.

CLEUTJENS, J. P., VERLUYTEN, M. J., SMITHS, J. F. & DAEMEN, M. J. 1995. Collagen remodeling after myocardial infarction in the rat heart. *Am J Pathol,* 147**,** 325-38.

COOPER, G., TOMANEK, R. J., EHRHARDT, J. C. & MARCUS, M. L. 1981. Chronic Progressive Pressure Overload of the Cat Right Ventricle. *Circ Res.,* 48**,** 488-497.

COX, R. D., HUGILL, A., PARKINSON, N., GLENISTER, P., BROWN, S. D. M., COGHILL, E. L., CLEMENTS, S., DAVISON, C. & HUNTER, J. 2002. A gene-driven approach to the identification of ENU mutants in the mouse. *Nat Genet,* 30**,** 255-256.

CRITTENDEN, L., BITGOOD, J. & BURT, D. 1995. Genetic nomenclature guide. Chick. *Trends in genetics***,** 33-34.

CRONE, S. A., ZHAO, Y.-Y., FAN, L., GU, Y., MINAMISAWA, S., LIU, Y., PETERSON, K. L., CHEN, J., KAHN, R., CONDORELLI, G., JR, J. R., CHIEN, K. R. & LEE, K.-F. 2002. ErbB2 is essential in the prevention of dilated cardiomyopathy. *Nat Med,* 8**,** 459-465.

D'AMATO, G., LUXÁN, G., DEL MONTE-NIETO, G., MARTÍNEZ-POVEDA, B., TORROJA, C., WALTER, W., BOCHTER, M. S., BENEDITO, R., COLE, S., MARTINEZ, F., HADJANTONAKIS, A.-K., UEMURA, A., JIMÉNEZ-BORREGUERO, L. J. & DE LA POMPA, J. L. 2016. Sequential Notch activation regulates ventricular chamber development. *Nat Cell Biol.,* 18**,** 7-20.

DAMMERT, M. A., BRÄGELMANN, J., OLSEN, R. R., BÖHM, S., MONHASERY, N., WHITNEY, C. P., CHALISHAZAR, M. D., TUMBRINK, H. L., GUTHRIE, M. R., KLEIN, S., IRELAND, A. S., RYAN, J., SCHMITT, A., MARX, A., OZRETIĆ, L., CASTIGLIONE, R., LORENZ, C., JACHIMOWICZ, R. D., WOLF, E., THOMAS, R. K., POIRIER, J. T., BÜTTNER, R., SEN, T., BYERS, L. A., REINHARDT, H. C., LETAI, A., OLIVER, T. G. & SOS, M. L. 2019. MYC paralog-dependent apoptotic priming orchestrates a spectrum of vulnerabilities in small cell lung cancer. *Nat Commun.,* 10**,** 3485-11.

DAREHZERESHKI, A., RUBIN, N., GAMBA, L., KIM, J., FRASER, J., HUANG, Y., BILLINGS, J., MOHAMMADZADEH, R., WOOD, J., WARBURTON, D., KAARTINEN, V. & LIEN, C.-L. 2015. Differential regenerative capacity of neonatal mouse hearts after cryoinjury. *Dev Biol.,* 399**,** 91-99.

DAS, D. K., ENGELMAN, R. M., ROUSOU, J. A. & BREYER, R. H. 1987. Aerobic vs anaerobic metabolism during ischemia in heart muscle. *Ann Chir Gynaecol,* 76**,** 68-76.

DAVIDSON, B. & LEVINE, M. 2003. Evolutionary Origins of the Vertebrate Heart: Specification of the Cardiac Lineage in Ciona intestinalis. *Proc Natl Acad Sci U S A.,* 100**,** 11469-11473.

DAVIDSON, B., SMITH WALLACE, S., HOWSMON, R. & SWALLA, B. 2003. A morphological and genetic characterization of metamorphosis in the ascidian Boltenia villosa. *Dev Genes Evol.,* 213**,** 601-611.

DAVISSON, M. T. 1995. Genetic nomenclature guide. Mouse. *Trends in genetics***,** 35-38.

DE CAMPOS-BAPTISTA, M. I. M., HOLTZMAN, N. G., YELON, D. & SCHIER, A. F. 2008. Nodal signaling promotes the speed and directional movement of cardiomyocytes in zebrafish. *Dev Dyn.,* 237**,** 3624-3633.

DE PATER, E., CLIJSTERS, L., MARQUES, S. R., LIN, Y.-F., GARAVITO-AGUILAR, Z. V., YELON, D. & BAKKERS, J. 2009. Distinct phases of cardiomyocyte differentiation regulate growth of the zebrafish heart. *Development,* 136**,** 1633-41.

DE PREUX CHARLES, A.-S., BISE, T., BAIER, F., MARRO, J. & JAŹWIŃSKA, A. 2016. Distinct effects of inflammation on preconditioning and regeneration of the adult zebrafish heart. *Open Biol,* 6**,** 160102.

DE RIDDER, W., NELSON, I., ASSELBERGH, B., DE PAEPE, B., BEUVIN, M., BEN YAOU, R., MASSON, C., BOLAND, A., DELEUZE, J. F., MAISONOBE, T., EYMARD, B., SYMOENS, S., SCHINDLER, R., BRAND, T., JOHNSON, K., TÖPF, A., STRAUB, V., DE JONGHE, P., DE BLEECKER, J., BONNE, G. & BAETS, J. 2019. Muscular dystrophy with arrhythmia caused by loss-of-function mutations in BVES. *Neurol Genet.,* 5**,** e321.

DE VILLIERS, C. & RILEY, P. R. 2020. Mouse models of myocardial infarction: comparing permanent ligation and ischaemia-reperfusion. *Dis Model Mech.,* 13**,** dmm046565.

DEL PULGAR, T. G., BENITAH, S. A., VALERÓN, P. F., ESPINA, C. & LACAL, J. C. 2005. Rho GTPase expression in tumourigenesis: Evidence for a significant link. *Bioessays,* 27**,** 602-613.

DESGRANGE, A., LE GARREC, J.-F. & MEILHAC, S. M. 2018. Left-right asymmetry in heart development and disease: forming the right loop. *Development,* 145**,** dev162776.

DEVEAU, H., BARRANGOU, R., GARNEAU, J. E., LABONTE, J., FREMAUX, C., BOYAVAL, P., ROMERO, D. A., HORVATH, P. & MOINEAU, S. 2007. Phage Response to CRISPR-Encoded Resistance in Streptococcus thermophilus. *J Bacteriol,* 190**,** 1390-1400.

DICKS, S., JÜRGENSEN, L., LEUSCHNER, F., HASSEL, D., ANDRIEUX, G. & BOERRIES, M. 2020. Cardiac Regeneration and Tumor Growth-What Do They Have in Common? *Front Genet.,* 9**,** 586658-586658.

DIGITAL HEALTH AND CARE WALES 2020. The Patient Episode Database for Wales - 2018/19. https://nwis.nhs.wales.

DIGITAL NHS 2020. Hospital Admitted Patient Care Activity 2019-20. *Data and Information.* https://digital.nhs.uk: NHS England.

DIMMELER, S., ZEIHER, A. M. & SCHNEIDER, M. D. 2005. Unchain my heart: the scientific foundations of cardiac repair. *J Clin Invest.,* 115**,** 572-583.

DOBACZEWSKI, M., BUJAK, M., ZYMEK, P., REN, G., ENTMAN, M. L. & FRANGOGIANNIS, N. G. 2006. Extracellular matrix remodeling in canine and mouse myocardial infarcts. *Cell Tissue Res,* 324**,** 475-88.

DOBACZEWSKI, M., GONZALEZ-QUESADA, C. & FRANGOGIANNIS, N. G. 2010. The extracellular matrix as a modulator of the inflammatory and reparative response following myocardial infarction. *J Mol Cell Cardiol,* 48**,** 504-11.

DOENST, T., NGUYEN, T. D. & ABEL, E. D. 2013. Cardiac Metabolism in Heart Failure: Implications Beyond ATP Production. *Circ Res.,* 113**,** 709-724.

DOYON, Y., MCCAMMON, J. M., MILLER, J. C., FARAJI, F., NGO, C., KATIBAH, G. E., AMORA, R., HOCKING, T. D., ZHANG, L., REBAR, E. J., GREGORY, P. D., URNOV, F. D. & AMACHER, S. L. 2008. Heritable targeted gene disruption in zebrafish using designed zinc-finger nucleases. *Nat Biotechnol,* 26**,** 702-708.

EBERWINE, J., SUL, J.-Y., BARTFAI, T. & KIM, J. 2014. The promise of single-cell sequencing. *Nat Methods.,* 11**,** 25-27.

EGERMAN, MARC A., CADENA, SAMUEL M., GILBERT, JASON A., MEYER, A., NELSON, HALLIE N., SWALLEY, SUSANNE E., MALLOZZI, C., JACOBI, C., JENNINGS, LORI L., CLAY, I., LAURENT, G., MA, S., BRACHAT, S., LACH-TRIFILIEFF, E., SHAVLAKADZE, T., TRENDELENBURG, A.-U., BRACK, ANDREW S. & GLASS, DAVID J. 2015. GDF11 Increases with Age and Inhibits Skeletal Muscle Regeneration. *Cell Metab.,* 22**,** 164-174.

EISEN, J. S. & SMITH, J. C. 2008. Controlling morpholino experiments: don't stop making antisense. *Development,* 135**,** 1735-1743.

EISENBERG, L. M. & MARKWALD, R. R. 1995. Molecular Regulation of Atrioventricular Valvuloseptal Morphogenesis. *Circ Res.,* 77**,** 1-6.

ELLIS, J. M., MENTOCK, S. M., DEPETRILLO, M. A., KOVES, T. R., SEN, S., WATKINS, S. M., MUOIO, D. M., CLINE, G. W., TAEGTMEYER, H., SHULMAN, G. I., WILLIS, M. S. & COLEMAN, R. A. 2011. Mouse Cardiac Acyl Coenzyme A Synthetase 1 Deficiency Impairs Fatty Acid Oxidation and Induces Cardiac Hypertrophy. *Mol Cell Biol.,* 31**,** 1252-1262.

ETOH, T., JOFFS, C., DESCHAMPS, A. M., DAVIS, J., DOWDY, K., HENDRICK, J., BAICU, S., MUKHERJEE, R., MANHAINI, M. & SPINALE, F. G. 2001. Myocardial and interstitial matrix metalloproteinase activity after acute myocardial infarction in pigs. *Am J Physiol Heart Circ Physiol.,* 281**,** 987-994.

FAJARDO, V. M., FENG, I., CHEN, B. Y., PEREZ-RAMIREZ, C. A., SHI, B., CLARK, P., TIAN, R., LIEN, C.-L., PELLEGRINI, M., CHRISTOFK, H., NAKANO, H. & NAKANO, A. 2021. GLUT1 overexpression enhances glucose metabolism and promotes neonatal heart regeneration. *Sci Rep.,* 11**,** 8669-8669.

FANG, Y., GUPTA, V., KARRA, R., HOLDWAY, J., E., KIKUCHI, K. & POSS, K., D. 2013. Translational profiling of cardiomyocytes identifies an early Jak1/Stat3 injury response required for zebrafish heart regeneration. *Proc Natl Acad Sci U S A,* 110**,** 13416-13421.

FELKER, A., PRUMMEL, K. D., MERKS, A. M., MICKOLEIT, M., BROMBACHER, E. C., HUISKEN, J., PANÁKOVÁ, D. & MOSIMANN, C. 2018. Continuous addition of progenitors forms the cardiac ventricle in zebrafish. *Nature commun.,* 9**,** 2001-2001.

FENG, Q., HAWES, S. E., STERN, J. E., WIENS, L., LU, H., DONG, Z. M., JORDAN, C. D., KIVIAT, N. B. & VESSELLE, H. 2008. DNA methylation in tumor and matched normal tissues from non-small cell lung cancer patients. *Cancer Epidemiol Biomarkers Prev.,* 17**,** 645-54.

FISH, J. E., WYTHE, J. D., XIAO, T., BRUNEAU, B. G., STAINIER, D. Y. R., SRIVASTAVA, D. & WOO, S. 2011. A Slit/miR-218/Robo regulatory loop is required during heart tube formation in zebrafish. *Development,* 138**,** 1409.

FITTIPALDI, S., MERCATELLI, N., DIMAURO, I., JACKSON, M. J., PARONETTO, M. P. & CAPOROSSI, D. 2015. Alpha B-crystallin induction in skeletal muscle cells under redox imbalance is mediated by a JNK-dependent regulatory mechanism. *Free Radic Biol Med,* 86**,** 331-42.

FRANCIS, S. C., MICHAEL, M. & ARISTIDES, P. 2003. The Human Genome Project: Lessons from Large-Scale Biology. *Science,* 300**,** 286-290.

FRANCIS STUART, S. D., DE JESUS, N. M., LINDSEY, M. L. & RIPPLINGER, C. M. 2016. The crossroads of inflammation, fibrosis, and arrhythmia following myocardial infarction. *J Mol Cell Cardiol,* 91**,** 114-22.

FRANK, S. R., PARISI, T., TAUBERT, S., FERNANDEZ, P., FUCHS, M., CHAN, H. M., LIVINGSTON, D. M. & AMATI, B. 2003. MYC recruits the TIP60 histone acetyltransferase complex to chromatin. *EMBO rep.,* 4**,** 575-580.

FREY, N. & OLSON, E. N. 2003. Cardiac hypertrophy: the good, the bad, and the ugly. *Annu Rev Physiol.,* 65**,** 45-79.

FRISCHMEYER, P. A. & DIETZ, H. C. 1999. Nonsense-mediated mRNA decay in health and disease. *Hum Mol Genet.,* 8**,** 1893-1900.

FROESE, A. & BRAND, T. 2008. Expression pattern of Popdc2 during mouse embryogenesis and in the adult. *Dev Dyn.,* 237**,** 780-787.

FROESE, A., BREHER, S. S., WALDEYER, C., SCHINDLER, R. F. R., NIKOLAEV, V. O., RINNE, S., WISCHMEYER, E., SCHLUETER, J., BECHER, J., SIMRICK, S., VAUTI, F., KUHTZ, J., MEISTER, P., KREISSL, S., TORLOPP, A., LIEBIG, S. K., LAAKMANN, S., MUELLER, T. D., NEUMANN, J., STIEBER, J., LUDWIG, A., MAIER, S. K., DECHER, N., ARNOLD, H. H., KIRCHHOF, P., FABRITZ, L. & BRAND, T. 2012. Popeye domain containing proteins are essential for stress-mediated modulation of cardiac pacemaking in mice. *J Clin Invest.,* 122**,** 1119-1130.

FUKUDA, R., MARÍN-JUEZ, R., EL-SAMMAK, H., BEISAW, A., RAMADASS, R., KUENNE, C., GUENTHER, S., KONZER, A., BHAGWAT, A. M., GRAUMANN, J. & STAINIER, D. Y. 2020. Stimulation of glycolysis promotes cardiomyocyte proliferation after injury in adult zebrafish. *EMBO Rep,* 21**,** e49752.

GAMBA, L., AMIN-JAVAHERI, A., KIM, J., WARBURTON, D. & LIEN, C.-L. 2017. Collagenolytic Activity Is Associated with Scar Resolution in Zebrafish Hearts after Cryoinjury. *J Cardiovasc Dev Dis.,* 4**,** 2.

GAMPERL, A. K. & FARRELL, A. P. 2004. Cardiac plasticity in fishes: environmental influences and intraspecific differences. *J Exp Biol.,* 207**,** 2539-2550.

GARAVITO-AGUILAR, Z. V., RILEY, H. E. & YELON, D. 2010. Hand2 ensures an appropriate environment for cardiac fusion by limiting Fibronectin function. *Development,* 137**,** 3215.

GARRITY, D. M., CHILDS, S. & FISHMAN, M. C. 2002. The heartstrings mutation in zebrafish causes heart/fin Tbx5 deficiency syndrome. *Development,* 129**,** 4635-4645.

GASSMANN, M., CASAGRANDA, F., ORIOLI, D., SIMON, H., LAI, C., KLEIN, R. & LEMKE, G. 1995. Aberrant neural and cardiac development in mice lacking the ErbB4 neuregulin receptor. *Nature,* 378**,** 390-394.

GEMBERLING, M., KARRA, R., DICKSON, A. L. & POSS, K. D. 2015. Nrg1 is an injury-induced cardiomyocyte mitogen for the endogenous heart regeneration program in zebrafish. *eLife,* 4**,** e05871.

GENE ONTOLOGY CONSORTIUM 2006. The Gene Ontology (GO) project in 2006. *Nucleic Acids Res,* 34**,** D322-6.

GEORGE, E. L., BALDWIN, H. S. & HYNES, R. O. 1997. Fibronectins are essential for heart and blood vessel morphogenesis but are dispensable for initial specification of precursor cells. *Blood,* 90**,** 3073.

GILCHRIST, E. J., O'NEIL, N. J., ROSE, A. M., ZETKA, M. C. & HAUGHN, G. W. 2006. TILLING is an effective reverse genetics technique for Caenorhabditis elegans. *BMC Genomics,* 7**,** 262-262.

GILCHRIST, M., HENDERSON, J. W. R., CLARK, A. E., SIMMONS, R. M., YE, X., SMITH, K. D. & ADEREM, A. 2008. Activating transcription factor 3 is a negative regulator of allergic pulmonary inflammation. *J Exp Med.,* 205**,** 2349-2357.

GINGOLD-BELFER, R., KESSLER-ICEKSON, G., MORGENSTERN, S., RATH-WOLFSON, L., ZEMEL, R., BOLTIN, D., LEVI, Z. & HERMAN-EDELSTEIN, M. 2021. The Transition from Gastric Intestinal Metaplasia to Gastric Cancer Involves POPDC1 and POPDC3 Downregulation. *Int J Mol Sci,* 22**,** 5359.

GITTENBERGER-DE GROOT, A. C., VRANCKEN PEETERS, M.-P. F. M., MENTINK, M. M. T., GOURDIE, R. G. & POELMANN, R. E. 1998. Epicardium-Derived Cells Contribute a Novel Population to the Myocardial Wall and the Atrioventricular Cushions. *Circ Res,* 82**,** 1043-1052.

GLICKMAN, N. S. & YELON, D. 2002. Cardiac development in zebrafish: coordination of form and function. *Semin Cell Dev Biol.,* 13**,** 507-513.

GONZÁLEZ-ROSA, J. M., GUZMÁN-MARTÍNEZ, G., MARQUES, I. J., SÁNCHEZ-IRANZO, H., JIMÉNEZ-BORREGUERO, L. J. & MERCADER, N. 2014. Use of echocardiography reveals reestablishment

of ventricular pumping efficiency and partial ventricular wall motion recovery upon ventricular cryoinjury in the zebrafish. *PloS one,* 9**,** 115604-115604.

GONZÁLEZ-ROSA, J. M., MARTÍN, V., PERALTA, M., TORRES, M. & MERCADER, N. 2011. Extensive scar formation and regression during heart regeneration after cryoinjury in zebrafish. *Development,* 138**,** 1663.

GONZÁLEZ-ROSA, J. M. & MERCADER, N. 2012. Cryoinjury as a myocardial infarction model for the study of cardiac regeneration in the zebrafish. *Nat Protoc.,* 7**,** 782-8.

GONZÁLEZ-ROSA, J. M., PERALTA, M. & MERCADER, N. 2012. Pan-epicardial lineage tracing reveals that epicardium derived cells give rise to myofibroblasts and perivascular cells during zebrafish heart regeneration. *Dev Biol,* 370**,** 173-186.

GONZÁLEZ-ROSA, J. M., SHARPE, M., FIELD, D., SOONPAA, M. H., FIELD, L. J., BURNS, C. E. & BURNS, C. G. 2018. Myocardial Polyploidization Creates a Barrier to Heart Regeneration in Zebrafish. *Dev Cell.,* 44**,** 433-446.

GONZÁLEZ-ROSA, J. M., BURNS, C. E. & BURNS, C. G. 2017. Zebrafish heart regeneration: 15 years of discoveries. *Regeneration,* 4**,** 105-123.

GORDON, E. M., RAVICZ, J. R., LIU, S., CHAWLA, S. P. & HALL, F. L. 2018. Cell cycle checkpoint control: The cyclin G1/Mdm2/p53 axis emerges as a strategic target for broad-spectrum cancer gene therapy - A review of molecular mechanisms for oncologists. *Mol Clin Oncol,* 9**,** 115-134.

GRAHAM, M. & FARREL, A. 1989. The Effect of Temperature Acclimation and Adrenaline on the performance of a perfused Trout Heart. *Physiol. Zool.,* 62**,** 33-61.

GRAJEVSKAJA, V., CAMEROTA, D., BELLIPANNI, G., BALCIUNIENE, J. & BALCIUNAS, D. 2018. Analysis of a conditional gene trap reveals that tbx5a is required for heart regeneration in zebrafish. *PloS one,* 13**,** 0197293-0197293.

GRIMES, A. C. & KIRBY, M. L. 2009. The outflow tract of the heart in fishes: anatomy, genes and evolution. *J Fish Biol,* 74**,** 983-1036.

GRIMES, A. C., STADT, H. A., SHEPHERD, I. T. & KIRBY, M. L. 2006. Solving an enigma: Arterial pole development in the zebrafish heart. *Dev Biol,* 290**,** 265-276.

GRIVAS, D., GONZÁLEZ-RAJAL, Á. & DE LA POMPA, J. L. 2021. Midkine-a Regulates the Formation of a Fibrotic Scar During Zebrafish Heart Regeneration. *Frontiers in cell and developmental biology,* 9**,** 669439-669439.

GUERRERO, A., ICARDO, J. M., DURÁN, A. C., GALLEGO, A., DOMEZAIN, A., COLVEE, E. & SANS-COMA, V. 2004. Differentiation of the cardiac outflow tract components in alevins of the sturgeon Acipenser naccarii (Osteichthyes, Acipenseriformes): implications for heart evolution. *J Morphol,* 260**,** 172-83.

GUO, X., STAFFORD, L. J., BRYAN, B., XIA, C., MA, W., WU, X., LIU, D., SONGYANG, Z. & LIU, M. 2003. A Rac/Cdc42-specific Exchange Factor, GEFT, Induces Cell Proliferation, Transformation, and Migration. *J Biol Chem,* 278**,** 13207-13215.

GUPTA, V., GEMBERLING, M., KARRA, R., ROSENFELD, GABRIEL E., EVANS, T. & POSS, KENNETH D. 2013. An Injury-Responsive Gata4 Program Shapes the Zebrafish Cardiac Ventricle. *Curr Biol.,* 23**,** 1221-1227.

GUPTA, V. & POSS, K. D. 2012. Clonally dominant cardiomyocytes direct heart morphogenesis. *Nature,* 484**,** 479-484.

GÁLVEZ-SANTISTEBAN, M., CHEN, D., ZHANG, R., SERRANO, R., NGUYEN, C., ZHAO, L., NERB, L., MASUTANI, E. M., VERMOT, J., BURNS, C. G., BURNS, C. E., DEL ÁLAMO, J. C. & CHI, N. C. 2019. Hemodynamic-mediated endocardial signaling controls in vivo myocardial reprogramming. *eLife,* 25**,** e44816.

HAACK, T. & ABDELILAH-SEYFRIED, S. 2016. The force within: endocardial development, mechanotransduction and signalling during cardiac morphogenesis. *Development,* 143**,** 373.

HAGER, H. A., CROSS, E. E., BADER, D. M., ROBERTS, R. J. & PROUX-GILLARDEAUX, V. 2010. Identification of a novel Bves function: regulation of vesicular transport. *EMBO J,* 29**,** 532-545.

HAI, T., LIU, F., COUKOS, W. J. & GREEN, M. R. 1989. Transcription factor ATF cDNA clones: an extensive family of leucine zipper proteins able to selectively form DNA-binding heterodimers. *Genes Dev.,* 3**,** 2083-2090.

HAI, T., WOLFORD, C. C. & CHANG, Y.-S. 2010. ATF3, a hub of the cellular adaptive-response network, in the pathogenesis of diseases: is modulation of inflammation a unifying component? *Gene Expr,* 15**,** 1-11.

HAMI, D., GRIMES, A. C., TSAI, H.-J. & KIRBY, M. L. 2011. Zebrafish cardiac development requires a conserved secondary heart field. *Development,* 138**,** 2389.

HAMMERS, D. W., MERSCHAM-BANDA, M., HSIAO, J. Y., ENGST, S., HARTMAN, J. J. & SWEENEY, H. L. 2017. Supraphysiological levels of GDF11 induce striated muscle atrophy. *EMBO Mol Med.,* 9**,** 531-544.

HAN, P., FU, Y., LIU, J., WANG, Y., HE, J., GONG, J., LI, M., TAN, Q., LI, D., LUO, Y., HAN, J., LIU, J., TU, W., WANG, Y., TIAN, D. & YAN, W. 2015. Netrin-1 promotes cell migration and invasion by down-regulation of BVES expression in human hepatocellular carcinoma. *Am J Cancer Res.,* 5**,** 1396-409.

HAN, P., FU, Y., LUO, M., HE, J., LIU, J., LIAO, J., TIAN, D. & YAN, W. 2014. BVES inhibition triggers epithelial-mesenchymal transition in human hepatocellular carcinoma. *Dig Dis Sci,* 59**,** 992-1000.

HAN, R., BANSAL, D., MIYAKE, K., MUNIZ, V. P., WEISS, R. M., MCNEIL, P. L. & CAMPBELL, K. P. 2007. Dysferlin-mediated membrane repair protects the heart from stress-induced left ventricular injury. *J Clin Invest,* 117**,** 1805-1813.

HARADA, K., FRIEDMAN, M., LOPEZ, J. J., WANG, S. Y., LI, J., PRASAD, P. V., PEARLMAN, J. D., EDELMAN, E. R., SELLKE, F. W. & SIMONS, M. 1996. Vascular endothelial growth factor administration in chronic myocardial ischemia. *Am J Physiol.,* 270**,** H1791-H1802.

HARRISON, MICHAEL R. M., BUSSMANN, J., HUANG, Y., ZHAO, L., OSORIO, A., BURNS, C. G., BURNS, CAROLINE E., SUCOV, HENRY M., SIEKMANN, ARNDT F. & LIEN, C.-L. 2015. Chemokine-Guided Angiogenesis Directs Coronary Vasculature Formation in Zebrafish. *Dev Cell,* 33**,** 442-454.

HARVARD CHAN BIOINFORMATICS CORE. 2021. *Single-cell RNA-seq: Quality control* [Online]. https://hbctraining.github.io/scRNA-seq/lessons/04_SC_quality_control.html: GitHub. [Accessed 16th June 2021].

HAUBNER, B. J., ADAMOWICZ-BRICE, M., KHADAYATE, S., TIEFENTHALER, V., METZLER, B., AITMAN, T. & PENNINGER, J. M. 2012. Complete cardiac regeneration in a mouse model of myocardial infarction. *Aging (Albany NY),* 4**,** 966-977.

HE, X., XU, H., ZHAO, W., ZHAN, M., LI, Y., LIU, H., TAN, L. & LU, L. 2019. POPDC3 is a potential biomarker for prognosis and radioresistance in patients with head and neck squamous cell carcinoma. *Oncol Lett.,* 18**,** 5468-5480.

HEALTH NI 2020. Northern Ireland Episode Based Inpatient abd Day Case Activity Data (2018/2019). http://www.health-ni.gov.uk.

HEATHER, L. C., COLE, M. A., LYGATE, C. A., EVANS, R. D., STUCKEY, D. J., MURRAY, A. J., NEUBAUER, S. & CLARKE, K. 2006. Fatty acid transporter levels and palmitate oxidation rate correlate with ejection fraction in the infarcted rat heart. *Cardiovasc Res.,* 72**,** 430-437.

HEERBOTH, S., HOUSMAN, G., LEARY, M., LONGACRE, M., BYLER, S., LAPINSKA, K., WILLBANKS, A. & SARKAR, S. 2015. EMT and tumor metastasis. *Clin Transl Med,* 4**,** 1-13.

HEIL, M. & SCHAPER, W. 2004. Influence of Mechanical, Cellular, and Molecular Factors on Collateral Artery Growth (Arteriogenesis). *Circ Res.,* 95**,** 449-458.

HEIN, S., KOSTIN, S., HELING, A., MAENO, Y. & SCHAPER, J. 2000. The role of the cytoskeleton in heart failure. *Cardiovasc Res.,* 45**,** 273-278.

HEIN, S. J., LEHMANN, L. H., KOSSACK, M., JUERGENSEN, L., FUCHS, D., KATUS, H. A. & HASSEL, D. 2015. Advanced echocardiography in adult zebrafish reveals delayed recovery of heart function after myocardial cryoinjury. *PloS one,* 10**,** 0122665-0122665.

HERTZ, A. L., BENDER, A. T., SMITH, K. C., GILCHRIST, M., AMIEUX, P. S. & BEAVO, J. A. 2009. PDE4 inhibitors can induce pro-inflammatory chemokine expression in human macrophages. *Proc Natl Acad Sci U S A.,* 23**,** 891.2-891.2.

HICKMAN, C. P., ROBERTS, L. S. & HICKMAN, F. M. 1988. *Integrated Principles of Zoology,* New York, New York, McGraw-Hill Education.

HIROSE, K., PAYUMO, A. Y., CUTIE, S., HOANG, A., ZHANG, H., GUYOT, R., LUNN, D., BIGLEY, R. B., YU, H., WANG, J., SMITH, M., GILLETT, E., MUROY, S. E., SCHMID, T., WILSON, E., FIELD, K. A., REEDER, D. M., MADEN, M., YARTSEV, M. M., WOLFGANG, M. J., GRÜTZNER, F., SCANLAN, T. S., SZWEDA, L. I., BUFFENSTEIN, R., HU, G., FLAMANT, F., OLGIN, J. E. & HUANG, G. N. 2019. Evidence for hormonal control of heart regenerative capacity during endothermy acquisition. *Science,* 364**,** 184-188.

HOFSTEEN, P., ROBITAILLE, A. M., CHAPMAN, D. P., MOON, R. T. & MURRY, C. E. 2016. Quantitative proteomics identify DAB2 as a cardiac developmental regulator that inhibits WNT/β-catenin signaling. *Proc Natl Acad Sci U S A.,* 113**,** 1002-1007.

HOLT, I., FULLER, H. R., SCHINDLER, R. F. R., SHIRRAN, S. L., BRAND, T. & MORRIS, G. E. 2020. An interaction of heart disease-associated proteins POPDC1/2 with XIRP1 in transverse tubules and intercalated discs. *BMC Mol Cell Biol,* 21**,** 88.

HOLTZMAN, N. G., SCHOENEBECK, J. J., TSAI, H.-J. & YELON, D. 2007. Endocardium is necessary for cardiomyocyte movement during heart tube assembly. *Development,* 134**,** 2379.

HONKOOP, H., DE BAKKER, D. E., AHARONOV, A., KRUSE, F., SHAKKED, A., NGUYEN, P. D., DE HEUS, C., GARRIC, L., MURARO, M. J., SHOFFNER, A., TESSADORI, F., PETERSON, J. C., NOORT, W., BERTOZZI, A., WEIDINGER, G., POSTHUMA, G., GRUN, D., VAN DER LAARSE, W. J., KLUMPERMAN, J., JASPERS, R. T., POSS, K. D., VAN OUDENAARDEN, A., TZAHOR, E. & BAKKERS, J. 2019. Single-cell analysis uncovers that metabolic reprogramming by ErbB2 signaling is essential for cardiomyocyte proliferation in the regenerating heart. *eLife,* 8**,** e50163.

HOOVER, K. B., LIAO, S. Y. & BRYANT, P. J. 1998. Loss of the tight junction MAGUK ZO-1 in breast cancer: Relationship to glandular differentiation and loss of heterozygosity. *Am J Pathol,* 153**,** 1767-1773.

HOWE, K., CLARK, M., TORROJA, C. F., TORRANCE, J., BERTHELOT, C., MUFFATO, M., COLLINS, J., E., HUMPHRAY, S., MCLAREN, K., MATTHEWS, L., MCLAREN, S., SEALY, I., CACCAMO, M., CHURCHER, C., SCOTT, C., BARRETT, J. C., KOCH, R., RAUCH, G.-J., WHITE, S., CHOW, W., KILIAN, B., QUINTAIS, L. T., GUERRA-ASSUNÇÃO, J. A., ZHOU, Y., GU, Y., YEN, J., VOGEL, J.-H., EYRE, T., REDMOND, S., BANERJEE, R., CHI, J., FU, B., LANGLEY, E., MAGUIRE, S. F., LAIRD, G. K., LLOYD, D., KENYON, E., DONALDSON, S., SEHRA, H., ALMEIDA-KING, J., LOVELAND, J., TREVANION, S., JONES, M., QUAIL, M., WILLEY, D., HUNT, A., BURTON, J., SIMS, S., MCLAY, K., PLUMB, B., DAVIS, J., CLEE, C., OLIVER, K., CLARK, R., RIDDLE, C., ELIOTT, D., THREADGOLD, G., HARDEN, G., WARE, D., MORTIMER, B., KERRY, G., HEATH, P., PHILLIMORE, B., TRACEY, A., CORBY, N., DUNN, M., JOHNSON, C., WOOD, J., CLARK, S., PELAN, S., GRIFFITHS, G., SMITH, M., GLITHERO, R., HOWDEN, P., BARKER, N., STEVENS, C., HARLEY, J., HOLT, K., PANAGIOTIDIS, G., LOVELL, J., BEASLEY, H., HENDERSON, C., GORDON, D., AUGER, K., WRIGHT, D., COLLINS, J., RAISEN, C., DYER, L., LEUNG, K., ROBERTSON, L., AMBRIDGE, K., LEONGAMORNLERT, D., MCGUIRE, S., GILDERTHORP, R., GRIFFITHS, C., MANTHRAVADI, D., NICHOL, S., BARKER, G., WHITEHEAD, S. & KAY, M. 2013. The zebrafish reference genome sequence and its relationship to the human genome. *Nature,* 496**,** 498.

HU, N., SEDMERA, D., YOST, H. J. & CLARK, E. B. 2000. Structure and function of the developing zebrafish heart. *Anat Rec.,* 260**,** 148-157.

HU, N., YOST, H. J. & CLARK, E. B. 2001. Cardiac morphology and blood pressure in the adult zebrafish. *Anat Rec.,* 264**,** 1-12.

HUANG, P., XIAO, A., ZHOU, M., ZHU, Z., LIN, S. & ZHANG, B. 2011. Heritable gene targeting in zebrafish using customized TALENs. *Nat Biotechnol,* 29**,** 699-700.

HUANG, W.-C., YANG, C.-C., CHEN, I. H., LIU, Y.-M. L., CHANG, S.-J. & CHUANG, Y.-J. 2013. Treatment of Glucocorticoids Inhibited Early Immune Responses and Impaired Cardiac Repair in Adult Zebrafish. *PloS one,* 8**,** e66613-e66613.

HWANG, W. Y., FU, Y., REYON, D., MAEDER, M. L., TSAI, S. Q., SANDER, J. D., PETERSON, R. T., YEH, J. R. J. & JOUNG, J. K. 2013. Efficient genome editing in zebrafish using a CRISPR-Cas system. *Nat Biotechnol,* 31**,** 227-229.

ICARDO, J. M. 2006. Conus arteriosus of the teleost heart: dismissed, but not missed. *Anat Rec A Discov Mol Cell Evol Biol,* 288**,** 900-8.

IEDA, M., FU, J.-D., DELGADO-OLGUIN, P., VEDANTHAM, V., HAYASHI, Y., BRUNEAU, B. G. & SRIVASTAVA, D. 2010. Direct Reprogramming of Fibroblasts into Functional Cardiomyocytes by Defined Factors. *Cell,* 142**,** 375-386.

INDRAWATI, L. A., IIDA, A., TANAKA, Y., HONMA, Y., MIZOGUCHI, K., YAMAGUCHI, T., IKAWA, M., HAYASHI, S., NOGUCHI, S. & NISHINO, I. 2020. Two Japanese LGMDR25 patients with a biallelic recurrent nonsense variant of BVES. *Neuromuscul Disord.,* 30**,** 674-679.

ISHINO, Y., SHINAGAWA, H., MAKINO, K., AMEMURA, M. & NAKATA, A. 1987. Nucleotide sequence of the iap gene, responsible for alkaline phosphatase isozyme conversion in Escherichia coli, and identification of the gene product. *J Bacteriol,* 169**,** 5429-5433.

ISLAM, S., ZEISEL, A., JOOST, S., LA MANNO, G., ZAJAC, P., KASPER, M., LÖNNERBERG, P. & LINNARSSON, S. 2014. Quantitative single-cell RNA-seq with unique molecular identifiers. *Nat Methods.,* 11**,** 163-166.

ITO, K., MORIOKA, M., KIMURA, S., TASAKI, M., INOHAYA, K. & KUDO, A. 2014. Differential reparative phenotypes between zebrafish and medaka after cardiac injury. *Dev Dyn,* 243**,** 1106-1115.

JACKSON, T., ALLARD, M. F., SREENAN, C. M., DOSS, L. K., BISHOP, S. P. & SWAIN, J. L. 1990. The c- myc proto- oncogene regulates cardiac development in transgenic mice. *Mol Cell Biol.,* 10**,** 3709.

JEAN, M. J., DEVERTEUIL, P., LOPEZ, N. H., TAPIA, J. D. & SCHOFFSTALL, B. 2012. Adult Zebrafish Hearts Efficiently Compensate for Excessive Forced Overload Cardiac Stress with Hyperplastic Cardiomegaly. *BioResearch open access,* 1**,** 88-91.

JENNI, R., ROJAS, J. & OECHSLIN, E. 1999. Isolated Noncompaction of the Myocardium. *N Engl J Med,* 340**,** 966-967.

JENSEN, B., BOUKENS, B. J. D., POSTMA, A. V., GUNST, Q. D., VAN DEN HOFF, M. J. B., MOORMAN, A. F. M., WANG, T. & CHRISTOFFELS, V. M. 2012. Identifying the Evolutionary Building Blocks of the Cardiac Conduction System. *PloS one,* 7**,** e44231-e44231.

JENSEN, B., VAN DER WAL, A. C., MOORMAN, A. F. M. & CHRISTOFFELS, V. M. 2017. Excessive trabeculations in noncompaction do not have the embryonic identity. *Int J Cardiol,* 227**,** 325-330.

JIANYI, W., RICHARD, B. S., MARK, D. R., JEFFREY, E. S. & JOHN, P. B. 2001. Morphological and membrane characteristics of spider and spindle cells isolated from rabbit sinus node. *Am J Physiol Heart Circ Physiol,* 280**,** 1232-1240.

JINEK, M., CHYLINSKI, K., FONFARA, I., HAUER, M., DOUDNA, J. A. & CHARPENTIER, E. 2012. A Programmable Dual-RNA-Guided DNA Endonuclease in Adaptive Bacterial Immunity. *Science,* 337**,** 816-821.

JOHNSON, S. L. & WESTON, J. A. 1995. Temperature-sensitive mutations that cause stage-specific defects in Zebrafish fin regeneration. *Genetics,* 141**,** 1583.

JONES, D. R., LANGILLE, B. L., RANDALL, D. J. & SHELTON, G. 1974. Blood flow in dorsal and ventral aortas of the cod, Gadus morhua. *Am J Physiol.,* 226**,** 90-95.

JOPLING, C., SLEEP, E., RAYA, M., MARTI, M., RAYA, A. & IZPISUA BELMONTE, J. C. 2010. Zebrafish heart regeneration occurs by cardiomyocyte dedifferentiation and proliferation. *Nature,* 464**,** 606-609.

JOPLING, C., SUNE, G., FAUCHERRE, A., FABREGAT, C. & IZPISUA BELMONTE, J. C. 2012. Hypoxia Induces Myocardial Regeneration in Zebrafish. *Circulation,* 126**,** 3017-3027.

JURD, R., MOSS, S. J. & JACOB, T. C. 2008. GABA A receptor trafficking and its role in the dynamic modulation of neuronal inhibition. *Nat Rev Neurosci.,* 9**,** 331-343.

KALFON, R., KOREN, L., AVIRAM, S., SCHWARTZ, O., HAI, T. & ARONHEIM, A. 2017. ATF3 expression in cardiomyocytes preserves homeostasis in the heart and controls peripheral glucose tolerance. *Cardiovasc Res.,* 113**,** 134-146.

KAMATHAM, S., WATERS, C. M., SCHWINGSHACKL, A. & MANCARELLA, S. 2019. TREK-1 protects the heart against ischemia-reperfusion-induced injury and from adverse remodeling after myocardial infarction. *Pflugers Arch,* 471**,** 1263-1272.

KATO, T., NIIZUMA, S., INUZUKA, Y., KAWASHIMA, T., OKUDA, J., TAMAKI, Y., IWANAGA, Y., NARAZAKI, M., MATSUDA, T., SOGA, T., KITA, T., KIMURA, T. & SHIOI, T. 2010. Analysis of metabolic remodeling in compensated left ventricular hypertrophy and heart failure. *Circ Heart Fail.,* 3**,** 420-430.

KATZ, TAMAR C., SINGH, MANVENDRA K., DEGENHARDT, K., RIVERA-FELICIANO, J., JOHNSON, RANDY L., EPSTEIN, JONATHAN A. & TABIN, CLIFFORD J. 2012. Distinct Compartments of the Proepicardial Organ Give Rise to Coronary Vascular Endothelial Cells. *Dev Cell,* 22**,** 639-650.

KAWAGUCHI, M., HAGER, H. A., WADA, A., KOYAMA, T., CHANG, M. S. & BADER, D. M. 2008. Identification of a novel intracellular interaction domain essential for Bves function. *PLoS One,* 3**,** e2261.

KAYKAS, A., KOHN, A. D., FERRARI, G. V. D. & MOON, R. T. 2004. WNT and β-catenin signalling: diseases and therapies. *Nat Rev Genet,* 5**,** 691-701.

KEEGAN, B. R., MEYER, D. & YELON, D. 2004. Organization of cardiac chamber progenitors in the zebrafish blastula. *Development,* 131**,** 3081.

KELLY, R. G., BROWN, N. A. & BUCKINGHAM, M. E. 2001. The Arterial Pole of the Mouse Heart Forms from Fgf10-Expressing Cells in Pharyngeal Mesoderm. *Dev Cell.,* 1**,** 435-440.

KIKUCHI, K. 2015. Dedifferentiation, Transdifferentiation, and Proliferation: Mechanisms Underlying Cardiac Muscle Regeneration in Zebrafish. *Curr Pathobiol Rep,* 3**,** 81-88.

KIKUCHI, K., GUPTA, V., WANG, J., HOLDWAY, J. E., WILLS, A. A., FANG, Y. & POSS, K. D. 2011a. tcf21+ epicardial cells adopt non-myocardial fates during zebrafish heart development and regeneration. *Development,* 138**,** 2895-2902.

KIKUCHI, K., HOLDWAY, JENNIFER E., MAJOR, ROBERT J., BLUM, N., DAHN, RANDALL D., BEGEMANN, G. & POSS, KENNETH D. 2011b. Retinoic Acid Production by Endocardium and Epicardium Is an Injury Response Essential for Zebrafish Heart Regeneration. *Dev Cell.,* 20**,** 397-404.

KIKUCHI, K., HOLDWAY, J. E., WERDICH, A. A., ANDERSON, R. M., YI, F., EGNACZYK, G. F., EVANS, T., MACRAE, C. A., STAINIER, D. Y. R. & POSS, K. D. 2010. Primary contribution to zebrafish heart regeneration by gata4+ cardiomyocytes. *Nature,* 464**,** 601-605.

KIM, J., WU, Q., ZHANG, Y., WIENS, K. M., HUANG, Y., RUBIN, N., SHIMADA, H., HANDIN, R. I., CHAO, M. Y., TUAN, T.-L., STARNES, V. A. & LIEN, C.-L. 2010a. PDGF signaling is required for epicardial function and blood vessel formation in regenerating zebrafish hearts. *Proceedings of the National Academy of Sciences - PNAS,* 107**,** 17206-17210.

KIM, M., JANG, H.-R., HAAM, K., KANG, T.-W., KIM, J.-H., KIM, S.-Y., NOH, S.-M., SONG, K.-S., CHO, J.-S., JEONG, H.-Y., KIM, J. C., YOO, H.-S. & KIM, Y. S. 2010b. Frequent silencing of popeye domain-containing genes, BVES and POPDC3 , is associated with promoter hypermethylation in gastric cancer. *Carcinogenesis,* 31**,** 1685-1693.

KIRCHMAIER, B. C., POON, K. L., SCHWERTE, T., HUISKEN, J., WINKLER, C., JUNGBLUT, B., STAINIER, D. Y. & BRAND, T. 2012. The Popeye domain containing 2 (popdc2) gene in zebrafish is required for heart and skeletal muscle development. *Dev Biol,* 363**,** 438-450.

KISHIMOTO, Y., LEE, K. H., ZON, L., HAMMERSCHMIDT, M. & SCHULTE-MERKER, S. 1997. The molecular nature of zebrafish swirl: BMP2 function is essential during early dorsoventral patterning. *Development (Cambridge, England),* 124**,** 4457.

KLIMINSKI, V., UZIEL, O. & KESSLER-ICEKSON, G. 2017. Popdc1/Bves Functions in the Preservation of Cardiomyocyte Viability While Affecting Rac1 Activity and Bnip3 Expression. *J Cell Biochem,* 118**,** 1505-1517.

KLINKE, N. D. J., HORVATH, N., CUPPETT, V., WU, Y., DENG, W. & KANJ, R. 2015. Interlocked positive and negative feedback network motifs regulate β-catenin activity in the adherens junction pathway. *Mol Biol Cell.,* 26**,** 4135-4148.

KNIGHT, R. F., BADER, D. M. & BACKSTROM, J. R. 2003. Membrane topology of Bves/Pop1A, a cell adhesion molecule that displays dynamic changes in cellular distribution during development. *J Biol Chem.,* 278**,** 32872-32879.

KOIVISTO, E., JURADO ACOSTA, A., MOILANEN, A.-M., TOKOLA, H., ARO, J., PENNANEN, H., SÄKKINEN, H., KAIKKONEN, L., RUSKOAHO, H. & RYSÄ, J. 2014. Characterization of the regulatory mechanisms of activating transcription factor 3 by hypertrophic stimuli in rat cardiomyocytes. *PloS one,* 9**,** e105168.

KOK, FATMA O., SHIN, M., NI, C.-W., GUPTA, A., GROSSE, ANN S., VAN IMPEL, A., KIRCHMAIER, BETTINA C., PETERSON-MADURO, J., KOURKOULIS, G., MALE, I., DESANTIS, DANA F., SHEPPARD-TINDELL, S., EBARASI, L., BETSHOLTZ, C., SCHULTE-MERKER, S., WOLFE, SCOT A. & LAWSON, NATHAN D. 2015. Reverse Genetic Screening Reveals Poor Correlation between Morpholino-Induced and Mutant Phenotypes in Zebrafish. *Dev Cell,* 32**,** 97-108.

KOLODZIEJCZYK, ALEKSANDRA A., KIM, J. K., SVENSSON, V., MARIONI, JOHN C. & TEICHMANN, SARAH A. 2015. The Technology and Biology of Single-Cell RNA Sequencing. *Mol Cell.,* 58**,** 610-620.

KOMIYA, Y. & HABAS, R. 2008. Wnt signal transduction pathways. *Organogenesis,* 4**,** 68-75.

KOMURO, I. & YAZAKI, Y. 1993. Control of cardiac gene expression by mechanical stress. *Annual review of physiology,* 55**,** 55-75.

KOPP, R., BAUER, I., RAMALINGAM, A., EGG, M. & SCHWERTE, T. 2014. Prolonged hypoxia increases survival even in Zebrafish (Danio rerio) showing cardiac arrhythmia. *PloS one,* 9**,** e89099-e89099.

KOREN, L., ELHANANI, O., KEHAT, I., HAI, T. & ARONHEIM, A. 2013. Adult cardiac expression of the activating transcription factor 3, ATF3, promotes ventricular hypertrophy. *PloS one,* 8**,** e68396.

KOTH, J., WANG, X., KILLEN, A. C., STOCKDALE, W. T., POTTS, H. G., JEFFERSON, A., BONKHOFER, F., RILEY, P. R., PATIENT, R. K., GÖTTGENS, B. & MOMMERSTEEG, M. T. M. 2020. Runx1 promotes scar deposition and inhibits myocardial proliferation and survival during zebrafish heart regeneration. *Development,* 147**,** dev186569.

KOTKAMP, K., KUR, E., WENDIK, B., POLOK, B. K., BEN-DOR, S., ONICHTCHOUK, D. & DRIEVER, W. 2014. Pou5f1/Oct4 promotes cell survival via direct activation of mych expression during zebrafish gastrulation. *PloS one,* 9**,** e92356-e92356.

KREIPKE, E. R., WANG, Y., MIKLAS, J. W., MATHIEU, J. & RUOHOLA-BAKER, H. 2016. Metabolic remodeling in early development and cardiomyocyte maturation. *Semin Cell Dev Biol,* 52**,** 84-92.

KRISHNAMURTI, U. & SILVERMAN, J. F. 2014. HER2 in Breast Cancer: A Review and Update. *Adv Anat Pathol,* 21**,** 100-107.

KUMAR, N., GUPTA, S., DABRAL, S., SINGH, S. & SEHRAWAT, S. 2017. Role of exchange protein directly activated by cAMP (EPAC1) in breast cancer cell migration and apoptosis. *Mol Cell Biochem,* 430**,** 115-125.

KÜCHLER, A. M., GJINI, E., PETERSON-MADURO, J., CANCILLA, B., WOLBURG, H. & SCHULTE-MERKER, S. 2006. Development of the Zebrafish Lymphatic System Requires Vegfc Signaling. *Curr Biol.,* 16**,** 1244-1248.

LAFOREST, B. & NEMER, M. 2011. GATA5 interacts with GATA4 and GATA6 in outflow tract development. *Dev Biol,* 358**,** 368-78.

LAI, S.-L., MARÍN-JUEZ, R., MOURA, P. L., KUENNE, C., LAI, J. K. H., TSEDEKE, A. T., GUENTHER, S., LOOSO, M. & STAINIER, D. Y. 2017. Reciprocal analyses in zebrafish and medaka reveal that harnessing the immune response promotes cardiac regeneration. *eLife,* 6**,** e25605.

LAKE, B. B., AI, R., KAESER, G. E., SALATHIA, N. S., YUNG, Y. C., LIU, R., WILDBERG, A., GAO, D., FUNG, H.-L., CHEN, S., VIJAYARAGHAVAN, R., WONG, J., CHEN, A., SHENG, X., KAPER, F., SHEN, R., RONAGHI, M., FAN, J.-B., WANG, W., CHUN, J. & ZHANG, K. 2016. Neuronal subtypes and diversity revealed by single-nucleus RNA sequencing of the human brain. *Science,* 352**,** 1586-1590.

LAKE, B. B., CODELUPPI, S., YUNG, Y. C., GAO, D., CHUN, J., KHARCHENKO, P. V., LINNARSSON, S. & ZHANG, K. 2017. A comparative strategy for single-nucleus and single-cell transcriptomes confirms accuracy in predicted cell-type expression from nuclear RNA. *Sci Rep.,* 7**,** 6031-8.

LANG, J. C., WHITELAW, B., TALBOT, S. & WILKIE, N. M. 1988. Transcriptional regulation of the human c- myc gene. *Br J Cancer Suppl.,* 9**,** 62-6.

LAVINE, K. J., YU, K., WHITE, A. C., ZHANG, X., SMITH, C., PARTANEN, J. & ORNITZ, D. M. 2005. Endocardial and Epicardial Derived FGF Signals Regulate Myocardial Proliferation and Differentiation In Vivo. *Dev Cell,* 8**,** 85-95.

LAZIC, S. & SCOTT, I. C. 2011. Mef2cb regulates late myocardial cell addition from a second heart field-like population of progenitors in zebrafish. *Dev Biol.,* 354**,** 123-133.

LECLAIR, E. E. & TOPCZEWSKI, J. 2010. Development and Regeneration of the Zebrafish Maxillary Barbel: A Novel Study System for Vertebrate Tissue Growth and Repair (Zebrafish Maxillary Barbels). *PLoS ONE,* 5**,** e8737.

LEE, K.-F., SIMON, H., CHEN, H., BATES, B., HUNG, M.-C. & HAUSER, C. 1995. Requirement for neuregulin receptor erbB2 in neural and cardiac development. *Nature,* 378**,** 394-398.

LEE, K.-H., XU, Q. & BREITBART, R. E. 1996. A Newtinman-Related Gene,nkx2.7,Anticipates the Expression ofnkx2.5andnkx2.3in Zebrafish Heart and Pharyngeal Endoderm. *Dev Biol.,* 180**,** 722-731.

LEE, R. K., STAINIER, D. Y., WEINSTEIN, B. M. & FISHMAN, M. C. 1994. Cardiovascular development in the zebrafish. II. Endocardial progenitors are sequestered within the heart field. *Development,* 120**,** 3361.

LEE, S. H., WOLF, P. L., ESCUDERO, R., DEUTSCH, R., JAMIESON, S. W. & THISTLETHWAITE, P. A. 2000. Early Expression of Angiogenesis Factors in Acute Myocardial Ischemia and Infarction. *N Engl J Med.,* 342**,** 626-633.

LEPILINA, A., COON, A. N., KIKUCHI, K., HOLDWAY, J. E., ROBERTS, R. W., BURNS, C. G. & POSS, K. D. 2006. A Dynamic Epicardial Injury Response Supports Progenitor Cell Activity during Zebrafish Heart Regeneration. *Cell,* 127**,** 607-619.

LI, P., CAVALLERO, S., GU, Y., CHEN, T. H. P., HUGHES, J., HASSAN, A. B., BRUNING, J. C., PASHMFOROUSH, M. & SUCOV, H. M. 2011. IGF signaling directs ventricular cardiomyocyte proliferation during embryonic heart development. *Development,* 138**,** 1795-1805.

LIEN, C.-L., SCHEBESTA, M., MAKINO, S., WEBER, G. J. & KEATING, M. T. 2006. Gene expression analysis of zebrafish heart regeneration. *PLoS biol.,* 4**,** e260-e260.

LIN, S., ZHAO, D. & BOWNES, M. 2007. Blood vessel/ epicardial substance (bves) expression, essential for embryonic development, is down regulated by Grk/ EFGR signalling. *Int J Dev Biol.,* 51**,** 37-44.

LITVINUKOVA, M., TALAVERA-LOPEZ, C., MAATZ, H., REICHART, D., WORTH, C. L., LINDBERG, E. L., KANDA, M., POLANSKI, K., HEINIG, M., LEE, M., NADELMANN, E. R., ROBERTS, K., TUCK, L., FASOULI, E. S., DELAUGHTER, D. M., MCDONOUGH, B., WAKIMOTO, H., GORHAM, J. M., SAMARI, S., MAHBUBANI, K. T., SAEB-PARSY, K., PATONE, G., BOYLE, J. J., ZHANG, H., VIVEIROS, A., OUDIT, G. Y., BAYRAKTAR, O. A., SEIDMAN, J. G., SEIDMAN, C. E., NOSEDA, M., HUBNER, N. & TEICHMANN, S. A. 2020. Cells of the adult human heart. *Nature,* 558**,** 466-472.

LIU, H., ZHANG, C.-H., AMMANAMANCHI, N., SURESH, S., LEWARCHIK, C., RAO, K., UYS, G. M., HAN, L., ABRIAL, M., YIMLAMAI, D., GANAPATHY, B., GUILLERMIER, C., CHEN, N., KHALADKAR, M., SPAETHLING, J., EBERWINE, J. H., KIM, J., WALSH, S., CHOUDHURY, S., LITTLE, K., FRANCIS, K., SHARMA, M., VIEGAS, M., BAIS, A., KOSTKA, D., DING, J., BAR-JOSEPH, Z., WU, Y., YECHOOR, V., MOULIK, M., JOHNSON, J., WEINBERG, J., REYES-MÚGICA, M., STEINHAUSER, M. L. & KÜHN, B.

2019. Control of cytokinesis by β-adrenergic receptors indicates an approach for regulating cardiomyocyte endowment. *Sci Transl Med.,* 11.

LIU, J., BRESSAN, M., HASSEL, D., HUISKEN, J., STAUDT, D., KIKUCHI, K., POSS, K. D., MIKAWA, T. & STAINIER, D. Y. R. 2010. A dual role for ErbB2 signaling in cardiac trabeculation. *Development,* 137**,** 3867-3875.

LIU, J. & STAINIER, D. Y. R. 2010. Tbx5 and Bmp Signaling Are Essential for Proepicardium Specification in Zebrafish. *Circ Res.,* 106**,** 1818-1828.

LIU, X., TESFAI, J., EVRARD, Y. A., DENT, S. Y. R. & MARTINEZ, E. 2003. c-Myc transformation domain recruits the human STAGA complex and requires TRRAP and GCN5 acetylase activity for transcription activation. *J Biol Chem.,* 278**,** 20405.

LOHSE, C., BOCK, A., MAIELLARO, I., HANNAWACKER, A., SCHAD, L. R., LOHSE, M. J. & BAUER, W. R. 2017. Experimental and mathematical analysis of cAMP nanodomains. *PLoS One,* 12**,** e0174856.

LOMBARDO, V. A., HEISE, M., MOGHTADAEI, M., BORNHORST, D., MÄNNER, J. & ABDELILAH-SEYFRIED, S. 2019. Morphogenetic control of zebrafish cardiac looping by Bmp signaling. *Development,* 146**,** dev180091.

LONG, S., AHMAD, N. & REBAGLIATI, M. 2003. The zebrafish nodal-related gene southpaw is required for visceral and diencephalic left-right asymmetry. *Development,* 130**,** 2303-2316.

LOPASCHUK, G. D., BELKE, D. D., GAMBLE, J., ITOI, T. & SCHÖNEKESS, B. O. 1994. Regulation of fatty acid oxidation in the mammalian heart in health and disease. *Biochim Biophys Acta,* 1213**,** 263-76.

LOPASCHUK, G. D., COLLINS-NAKAI, R. L. & ITOI, T. 1992. Developmental changes in energy substrate use by the heart. *Cardiovasc Res.,* 26**,** 1172-1180.

LOPASCHUK, G. D., USSHER, J. R., FOLMES, C. D. L., JASWAL, J. S. & STANLEY, W. C. 2010. Myocardial Fatty Acid Metabolism in Health and Disease. *Physiological Reviews,* 90**,** 207-258.

LU, F., LANGENBACHER, A. & CHEN, J.-N. 2017. Tbx20 drives cardiac progenitor formation and cardiomyocyte proliferation in zebrafish. *Dev Biol.,* 421**,** 139-148.

LUO, D., HUANG, H., LU, M.-L., ZHAO, G.-F., CHANG, J., ZHENG, M.-Y. & WANG, Y. 2012a. Abnormal Expression of Adhesion Protein Bves is Associated with Gastric Cancer Progression and Poor Survival. *Pathol Oncol Res.,* 18**,** 491-497.

LUO, D., LU, M.-L., ZHAO, G.-F., HUANG, H., ZHENG, M.-Y., CHANG, J., LV, L. & LUO, J.-B. 2012b. Reduced Popdc3 expression correlates with high risk and poor survival in patients with gastric cancer. *World J Gastroenterol.,* 18**,** 2423-2429.

LUTTERBACH, B. & HANN, S. R. 1994. Hierarchical phosphorylation at N- terminal transformation-sensitive sites in c- Myc protein is regulated by mitogens and in mitosis. *Mol Cell Biol.,* 14**,** 5510.

MACHACKOVA, J., BARTA, J. & DHALLA, N. S. 2006. Myofibrillar remodelling in cardiac hypertrophy, heart failure and cardiomyopathies. *Can J Cardiol,* 22**,** 953-968.

MAGADUM, A., SINGH, N., KURIAN, A. A., SHARKAR, M. T. K., CHEPURKO, E. & ZANGI, L. 2018. Ablation of a Single N-Glycosylation Site in Human FSTL 1 Induces Cardiomyocyte Proliferation and Cardiac Regeneration. *Mol Ther Nucleic Acids,* 13**,** 133-143.

MARTIK, M. L. 2020. Metabolism makes and mends the heart. *eLife,* 9**,** e54665.

MARTIN-PUIG, S., WANG, Z. & CHIEN, K. R. 2008. Lives of a heart cell: tracing the origins of cardiac progenitors. *Cell Stem Cell,* 2**,** 320-331.

MARTINATO, F., CESARONI, M., AMATI, B. & GUCCIONE, E. 2008. Analysis of Myc-Induced Histone Modifications on Target Chromatin (Myc-Induced HMs). *PLoS One,* 3**,** e3650.

MARÍN-JUEZ, R., MARASS, M., GAUVRIT, S., ROSSI, A., LAI, S.-L., MATERNA, S. C., BLACK, B. L. & STAINIER, D. Y. R. 2016. Fast revascularization of the injured area is essential to support zebrafish heart regeneration. *Proc Natl Acad Sci U S A,* 113**,** 11237-11242.

MASTERS, M. & RILEY, P., R. 2014. The epicardium signals the way towards heart regeneration. *Stem Cell Res,* 13**,** 683-692.

MATTER, K. & BALDA, M. S. 2000. The tight junction protein ZO-1 and an interacting transcription factor regulate ErbB-2 expression. *EMBO J,* 19**,** 2024-2033.
MAURICE, D. H., KE, H., AHMAD, F., WANG, Y., CHUNG, J. & MANGANIELLO, V. C. 2014. Advances in targeting cyclic nucleotide phosphodiesterases. *Nat Rev Drug Discov,* 13**,** 290-314.
MCALPINE, P. 1995. Genetic nomenclature guide. Human. *Trends in genetics***,** 39-42.
MCCALLUM, C. M., COMAI, L., GREENE, E. A. & HENIKOFF, S. 2000. Targeted screening for induced mutations. *Nat Biotechnol,* 18**,** 455-457.
MCCARROLL, C. S., HE, W., FOOTE, K., BRADLEY, A., MCGLYNN, K., VIDLER, F., NIXON, C., NATHER, K., FATTAH, C., RIDDELL, A., BOWMAN, P., ELLIOTT, E. B., BELL, M., HAWKSBY, C., MACKENZIE, S. M., MORRISON, L. J., TERRY, A., BLYTH, K., SMITH, G. L., MCBRIDE, M. W., KUBIN, T., BRAUN, T., NICKLIN, S. A., CAMERON, E. R. & LOUGHREY, C. M. 2018. Runx1 Deficiency Protects Against Adverse Cardiac Remodeling After Myocardial Infarction. *Circulation,* 137**,** 57-70.
MCMAHON, S. B., WOOD, M. A. & COLE, M. D. 2000. The Essential Cofactor TRRAP Recruits the Histone Acetyltransferase hGCN5 to c-Myc. *Mol Cell Biol.,* 20**,** 556.
MCPHERRON, A. C., LAWLER, A. M. & LEE, S. J. 1997. Regulation of skeletal muscle mass in mice by a new TGF-β superfamily member. *Nature,* 387**,** 83-90.
MEILHAC, S. M., ESNER, M., KELLY, R. G., NICOLAS, J.-F. & BUCKINGHAM, M. E. 2004. The Clonal Origin of Myocardial Cells in Different Regions of the Embryonic Mouse Heart. *Dev Cell,* 6**,** 685-698.
MENENDEZ-MONTES, I., ESCOBAR, B., PALACIOS, B., GÓMEZ, M. J., IZQUIERDO-GARCIA, J. L., FLORES, L., JIMÉNEZ-BORREGUERO, L. J., ARAGONES, J., RUIZ-CABELLO, J., TORRES, M. & MARTIN-PUIG, S. 2016. Myocardial VHL-HIF Signaling Controls an Embryonic Metabolic Switch Essential for Cardiac Maturation. *Dev Cell,* 39**,** 724-739.
MEYER, A. & SCHARTL, M. 1999. Gene and genome duplications in vertebrates: the one-to-four (-to-eight in fish) rule and the evolution of novel gene functions. *Curr Opin Cell Biol,* 11**,** 699-704.
MEYERS, S., DOWNING, J. R. & HIEBERT, S. W. 1993. Identification of AML-1 and the (8;21) translocation protein (AML-1/ETO) as sequence-specific DNA-binding proteins: the runt homology domain is required for DNA binding and protein-protein interactions. *Mol Cell Biol,* 13**,** 6336-6345.
MEYSEN, S., MARGER, L., HEWETT, K. W., JARRY-GUICHARD, T., AGARKOVA, I., CHAUVIN, J. P., PERRIARD, J. C., IZUMO, S., GOURDIE, R. G., MANGONI, M. E., NARGEOT, J., GROS, D. & MIQUEROL, L. 2007. Nkx2.5 cell-autonomous gene function is required for the postnatal formation of the peripheral ventricular conduction system. *Dev Biol,* 303**,** 740-53.
MIAO, M., BRUCE, A. E., BHANJI, T., DAVIS, E. C. & KEELEY, F. W. 2007. Differential expression of two tropoelastin genes in zebrafish. *Matrix Biol,* 26**,** 115-24.
MIKAWA, T. & GOURDIE, R. G. 1996. Pericardial Mesoderm Generates a Population of Coronary Smooth Muscle Cells Migrating into the Heart along with Ingrowth of the Epicardial Organ. *Dev Biol,* 174**,** 221-232.
MILLER, W. R. 2002. Regulatory Subunits of PKA and Breast Cancer. *Ann N Y Acad Sci,* 968**,** 37-48.
MIQUEROL, L., MORENO-RASCON, N., BEYER, S., DUPAYS, L., MEILHAC, S. M., BUCKINGHAM, M. E., FRANCO, D. & KELLY, R. G. 2010. Biphasic Development of the Mammalian Ventricular Conduction System. *Circ Res,* 107**,** 153-161.
MITCHELL, I. C., BROWN, T. S., TERADA, L. S., AMATRUDA, J. F. & NWARIAKU, F. E. 2010. Effect of Vascular Cadherin Knockdown on Zebrafish Vasculature during Development (VE–Cad Knockdown Zebrafish). *PLoS ONE,* 5**,** e8807.
MITRA, S., SHARMA, P., KAUR, S., KHURSHEED, M. A., GUPTA, S., CHAUDHARY, M., KURUP, A. J. & RAMACHANDRAN, R. 2019. Dual regulation of lin28a by Myc is necessary during zebrafish retina regeneration. *J Cell Biol,* 218**,** 489-507.
MIURA, G. I. & YELON, D. 2011. A Guide to Analysis of Cardiac Phenotypes in the Zebrafish Embryo. *Methods Cell Biol,* 101**,** 161-180.
MIYAMOTO, D. T., ZHENG, Y., WITTNER, B. S., LEE, R. J., ZHU, H., BRODERICK, K. T., DESAI, R., FOX, D. B., BRANNIGAN, B. W., TRAUTWEIN, J., ARORA, K. S., DESAI, N., DAHL, D. M., SEQUIST, L. V., SMITH, M. R., KAPUR, R., WU, C.-L., SHIODA, T., RAMASWAMY, S., TING, D. T., TONER, M.,

MAHESWARAN, S. & HABER, D. A. 2015. RNA-Seq of single prostate CTCs implicates noncanonical Wnt signaling in antiandrogen resistance. *Science. ,* 349**,** 1351-1356.
MJAATVEDT, C. H., NAKAOKA, T., MORENO-RODRIGUEZ, R., NORRIS, R. A., KERN, M. J., EISENBERG, C. A., TURNER, D. & MARKWALD, R. R. 2001. The outflow tract of the heart is recruited from a novel heart-forming field. *Dev Biol,* 238**,** 97-109.
MOENS, C. B., DONN, T. M., WOLF-SAXON, E. R. & MA, T. P. 2008. Reverse genetics in zebrafish by TILLING. *Brief Funct Genomic Proteomic,* 7**,** 454-459.
MORGENTHAU, A. & FRISHMAN, W. H. 2018. Genetic Origins of Tetralogy of Fallot. *Cardiol Rev,* 26**,** 86-92.
MOVSESIAN, M. 2004. Altered cAMP-mediated signalling and its role in the pathogenesis of dilated cardiomyopathy. *Cardiovasc Res,* 62**,** 450-459.
MULLINS, M. 1995. Genetic nomenclature guide. Zebrafish. *Trends in genetics***,** 31-32.
MULLINS, M. C., HAMMERSCHMIDT, M., HAFFTER, P. & NÜSSLEIN-VOLHARD, C. 1994. Large-scale mutagenesis in the zebrafish: in search of genes controlling development in a vertebrate. *Curr Biol,* 4**,** 189-202.
MÄNNER, J. 2009. The anatomy of cardiac looping: A step towards the understanding of the morphogenesis of several forms of congenital cardiac malformations. *Clin Anat,* 22**,** 21-35.
MÜNCH, J., GRIVAS, D., GONZÁLEZ-RAJAL, Á., TORREGROSA-CARRIÓN, R. & DE LA POMPA, J. L. 2017. Notch signalling restricts inflammation and serpine1 expression in the dynamic endocardium of the regenerating zebrafish heart. *Development,* 144**,** 1425-1440.
NASEVICIUS, A. & EKKER, S. C. 2000. Effective targeted gene 'knockdown' in zebrafish. *Nat Genet,* 26**,** 216-220.
NESBIT, C., E., TERSAK, J. M. & PROCHOWNIK, E. 1999. MYC oncogenes and human neoplastic disease. *Oncogene,* 18**,** 3004-16.
NOVODVORSKY, P., WATSON, O., GRAY, C., WILKINSON, R. N., REEVE, S., SMYTHE, C., BENISTON, R., PLANT, K., MAGUIRE, R., M. K. ROTHMAN, A., ELWORTHY, S., VAN EEDEN, F. J. M. & CHICO, T. J. A. 2015. klf2ash317 Mutant Zebrafish Do Not Recapitulate Morpholino-Induced Vascular and Haematopoietic Phenotypes. *PloS one,* 10**,** e0141611.
NOWBAR, A. N., GITTO, M., HOWARD, J., FRANCIS, D. & AL-LAMEE, R. 2019. Mortality from Ischaemic Heart Disease: analysis of data from the World Health Organization and coronary artery disease risk factors from NCD-RisC. *Circ Cardiovasc qual outcomes,* 12**,** e005375.
OBERPRILLER, J. & OBERPRILLER, J. 1974. Response of the adult newt ventricle to injury. *J Exp Zool,* 187**,** 249-253.
OGAWA, M., GENG, F.-S., HUMPHREYS, D. T., KRISTIANTO, E., SHENG, D. Z., HUI, S. P., ZHANG, Y., SUGIMOTO, K., NAKAYAMA, M., ZHENG, D., HESSELSON, D., HODSON, M. P., BOGDANOVIC, O. & KIKUCHI, K. 2021. Krüppel-like factor 1 is a core cardiomyogenic trigger in zebrafish. *Science,* 372**,** 201-205.
OGRYZKO, N. V., HOGGETT, E. E., SOLAYMANI-KOHAL, S., TAZZYMAN, S., CHICO, T. J. A., RENSHAW, S. A. & WILSON, H. L. 2014. Zebrafish tissue injury causes upregulation of interleukin-1 and caspase-dependent amplification of the inflammatory response. *Dis Model Mech,* 7**,** 259-264.
OKAMOTO, K., LI, H., JENSEN, M. R., ZHANG, T., TAYA, Y., THORGEIRSSON, S. S. & PRIVES, C. 2002. Cyclin G Recruits PP2A to Dephosphorylate Mdm2. *Mol Cell,* 9**,** 761-771.
OKUDA, T., VAN DEURSEN, J., HIEBERT, S. W., GROSVELD, G. & DOWNING, J. R. 1996. AML1, the Target of Multiple Chromosomal Translocations in Human Leukemia, Is Essential for Normal Fetal Liver Hematopoiesis. *Cell,* 84**,** 321-330.
ONS. 2020. *Deaths from diseases of the cardiovascular system and ischaemic heart disease, males and females, by age and month of occurrence, England and Wales, deaths occurring in 2010 to 2018* [Online]. https://www.ons.gov.uk/peoplepopulationandcommunity/birthsdeathsandmarriages/deaths/adhocs/112000deathsfromdiseasesofthecardiovascularsystemandischaemicheartdiseasemale

sandfemalesbyageandmonthofoccurrenceenglandandwalesdeathsoccurringin2010to2018: Office for National Statistics. [Accessed 15 June 2021].
OPIE, L. H. M. D. D. D. & KNUUTI, J. M. D. P. 2009. The Adrenergic-Fatty Acid Load in Heart Failure. *J Am Coll Cardiol,* 54**,** 1637-1646.
OSKARSSON, T., TRUMPP, A., MURPHY, M., BISHOP, J. M., REFAELI, Y., GASSER, S. & MARTIN, G. R. 2001. c-Myc regulates mammalian body size by controlling cell number but not cell size. *Nature,* 414**,** 768-773.
OSLER, M. E. & BADER, D. M. 2004. Bves expression during avian embryogenesis. *Dev Dyn,* 229**,** 658-667.
OSLER, M. E., CHANG, M. S. & BADER, D. M. 2005. Bves modulates epithelial integrity through an interaction at the tight junction. *J Cell Sci,* 118**,** 4667.
OSLER, M. E., SMITH, T. K. & BADER, D. M. 2006. Bves , a member of the Popeye domain- containing gene family. *Dev Dyn,* 235**,** 586-593.
OSORIO, J. C., STANLEY, W. C., LINKE, A., CASTELLARI, M., DIEP, Q. N., PANCHAL, A. R., HINTZE, T. H., LOPASCHUK, G. D. & RECCHIA, F. A. 2002. Impaired myocardial fatty acid oxidation and reduced protein expression of retinoid X receptor-α in pacing-induced heart failure. *Circulation,* 106**,** 606-612.
OTTEN, C., VAN DER VEN, P. F., LEWRENZ, I., PAUL, S., STEINHAGEN, A., BUSCH-NENTWICH, E., EICHHORST, J., WIESNER, B., STEMPLE, D., STRÄHLE, U., FÜRST, D. O. & ABDELILAH-SEYFRIED, S. 2012. Xirp proteins mark injured skeletal muscle in zebrafish. *PloS one,* 7**,** e31041-e31041.
PADMANABHAN, A., LI, X. & BIEBERICH, C. J. 2013. Protein kinase A regulates MYC protein through transcriptional and post-translational mechanisms in a catalytic subunit isoform-specific manner. *J Biol Chem,* 288**,** 14158.
PAFFETT-LUGASSY, N., NOVIKOV, N., JEFFREY, S., ABRIAL, M., GUNER-ATAMAN, B., SAKTHIVEL, S., BURNS, C. E. & BURNS, C. G. 2017. Unique developmental trajectories and genetic regulation of ventricular and outflow tract progenitors in the zebrafish second heart field. *Development,* 144**,** 4616-4624.
PALATINUS, J. A., O'QUINN, M. P., BARKER, R. J., HARRIS, B. S., JOURDAN, J. & GOURDIE, R. G. 2011. ZO-1 determines adherens and gap junction localization at intercalated disks. *Am J Physiol Heart Circ Physiol,* 300**,** 583-594.
PALENCIA-DESAI, S., KOHLI, V., KANG, J., CHI, N. C., BLACK, B. L. & SUMANAS, S. 2011. Vascular endothelial and endocardial progenitors differentiate as cardiomyocytes in the absence of Etsrp/Etv2 function. *Development,* 138**,** 4721.
PARANG, B., KAZ, A. M., BARRETT, C. W., SHORT, S. P., NING, W., KEATING, C. E., MITTAL, M. K., NAIK, R. D., WASHINGTON, M. K., REVETTA, F. L., SMITH, J. J., CHEN, X., WILSON, K. T., BRAND, T., BADER, D. M., TANSEY, W. P., CHEN, R., BRENTNALL, T. A., GRADY, W. M. & WILLIAMS, C. S. 2016. BVES regulates c-Myc stability via PP2A and suppresses colitis-induced tumourigenesis. *Gut,* 66**,** 852-862.
PARRIE, L. E., RENFREW, E. M., WAL, A. V., MUELLER, R. L. & GARRITY, D. M. 2013. Zebrafish tbx5 paralogs demonstrate independent essential requirements in cardiac and pectoral fin development. *Dev Dyn,* 242**,** 485-502.
PATTERSON, M., BARSKE, L., VAN HANDEL, B., RAU, C. D., GAN, P., SHARMA, A., PARIKH, S., DENHOLTZ, M., HUANG, Y., YAMAGUCHI, Y., SHEN, H., ALLAYEE, H., CRUMP, J. G., FORCE, T. I., LIEN, C.-L., MAKITA, T., LUSIS, A. J., KUMAR, S. R. & SUCOV, H. M. 2017. Frequency of mononuclear diploid cardiomyocytes underlies natural variation in heart regeneration. *Nat Genet,* 49**,** 1346-1353.
PAUL, M. H., HARVEY, R. P., WEGNER, M. & SOCK, E. 2014. Cardiac outflow tract development relies on the complex function of Sox4 and Sox11 in multiple cell types. *Cell Mol Life Sci,* 71**,** 2931-45.
PENNISI, D. J. & MIKAWA, T. 2005. Normal patterning of the coronary capillary plexus is dependent on the correct transmural gradient of FGF expression in the myocardium. *Dev Biol,* 279**,** 378-390.
PERALTA, M., STEED, E., HARLEPP, S., GONZÁLEZ-ROSA, JUAN M., MONDUC, F., ARIZA-COSANO, A., CORTÉS, A., RAYÓN, T., GÓMEZ-SKARMETA, J.-L., ZAPATA, A., VERMOT, J. & MERCADER, N.

2013. Heartbeat-Driven Pericardiac Fluid Forces Contribute to Epicardium Morphogenesis. *Curr Biol,* 23**,** 1726-1735.
PESHKOVSKY, C., TOTONG, R. & YELON, D. 2011. Dependence of cardiac trabeculation on neuregulin signaling and blood flow in zebrafish. *Dev Dyn,* 240**,** 446-56.
PFEFFER, A. M. & BRAUNWALD, A. E. 1990. Ventricular Remodeling After Myocardial Infarction: Experimental Observations and Clinical Implications. *Circulation,* 81**,** 1161-1172.
PFEFFERLI, C. & JAŹWIŃSKA, A. 2017. The careg element reveals a common regulation of regeneration in the zebrafish myocardium and fin. *Nat Commun,* 8**,** 15151.
PHAM, V. N., LAWSON, N. D., MUGFORD, J. W., DYE, L., CASTRANOVA, D., LO, B. & WEINSTEIN, B. M. 2007. Combinatorial function of ETS transcription factors in the developing vasculature. *Dev Biol,* 303**,** 772-783.
PIQUEREAU, J. & VENTURA-CLAPIER, R. 2018. Maturation of Cardiac Energy Metabolism During Perinatal Development. *Front Physiol,* 9**,** 959-959.
PLAVICKI, J. S., HOFSTEEN, P., YUE, M. S., LANHAM, K. A., PETERSON, R. E. & HEIDEMAN, W. 2014. Multiple modes of proepicardial cell migration require heartbeat. *BMC Dev Biol,* 14**,** 18-18.
POELMANN, R. E., LIE-VENEMA, H. & GITTENBERGER-DE GROOT, A. C. 2002. The role of the epicardium and neural crest as extracardiac contributors to coronary vascular development. *Tex Heart Inst J,* 29**,** 255-261.
POLLACK, P. S. 1995. Proto-oncogenes and the Cardiovascular System. *Chest,* 107**,** 826-835.
POLLACK, P. S., HOUSER, S. R., BUDJAK, R. & GOLDMAN, B. 1994. c-myc Gene expression is localized to the myocyte following hemodynamic overload in vivo. *J Cell Biochem,* 54**,** 78-84.
PORRELLO, E., R. & OLSON, E., N. 2014. A neonatal blueprint for cardiac regeneration. *Stem Cell Res,* 13**,** 556-570.
PORRELLO, E. R., MAHMOUD, A. I., SIMPSON, E., HILL, J. A., RICHARDSON, J. A., OLSON, E. N. & SADEK, H. A. 2011. Transient regenerative potential of the neonatal mouse heart. *Science,* 331**,** 1078.
PORRELLO, E. R., MAHMOUD, A. I., SIMPSON, E., JOHNSON, B. A., GRINSFELDER, D., CANSECO, D., MAMMEN, P. P., ROTHERMEL, B. A., OLSON, E. N. & SADEK, H. A. 2013. Regulation of neonatal and adult mammalian heart regeneration by the miR-15 family. *Proc Natl Acad Sci U S A,* 110**,** 187.
POSS, K., WILSON, L. & KEATING, M. 2002. Heart regeneration in zebrafish. *Science,* 298**,** 2188-2190.
PRICE, E. L., VIEIRA, J. M. & RILEY, P. R. 2019. Model organisms at the heart of regeneration. *Dis Model Mech,* 12**,** dmm040691.
PÉREZ-POMARES, J. M., PHELPS, A., SEDMEROVA, M. & WESSELS, A. 2003. Epicardial-like cells on the distal arterial end of the cardiac outflow tract do not derive from the proepicardium but are derivatives of the cephalic pericardium. *Dev Dyn,* 227**,** 56-68.
QUIJADA, P., TREMBLEY, M. A. & SMALL, E. M. 2020. The Role of the Epicardium During Heart Development and Repair. *Circ Res,* 126**,** 377-394.
RAMBEAU, P., FAURE, E., THÉRON, A., AVIERINOS, J. F., JOPLING, C., ZAFFRAN, S. & FAUCHERRE, A. 2017. Reduced aggrecan expression affects cardiac outflow tract development in zebrafish and is associated with bicuspid aortic valve disease in humans. *Int J Cardiol,* 249**,** 340-343.
RASOULI, S. J. & STAINIER, D. Y. R. 2017. Regulation of cardiomyocyte behavior in zebrafish trabeculation by Neuregulin 2a signaling. *Nat Commun,* 8**,** 15281.
RED-HORSE, K., UENO, H., WEISSMAN, I. L. & KRASNOW, M. A. 2010. Coronary arteries form by developmental reprogramming of venous cells. *Nature,* 464**,** 549-553.
REDDY, V. K., SHORT, S. P., BARRETT, C. W., MITTAL, M. K., KEATING, C. E., THOMPSON, J. J., HARRIS, E. I., REVETTA, F., BADER, D. M., BRAND, T., WASHINGTON, M. K. & WILLIAMS, C. S. 2016. BVES Regulates Intestinal Stem Cell Programs and Intestinal Crypt Viability after Radiation. *STEM CELLS,* 34**,** 1626-1636.
REES, B. B., SUDRADJAT, F. A. & LOVE, J. W. 2001. Acclimation to hypoxia increases survival time of zebrafish, Danio rerio, during lethal hypoxia. *J Exp Zool,* 289**,** 266-72.

REESE, D. E. & BADER, D. M. 1999. Cloning and expression of hbves, a novel and highly conserved mRNA expressed in the developing and adult heart and skeletal muscle in the human. *Mamm Genome,* 10**,** 913-915.

REESE, D. E., ZAVALJEVSKI, M., STREIFF, N. L. & BADER, D. 1999. bves:A Novel Gene Expressed during Coronary Blood Vessel Development. *Dev Biol,* 209**,** 159-171.

REITER, J. F., ALEXANDER, J., RODAWAY, A., YELON, D., PATIENT, R., HOLDER, N. & STAINIER, D. Y. 1999. Gata5 is required for the development of the heart and endoderm in zebrafish. *Genes Dev,* 13**,** 2983.

RIBAS, L., VALDIVIESO, A., DÍAZ, N. & PIFERRER, F. 2017. Response to "The importance of controlling genetic variation - remarks on 'Appropriate rearing density in domesticated zebrafish to avoid masculinization: links with the stress response'". *J Exp Biol,* 220**,** 4079-4080.

RINNÉ, S., ORTIZ-BONNIN, B., STALLMEYER, B., KIPER, A. K., FORTMÜLLER, L., SCHINDLER, R. F. R., HERBORT-BRAND, U., KABIR, N. S., DITTMANN, S., FRIEDRICH, C., ZUMHAGEN, S., GUALANDI, F., SELVATICI, R., RAPEZZI, C., ARBUSTINI, E., FERLINI, A., FABRITZ, L., SCHULZE-BAHR, E., BRAND, T. & DECHER, N. 2020. POPDC2 a novel susceptibility gene for conduction disorders. *J Mol Cell Cardiol,* 145**,** 74-83.

RIPLEY, A. N., OSLER, M. E., WRIGHT, C. V. E. & BADER, D. 2006. Xbves is a regulator of epithelial movement during early Xenopus laevis development. *Proc Natl Acad Sci U S A,* 103**,** 614-619.

RODRÍGUEZ-ESTEBAN , CONCEPCIÓN., CAPDEVILA , JAVIER., KAWAKAMI , YASUHIKO., IZPISÚA BELMONTE & CARLOS., J. 2001. Wnt signaling and PKA control Nodal expression and left-right determination in the chick embryo. *Development,* 128**,** 3189-3195.

ROWLERSON, A., RADAELLI, G., MASCARELLO, F. & VEGGETTI, A. 1997. Regeneration of skeletal muscle in two teleost fish: Sparus aurata and Brachydanio rerio. *Cell Tissue Res,* 289**,** 311-322.

RUDAT, C. & KISPERT, A. 2012. Wt1 and Epicardial Fate Mapping. *Circ Res,* 111**,** 165-169.

RUSS, P. K., PINO, C. J., WILLIAMS, C. S., BADER, D. M., HASELTON, F. R. & CHANG, M. S. 2011. Bves Modulates Tight Junction Associated Signaling (Bves Modulates Signaling). *PLoS ONE,* 6**,** e14563.

RYAN, R., MOYSE, B. R. & RICHARDSON, R. J. 2020. Zebrafish cardiac regeneration—looking beyond cardiomyocytes to a complex microenvironment. *Histochem Cell Biol,* 154**,** 533-548.

SALLIN, P. & JAŹWIŃSKA, A. 2016. Acute stress is detrimental to heart regeneration in zebrafish. *Open Biol,* 6**,** 160012.

SAMSA, L. A., GIVENS, C., TZIMA, E., STAINIER, D. Y. R., QIAN, L. & LIU, J. 2015. Cardiac contraction activates endocardial Notch signaling to modulate chamber maturation in zebrafish. *Development,* 142**,** 4080-4091.

SAMSA, L. A., YANG, B. & LIU, J. 2013. Embryonic cardiac chamber maturation: Trabeculation, conduction, and cardiomyocyte proliferation. *Am J Med Genet C Semin Med Genet,* 163**,** 157-168.

SANDE-MELÓN, M., MARQUES, I. J., GALARDI-CASTILLA, M., LANGA, X., PÉREZ-LÓPEZ, M., BOTOS, M.-A., SÁNCHEZ-IRANZO, H., GUZMÁN-MARTÍNEZ, G., FERREIRA FRANCISCO, D. M., PAVLINIC, D., BENES, V., BRUGGMANN, R. & MERCADER, N. 2019. Adult sox10+ Cardiomyocytes Contribute to Myocardial Regeneration in the Zebrafish. *Cell Rep,* 29**,** 1041-1054.e5.

SANDER, J. D. & JOUNG, J. K. 2014. CRISPR-Cas systems for genome editing, regulation and targeting. *Nat Biotechnol,* 32**,** 347-355.

SANDER, V., SUÑE, G., JOPLING, C., MORERA, C. & BELMONTE, J. C. 2013. Isolation and in vitro culture of primary cardiomyocytes from adult zebrafish hearts. *Nat Protoc,* 8**,** 800-9.

SANZ-MOREJÓN, A. & MERCADER, N. 2020. Recent insights into zebrafish cardiac regeneration. *Curr Opin Genet Dev,* 64**,** 37-43.

SAWADA, N., MURATA, M., KIKUCHI, K., OSANAI, M., TOBIOKA, H., KOJIMA, T. & CHIBA, H. 2003. Tight junctions and human diseases. *Med Electron Microsc,* 36**,** 147-56.

SCHIB, J. L., ICARDO, J. M., DURÁN, A. C., GUERRERO, A., LÓPEZ, D., COLVEE, E., DE ANDRÉS, A. V. & SANS-COMA, V. 2002. The conus arteriosus of the adult gilthead seabream (Sparus auratus). *J Anat,* 201**,** 395-404.

SCHINDELIN, J., ARGANDA-CARRERAS, I., FRISE, E., KAYNIG, V., LONGAIR, M., PIETZSCH, T., PREIBISCH, S., RUEDEN, C., SAALFELD, S., SCHMID, B., TINEVEZ, J.-Y., WHITE, D. J., HARTENSTEIN, V., ELICEIRI, K., TOMANCAK, P. & CARDONA, A. 2012. Fiji: an open-source platform for biological-image analysis. *Nat Methods,* 9**,** 676-682.

SCHINDLER, F. R., SCOTTON, C., FRENCH, V., FERLINI, A. & BRAND, T. 2016a. The Popeye Domain Containing Genes and Their Function in Striated Muscle. *J Cardiovasc Dev Dis,* 13**,** 18.

SCHINDLER, R. F., POON, K. L., SIMRICK, S. & BRAND, T. 2012. The Popeye domain containing genes: essential elements in heart rate control. *Cardiovasc Diagn Ther,* 2**,** 308-19.

SCHINDLER, R. F. R. & BRAND, T. 2016. The Popeye domain containing protein family – A novel class of cAMP effectors with important functions in multiple tissues. *Prog Biophys Mol Biol,* 120**,** 28-36.

SCHINDLER, R. F. R., SCOTTON, C., ZHANG, J., PASSARELLI, C., ORTIZ-BONNIN, B., SIMRICK, S., SCHWERTE, T., POON, K.-L., FANG, M., RINNÉ, S., FROESE, A., NIKOLAEV, V. O., GRUNERT, C., MÜLLER, T., TASCA, G., SARATHCHANDRA, P., DRAGO, F., DALLAPICCOLA, B., RAPEZZI, C., ARBUSTINI, E., DI RAIMO, F. R., NERI, M., SELVATICI, R., GUALANDI, F., FATTORI, F., PIETRANGELO, A., LI, W., JIANG, H., XU, X., BERTINI, E., DECHER, N., WANG, J., BRAND, T. & FERLINI, A. 2016b. POPDC1(S201F) causes muscular dystrophy and arrhythmia by affecting protein trafficking. *J Clin Invest,* 126**,** 239-253.

SCHNABEL, K., WU, C.-C., KURTH, T. & WEIDINGER, G. 2011. Regeneration of Cryoinjury Induced Necrotic Heart Lesions in Zebrafish Is Associated with Epicardial Activation and Cardiomyocyte Proliferation (Zebrafish Regenerate Necrotic Heart Lesions). *PLoS ONE,* 6**,** e18503.

SCHNEIDER, M. D., PAYNE, P. A., UENO, H., PERRYMAN, M. B. & ROBERTS, R. 1986. Dissociated expression of c-myc and a fos-related competence gene during cardiac myogenesis. *Mol Cell Biol.,* 6**,** 4140-4143.

SCHNITT, J. S., STILLMAN, E. I., OWINGS, V. D., KISHIMOTO, F. C., DVORAK, H. H. & ABELMANN, H. W. 1993. Myocardial Fibrin Deposition in Experimental Viral Myocarditis That Progresses to Dilated Cardiomyopathy. *Circ Res,* 72**,** 914-920.

SCHOENEBECK, J. J., KEEGAN, B. R. & YELON, D. 2007. Vessel and Blood Specification Override Cardiac Potential in Anterior Mesoderm. *Dev Cell,* 13**,** 254-267.

SCHREIBER-AGUS, N., HORNER, J., TORRES, R., CHIU, F. C. & DEPINHO, R. A. 1993. Zebra fish myc family and max genes: differential expression and oncogenic activity throughout vertebrate evolution. *Mol Cell Biol,* 13**,** 2765-75.

SCHWARTZ, K., DE LA BASTIE, D., BOUVERET, P., OLIVIÉRO, P., ALONSO, S. & BUCKINGHAM, M. 1986. α-Skeletal Muscle Actin mRNA's Accumulate in Hypertrophied Adult Rat Hearts. *Circ Res,* 59**,** 551-555.

SCOTLAND, P. H. 2020. Heart Failure Outpatient Numbers.

SEARS, R., NUCKOLLS, F., HAURA, E., TAYA, Y., TAMAI, K. & NEVINS, J. R. 2000. Multiple Ras-dependent phosphorylation pathways regulate Myc protein stability. *Genes Dev,* 14**,** 2501-2514.

SEDMERA, D., PEXIEDER, T., VUILLEMIN, M., THOMPSON, R. P. & ANDERSON, R. H. 2000. Developmental patterning of the myocardium. *Anat Rec,* 258**,** 319-337.

SEDMERA, D., RECKOVA, M., DEALMEIDA, A., SEDMEROVA, M., BIERMANN, M., VOLEJNIK, J., SARRE, A., RADDATZ, E., MCCARTHY, R. A., GOURDIE, R. G. & THOMPSON, R. P. 2003. Functional and morphological evidence for a ventricular conduction system in zebrafish and Xenopus hearts. *Am J Physiol Heart Circ Physiol,* 284**,** H1152-H1160.

SEE, K., TAN, W. L. W., LIM, E. H., TIANG, Z., LEE, L. T., LI, P. Y. Q., LUU, T. D. A., ACKERS-JOHNSON, M. & FOO, R. S. 2017. Single cardiomyocyte nuclear transcriptomes reveal a lincRNA-regulated de-differentiation and cell cycle stress-response in vivo. *Nat Commun,* 8**,** 225-225.

SEIGO, I., BERNARDO, N.-G. & VIJAK, M. 1988. Protooncogene Induction and Reprogramming of Cardiac Gene Expression Produced by Pressure Overload. *Proc Natl Acad Sci U S A,* 85**,** 339-343.

SERGEEVA, I. A., HOOIJKAAS, I. B., VAN DER MADE, I., JONG, W. M. C., CREEMERS, E. E. & CHRISTOFFELS, V. M. 2014. A transgenic mouse model for the simultaneous monitoring of ANF and BNP gene activity during heart development and disease. *Cardiovasc Res,* 101**,** 78-86.

SERLUCA, F. C. 2008. Development of the proepicardial organ in the zebrafish. *Dev Biol,* 315**,** 18-27.

SHEN, H., CUI, G., LI, Y., YE, W., SUN, Y., ZHANG, Z., LI, J., XU, G., ZENG, X., ZHANG, Y., ZHANG, W., HUANG, Z., CHEN, W. & SHEN, Z. 2019. Follistatin-like 1 protects mesenchymal stem cells from hypoxic damage and enhances their therapeutic efficacy in a mouse myocardial infarction model. *Stem Cell Res Ther,* 10**,** 17.

SHETTY, M. S., RIS, L., SCHINDLER, R. F. R., MIZUNO, K., FEDELE, L., GIESE, K. P., BRAND, T. & ABEL, T. 2021. Mice lacking the cAMP effector protein POPDC1 show enhanced hippocampal synaptic plasticity. *bioRxiv***,** 2021.05.12.443909.

SHI, Y., LI, Y., WANG, Y., ZHU, P., CHEN, Y., WANG, H., YUE, S., XIA, X., CHEN, J., JIANG, Z., ZHOU, C., CAI, W., YUAN, H., WU, Y., WAN, Y., LI, X., ZHU, X., ZHOU, Z., DAI, G., LI, F., MO, X., YE, X., FAN, X., ZHUANG, J., WU, X. & YUAN, W. 2020. BVES downregulation in non-syndromic tetralogy of fallot is associated with ventricular outflow tract stenosis. *Sci Rep,* 10**,** 14167-14167.

SHI, Y., LI, Y., WANG, Y., ZHUANG, J., WANG, H., HU, M., MO, X., YUE, S., CHEN, Y., FAN, X., CHEN, J., CAI, W., ZHU, X., WAN, Y., ZHONG, Y., YE, X., LI, F., ZHOU, Z., DAI, G., LUO, R., OCORR, K., JIANG, Z., LI, X., ZHU, P., WU, X. & YUAN, W. 2019. The Functional Polymorphism R129W in the BVES Gene Is Associated with Sporadic Tetralogy of Fallot in the Han Chinese Population. *Genet Test Mol Biomarkers,* 23**,** 61-609.

SICCARDI, R. A. J., GARRIS, H. W., JONES, W. T., MOSELEY, D. B., D'ABRAMO, L. R. & WATTS, S. A. 2009. Growth and survival of zebrafish (Danio rerio) fed different commercial and laboratory diets. *Zebrafish,* 6**,** 275-280.

SIMRICK, S., KREUTZER, R., RAO, C., TERRACCIANO, C., KIRCHHOF, P., FABRITZ, L. & BRAND, T. 2012. Pronounced stress-induced lethality in popdc1/2 null mutants. *Cardiovascular Research, 93***,** 52-87.

SIMRICK, S., SCHINDLER, R. F., POON, K.-L. & BRAND, T. 2013. Popeye domain- containing proteins and stress- mediated modulation of cardiac pacemaking. *Trends Cardiovasc Med,* 23**,** 257-263.

SIMÕES, F. C., CAHILL, T. J., KENYON, A., GAVRIOUCHKINA, D., VIEIRA, J. M., SUN, X., PEZZOLLA, D., RAVAUD, C., MASMANIAN, E., WEINBERGER, M., MAYES, S., LEMIEUX, M. E., BARNETTE, D. N., GUNADASA-ROHLING, M., WILLIAMS, R. M., GREAVES, D. R., TRINH, L. A., FRASER, S. E., DALLAS, S. L., CHOUDHURY, R. P., SAUKA-SPENGLER, T. & RILEY, P. R. 2020. Macrophages directly contribute collagen to scar formation during zebrafish heart regeneration and mouse heart repair. *Nat Commun,* 11**,** 600-600.

SINCLAIR , J. W., HOYING , D. R., BRESCIANI , E., NOGARE, D. D., NEEDLE, C. D., WU, W., BISHOP, K., ELKAHLOUN, A. G., CHITNIS, A., LIU, P. & BURGESS, S. M. 2020. A metabolic shift to glycolysis promotes zebrafish tail regeneration through TGF-b dependent dedifferentiation of notochord cells to form the blastema. *bioRxiv***,** 385.

SINGLEMAN, C. & HOLTZMAN, N. G. 2012. Analysis of postembryonic heart development and maturation in the zebrafish, Danio rerio. *Dev Dyn,* 241**,** 1993-2004.

SMART, N., RISEBRO, C. A., MELVILLE, A. A. D., MOSES, K., SCHWARTZ, R. J., CHIEN, K. R. & RILEY, P. R. 2007. Thymosin beta4 induces adult epicardial progenitor mobilization and neovascularization. *Nature,* 445**,** 177.

SMITH, K. A. & MOMMERSTEEG, M. T. M. 2020. Talkin' 'bout regeneration: new advances in cardiac regeneration using the zebrafish. *Curr Opin Physiol,* 14**,** 48-55.

SMITH, T. K. & BADER, D. M. 2006. Characterization of Bves expression during mouse development using newly generated immunoreagents. *Dev Dyn,* 235**,** 1701-1708.

SMITH, T. K., HAGER, H. A., FRANCIS, R., KILKENNY, D. M., LO, C. & BADER, D. M. 2008. Bves Directly Interacts with GEFT, and Controls Cell Shape and Movement through Regulation of Rac1/Cdc42 Activity. *Proc Natl Acad Sci U S A,* 105**,** 8298-8303.

SOOD, R., ENGLISH, M. A., JONES, M., MULLIKIN, J., WANG, D.-M., ANDERSON, M., WU, D., CHANDRASEKHARAPPA, S. C., YU, J., ZHANG, J. & PAUL LIU, P. 2006. Methods for reverse genetic screening in zebrafish by resequencing and TILLING. *Methods,* 39**,** 220-227.

SOOD, R., KAMIKUBO, Y. & LIU, P. 2017. Role of RUNX1 in hematological malignancies. *Blood,* 129**,** 2070-2082.

SPINA, A., DI MAIOLO, F., ESPOSITO, A., SAPIO, L., CHIOSI, E., SORVILLO, L. & NAVIGLIO, S. 2012. cAMP Elevation Down-Regulates β 3 Integrin and Focal Adhesion Kinase and Inhibits Leptin-Induced Migration of MDA-MB-231 Breast Cancer Cells. *Biores Open Access,* 1**,** 324-332.

STAINIER, D. Y., LEE, R. K. & FISHMAN, M. C. 1993. Cardiovascular development in the zebrafish. I. Myocardial fate map and heart tube formation. *Development,* 119**,** 31.

STAINIER, D. Y., WEINSTEIN, B. M., DETRICH, H. W., ZON, L. I. & FISHMAN, M. C. 1995. Cloche, an early acting zebrafish gene, is required by both the endothelial and hematopoietic lineages. *Development,* 121**,** 3141.

STANLEY, W. C. & CHANDLER, M. P. 2002. Energy metabolism in the normal and failing heart: potential for therapeutic interventions. *Heart Fail Rev,* 7**,** 115-30.

STAUDT, D. W., LIU, J., THORN, K. S., STUURMAN, N., LIEBLING, M. & STAINIER, D. Y. R. 2014. High-resolution imaging of cardiomyocyte behavior reveals two distinct steps in ventricular trabeculation. *Development,* 141**,** 585-593.

STEIN, C., CACCAMO, M., LAIRD, G. & LEPTIN, M. 2007. Conservation and divergence of gene families encoding components of innate immune response systems in zebrafish. *Genome Biol,* 8**,** R251-R251.

STOCKDALE, W. T., LEMIEUX, M. E., KILLEN, A. C., ZHAO, J., HU, Z., RIEPSAAME, J., HAMILTON, N., KUDOH, T., RILEY, P. R., VAN AERLE, R., YAMAMOTO, Y. & MOMMERSTEEG, M. T. M. 2018. Heart Regeneration in the Mexican Cavefish. *Cell Rep,* 25**,** 1997-2007.e7.

STREISINGER , G., WALKER , C. & DOWER , N. K., DONNASINGER, FRED 1981. Production of clones of homozygous diploid zebra fish (*Brachydanio rerio*). *Nature,* 291**,** 293-296.

SUMANAS, S. & LIN, S. 2006. Ets1-Related Protein Is a Key Regulator of Vasculogenesis in Zebrafish (Zebrafish Etsrp Regulates Vasculogenesis). *PLoS Biol,* 4**,** e10.

SUSANNE, W. M. V. D. B., JAVIER, D., BLANKESTEIJN, W. M., JOHAN, V., LEO, H. & JAGAT, N. 2009. Myocardial remodeling after infarction: the role of myofibroblasts. *Nat Rev Cardiol,* 7**,** 30-7.

SWAN, A., GRUSCHESKI, L., BOLAND, L. & BRAND, T. 2019. The Popeye domain containing gene family encoding a family of cAMP-effector proteins with important functions in striated muscle and beyond. *J Muscle Res Cell Motil,* 40**,** 169–183.

SÁNCHEZ-IRANZO, H., GALARDI-CASTILLA, M., MINGUILLÓN, C., SANZ-MOREJÓN, A., GONZÁLEZ-ROSA, J. M., FELKER, A., ERNST, A., GUZMÁN-MARTÍNEZ, G., MOSIMANN, C. & MERCADER, N. 2018. Tbx5a lineage tracing shows cardiomyocyte plasticity during zebrafish heart regeneration. *Nat Commun,* 9**,** 428-428.

TAKASHI, M. & DONALD, A. F. 1992. Retroviral Analysis of Cardiac Morphogenesis: Discontinuous Formation of Coronary Vessels. *Proc Natl Acad Sci U S A,* 89**,** 9504-9508.

TANIGUCHI, Y., TAKEDA, S., FURUTANI-SEIKI, M., KAMEI, Y., TODO, T., SASADO, T., DEGUCHI, T., KONDOH, H., MUDDE, J., YAMAZOE, M., HIDAKA, M., MITANI, H., TOYODA, A., SAKAKI, Y., PLASTERK, R. H. A. & CUPPEN, E. 2006. Generation of medaka gene knockout models by target-selected mutagenesis. *Genome Biol,* 7**,** R116-R116.

TATSUMOTO, T., XIE, X., BLUMENTHAL, R., OKAMOTO, I. & MIKI, T. 1999. Human ECT2 Is an Exchange Factor for Rho GTPases, Phosphorylated in G2/M Phases, and Involved in Cytokinesis. *J Cell Biol,* 147**,** 921-927.

TEKELI, I., GARCIA-PUIG, A., NOTARI, M., GARCÍA-PASTOR, C., AUJARD, I., JULLIEN, L. & RAYA, A. 2017. Fate predetermination of cardiac myocytes during zebrafish heart regeneration. *Open Biol,* 7**,** 170116.

TEO, J.-L. & KAHN, M. 2010. The Wnt signaling pathway in cellular proliferation and differentiation: A tale of two coactivators. *Adv Drug Deliv Rev,* 62**,** 1149-1155.

TERNS, M. P. & TERNS, R. M. 2011. CRISPR-based adaptive immune systems. *Curr Opin Microbiol,* 14**,** 321-327.

THOMAS, P. D., CAMPBELL, M. J., KEJARIWAL, A., MI, H., KARLAK, B., DAVERMAN, R., DIEMER, K., MURUGANUJAN, A. & NARECHANIA, A. 2003. PANTHER: a library of protein families and subfamilies indexed by function. *Genome Res,* 13**,** 2129-2141.

THOMPSON, J. J., CHOKSI, Y. A., BROWN, R. E., SHORT, S. P., BRAND, T., LEE, E. & WILLIAMS, C. S. 2019. Blood Vessel Epicardial Substance (BVES) Coordinately Reduces LRP6 Receptor and Cytoplasmic β-Catenin Levels to Modulate WNT Signaling and Intestinal Homeostasis. *Carcinogenesis,* 10**,** 1086-1098.

THRUPP, N., FRIGERIO, C. S., WOLFS, L., SKENE, N. G., FATTORELLI, N., POOVATHINGAL, S., FOURNE, Y., MATTHEWS, P. M., THEYS, T., MANCUSO, R., DE STROOPER, B. & FIERS, M. 2020. Single-nucleus RNA-seq is not suitable for detection of microglial activation genes in humans. *Cell Rep,* 32**,** 108189.

TIBBO, A. J., DOBI, S., MCFALL, A., TEJEDA, G. S., BLAIR, C., MACLEOD, R., MACQUAIDE, N., GÖK, C., FULLER, W., SMITH, B. O., SMITH, G. L., BRAND, T. & BAILLIE, G. S. 2020. Phosphodiesterase Type 4 anchoring regulates cAMP signaling to Popeye domain-containing proteins. *bioRxiv*.

TILL, B. J., REYNOLDS, S. H., WEIL, C., SPRINGER, N., BURTNER, C., YOUNG, K., BOWERS, E., CODOMO, C. A., ENNS, L. C., ODDEN, A. R., GREENE, E. A., COMAI, L. & HENIKOFF, S. 2004. Discovery of induced point mutations in maize genes by TILLING. *BMC Plant Biol,* 4**,** 12.

TILL, B. J., ZERR, T., BOWERS, E., GREENE, E. A., COMAI, L. & HENIKOFF, S. 2006. High-throughput discovery of rare human nucleotide polymorphisms by Ecotilling. *Nucleic Acids Res,* 34**,** e99-e99.

TIMMERS, L., PASTERKAMP, G., DE HOOG, V. C., ARSLAN, F., APPELMAN, Y. E. A. & DE KLEIJN, D. P. V. 2012. The innate immune response in reperfused myocardium. *Cardiovasc Res,* 94**,** 276-283.

TOGO, T. 2019. Autocrine purinergic signaling stimulated by cell membrane disruption is involved in both cell membrane repair and adaptive response in MDCK cells. *Biochem Biophys Res Commun,* 511**,** 161-164.

TORLOPP, A., BREHER, S. S., SCHLÜTER, J. & BRAND, T. 2006. Comparative analysis of mRNA and protein expression of Popdc1 (Bves) during early development in the chick embryo. *Dev Dyn,* 235**,** 691-700.

TSEDEKE, A. T., ALLANKI, S., GENTILE, A., JIMENEZ-AMILBURU, V., RASOULI, S. J., GUENTHER, S., LAI, S.-L., STAINIER, D. Y. R. & MARÍN-JUEZ, R. 2021. Cardiomyocyte heterogeneity during zebrafish development and regeneration. *Dev Biol,* 476**,** 259-271.

TU, C.-T., YANG, T.-C. & TSAI, H.-J. 2009. Nkx2.7 and Nkx2.5 Function Redundantly and Are Required for Cardiac Morphogenesis of Zebrafish Embryos (Nkx in Cardiac Morphogenesis). *PLoS ONE,* 4**,** e4249.

UNAL, B., CRITCHLEY, J. A. & CAPEWELL, S. 2005. Modelling the decline in coronary heart disease deaths in England and Wales, 1981- 2000: comparing contributions from primary prevention and secondary prevention. *BMJ,* 331**,** 614.

UNG, C. Y., LAM, S. H. & GONG, Z. 2009. Comparative transcriptome analyses revealed conserved biological and transcription factor target modules between the zebrafish and human tumors. *Zebrafish,* 6**,** 425.

VAGNOZZI, R. J., GATTO, J. G. J., KALLANDER, L. S., HOFFMAN, N. E., MALLILANKARAMAN, K., BALLARD, V. L. T., LAWHORN, B. G., STOY, P., PHILP, J., GRAVES, A. P., NAITO, Y., LEPORE, J. J., GAO, E., MADESH, M. & FORCE, T. 2013. Inhibition of the cardiomyocyte-specific kinase TNNI3K limits oxidative stress, injury, and adverse remodeling in the ischemic heart. *Sci Transl Med,* 5**,** 207.

VAN DER OOST, J., JORE, M. M., WESTRA, E. R., LUNDGREN, M. & BROUNS, S. J. J. 2009. CRISPR-based adaptive and heritable immunity in prokaryotes. *Trends Biochem Sci,* 34**,** 401-407.

VAN DER POL, A., HOES, M. F., DE BOER, R. A. & VAN DER MEER, P. 2020. Cardiac foetal reprogramming: a tool to exploit novel treatment targets for the failing heart. *J Intern Med,* 288**,** 491-506.

VAN IMPEL, A., ZHAO, Z., HERMKENS, D. M. A., ROUKENS, M. G., FISCHER, J. C., PETERSON-MADURO, J., DUCKERS, H., OBER, E. A., INGHAM, P. W. & SCHULTE-MERKER, S. 2014. Divergence of zebrafish and mouse lymphatic cell fate specification pathways. *Development,* 141**,** 1228-1238.

VASAVADA, T. K., DIANGELO, J. R. & DUNCAN, M. K. 2004. Developmental Expression of Pop1/Bves. *J Histochem Cytochem,* 52**,** 371-377.

VEGA-HERNANDEZ, M., KOVACS, A., DE LANGHE, S. & ORNITZ, D. M. 2011. FGF10/FGFR2b signaling is essential for cardiac fibroblast development and growth of the myocardium. *Development,* 138**,** 3331-3340.

VERVOORTS, J., LÜSCHER-FIRZLAFF, J. & LÜSCHER, B. 2006. The ins and outs of MYC regulation by posttranslational mechanisms. *J Biol Chem,* 281**,** 34725-9.

VIRANI, S. S., ALONSO, J. A., BENJAMIN, S. E., BITTENCOURT, W. M., CALLAWAY, P. C., CARSON, M. A., CHAMBERLAIN, R. A., CHANG, N. A., CHENG, S. V. S., DELLING, F. F., DJOUSSE, S. L., ELKIND, M. M., FERGUSON, L. J., FORNAGE, W. M., KHAN, T. S., KISSELA, T. B., KNUTSON, H. K., KWAN, T. T., LACKLAND, S. D. & LEWIS 2020. Heart Disease and Stroke Statistics—2020 Update: A Report From the American Heart Association. *Circulation,* 141**,** e139-e151.

VISSING, J., JOHNSON, K., TÖPF, A., NAFISSI, S., DÍAZ-MANERA, J., FRENCH, V. M., SCHINDLER, R. F., SARATHCHANDRA, P., LØKKEN, N., RINNÉ, S., FREUND, M., DECHER, N., MÜLLER, T., DUNO, M., KRAG, T., BRAND, T. & STRAUB, V. 2019. POPDC3 Gene Variants Associate with a New Form of Limb Girdle Muscular Dystrophy. *Ann Neurol,* 86**,** 832-843.

VIVIEN, C. J., HUDSON, J. E. & PORRELLO, E. R. 2016. Evolution, comparative biology and ontogeny of vertebrate heart regeneration. *NPJ Regen Med,* 28**,** 16012.

WALDO, K. L., HUTSON, M. R., STADT, H. A., ZDANOWICZ, M., ZDANOWICZ, J. & KIRBY, M. L. 2005a. Cardiac neural crest is necessary for normal addition of the myocardium to the arterial pole from the secondary heart field. *Dev Biol,* 281**,** 66-77.

WALDO, K. L., HUTSON, M. R., WARD, C. C., ZDANOWICZ, M., STADT, H. A., KUMISKI, D., ABU-ISSA, R. & KIRBY, M. L. 2005b. Secondary heart field contributes myocardium and smooth muscle to the arterial pole of the developing heart. *Dev Biol,* 281**,** 78-90.

WALDO, K. L., KUMISKI, D. H., WALLIS, K. T., STADT, H. A., HUTSON, M. R., PLATT, D. H. & KIRBY, M. L. 2001. Conotruncal myocardium arises from a secondary heart field. *Development,* 128**,** 3179-3188.

WANG, J., KARRA, R., DICKSON, A. L. & POSS, K. D. 2013. Fibronectin is deposited by injury-activated epicardial cells and is necessary for zebrafish heart regeneration. *Dev Biol,* 382**,** 427-35.

WANG, J., PANÁKOVÁ, D., KIKUCHI, K., HOLDWAY, J. E., GEMBERLING, M., BURRIS, J. S., SINGH, S. P., DICKSON, A. L., LIN, Y.-F., SABEH, M. K., WERDICH, A. A., YELON, D., MACRAE, C. A. & POSS, K. D. 2011. The regenerative capacity of zebrafish reverses cardiac failure caused by genetic cardiomyocyte depletion. *Development,* 138**,** 3421.

WANG, S.-C., LIN, X.-L., LI, J., ZHANG, T.-T., WANG, H.-Y., SHI, J.-W., YANG, S., ZHAO, W.-T., XIE, R.-Y., WEI, F., QIN, Y.-J., CHEN, L., YANG, J., YAO, K.-T. & XIAO, D. 2014. MicroRNA-122 triggers mesenchymal-epithelial transition and suppresses hepatocellular carcinoma cell motility and invasion by targeting RhoA. *PloS one,* 9**,** e101330.

WEI, K., SERPOOSHAN, V., HURTADO, C., DIEZ-CUNADO, M., ZHAO, M., MARUYAMA, S., ZHU, W., FAJARDO, G., NOSEDA, M., NAKAMURA, K., TIAN, X., LIU, Q., WANG, A., MATSUURA, Y., BUSHWAY, P., CAI, W., SAVCHENKO, A., MAHMOUDI, M., SCHNEIDER, M. D., VAN DEN HOFF, M. J. B., BUTTE, M. J., YANG, P. C., WALSH, K., ZHOU, B., BERNSTEIN, D., MERCOLA, M. & RUIZ-LOZANO, P. 2015. Epicardial FSTL1 reconstitution regenerates the adult mammalian heart. *Nature,* 525**,** 479-85.

WEN, L. & TANG, F. 2018. Boosting the power of single-cell analysis. *Nat Biotechnol,* 36**,** 408-409.

WENDE, A. R. P., BRAHMA, M. K. P., MCGINNIS, G. R. P. & YOUNG, M. E. D. 2017. Metabolic Origins of Heart Failure. *JACC Basic Transl Sci,* 2**,** 297-310.

WHITE, J. A., BOFFA, M. B., JONES, B. & PETKOVICH, M. 1994. A zebrafish retinoic acid receptor expressed in the regenerating caudal fin. *Development,* 120**,** 1861.

WHO. 2015. *The leading causes of death* [Online]. https://www.who.int/data/gho/data/themes/mortality-and-global-health-estimates/ghe-leading-causes-of-death: World Health Organisation. [Accessed 15th June 2021].
WIEDENHEFT, B., STERNBERG, S. H. & DOUDNA, J. A. 2012. RNA-guided genetic silencing systems in bacteria and archaea. *Nature,* 482**,** 331-338.
WIENHOLDS, E. 2002. Target-Selected Inactivation of the Zebrafish rag1 Gene. *Science,* 297**,** 99-102.
WIENHOLDS, E., VAN EEDEN, F., KOSTERS, M., MUDDE, J. B., PLASTERK, R. & CUPPEN, E. 2003. Efficient target-selected mutagenesis in zebrafish. *Genome Res,* 13**,** 2700-2707.
WILLIAMS, C. S., ZHANG, B., SMITH, J. J., JAYAGOPAL, A., BARRETT, C. W., PINO, C., RUSS, P., PRESLEY, S. H., PENG, D., ROSENBLATT, D. O., HASELTON, F. R., YANG, J.-L., WASHINGTON, M. K., CHEN, X., ESCHRICH, S., YEATMAN, T. J., EL-RIFAI, W., BEAUCHAMP, R. D. & CHANG, M. S. 2011. BVES regulates EMT in human corneal and colon cancer cells and is silenced via promoter methylation in human colorectal carcinoma. *J Clin Invest,* 121**,** 4056.
WILLS, A. A., HOLDWAY, J. E., MAJOR, R. J. & POSS, K. D. 2007. Regulated addition of new myocardial and epicardial cells fosters homeostatic cardiac growth and maintenance in adult zebrafish. *Development,* 135**,** 183-192.
WOLF, F. A., ANGERER, P. & THEIS, F. J. 2018. SCANPY: large-scale single-cell gene expression data analysis. *Genome Biol,* 19**,** 15.
WOLOCK, S. L., LOPEZ, R. & KLEIN, A. M. 2019. Scrublet: Computational Identification of Cell Doublets in Single-Cell Transcriptomic Data. *Cell Syst,* 8**,** 281-291.e9.
WU, C.-C., KRUSE, F., VASUDEVARAO, M. D., JUNKER, J. P., ZEBROWSKI, D. C., FISCHER, K., NOËL, E. S., GRÜN, D., BEREZIKOV, E., ENGEL, F. B., VAN OUDENAARDEN, A., WEIDINGER, G. & BAKKERS, J. 2016. Spatially Resolved Genome-wide Transcriptional Profiling Identifies BMP Signaling as Essential Regulator of Zebrafish Cardiomyocyte Regeneration. *Dev Cell,* 36**,** 36-49.
WU, K.-J., MATTIOLI, M., MORSE, H. C. & DALLA-FAVERA, R. 2002. c-MYC activates protein kinase A (PKA) by direct transcriptional activation of the PKA catalytic subunit beta (PKA-Cβ) gene. *Oncogene,* 21**,** 7872-7882.
WU, Y.-C., LIU, C.-Y., CHEN, Y.-H., CHEN, R.-F., HUANG, C.-J. & WANG, I. J. 2012. Blood Vessel Epicardial Substance (Bves) Regulates Epidermal Tight Junction Integrity through Atypical Protein Kinase C. *J Biol Chem,* 287**,** 39887-39897.
XIAO, G., MAO, S., BAUMGARTEN, G., SERRANO, J., JORDAN, M. C., ROOS, K. P., FISHBEIN, M. C. & MACLELLAN, W. R. 2001. Inducible Activation of c-Myc in Adult Myocardium In Vivo Provokes Cardiac Myocyte Hypertrophy and Reactivation of DNA Synthesis. *Circ Res,* 89**,** 1122-1129.
XU, S., LIU, C., XIE, F., TIAN, L., MANNO, S. H., MANNO, F. A. M., 3RD, FALLAH, S., PELSTER, B., TSE, G. & CHENG, S. H. 2019. Excessive inflammation impairs heart regeneration in zebrafish breakdance mutant after cryoinjury. *Fish Shellfish Immunol,* 89**,** 117-126.
XU, S., WEBB, S. E., LAU, T. C. K. & CHENG, S. H. 2018. Matrix metalloproteinases (MMPs) mediate leukocyte recruitment during the inflammatory phase of zebrafish heart regeneration. *Sci Rep,* 8**,** 7199-14.
YANAGISAWA-MIWA, A., UCHIDA, Y., NAKAMURA, F., TOMARU, T., KIDO, H., KAMIJO, T., SUGIMOTO, T., KAJI, K., UTSUYAMA, M. & KURASHIMA, C. 1992. Salvage of Infarcted Myocardium by Angiogenic Action of Basic Fibroblast Growth Factor. *Science,* 257**,** 1401-1403.
YANG, F., LIU, Y. H., YANG, X. P., XU, J., KAPKE, A. & CARRETERO, O. A. 2002. Myocardial Infarction and Cardiac Remodelling in Mice. *Exp Physiol,* 87**,** 547-555.
YANO, T., MIURA, T., IKEDA, Y., MATSUDA, E., SAITO, K., MIKI, T., KOBAYASHI, H., NISHINO, Y., OHTANI, S. & SHIMAMOTO, K. 2005. Intracardiac fibroblasts, but not bone marrow derived cells, are the origin of myofibroblasts in myocardial infarct repair. *Cardiovasc Pathol,* 14**,** 241-6.
YEH, E., CUNNINGHAM, M., ARNOLD, H., CHASSE, D., MONTEITH, T., IVALDI, G., HAHN, W., C., STUKENBERG, P. T., SHENOLIKAR, S., UCHIDA, T., COUNTER, C., M., NEVINS, J., R., MEANS, A., R. & SEARS, R. 2004. A signalling pathway controlling c- Myc degradation that impacts oncogenic transformation of human cells. *Nat Cell Biol,* 6**,** 308-18.

YELON, D., HORNE, S. A. & STAINIER, D. Y. R. 1999. Restricted Expression of Cardiac Myosin Genes Reveals Regulated Aspects of Heart Tube Assembly in Zebrafish. *Dev Biol* 214**,** 23-37.

YOW, A., RAJASURYA, V. & SHARMA, S. 2021. Sudden Cardiac Death. *StatPerls,* 2021.

ZHAN, T., RINDTORFF, N. & BOUTROS, M. 2017. Wnt signaling in cancer. *Oncogene,* 36**,** 1461-1473.

ZHANG, H., FUTAMI, K. & OKAMOTO, N. 2003. Isolation of c- myc genes from goldfish and their tissue specific expression. *J. Fish Biol,* 63**,** 1266-1273.

ZHANG, Y., ZHENG, L., ZHANG, L., HU, X., REN, X. & ZHANG, Z. 2019. Deep single-cell RNA sequencing data of individual T cells from treatment-naïve colorectal cancer patients. *Sci Data,* 6**,** 131-15.

ZHAO, L., BORIKOVA, A. L., BEN-YAIR, R., GUNER-ATAMAN, B., MACRAE, C. A., LEE, R. T., GEOFFREY BURNS, C. & BURNS, C. E. 2014. Notch signaling regulates cardiomyocyte proliferation during zebrafish heart regeneration. *Proc Natl Acad Sci U S A,* 111**,** 1403-1408.

ZHENG, G. X. Y., TERRY, J. M., BELGRADER, P., RYVKIN, P., BENT, Z. W., WILSON, R., ZIRALDO, S. B., WHEELER, T. D., MCDERMOTT, G. P., ZHU, J., GREGORY, M. T., SHUGA, J., MONTESCLAROS, L., UNDERWOOD, J. G., MASQUELIER, D. A., NISHIMURA, S. Y., SCHNALL-LEVIN, M., WYATT, P. W., HINDSON, C. M., BHARADWAJ, R., WONG, A., NESS, K. D., BEPPU, L. W., DEEG, H. J., MCFARLAND, C., LOEB, K. R., VALENTE, W. J., ERICSON, N. G., STEVENS, E. A., RADICH, J. P., MIKKELSEN, T. S., HINDSON, B. J. & BIELAS, J. H. 2017. Massively parallel digital transcriptional profiling of single cells. *Nat Commun,* 8**,** 14049.

ZHOU, B., MA, Q., RAJAGOPAL, S., WU, S. M., DOMIAN, I., RIVERA-FELICIANO, J., JIANG, D., VON GISE, A., IKEDA, S., CHIEN, K. R. & PU, W. T. 2008. Epicardial progenitors contribute to the cardiomyocyte lineage in the developing heart. *Nature,* 454**,** 109-113.

ZHOU, H., LI, N., YUAN, Y., JIN, Y. G., GUO, H., DENG, W. & TANG, Q. Z. 2018. Activating transcription factor 3 in cardiovascular diseases: a potential therapeutic target. *Basic Res Cardiol,* 113**,** 37.

ZHOU, H., SHEN, D.-F., BIAN, Z.-Y., ZONG, J., DENG, W., ZHANG, Y., GUO, Y.-Y., LI, H. & TANG, Q.-Z. 2011a. Activating transcription factor 3 deficiency promotes cardiac hypertrophy, dysfunction, and fibrosis induced by pressure overload. *PloS one,* 6**,** e26744.

ZHOU, J., LIAO, M., HATTA, T., TANAKA, M., XUAN, X. & FUJISAKI, K. 2006. Identification of a follistatin-related protein from the tick Haemaphysalis longicornis and its effect on tick oviposition. *Gene,* 372**,** 191-8.

ZHOU, Y., CASHMAN, T., J., NEVIS, K. R., OBREGON, P., CARNEY, S. A., LIU, Y., GU, A., MOSIMANN, C., SONDALLE, S., PETERSON, R. E., HEIDEMAN, W., BURNS, C. E. & BURNS, G. 2011b. Latent TGF-β binding protein 3 identifies a second heart field in zebrafish. *Nature,* 474**,** 645.

ZHOU, Y., CASHMAN, T. J., NEVIS, K. R., OBREGON, P., CARNEY, S. A., LIU, Y., GU, A., MOSIMANN, C., SONDALLE, S., PETERSON, R. E., HEIDEMAN, W., BURNS, C. E. & BURNS, C. G. 2011c. Latent TGF-βbinding protein 3 identifies a second heart field in zebrafish. *Nature,* 474**,** 645-648.

ZOGBI, C., SATURI DE CARVALHO, A. E. T., NAKAMUTA, J. S., CACERES, V. D. M., PRANDO, S., GIORGI, M. C. P., ROCHITTE, C. E., MENEGHETTI, J. C. & KRIEGER, J. E. 2014. Early postnatal rat ventricle resection leads to long-term preserved cardiac function despite tissue hypoperfusion. *Physiol Rep,* 2**,** e12115.

Appendix

Permissions

World Health Organisation (WHO, 2015)

No permission required

Data used to create Figure 1

Disclaimer for data taken from the World Health Organisation. In figure 1 I used data taken from the World Health Organisation's mortality database. Although the data was from the organisation I take responsibility for the visualisation and the analysis of this data. Any interpretations and conclusions drawn from this data are my own. The World Health Organisation is only responsible for the provision of this data and not from any conclusions which I have drawn from it.

ONS (ONS, 2020) and NHS England, Wales and Northern Ireland (Digital NHS, 2020, Digital Health and Care Wales, 2020, Health NI, 2020)

No permission required

Data used to create Figure 2

Re-using Crown copyright material © Crown copyright

You may use and re-use the information featured on this website (not including logos) free of charge in any format or medium, under the terms of the Open Government Licence with only a few conditions.

Open Government Licence

Using Information under this licence

Use of copyright and database right material expressly made available under this licence (the 'Information') indicates your acceptance of the terms and conditions below.

The Licensor grants you a worldwide, royalty-free, perpetual, non-exclusive licence to use the Information subject to the conditions below.

This licence does not affect your freedom under fair dealing or fair use or any other copyright or database right exceptions and limitations.

You are free to:

- copy, publish, distribute and transmit the Information;
- adapt the Information;
- exploit the Information commercially and non-commercially for example, by combining it with other Information, or by including it in your own product or application.

NHS Scotland (Scotland, 2020)

No permission required

Data used to create Figure 2

Content on this website is © copyright Public Heath Scotland unless otherwise stated.
Organisations may copy, quote, publish and broadcast material from this website without payment and without approval provided they observe the conditions below. Other users may copy or download material from this website for private research and study without payment and without approval provided they observe the conditions below:

- the source is attributed to Public Health Scotland
- the material is not used in a misleading context or in a way that might damage Public Health Scotland's reputation
- the material is not used for commercial purposes
- a copy is sent to the Organisational Lead for Publishing Services via PHS-publications@nhs.net

Journal of Muscle Research and Cell Motility (Swan *et al.*, 2019)

No Permission required

Figure panels copied to create figure 6

Journal of Muscle Research and Cell Motility publishes open access articles. Authors of open access articles published in this journal retain the copyright of their articles and are free to reproduce and disseminate their work.

We are the authors of this work and so retain the copyright of this figure.

Materials

Table 18 Details of equipment used in this study

Name	Make	Model
15 ml Tubes	SARSTEDT	62.554.502
384-Well reaction plate	Applied Biosystems	I30F8 Q716
50 ml Tubes	SARSTEDT	62.547.254
Agarose electrophoresis system	peqlab Biotechnologie GmbH	40-07-08
Aspirator	Vacuubrand	BVC Control
Balance	Denver Instrument	SI-2002
Bioanalyzer	Agilent	2100 Bioanalyzer Instrument
Blotter	Thermo Scientific	OWL HEP1
Breeding tanks	-	-
Bunsen burner	-	-
Cassettes	Leica	3802757
Cell counter	Beckman coulter	Vi-cell™ XR
Cell culture hood	Contained Air Solutions	Biomat 2
Cell culture incubator	New Brunswick	Galaxy 170 S
Cell Scrapers	SARTEDT	83.183
Cell Sorter	BD Biosciences	BD FACSAria™ Fusion Cell Sorter
Cell strainers	pluriSelect	pluriStrainer Mini 40um
Cell strainers	pluriSelect	pluriStrainer Mini 70um
Centrifuge	Eppendorf	5415R
Centrifuge	Sorvall	Discovery 90SE
Centrifuge	Eppendorf	5810 R
Centrifuge	Boeco	C-28
Chromium Single Cell product	10x Genomics	Chromium Controller
Coffee Filters	Selecta	1117.5

Combination refrigerator-freezer	Liebherr	SN-ST
Combination refrigerator-freezer	Vestfrost	SZ301M
Computer	Hewlett-Packard®	QV993AV
Confocal Microscope	Zeiss	LSM-780
Coplin Jars	-	-
Coverslips 13mm diameter	VWR	631-0150
Coverslips 24x60mm	VWR	631-1575
Cryostat	Leica	CM1850
Dissection forceps	Dumont	FST no. 5
Dissection Microscope	Zeiss	KL7500
Dissection scissors	Deutsche Biomedzin	DB1005
Dounce Homogeniser	Sigma Aldrich	D9063-1SET
Embedding moulds	Agar Scientific	G3555
External light source for fluorescence excitation	Leica	Kubler Codix
Fine Balance	Sartorius	CP 124 S
Fish system	Aquaneering	Zebrafish Stand Alone Rack
Flow cytometer and Imager	Amnis®	Amnis® ImageStream®XMk II
Freezer	Lec+	ISU 57
Freezer	Liebherr	A61794
Freezer	Liebherr	SN-T
Freezer	Vestfrost	CFS344
Gel imager	Syngene	g:box
Glass pipettes	VWR	612-1701
Glass pipettes	VWR	612-1702
Hemocytometer	Marienfeld	
Hot plate	Leica	HI1220
Incubator (fish room)	Memmert	INE 200
Incubator (Lab)	Heraeus	
Incubator Shaker	New Brunswick Scientific	Excella E24
Laptop	Apple	MacBook Pro
Laptop	Dell	XPS13
Lightbox	Leica	KL 1500 LCD
Magnetic Stirrer	IKA Werke	Basic 2
Microcentrifuge tubes	SARTEDT	72.690.001
Microscope (cell culture)	Leica	DMi1
Microscope (fish room)	Leica	MZFLIII
Microscope slides	MARIENFELD	704002
Microtome	Leica	RM2255
Microwave	Panasonic	
Needle	Terumo	Aganti needle
Optical adhesive covers	Applied Biosystems	4360954
Parafilm	Pechiney Plastic Packaging	PM-922
PCR tubes	SARTEDT	72.737.002

Petri dishes	Thermo Scientific	90mm Petri dish triple vent
pH Meter	Orion Research	
Pipetman	Brand®	Accu-jet ® pro
Pipette	Eppendorf	Research plus G23402E
Pipette	Eppendorf	Research plus K21025E
Pipette	Eppendorf	Research plus J33426E
Pipette	Gilson	Pipetman DLS8307
Pipette	Gilson	Pipetman DK61210
Pipette	Gilson	Pipetman DB63368
Pipette	Gilson	Pipetman P55703A
Pipette tips	TipOne	S1111-6001
Pipette tips	TipOne	S1113-1006
Pipette tips	TipOne	S1110-3000
Plastic Pasture pipette	VWR	612-2850
Plate reader	Beckman coulter	Detection Paradigim
Plate Spinner	Labnet	MPS 1000
Power Pack	Bio-Rad	PowerPac HC
Polypropylene round-bottom tubes	Corning Science	352063
Polypropylene round-bottom tubes	Corning Science	352059
qPCR Machine	Applied Biosystems	Quanti studio 6
Refrigerator	Derby	GLOBAL48C-02
Refrigerator	Lec+	LR507
Retention Filter tips	SARTEDT	70.1116.215
Retractable scalpel	Swan-Morton®	6731704
Roller	DENLEY	Spiramix 5
Rotator	Labinco	L28
SDS-PAGE gel electrophoresis system	Bio-Rad	mini-PROTEAN®
Shaker	Lab Biometra	WT16
Sonifier	Soniprep	150
Spectrophotometers	Thermo Scientific	ND-8000
Stereomicroscope	Leica	M205 FA
Stripettes	Greiner Bio-one	760160
Stripettes	Greiner Bio-one	606180
Stripettes	Greiner Bio-one	607180
Superfrost Glass slides	Thermo Scientific	Polysine® Slides
Superspeed centrifuge	Sorvall	Evolution RC
Syringe	Terumo	197
Thermocycler	Applied Biosystems	Veriti 96 well thermal cycler
Thermocycler	Biometra	T3000
Tissue culture dishes	Corning Incorporated	353004
Tissue culture dishes	Corning Incorporated	3516
Tissue culture dishes	SARSTEDT	83.3902.300
Tissue embedder	Sakura	Tissue TEK
Tissue processor	Sakura	Tissue VIP

Ultra-low temperature freezer	New Brunswick Scientific	U570
Ultrapure water system	Millipore	Milli-Q® Integral 3
Vortex	Scientific Industries	Vortex gene 2 G560E
Water bath	Grant	OLS200
Water bath	Leica	HI1210
Weigh Tray	SARTEDT	71.9923.212
Whatman filter paper	GE Healthcare Lifesciences	3030-917
Widefield Microscope	Zeiss	Axio observer widefield

Table 19 Details of software used in this study

Name	Source
2100 Expert Software	Agilent
Anaconda	Anaconda Inc
Annadata 0.7.5	F. Alexander Wolf, Philipp Angerer & Fabian J. Theis
Cell Ranger 5.0.1	10x Genomics
Clustal Omega	EMBL-EBI
Endnote	Clarivate Analytics
FIJI	Open Source
GeneSnap	SynGene
GraphPad Prism 5	GraphPad Software
Harmonpy	Ilya Korsunsky, Nghia Millard, Jean Fan, Kamil Slowikowski, Fan Zhang, Kevin Wei, Yuriy Baglaenko, Michael Brenner, Po-ru Loh & Soumya Raychaudhuri
iCn3D	National Centre for Biotechnology Information
IDEAS®	Amnis®
IMAGE®	Amnis®
InkScape	Open Source
LasX	Leica
Matplotlib 3.2.1	NumFOCUS
Micosoft Excel	Microsoft
Microsoft PowerPoint	Microsoft
Microsoft Word	Microsoft
ND8000 2.3.2	Thermo Fisher Scientific
Notepad++	Open Source
Pandas 1.1.5	NumFOCUS
PANTHER DB	Thomas lab at the University of Southern California.

PHYRE2	Structural Bioinformatics Group, Imperial College, London
PuTTY	Simon Tatham/ Open Source
Python 3.6.10	Python Software Foundation
QuantStudio™ Real-Time PCR System	Thermo Fisher Scientific
Scanpy 1.7.0	F. Alexander Wolf, Philipp Angerer & Fabian J. Theis
scrublet	Samuel L. Wolock, Romain Lopez & Allon M. Klein
Servier Medical Art	Servier
SnapGene Viewer	Insightful Science
SoftMax® Pro 7.0.2	Molecular Devices
Vi-CELL XR 2.04	Beckman Coulter, Inc
ZEN (black edition)	Zeiss
ZEN 2 (blue edition)	Zeiss
ZEN 3.3 (blue edition)	Zeiss

Coding

Notebooks for all of the coding completed in this these can be found on GitHub with the following address;

https://github.com/lboland16/popdc1_zfish